MECHANISTIC UNDERSTANDING OF EMULSION FORMATION DURING PROCESSING

by

Nima Niknafs

A thesis submitted to
The University of Birmingham
For the degree of
DOCTOR OF PHILOSOPHY

School of Chemical Engineering
College of Physical and Engineering Sciences
The University of Birmingham
November 2011

تقدیم به

خانواده عزیزم ، پدربزرگوار ، مادر عزیز و خواهران مهربانم، زیرا که بدون وجود پشتیباني بي دریغ آنها انجام این مقوله میسر نبود

Abstract

In the light of the recent research interest in emulsion formation, this PhD thesis seeks to expand the current body of knowledge regarding the role of various emulsifiers on emulsion formation mechanisms. This study is particularly relevant to the food industries, where formulated emulsions often result in complex microstructures. Therefore, controlling the production processes requires knowledge regarding the effect of individual constituents on the final product.

The experimental investigation presented here examines emulsion behaviour during processing. Attempts have been initially focused on the development of a technique (reflectance technique), and subsequently a methodology, to investigate droplet size evolution during processing. This technique is based on the relationship between reflected light from the emulsion and the droplet size, at any given dispersed phase volume fraction, and emulsifier type. Consequently, measurements of the 'light reflectance' during the process can be used to determine the droplet size evolution in real-time. This technique was applied to the study of emulsification in batch mixing systems.

The developed methodology was used to investigate the effect of various operating parameters and formulations on the droplet size evolution during processing. These parameters include: the emulsifier type (surfactants, proteins, solid particles and mixed-emulsifier systems) and concentration; hydrodynamic condition of the process; and the dispersed phase volume fraction.

It was shown that using emulsifiers results in a higher droplet break-up frequency at the early stages of the process. The break-up frequencies remained the same in the presence of a range of emulsifier concentrations. Out of all the emulsifiers used, silica particles showed

the lowest droplet break-up frequency. This is because the interfacial tension is not affected when silica particles are adsorbed on the interface of droplets.

It was further shown that the final droplet size is mostly affected by the extent of droplet break-up, whilst droplet coalescence has minimal influence. Therefore, using a higher concentration of emulsifier results in a lower final droplet size, as a consequence of higher adsorption rate of remaining emulsifiers in the aqueous phase, which in turn increases the droplet break-up frequency through decreasing the interfacial tension. This hypothesis was demonstrated by using solid particles in emulsification which showed similar final droplet size to the experiment in the absence of added emulsifier, since interfacial tension is not affected by their adsorption.

It is demonstrated that the droplet coalescence cannot be completely suppressed by the presence of surfactants (Tween 20) or proteins (sodium caseinate or WPI), due to the desorption of these emulsifiers from the interface. On the other hand, droplet coalescence was arrested in the presence of solid particles, since their adsorption can be considered an irreversible phenomenon.

When the dispersed phase volume fraction was increased up to 50 %, a minimum was observed in the droplet break-up frequency at the dispersed phase volume fraction of 20 %. This was caused by the influence of two opposing factors; the increase in the dispersed phase volume fraction dampens the energy dissipation in the system, which tends to decrease the droplet break-up. In contrast, larger droplets are involved in break-up phenomena at higher dispersed phase volume fractions, which promote the droplet breakup. Increasing the dispersed phase volume fraction, on the other hand, resulted in a decrease in droplet coalescence, caused by an increase in the dampening effect of the dispersed phase, which decreases the energy dissipation in the system.

Acknowledgements

I wish to express my sincere gratitude to my supervisors at the University of Birmingham, Professor Ian T. Norton and Dr. Fotis Spyropoulos for their help and guidance throughout the duration of this work. They not only served as my supervisors but also encouraged and challenged me throughout my PhD.

My gratitude is also extended to the faculty at the school of Chemical Engineering, in particular to Dr. Taghi Miri, and the Engineering support staff, in particular Mrs Lynn Draper.

Several of my colleagues in microstructure group supported me throughout the PhD period, in particular I want to express my gratefulness to Aleksandra Pawlik, Asja Portsch, Jennifer Norton, Robin Hancock and Tom Mills.

I would like to thank Dr. Ali Hosseini, David Garrec, Marjan Rafee and Sarah Frasch-Melnik for their constant support and friendship who made the PhD experience a pleasurable one.

I would specially like to thank Dr. Ali Nazemi, Dr. Andrea Gabriele and Dr. Hamza Mounzer for being such good friends and for all the fun times.

Most of all I would like to thank my father and mother for their incredible support and interest they have shown for everything in my life, and my sisters, Niki and Nasim, for always being there for me and inspiring me in many ways.

Table of Content

List of Figures

List of Tables

List of Symbols

A	Coalescence rate
a^*, b^*	Colour coordinates
A_H	Hamaker constant
A_{oil}	Oil Hamaker constant
A_v	Surface area of droplets in unit volume
A_{water}	Water Hamaker constant
B	Break-up rate
c	Emulsifier concentration
C_i	Constants i=1,2,3...
c_{ini}	Initial emulsifier concentration
Cr	Chroma
C_T	Clearance between impeller and the bottom of the mixing vessel
D	Impeller diameter
d	Droplet diameter
d_{32}	Sauter mean diameter of droplets
$d_{32,eq}$	Sauter mean diameter when it reaches equilibrium
$d_{32,t}$	Sauter mean diameter at any given time
d_i	Diameter of droplets in size clss i
$d_{max,I}$	Maximum stable droplet in inertial sub-range of the turbulent regime
$d_{max,I,visc}$	Maximum stable droplet in inertial sub-range of the turbulent regime by considering the viscous stresses
D_T	Diameter of the mixing vessel
e	Elementary charge
E_{kin}	Kinetic energy of eddies
E_σ	Surface energy of droplets
$F_{droplet}$	Droplet interaction force
F_{ele}	Interaction force induced by electrostatic interactions
F_{vw}	Interaction force induced by Van der Wals interactions
$\bar{F}$	Mean turbulent force
H	Height of material in the mixing vessel
h	Continuous film thickness
h_d	Collision rate between an eddy and a droplet
h_{inv}	Inversion thickness
j	Power-law index
K	Consistency constant

K_B	Boltzmann constant
K_φ	Crowding factor
L^*	Lightness
m_s	Amount of surfactant in the continuous phase
N	Impeller rotational speed
n	Number concentration of droplets
n_0	Initial number concentration of droplets
$n0$	Electrolyte number
N_A	Avogadro constant
n_d	Number concentration of droplets with diameter d
N_{eff}	Corrected impeller rotational speed
n_i	Number of droplets in size class i
P_{cap}	Capillary pressure of a droplet
$\overline{\Delta P_d}$	Mean pressure fluctuation
Po	Power number
R	Droplet radius
Re	Reynolds number
Re_λ	Eddy Reynolds number
R_{film}	Radius of the flattened area of the droplet
$S_{1,2}$	Cross-section of collision between two droplets
$S_{d,e}$	Cross-section of collision between an eddy and a droplet
t	Time
T	Temperature
t_A	Surfactant adsorption time
U	Eddy velocity
$U_{relative}$	Droplets approach velocity
$\overline{U_\varphi{}^2}$	Mean square velocity of eddy in the presence of the dispersed phase
$\overline{U^2}$	Mean square velocity of eddy
$\overline{U_d}$	Mean velocity of droplets
We	Webber number
W_{planar}	Interaction energy between two planar surfaces
W_{vw}	Interaction energy induced by Van der Wals interactions
Y	Light reflectance
Y_d	Breakage efficiency
Y_n	Tristimulus value of perfect diffuser
Z	Ionic valency
α	Coalescence frequency
β	Break-up frequency
Γ	Concentration of a monolayer emulsifier on the interface

Γ^*	Threshold concentration of emulsifier on the interface
ε	Energy dissipation per unit mass
ε_c	Energy dissipation of the processing of only the continuous phase
ε_e	Energy dissipation of the emulsification
ε_{max}	Maximum energy dissipation of the mixing vessel
$\bar{\varepsilon}$	Average energy dissipation of the mixing vessel
ε_0	Permittivity of vacuum
ε_r	Relative permeability
ζ	Zeta potential of droplets
θ	Contact angle
κ	Eddy wave number
κ_D	Debye screening length
$\dot{\gamma}$	Shear rate
λ	Eddy size
λ_k	Kolmogorov microscale
μ	Viscosity
μ_d	Viscosity of the dispersed phase
μ_e	Viscosity of the emulsion
μ_r	Relative viscosity
ν	Kinematic viscosity
ν_c	Kinematic viscosity of the continuous phase
ν_e	Kinematic viscosity of the emulsion
ξ	Collision efficiency between two droplets
ρ_c	Density of the continuous phase
ρ_d	Density of the dispersed phase
ρ_e	Density of the emulsion
σ	Interfacial tension
τ	Shear stress
τ_d	Viscous stress inside the deforming droplet
φ	The dispersed phase volume fraction
χ	Collision rate between two droplets
Ψ_s	Electrical surface potential of droplets

Chapter 1

Introduction

1.1 Background

Emulsions have numerous applications in the food industry; many processed foods either partly or wholly contain emulsions (McClements, 2005). The examples of such foods include mayonnaise, milk, soup, beverages and many more. Emulsions induce numerous physical, chemical and sensory attributes to the products that they form. For example, they impart a variety of mouthfeels, textures and shelf-lives. These attributes are the result of the choice of the ingredients and the type and condition of the process employed for producing these food products. Therefore, understanding and controlling their functionality requires knowledge regarding the emulsion formation, stability, storage, and how these systems break-down upon consumption.

Conventionally, the food industry largely relied on tradition for the formulation of emulsion-based food products and the choice of processing types and conditions. This approach cannot be employed for the modern food industry as a result of the rapid change in the formulations and required processes (McClements, 2005). This is a consequence of the rapidly changing market and consumer needs, as the preferences are largely shifting towards healthier products. Moreover, the need for large quantity of food products requires that food producers operate at large scales, with relatively low costs. Consequently, a thorough understanding of the production process is required.

Most of the research performed, investigating the emulsion formation, has been carried out on static emulsions; meaning that the study was conducted after emulsification had finished. This was partly caused by the lack of convenient methods to study the formation and transient behaviour of the emulsion during processing. Moreover, most of these studies did not focus on formulation or choice of ingredients. More specifically, the effect of type and concentration of emulsifiers on underlying sub-processes has not been the focus of many

studies. Consequently, a gap in the knowledge is evident in understanding of the transient behaviour of emulsions during production processes with respect to the choice of emulsifier.

There are two reasons that make it necessary to investigate the effect of emulsifier type and concentration. The first is an economical reason, stemming from the fact that emulsifiers are among the most expensive ingredients in any given food formulation. The second reason relates to the fact that every added ingredient for controlling the food microstructure in food formulations should be justified by the added functionality. The amount of which should be in the limits prescribed by regulatory bodies (for example Food Standard Agency in UK). Therefore, food companies should determine the critical concentration of emulsifier in each formulation to address these cost and regulatory issues. This can be achieved by thoroughly understanding the mechanisms involved in the production processes and the influence of individual ingredients on the end product.

1.2 The scope of the current study

The obvious gap in knowledge leaves the aim of this study to further explore the effect of emulsifier type and concentration on the underlying mechanisms of emulsification processes. Attempts to achieve this aim are focused on monitoring the droplet size evolution during processing. Controlling the droplet size of the emulsion is one of the means to induce certain functionalities; droplet size influences important emulsion properties such as stability, colour and shelf-life (Henry *et al.*, 2009). The final average emulsion droplet size is the result of the dynamic balance between the two sub-processes of droplet break-up and coalescence, which occur simultaneously during emulsification. Despite previous studies, a lack of understanding of physical behaviour of emulsions during processing remains, mostly due to a lack of direct measurement techniques for monitoring the emulsification in real-time.

Subsequently, by using an online measurement technique, the mechanism of emulsification in the mixing systems was investigated. The choice of mixing process is justified by the numerous studies already performed on these systems, which provide sufficient information in order to better design the experiments. Moreover, the mixing process is still part of widely used processes in food industries. By carefully manipulating the processing conditions, it is possible to monitor the two sub-processes of droplet break-up and coalescence, individually.

The developed experimental set-up and methodology was employed to increase insight into processes with limited available information. It is well accepted that increasing the dispersed phase volume fraction results in an increase in droplet size. However, the underlying reasons are not fully explored. Therefore, investigating the emulsification mechanism in the presence of varying dispersed phase volume fractions was part of the focus of this work.

Finally, the influence of various emulsifier types and concentrations were studied. The selected emulsifiers include surfactants, proteins and solid particles. The influence of solid particles on emulsification mechanism is not well understood and very few studies are reported in the literature. Not only the effect of solid particles was studied individually, but also studies were conducted on the investigation of the influence of solid particles as part of mixed-emulsifier systems.

1.3 Thesis layout

The thesis structure is as follows. The introduction of the thesis is given in **CHAPTER 1**. A comprehensive literature survey was conducted prior to this study, and it is reported in **CHAPTER 2**. The materials, analytical techniques and experimental procedures are all explained in **CHAPTER 3**.

CHAPTER 4 is devoted to the method development followed by an explanation of mathematical treatment and theoretical analysis of the experimental data. In **CHAPTER 5**, the emulsification was studied in the presence of various concentrations of surfactants (Tween 20 and Brij 97) on emulsions containing 50 % volume fraction of the dispersed phase. In **CHAPTER 6**, the emulsification was studied with a range of dispersed phase volume fractions, in the presence of Tween 20. Various types of emulsifiers were employed in **CHAPTER 7**, including Tween 20, silica particles, sodium caseinate, whey protein isolate and mixed-emulsifier systems containing Tween 20 and silica particles. The studies conducted throughout this thesis are concluded in **CHAPTER 8**, and recommendations are given for enhancing the current study and the prospective work.

The results obtained during this study are published as follows:

- Niknafs, N., Spyropoulos, F., & Norton, I.T. 2011. Development of a new reflectance technique to investigate the mechanism of emulsification. *Journal of Food Engineering*, 104, (4) 603-611
- Niknafs, N., Spyropoulos, F., & Norton, I.T. 2010. The dynamic behaviour of pickering emulsification, *Proceedings of 5th World Congress on Emulsions,* Lyon, France
- Niknafs, N., Spyropoulos, F., & Norton, I.T. 2009. A new technique to understand emulsification processes, *Proceedings of the International Symposium on Food Rheology and Structure,* Zurich, Switzerland

The results obtained during this study were presented as follows:

- Niknafs, N., Spyropoulos, F., & Norton, I.T. The dynamic behaviour of pickering emulsification, *presented in 5th World Congress on Emulsions,* Lyon, France, October 2010.
- Niknafs, N., Spyropoulos, F., & Norton, I.T. The dynamic behaviour of emulsification in presence of hydrodolloids, *presented in 10th International Hydrocoloids Conference*, Shanghai, China, June 2010
- Niknafs, N., Spyropoulos, F., & Norton, I.T. 2010. The dynamic behaviour of emulsification in presence of milk proteins, *poster presentation in Formula VI*, Stockholm, June 2010
- Niknafs, N., Spyropoulos, F., & Norton, I.T. 2009. A new technique to understand emulsification processes, *presented in the International Symposium on Food Rheology and Structure,* Zurich, Switzerland, June 2009

Finally, the following parts of data obtained are in preparation for publication:

- Niknafs, N., Spyropoulos, F., & Norton, I.T. *Effect of dispersed phase volume fraction on emulsification in the presence of Tween 20 (in preparation)*
- Niknafs, N., Spyropoulos, F., & Norton, I.T. *Comparison between the effect of various emulsfier systems on emulsification (in preparation)*

Chapter 2

Literature survey

This chapter reviews the published literature regarding the theories and experimental studies carried out on emulsion composition and formation. It is divided into three sections. Firstly, emulsion composition and ingredients are introduced. In the second section a literature survey is presented on the experimental techniques used in the investigation of emulsion formation. Finally, theories of emulsion formation and experimental studies are summarised. The literature review concentrates on aspects relevant to the materials used in the work of this thesis.

2.1 Emulsion: chemistry and ingredients

An emulsion can be simply defined as "a system comprising of two immiscible liquids, one of which is dispersed as spherical droplets in the other" (Jafari *et al.*, 2007). Emulsions are typically defined according to the distribution of oil and aqueous phases (McClements, 2005). As the food industry mainly employs emulsions that consist of oil and water substances, an emulsion that consists of a dispersion of oil droplets in the aqueous phase is referred to as an oil-in-water emulsion (for example, milk, mayonnaise and soups), whereas an emulsion that consists of a dispersion of water droplets in the oil phase is referred to as a water-in-oil emulsion (for example, margarine, butter and spreads). Emulsions can also be classified with respect to droplet size in micro- (10-100 nm), mini- (100-1000 nm) or macro- (0.5-200 μm) emulsions. The food industry most frequently encounters macro-emulsions.

The presence of oil next to the aqueous phase is energetically unfavourable (Israelachvili, 1994). Consequently, energy is required to create such systems and, therefore, emulsions are typically produced by using mechanical devices to induce sufficient energy. The production processes of emulsions are referred to as 'emulsification' processes, during which larger droplets break down to smaller droplets as a result of energy input. The processes of breaking larger droplets into smaller ones are referred to as the 'droplet break-up' phenomena. Emulsions are thermodynamically unstable, since droplets merge into each other upon collision, which eventually results in complete phase separation. This process of merging droplets is referred to as 'droplet coalescence'. Nonetheless, it is possible to produce 'kinetically stable' emulsions over a desired period of time by employing substances called emulsifiers. Emulsifiers are 'amphiphilic' and 'surface active' materials which are able not only to facilitate droplet break-up, but also to suppress droplet coalescence.

2.1.1 Emulsion properties

2.1.1.1 Dispersed phase volume fraction

The concentration of the dispersed phase in an emulsion is normally described in terms of 'volume fraction' (φ) which is the ratio of the volume of the droplets to the volume of the whole emulsion. The dispersed phase volume fraction plays a major role in emulsification, as it not only influences droplet break-up and coalescence phenomena, but it also affects the choice of the relative quantity of ingredients (for example, emulsifier concentration) and process conditions.

2.1.1.2 Droplet size distribution

Controlling the droplet size of an emulsion is one of the means to induce certain functionality; droplet size influences important emulsion properties such as stability, colour and shelf-life (Henry *et al.*, 2009). The food industry most frequently encounters polydispersed emulsions, resulting in the presence of a distribution of droplet sizes.

Ideally, it is preferable to have information regarding all droplets in an emulsion. Nonetheless, in most situations, information regarding the mean (or average) droplet size and the width of the distribution is sufficient (Hunter, 1986) since the final average emulsion droplet size is the result of the dynamic balance between the two sub-processes of droplet break-up and coalescence.

The droplet size distribution is normally presented in the form of a continuous histogram of volume frequency of known size-class of droplets. A number of procedures exist to calculate the mean droplet size. Each of these methods results in the mean droplet size in units of 'length', however each of them stress on the different physical properties of the emulsion. One of the most useful mean droplet sizes is referred to as Sauter (or volume-surface) mean droplet size which is defined according to:

$$d_{32} = \frac{\sum n_i d_i^3}{\sum n_i d_i^2} \quad (2.1)$$

where n_i is the number of droplets and d_i is the droplet size of the given size class. The main reason that the Sauter mean diameter is normally employed in presenting the droplet size in emulsions is that it is related to the surface area of the droplets per unit volume (A_v) by:

$$A_v = \frac{6\varphi}{d_{32}} \quad (2.2)$$

where φ is the dispersed phase volume fraction. This relationship is particularly important since the total surface area of droplets can be estimated in any given emulsion.

2.1.1.3 Interfacial properties

The interface of two immiscible liquids is the narrow region that separates the oil phase from the aqueous phase. It affects directly the physicochemical properties of the emulsions including emulsion formation, rheology and stability (Everett, 1988). At the molecular level on the interface, the water and oil molecules intermingle and their composition varies across the interface. The presence of molecules in this manner results in the 'interfacial tension', (σ), between the two phases. Interfacial tension is a physical property of the system and is an indication of the 'imbalance' between molecular forces (Israelachvili, 1994).

In the presence of emulsifiers, the interfacial composition is changed since emulsifiers are adsorbed on the interface due to their 'surface activity', which is defined by the ability of the substance to accumulate on the interface. The surface activity of the emulsifier results from the amphiphilic nature of these substances; this implies that these types of material have both polar (favourable in the aqueous phase) and non-polar (favourable in the oil phase) heads. The 'sitting' of emulsifier molecules in this manner results in forming a 'shield'

between water and oil molecules which, in turn, reduces the interfacial tension between them (Israelachvili, 1994).

2.1.2 Emulsion ingredients

Emulsion-based foods are composed of a variety of chemical constituents which result in compositionally complex materials (Dickinson and Stainsby, 1982; Dickinson, 1992). These constituents interact chemically or physically with each other and the final physicochemical and/or organoleptic property of the final product is a result of all these interactions. Therefore, in order to efficiently produce emulsion-based foods which exhibit the desired functional properties, it is necessary to understand the influence of any individual constituent on the overall properties of the product, and how this contribution is affected by the presence of other chemical constituents.

This section briefly introduces the chemical characteristics of the emulsions that have been used throughout the work of this thesis. It should be noted that the descriptions of the continuous phase (water) and the dispersed phase (vegetable oil) are not provided.

2.1.2.1 Emulsifiers

The principle role of emulsifiers in emulsion-based foods is to facilitate and enhance their formation and stability. They can affect various properties of food emulsions such as viscosity or texture. Emulsifiers are amphiphilic and surface active and they can be divided in different categories such as surfactants and biopolymers. It should be noted that the descriptions given in this section concentrate on the emulsifiers employed in this study. For example, the description regarding biopolymers is limited to proteins only.

Additionally, a part of this section is devoted to the description regarding solid particles. These types of materials, by definition, are not associated with emulsifiers, since they do not reduce the interfacial tension and, therefore, they are part of stabilisers.

Nonetheless, in order to avoid confusion, they are categorised as emulsifiers and, in the respective chapter (Chapter 7), they are simply referred to as emulsifiers.

2.1.2.1.1 Surfactants

By definition, surfactants are amphiphilic molecules that can be represented by the formula *RX* (Dickinson and McClements, 1995) where *R* represents the hydrophilic 'head' part of a molecule and *X* represents the hydrophobic 'tail' part of the molecule. The properties of individual molecules are governed by the properties of the head and tail sections. The head part of the surfactant molecules employed in the food industry can be nonionic, anionic or zwitteronic. The tail part of surfactant molecules usually consists of one or more hydrocarbon chains. The surfactants employed in the work of this thesis all consist of nonionic head groups.

When surfactants are added into water they form a variety of thermodynamically stable structures known as 'association colloids'. Figure 2.1 shows a schematic representation of various association colloids. These structures are formed due to their tendency to minimise the unfavourable contact between water molecules and the non-polar tail parts of surfactant molecules. The type of association colloid is governed by the polarity and geometry of the surfactant molecules (Dickinson and McClements, 1995).

Figure 2.1. Various types of association colloids formed by surfactants in water.

Surfactants form micelles in the water when their concentration exceeds a critical level referred to as the 'critical micelle concentration' or *cmc* (Myers, 1988). Below the *cmc*

value, surfactants are dispersed mostly in the form of monomers, however, at concentrations higher than *cmc*, surfactants form micelles and the concentrations of monomers remain predominantly constant. Interestingly, despite the dynamic nature of micelles, their size and shape are well-defined under the given environmental conditions and addition of more surfactants mainly results in an increase in the number of micelles. Due to the fact that monomers and micelles have different properties, an abrupt change in some physicochemical properties is observed in surfactant solutions once the *cmc* value is exceeded (Myers, 1988). For example, surfactant monomers are highly surface active, whereas surfactant micelles have little surface activity due to their coverage by the hydrophilic head groups. Therefore, the surface tension of aqueous solutions (or, equivalently, the interfacial tension between oil and their solutions) decreases with an increase in surfactant concentration below *cmc*, but remains largely the same at concentrations higher than *cmc*.

In general, surfactants should possess three characteristics to be effective on emulsion production and long-term stability. Firstly, they should rapidly adsorb on the oil and water interface with relative high desorption activation energy (Hsu *et al.*, 2000). This results in strong adsorption on the interface and, consequently, the surfactants 'sit' firmly on the interface. Secondly, when the surfactants are adsorbed, they should have the ability to reduce the interfacial tension. This can facilitate droplet break-up since less energy is required for droplet disruption, resulting in smaller droplets. Finally, the surfactants should form a layer at the droplet interface to suppress droplet coalescence when droplets collide. Not only should this property be able to stabilise droplets during the shelf-life of a product, but also during emulsification. Depending on the type of the surfactants, they induce coalescence stability by various mechanisms. Nonionic surfactants, such as those employed in this work, generate such stability by a number of short-range repulsive forces such as steric overlap repulsion,

thermal fluctuation interactions and hydrations (McClements, 2005). Additionally, surfactants are able to stabilise droplets against coalescence by the so-called "Gibbs-Marangoni" effect (Walstra, 1993; Walstra and Smulders, 1998). This stability mechanism is based on the movement of the surfactant along the droplets interfaces. When two droplets collide the planar continuous phase squeezes out between droplets, dragging some of the surfactants. This action generates a concentration gradient along the interface. This results in a tendency of surfactants to move to the regions of low surfactant concentration, dragging some of the continuous phase along with them. This motion of the continuous phase causes an increase in the planar film thickness, hence stabilising the droplets. The combination of these factors results in the overall effectiveness of nonionic surfactants for emulsification.

Various rules have been proposed for surfactant classifications. One of the major classification methods, which is based on the chemical structure of surfactants, is the hydrophile-lipophile balance (*HLB*) (McClements, 2005). This method generates a value which indicates the affinity of surfactants to the oil or aqueous phase. Therefore, each surfactant is assigned an *HLB* value which is based on the chemical structure of such molecule and it is calculated using:

$$HLB = 7 + \sum hydrophilic\ group\ numbers - \sum lipophilic\ group\ numbers \quad (2.3)$$

Hydrophilic and lipophilic groups are assigned a group number which is used in equation 2.3 to calculate the respective *HLB* value. Oil-in-water emulsions are best stabilised by surfactants with *HLB* values between 8 and 12, an extremely high *HLB* value indicates that the surfactant is not particularly surface-active and preferentially they remain in one phase.

Nonetheless, surfactants cannot be chosen by relying solely on the proposed classification methods. For example, the speed by which a surfactant is adsorbed on the interface is of major importance on the minimum droplet size that can be achieved. Therefore,

more detailed experimental studies are needed to choose the most suitable surfactant for a given emulsion formulation.

2.1.2.1.2 Proteins

Proteins are widely employed by food manufacturers since they provide an important source of energy and they are part of the essential nutrients in the human diet. Moreover, due to their unique functional characteristics, they have the ability to modify the properties of emulsion-based foods such as appearance, texture and stability (Dickinson, 1992).

Proteins are polymers of amino acids and their functional properties are governed by their molecular characteristics such as molecular weight, flexibility and polarity. The molecular characteristics, in turn, are influenced by the type, number and sequence of the consisting monomers (Britten and Groux, 1990). The conformational structure of proteins can be divided into three categories, namely rod-like, random coil and globular (Figure 2.2). Globular and rod-like conformations are rigid structures, whereas random coil conformations have highly dynamic structures. It should be noted that the type of the conformational structures are affected by solvent conditions such as pH, ionic strength and temperature. In a solution, proteins may exist either as an isolated molecule or as part of an association with other molecules depending on the interaction energies and entropy effects (Dickinson and McClements, 1995). Proteins are normally added to the water phase in powder form. They mostly exhibit their best functionality when they are fully dissolved and distributed in the aqueous phase.

Flexible random-coil structure Rigid rod-like structure Rigid globular structure

Figure 2.2. Various conformational structures that proteins adopt in the aqueous solution.

Proteins are amphiphilic and surface-active molecules which are able to provide stability against coalescence due to the generation of a range of repulsive forces. Their surface activity is caused by a significant number of both polar and non-polar segments in their structure (Graham and Phillips, 1979; Dickinson and Gelin, 1992). Depending on the conformations at the oil and water interface, proteins are able to adapt various structures inducing different physicochemical properties (Dickinson *et al.*, 1985; Dickinson, 2001). Random-coil molecules, upon adsorption on the interface, predominantly form a structure with non-polar and polar segments protruding in the oil and aqueous phase (loops and tails), respectively, whereas neutral segments remain in direct contact with the oil and water interface (trains) (Figure 2.3). On the other hand, globular proteins 'sit' at the interface facing the non-polar segment toward the oil phase, while the polar segments remain in the water phase; therefore, they tend to have a definite orientation at the interface. It should be noted that, once adsorbed, globular proteins often undergo re-conformation, and 'unfold' at the interface. This results in an enhancement of chemical bonds with neighbouring molecules at the interface. Consequently, the interfacial layer that globular proteins form is thin and compact, exhibiting high visco-elasticity. In contrast, the interfacial layer formed by random-coil proteins tends to be open and thick showing low visco-elasticity, although these proteins undergo structural rearrangements more rapidly than globular proteins (Dickinson, 2001; Grigoriev and Miller, 2009). Therefore, the interfacial layer formed by globular molecules tends to be more resistant against rupture in comparison with that formed by random-coil molecules.

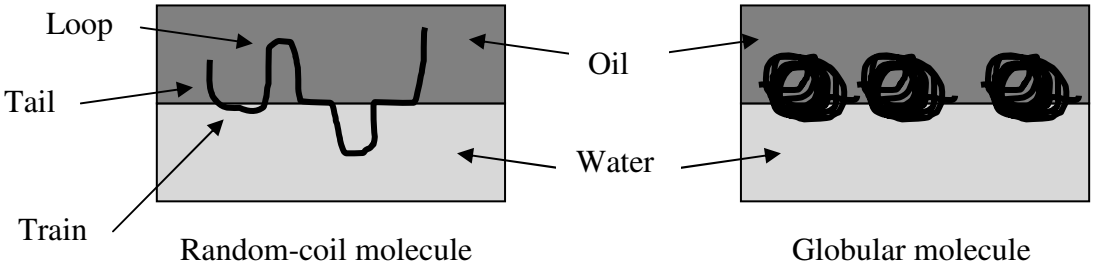

Figure 2.3. The structure of the oil-water interfacial layer depending on the type of protein.

Once absorbed on the interface, proteins are able to provide stability against aggregation by a number of mechanisms. Generally, all types of proteins provide stability against coalescence by close-range steric repulsive forces. In addition, if a protein is electrically charged it is able to provide a long-range electrostatic repulsive force against approaching droplets; this force is predominantly stronger than the steric repulsive forces. The strength of electrostatic repulsion, therefore, is highly influenced by pH and the ionic strength of the aqueous phase. At pH values close to the protein's iso-electric point, where the protein molecule does not have any net charge, or at high ionic strength, the electrostatic repulsive force is reduced significantly, in turn increasing the probability of droplet coalescence.

2.1.2.1.3 Solid particles

The fact that emulsions can be stabilised by solid particles was first reported over a century ago by Pickering who published a study on particle stabilised emulsions for plant spray applications (Pickering, 1907). Despite this early discovery, interest in these systems has increased only in the last two decades, and several studies have been carried out to characterise these types of emulsions. One of the main reasons that these systems have received much attention is their enhanced stability when compared with the more conventional surfactant- or protein-stabilised emulsions (Hunter *et al.*, 2008). This is a result of the differences between solid particle behaviour and that of more conventional emulsifiers.

It should be noted that an interest in particles already existed in the food industry, since particles play a decisive role in the microstructure of several products; such as, fat particles in whipping cream or ice crystals in the ice cream.

Despite the use of surfactants and proteins, most of the solid particles employed in the food industry are not amphiphilic (Tcholakova *et al.*, 2008). Moreover, upon adsorption, the interfacial tension between oil and water is not affected since they only 'sit' on the interface and they do not protrude in the dispersed phase, in contrast to surfactants and proteins. However, depending on their physicochemical characteristics they tend to generate oil-in-water or water-in-oil emulsions. Similarly to surfactants, solid particles can also be hydrophilic or hydrophobic. As the *HLB* value determines the nature of a surfactant (section 2.1.2.1.1), the relevant parameter for solid particles is the contact angle (θ) that the particle makes with the oil-water interface (Figure 2.4). Hydrophilic particles tend to make contact angles smaller than 90°; as a result, upon adsorption, most of the area containing hydrophilic solid particles remains in the aqueous phase. In contrast, the respective contact angle of hydrophobic particles with the oil-water interface is more than 90° (Binks and Lumsdon, 2000b; Binks, 2002). It should be noted that many methods now exist to chemically modify particles to be hydrophilic or hydrophobic (Binks, 2002). Therefore, particles with both hydrophobic and hydrophilic sides can be produced which are not only surface-active, but also amphiphilic. Such particles are referred to as "Janus" particles (Binks, 2002).

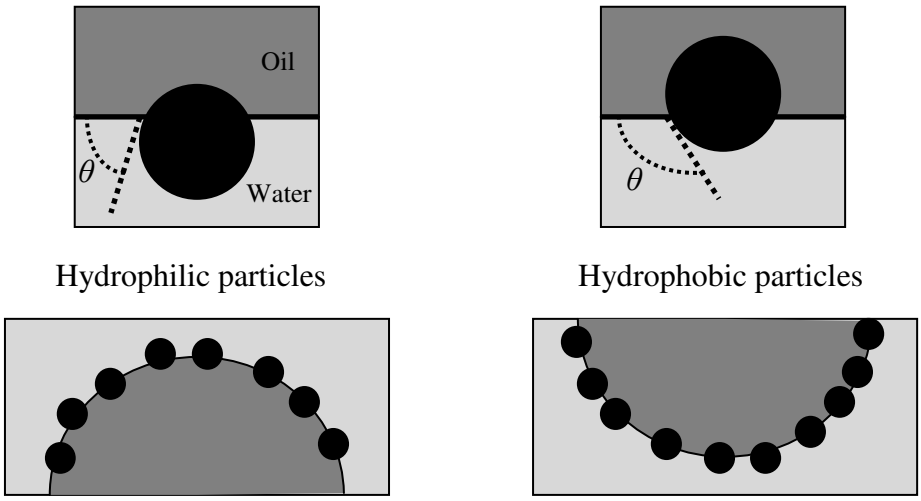

Figure 2.4. The position of solid particles on the oil-water interface depending on their physicochemical properties.

Nonetheless, the enhanced stability exhibited by these systems is mostly related to the fact that solid particles adsorb at the oil-water interface more strongly than small molecules. This is a consequence of the high attachment energy of particles relative to the thermal energy (K_BT), which cause their adsorption to be considered as an irreversible phenomenon (Aveyard *et al.*, 2003). In contrast, the adsorption and desorption of surfactants occur in relatively short timescales. It should be noted that the solid particles' attachment energy directly relates to the size of the particle; larger attachment energy is observed for larger particles, while the attachment energy is markedly reduced for smaller particles (Binks, 2002; Aveyard *et al.*, 2003; Hunter *et al*., 2008).

In most emulsions stabilised by solid particles a packed mono-layer of solid particles is formed on the interface (Figure 2.5), which due to the high desorption energy, induces a strong steric repulsive force against droplet coalescence (Binks, 2002). Other reported stability mechanisms in the presence of solid particles are the formation of a three-dimensional (3D) structure around the droplets due to inter-particle interactions, high capillary pressures between particles on the interface (Tcholakova *et al.*, 2008) and

electrostatic repulsive forces, if charged particles are used (Binks and Lumsdon, 2000a; Binks, 2002).

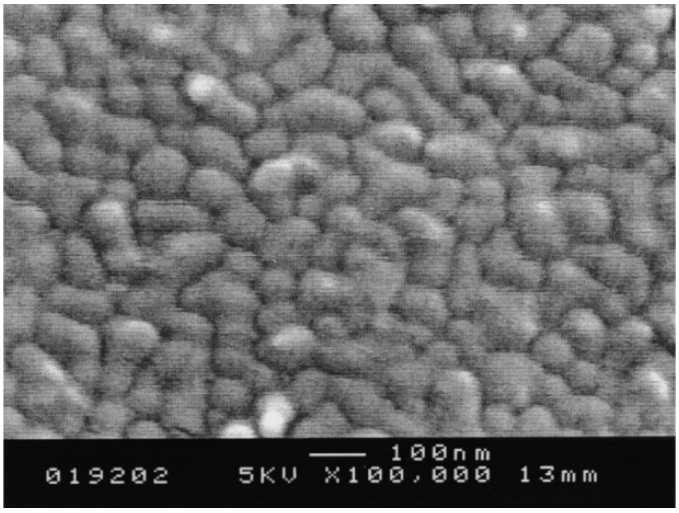

Figure 2.5. Freeze fracture SEM taken from oil (triglycerides) in water stabilised by silica particles (Binks and Kirkland, 2002).

The induced stability is highly dependent upon particle size, shape and concentration and interactions between particles. The latter are of major importance since silica particles form aggregates in the aqueous phase. An increase in the number of particle aggregates enhances the stability of emulsions against creaming and droplet coalescence. The number and structure of aggregates depends on the pH and ionic strength of the aqueous phase. For example, it has been shown that at lower pH values, where particles are neutralised, larger aggregates are produced, leading to the production of more stable emulsions (Binks and Rodrigues, 2007; Pichot *et al.*, 2009).

Another important feature of particles is their concentration. For example, it has been shown by Johansson *et al.* (1995) that low concentrations of fat crystals (monoglycerides) result in droplet coalescence or flocculation in water-in-oil emulsions. This has been related to the crossover action of particles, by which a bridge is formed between droplets, hence

inducing droplet coalescence. However, droplet coalescence is completely suppressed when high enough concentration of fat crystals were employed to cover all the droplets' interfaces.

In addition, particle-stabilised interfaces are much more rigid than those covered by small molecular emulsifiers; this results in a stronger resistance against coalescence. Zhai and Efrima (1996) showed that even millimetre-sized droplets covered by solid particles show strong stability against coalescence, a phenomenon never observed in emulsions stabilised by surfactants. Such large droplets are shown to roll over each other behaving as solid-like entities.

Due to the relatively large size of solid particles, their adsorption rates at the interface are lower than those of the much smaller surfactants. It has been shown that (Golemanov *et al.*, 2006), in contrast with surfactants and proteins whose adsorption rate depends on their respective concentrations in an emulsion, the adsorption rates of solid particles are directly related to their size. Therefore, it takes longer for them to be adsorbed. This means that surfactants and proteins are much more effective in terms of rapidly covering the naked interfaces during emulsification (Binks and Lumsdon, 2000b).

Due to the afore-mentioned property and the fact that solid particles do not affect the interfacial tension of droplets, emulsification in the presence of solely solid particles results mostly in large-sized droplets. Consequently, there has been some interest in the use of dual emulsifier systems in order to benefit from the respective advantages of both materials, namely solid particles and proteins or surfactants. The studies on this type of mixed systems report a synergistic effect related to the enhanced stability over using each emulsifier individually. For example, enhanced emulsion stability against droplet coalescence and creaming was reported when opposite charged surfactants and particles were employed (Koopal *et al.*, 1999; Binks and Rodrigues, 2007; Lan *et al.*, 2007; Torres *et al.*, 2007; Whitby

et al., 2009; Vashisth *et al.*, 2010). These observations are related to the influence of surfactants on the aggregation of particles in the aqueous phase. Surfactants adsorb on the particles' surfaces; consequently they neutralise the particles, thus promoting particle aggregation in the system. In addition, surfactants reduce the interfacial tension between continuous and dispersed phases, thus, facilitating droplet break-up and hence emulsions with smaller droplets are produced. Not only do the aggregates suppress droplet coalescence due to steric stabilisation, but also they stabilise emulsions against creaming by forming a 3D network in the aqueous phase.

Similarly enhanced stability has been reported when particles were employed with either hydrophilic (Midmore, 1998) or lipophilic (Pichot *et al.*, 2009; Wang *et al.*, 2009) nonionic surfactants. In these cases it was shown that the presence of surfactants does not affect aggregate formation. However, changing the pH of the aqueous phase promotes the reduction and stability of droplet size in the emulsions, since lower pH values neutralise the particles, therefore promoting aggregation. In addition to studies conducted on mixed-emulsifier systems containing surfactants and particles, similarly enhanced stability is reported when proteins are used with silica particles (Murray *et al.*, 2011).

Although a large number of studies have been conducted on mixed-emulsifier systems, their influence on emulsion formation and on the interfacial structure at the droplet interface are not yet well understood and there are still reports of experimental data with non-trivial results (Ghouchi Eskandar *et al.*, 2007; Tigges *et al.*, 2010; Vashisth *et al.*, 2010) which remain to be understood. Therefore, more experimental studies are required to fully understand mixed-emulsifier systems.

2.2 Experimental techniques employed to investigate emulsification processes

In a typical emulsification process, under steady-state conditions, which occur at longer times of the process, the droplet size is the result of the dynamic balance between droplet break-up and coalescence. However, the time-scales of the sub-processes in the early stages of the process are significantly shorter. Thus, droplet sizes and droplet size distributions of any process undergo rapid variations, which bring forward the necessity of robust measurement techniques. An overview of the measurement techniques developed for experimental studies of emulsification is shown schematically in Figure 2.6. These techniques can generally be divided into three categories, namely those monitoring droplet size and those that concentrate on droplet break-up or coalescence, individually.

Several techniques exist for offline measurement of droplet size using samples obtained from emulsification experiments. It should be noted that the reliability of the measurements on the samples depends on the stability of the samples after sampling and prior to the measurement. Therefore, it is often a problem to require precise measurements on samples that are not stable under natural conditions. In order to overcome this problem, after sampling, a large amount of stabiliser is added to the solution in order to ensure that the droplet size will not change until the time of the measurement. However, not only may the time from sampling until the addition to the solution be enough to change the droplet size, but also, in some cases, the addition of even small impurities may change the microstructure of the sample (Alban *et al.*, 2004). Moreover, in order to fully investigate and understand the dynamics of the processes during emulsification, there is a need to determine the droplet size during the process, which enables determination of the exact phenomena occurring in the processing vessel. Therefore, the major effort in this area is focused on the development of a technique that can be used online and during processing.

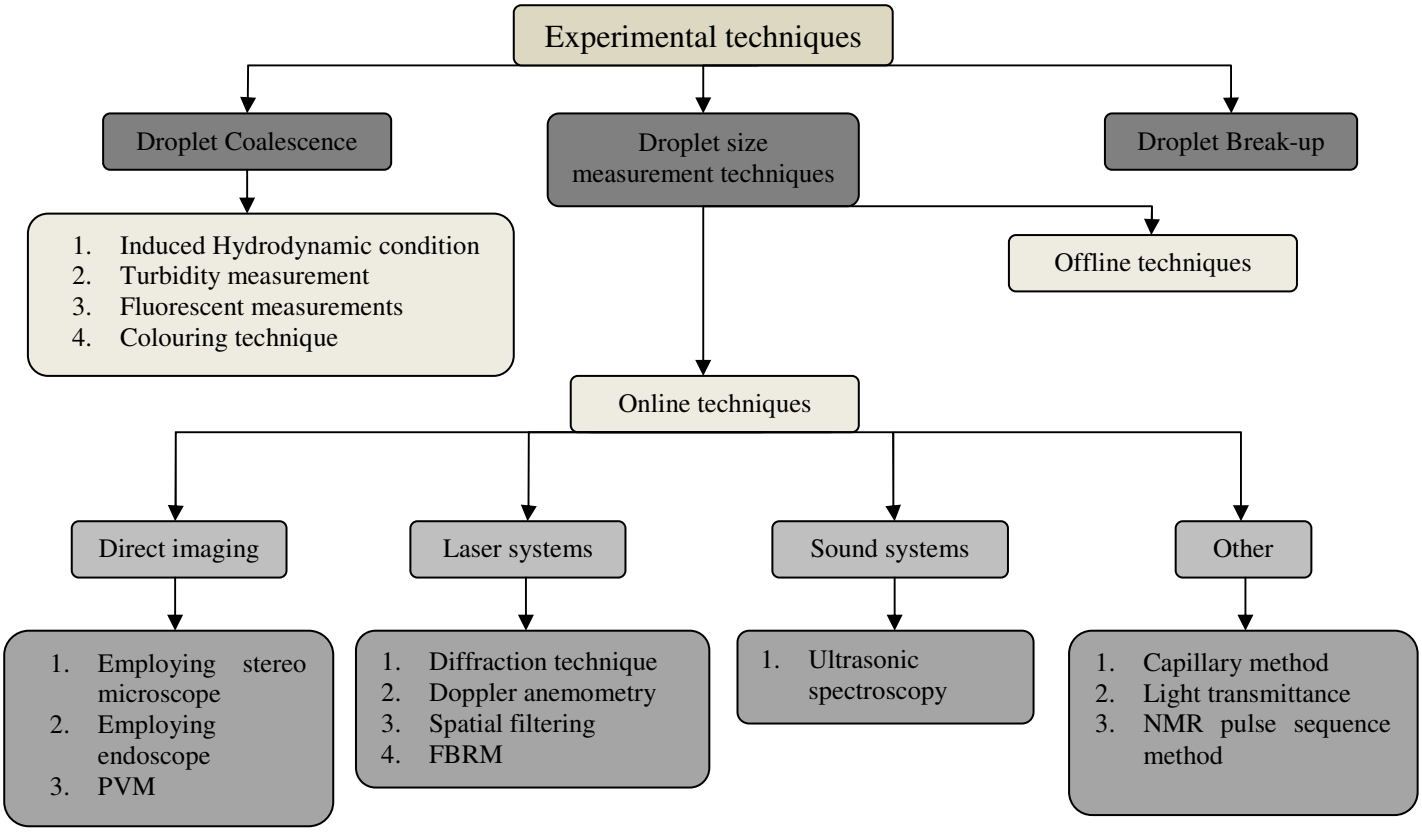

Figure 2.6. Schematic overview of the measurement techniques employed in studies on emulsification.

It should be noted that the techniques employed for droplet size monitoring are also employed in investigations on droplet break-up alone. The only difference is in the choice of processing conditions. In order to investigate droplet break-up individually, it should be separated from droplet coalescence. This is achieved by either reducing the dispersed phase volume fraction (φ<2%) while there is high emulsifier concentration, or by measuring the droplet size at certain times during processing, when droplet coalescence is minimal; for example, in the initial stages of the process (Sis and Chander, 2004; Vankova *et al.*, 2007). In this section, attention will be focused towards the online techniques.

2.2.1 Online droplet size measurement techniques

2.2.1.1 Laser systems

Measurement techniques which employ laser light to determine the droplet size are divided into four groups depending on the operating principle. Normally they can be used online and the data are collected rapidly, deeming these techniques suitable for emulsification processes. However, laser-based techniques have little application significance and some of the measurement techniques should be additionally calibrated.

One of the first and widely used techniques employs the diffraction of the propagated laser to determine the droplet size (Chatzi and Lee, 1987; Chatzi *et al.*, 1991). This technique is based on the measurement of diffracted light from droplets passing through the laser beam. The diffracted light is monitored by using a concentric annular probe so that each detector measures the scattered light at any angle. Finally these measurements are used to determine the droplet size distribution by employing Fraunhofer diffraction theory. The advantage of this technique is that it is fast and does not require any additional calibration. However, its main drawback is its limited applicability, as it can only be used for dilute emulsions.

In another approach, the phase Doppler anemometry (PDA) principle is employed for droplet size measurement (Zhou and Kresta, 1998; Wille *et al.*, 2001). This technique measures the phase difference between two scattered light signals at two collection points to determine the droplet size. This technique can only be used for systems which not only contain transparent continuous and dispersed phases, but where the entire emulsion is also transparent. Therefore PDA has little application in this framework.

The third approach (Petrak, 2002) uses modified spatial filtering velocimetry (SFV) by fibre-optical spot scanning (FSS) to measure droplet size. SFV is a method of measuring the velocity of a particle by observing it through a filter in front of a receiver. FSS is employed to observe the shadow image of a particle through a single optical fibre with small

size. This results in the generation of an impulse, the width of which depends on the droplet size and speed. The advantage of this technique is that it measures the droplet sizes and their velocity, which can be useful in emulsification studies. However, it can only be employed for emulsions containing low dispersed phase volume fractions (Maass *et al.*, 2009).

One of the most promising techniques using lasers is focused beam reflectance measurement (FBRM) (Alopaeus *et al.*, 2002). An infrared laser beam rotates at known velocity, propagating the laser beam through a lens on the probe tip. When the beam hits a droplet, the light is backscattered towards the probe window. The backscattered light is subsequently measured by a detector mounted behind the lens. Since the scanning velocity and the time delay of the backscattered light are known, the characteristic length is recorded. Given that the probability of the propagated beam hitting any part of the droplet is the same for any part of the droplet, the chord length is measured and transformed into the droplet size distribution. The main advantage of this technique is its simplicity and the robustness of the hardware required. In addition it can be employed for emulsions with dispersed phase volume fractions as high as 40% (Alopaeus *et al.*, 2002; Hu *et al.*, 2006). However, unsatisfactory results are observed when the measured droplet size distribution obtained by this technique is compared with that determined by other techniques (Worlitschek *et al.*, 2005). The reason for this is that, since the measured cord length is not always representative of the droplet diameter, various assumptions should be considered in the mathematical transformation of the data to droplet size distribution. Therefore, different mathematical approaches with different levels of sophistication have been developed (Tadayyon and Rohani, 1998; Worlitschek *et al.*, 2005; Hu *et al.*, 2006), which do not always result in similar droplet sizes. Therefore, although this technique is highly promising, it requires further development.

2.2.1.2 Sound systems

Ultrasonic spectroscopy, or acoustic droplet size measurement, has recently attracted considerable attention (Boscher *et al.*, 2009), due to its ability to measure droplet size in opaque systems such as milk and salad dressing. In addition, wider droplet size ranges can be detected by this technique than by those using laser techniques (Dukhin and Goetz, 2005). Ultrasonic spectroscopy is based on the measurement of the attenuation of ultrasound radiation propagated into an emulsion system. These data are, subsequently, transformed into droplet size distribution using theoretical models. Various mathematical models have been developed for this reason (Chanamai *et al.*, 1998; Chanamai *et al.*, 2002; Dukhin and Goetz 2005; Richter *et al.*, 2007) and they do not always generate similar results. Nonetheless, several applications have been reported where ultrasonic spectroscopy is used together with other techniques. An example of such an application is when this technique is employed in conjunction with electrophoresis for the measurement of the electric properties of an emulsion system in addition to the measurement of the droplet size (Dukhin and Goetz, 2005).

One of the main drawbacks is that ultrasonic spectroscopy has not found widespread use in industry and is related to the fact that it has an upper limit for the dispersed phase volume fraction of the emulsions in order to measure the droplet size accurately. Although in some cases 15% dispersed phase volume fraction has been used (Tong and Povey, 2002), most of the studies are performed on emulsions with dispersed phase volume fractions smaller than 5% (Dukhin and Goetz, 2005; Richter *et al.*, 2007; Boscher *et al.*, 2009). Nonetheless, the main drawback of this technique is that it is mostly suitable for offline droplet size measurement, although dilution is unnecessary. This is the result of the fact that, in order to determine droplet sizes within a broad range of sizes, ultrasonic spectroscopy employs acoustic waves with wide frequency range (1-100 MHz). Therefore, relatively long times (for example, 45 minutes (Boscher *et al.*, 2009), in comparison with emulsification time scales, is

required for droplet size measurement. It should be noted that a pulse-echo technique was developed for rapid measurement of the droplet size suitable for emulsification processes (Tong and Povey, 2002). This was achieved by reducing the range of sound frequencies and measuring the velocity of the sound instead of its attenuation. However, this approach requires further research and development in order to become fully operational for online droplet size measurement.

2.2.1.3 Direct imaging

Direct imaging methods are among the most conventional techniques employed for emulsification characterisation. They are the only techniques that can provide not only the droplet size distribution, but also they can determine the shape of the droplets. Three different approaches have been developed employing this concept.

The first online imaging technique was developed by Pacek *et al.* (1994) who employed a video camera attached to a stereo microscope. This measurement apparatus was set-up outside the mixing vessel, and in order to obtain clear pictures a stroboscope for illumination was introduced into the mixing vessel. The obtained images were subsequently analysed with the aid of semi-automatic image analysis software and the droplet size distribution was determined. Although this technique generates suitable data for determining droplet size distribution in timescales relevant to the emulsification processes, its main drawback is that the images are localised on the wall of the vessel at a depth up to 8 mm. Moreover, the introduction of a thick stroboscopic light source into the vessel may affect the process. Using this technique, droplet sizes greater than 10 μm can be characterised.

This technique was modified by Galindo *et al.* (2005) who replaced the video recording system with a CCD camera. This increased the depth of the image up to 20 mm. Moreover, fully-automated image analysis software was developed which employed the

Hough transformation. Although the proposed methodology improved the technique, the intrusive nature of this technique still persists due to the use of stroboscopic light source inside the vessel, in addition to the fact that only local images can be obtained.

Another approach using direct imaging was developed by Alban *et al.* (2004), using a stereo microscope combined with a recording system. They employed a stereo probe conventionally used for automated inspection applications. The stereo probe was a monochromic progressive-scan camera. Although the probe had the ability to record videos, it was not possible to obtain a clear image from the fast moving droplets. Therefore, a stroboscopic light source was attached to the stereo probe via an optical fibre. The obtained images were then analysed employing image analysis software. This methodology eliminates one of the main drawbacks of the technique developed by Pacek *et al.* (1994), enabling images to be freely obtained from various positions from the mixing vessel. However, the invasive nature of the technique remains, although to a lower extent. In addition, images were obtained from emulsification in the presence of 70% dispersed volume fractions (Alban *et al.*, 2004).

This approach was later used as the basis of a new measurement technique developed by Lasentech (USA) referred to as Particle Vision and Measurement (PVM®) (O'Rourke and MacLoughlin, 2005). Light from six laser sources is focused to generate a fixed (2 mm^2) area of illumination. When droplets are encountered within this area, they scatter the laser beam in all directions. The backscattered light is measured by a lensing system in the probe and then is relayed on a CCD array. The image captured on the CCD array is analysed by commercially available image analysis software. Although this technique has been shown to operate better than other commercially available techniques (Maass *et al.*, 2009), it has also been shown that a minimum time of three minutes is required to obtain a sufficient number of images for the

accurate determination of a representative droplet size distribution (O'Rourke and MacLoughlin, 2005). Therefore, this technique is not suitable for transient emulsification; for example, in the initial stages of the process. In addition, droplet sizes larger than 10 μm have been shown to be the limit of this technique (O'Rourke and MacLoughlin, 2005). It should be noted that the invasive nature of direct imaging techniques is significantly reduced by this method due to the 25 mm diameter of the probe; nonetheless, the problem persists in mixing vessels with smaller sizes.

2.2.1.4 Other techniques

In addition to the approaches described earlier, there are other techniques which cannot be categorised into any group. These techniques have often introduced novel approaches or applied new methods which require further attention in order to be employed in emulsification processes.

Bae and Tavlarides (1989) employed a capillary method to determine the droplet size distribution of the mixing tank. The system consists of a capillary tube positioned in the tank. Droplets during the process are forced into the capillary tube by using a vacuum pump. Consequently, droplets form cylindrical slugs when they are drawn into the capillary tube. A laser source is situated exactly in the middle of the tube. The device estimates the droplet size by measuring the difference between laser diffraction caused by the adsorption of the solute in the droplets. One of the advantages of this technique is that it can be employed for high dispersed phase volume fractions. However, it is limited to materials that have low molar adsorptivity. In addition, a calibration measurement is required to determine the relationship between the adsorption and droplet size. This technique was modified by Hocq *et al.* (1994) who, instead of using the difference in laser diffraction, used the difference between the conductivity of the phases to determine the droplet sizes. Although the limitations of the

technique with regard to the choice of materials are reduced by this modification, the other disadvantages of this technique remain.

Another approach was suggested by Hong and Lee (1983), who employed a light transmission method. A fibre-optic light guide received monochromatic light propagated from one end and transmitted the emergent light to the photocell. The probe had a 15 mm gap through which the emulsion sample passed. The relationship between the mean droplet size and the light transmission was determined using calibration studies on emulsions with known droplet sizes. Although this technique does not report the droplet size distribution, it can generate mean droplet size evolution data in the early stages of the process because of its fast data acquisition rate. The main drawback of this method is that the emulsions should be transparent. Therefore, the technique cannot be used for emulsions with high dispersed phase volume fractions.

Finally, Hollingsworth *et al.* (2004) developed a technique based on the nuclear magnetic resonance (NMR) pulse sequence Difftrain, which is able to measure the droplet size in emulsification processes with dispersed phase volume fractions up to 20 % during the mixing process. The mixing vessel was placed into an NMR spectrometer which operated by pulsed-field gradient (PFG) NMR, while the NMR spectrometer was modified to determine the droplet size during the process. Normally, the data acquisition time for PFG NMR is approximately 20 minutes. However, by taking advantage of Difftrain, the acquisition time was markedly reduced to 3-10 s, rendering the method suitable for emulsification studies. This technique benefits from the fact that it is non-invasive and can operate on the opaque systems. However, its development is still in the early stages of validation since the mixing vessel and the emulsion volume used are significantly different from those commonly used in industrial applications.

2.2.2 Techniques investigating droplet coalescence

Investigating droplet coalescence is more complex since it is more significant at higher dispersed phase volume fractions, thus limiting the use of online droplet size measurement techniques.

One of the first attempts was made by Howarth (1967) who carefully induced a sudden change in the hydrodynamic condition of the process (a mixing vessel) that provided conditions under which droplet break-up would no longer affect the droplet size. Consequently, droplet coalescence dominated and increased the droplet size. This was achieved by a step-change reduction in the impeller speed. Consequently, the initial stages of the process were dominated by droplet coalescence. A similar method was employed by Wright and Ramkrishna (1994) who determined the numerical values of droplet coalescence by systematic sampling and population balances. In addition, this approach was later employed by Mohan *et al.* (1997) and Narsimhan and Goel (2001) on homogeniser devices by inducing a sudden change in the hydrodynamic condition of the process by a step-change reduction in the homogenisation pressure. Although this technique can provide essential information, one of its main drawbacks is that droplet coalescence cannot be examined in the presence of droplet break-up (Lobo *et al.*, 2002).

This issue was resolved to a certain extent in an approach developed by Taisne *et al.* (1996) who prepared two coarse emulsions (pre-emulsions) under similar conditions but with two different groups of oil phases (dispersed phase). One group was used in the natural state, while the other was brominated; thus, the two groups differed in their refractive index. In addition to these oils, sucrose was employed to match the refractive indices of the respective aqueous phases to those of the oil phases. Subsequently, these two emulsions were added together and the mixture was homogenised. By monitoring the refractive index of the

homogenised emulsion, the extent of droplet coalescence was determined. If droplets coalesced, the refractive index of the homogenised emulsion would be bracketed between the refractive indices of the natural and brominated emulsions. Although this technique can indeed examine the droplet coalescence while droplet break-up occurs, it suffers from a major problem. The refractive index of an emulsion depends on the droplet size; hence, the pre-emulsions were prepared by passing the emulsions through homogenisers until the droplet size was the same for both pre-emulsions. Therefore, the coalescence study was conducted on emulsions where the equilibrium droplet size had already been achieved. Another problem with this method is the chemical modification of the oil phases which can indeed affect the physicochemical characteristics of the dispersed phase such as the interfacial tension.

A similar approach was followed by Lobo *et al.* (2002), however, instead of brominating the oil phase, they employed a fluorescent probe. This approach overcame the problem of dependency on the droplet size. Consequently, there was no requirement for keeping similar droplet size in the two pre-emulsions. Therefore it was possible to examine the droplet coalescence in the stages where a high frequency of droplet break-up is expected. In addition, a Monte Carlo simulation was employed to determine how random mixing affects the fluorescent signal. The simulation showed that the sensitivity of the technique can be tuned according to the process. Although this method resolved one of the major problems of the approach by Taisne *et al.* (1996), it had a new limitation, namely it can be employed only in emulsions that contain non-viscous dispersed phases.

Finally, a modification of the above approach was proposed by Danner (2001). He proposed a colouring technique where pre-emulsions were prepared by employing dispersed phases with various hydrophobic colorants. Therefore, the change in the colour of the droplets was linked with droplet coalescence. For example, yellow and blue dyes were employed to

colour the oil phases. Due to droplet coalescence the colour of the droplets would change to green. The colour change was observed by using optical microscopy and, subsequently, the coalescence was quantified by Monte Carlo simulation. This technique is bounded by the limitations imposed by optical microscopy. In addition, distinguishing the colour of droplets by optical microscopy is severely limited by the droplet size, as the colour of the smaller droplets cannot be determined.

2.3 Emulsification in the turbulent regime

Emulsification processes are often carried out in devices that introduce a large amount of energy into the system. A number of different devices are employed in the food industry, namely mixing vessels, homogenisers and rotor-stator systems. These systems, depending on the conditions employed, induce either laminar or turbulent regimes. An improved understanding of emulsification in these systems assists in the manufacturing and design of the novel products. For this reason, this section is fully devoted to the review of the current understanding of the mechanisms involved in emulsification, including droplet break-up and coalescence. It should be noted that the review is limited to emulsification processes in the turbulent regime, reflecting the choice of processes and conditions employed in the experiments undertaken in the work of this thesis.

2.3.1 Isotropic turbulent regime in mixing vessels

The hydrodynamic regimes that are present within mixing vessels used in the food industry are mostly turbulent, when materials with low viscosity fluids (with a viscosity less than 20 mPas) are employed. In the mixing tank during processing, different regions experience fast and slow mixing. In the impeller region, the mixing is faster, whereas less intense mixing occurs in the areas closer to the wall of the mixing vessel.

The hydrodynamic regimes within the stirrer tanks are determined through their respective Reynolds numbers. In cases where the Reynolds number is above 10^4 the Kolmogorov theory of local isotropic turbulence is employed to describe the presence of eddies (Leng and Calabrese, 2004). For sufficiently high Reynolds numbers, there is a range of smaller scale eddies that are statistically independent of the larger (energy containing) eddies which are present in the main flow region of the system. The small scale eddies are described as isotropic and are independent of the turbulence generating mechanism with physical properties that are dependent mainly on the local energy dissipation rate per unit mass (ε). Below the Kolmogorov microscale of turbulence (λ_k) the physical properties of the eddies depend on the kinematic viscosity (ν), whereas above λ_k, they are independent of the kinematic viscosity. The equilibrium size range of the eddies developed within the system is described as the universal equilibrium range. It is uniquely determined by the local energy dissipation rate and the kinematic viscosity.

Additionally, in the inertial sub-range of the turbulent regime (Figure 2.8) energy transfers from larger eddies that are of a size of the same order as the diameter of the impeller (D) to the smaller eddies' sizes (λ) without any dissipation of energy. Such energy transfers take place in the inertial sub-range of the turbulent regime. Viscous dissipation occurs for eddies with dimensions less than the Kolmogorov microscale, referred to as the viscous sub-range of the turbulent regime. A schematic representation of various regions in the turbulent regime is shown in the energy spectrum of Figure 2.7 (Harnby *et al.*, 1985).

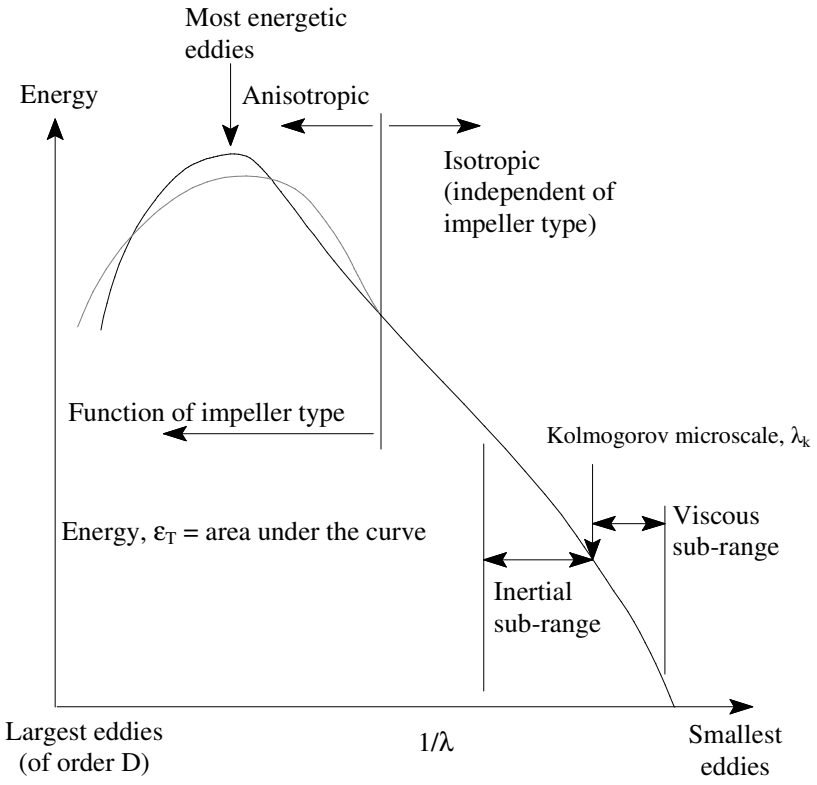

Figure 2.7. Energy spectrum of eddies with respect to their size. Different regions are indicated in the figure.

The Kolmogorov microscale is related to the conditions in which inertial forces of larger eddies are in equilibrium with the viscous forces induced by smaller eddies. In order to describe the Kolmogorov microscale mathematically, first the Reynolds number related to the eddies should be defined as:

$$Re_\lambda = \frac{\lambda U}{\nu} \tag{2.4}$$

where Re_λ is the Reynolds number of an eddy, λ is the eddy size, U is the velocity of an eddy and ν is the kinematic viscosity. The Reynolds number (equation 2.4) equals 1 when it is calculated for the Kolmogorov microscale. Consequently, the Kolmogorov microscale can be defined by:

$$\lambda_k = \left(\frac{\nu^3}{\varepsilon}\right)^{1/4} \tag{2.5}$$

where λ_k is the Kolmogorov microscale, ε is the energy dissipation and ν is the kinematic viscosity. Nonetheless, when the process conditions are such that the hydrodynamic regime

can be considered to be locally isotropic (where fluctuations in eddy sizes are restricted and do not have any directional bias) the eddy velocities (U) can be obtained by dimensional analysis for the inertial and viscous sub-ranges of the turbulent regime given in:

$$\overline{U^2} \approx (\varepsilon\lambda)^{2/3} \tag{2.6}$$

$$\overline{U^2} \approx \frac{\varepsilon\lambda^2}{\nu} \tag{2.7}$$

where the bar on the variables indicates the statistical average.

2.3.2 Emulsification in the turbulent regime

The first studies on emulsification in the turbulent regime were conducted by Kolmogorov (1949) and Hinze (1955) who showed that emulsification occurs in two different regimes, being the inertial sub-range and viscous sub-range. A number of mechanistic models were developed based on the Kolmogorov-Hinze theory, which are mostly modern modifications of the original model. Moreover, for mixing systems, due to simplifications induced by geometrical similarities, a number of semi-empirical approaches have been reported.

Apart from predictive models for droplet size distributions and mean droplet sizes, a number of models have been proposed for droplet break-up and coalescence rates, individually. In this section a brief overview of the emulsification mechanism and the most well-known models are presented in the inertial sub-range of turbulent regime.

2.3.2.1 Predicting droplet size in dilute (φ<5%) and non-coalescing emulsions in inertial sub-range of the turbulent regime

Kolmogorov-Hinze theory states that in the inertial sub-range of the turbulent regime droplets are larger than the Kolmogorov microscale and, therefore, the maximum droplet size that is able to resist flow fluctuations (maximum droplet size) is determined by the balance between flow pressure fluctuations (which tend to deform the droplets) and the droplet

capillary pressure (which resists the induced deformations). Figure 2.8 illustrates the mechanism of droplet disruption in the inertial sub-range of the turbulent regime.

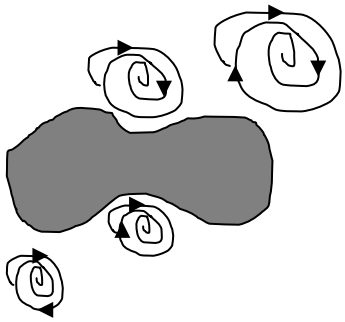

Figure 2.8. Droplet deformation caused by inertial stresses exerted by eddies on the droplet's interface.

Therefore, according to Kolmogorov-Hinze theory, in order to determine the maximum droplet size, the flow fluctuation magnitude should be comparable to the droplet capillary pressure. The fluctuation in the hydrodynamic pressure in the flow is expressed by:

$$\overline{\Delta P(d)} = C_1 \rho_c \overline{U^2} \tag{2.8}$$

where d is the droplet size, ρ_c is the density of the continuous phase, the velocity term, $\overline{U^2}$, is calculated from equation 2.6 and C_1 is the numerical constant in order of unity. The capillary pressure,P_{cap} , of the droplet is given by:

$$P_{cap} = \frac{4\sigma}{d} \tag{2.9}$$

where σ is the interfacial tension at the droplet interface. The maximum droplet size in the inertial sub-range ($d_{max,I}$) can be derived from equations 2.8 and 2.9:

$$d_{max,I} = C_2 \varepsilon^{-2/5} \sigma^{3/5} \rho_c{}^{-3/5} \tag{2.10}$$

where ε is the energy dissipation of the eddy. In geometrically similar mixing vessels the maximum energy dissipation (ε_{max}) is proportional to the average energy dissipation ($\bar{\varepsilon}$), which is effectively the power draw per unit mass of the fluid. A number of investigators have demonstrated that $d_{max,I}$ is proportional to d_{32}. Therefore, for such systems it has been proposed that equation 2.10 can be better expressed by:

$$\frac{d_{32}}{D} = C_3 We^{-3/5} \tag{2.11}$$

where D is the impeller diameter, C_3 is a constant and We is the Weber number of the process defined by:

$$We = \frac{\rho_c N^3 D^2}{\sigma} \tag{2.12}$$

where ρ_c is the density of the continuous phase, N is the impeller's rotational speed and σ is the interfacial tension between dispersed and continuous phases. As can be seen in equation 2.12, the Weber number is the ratio of the inertial (disruptive) forces over surface (cohesive) forces. Various studies have been conducted to determine C_3, which depends on the impeller size and type and the geometry of the mixing tank. In one particular study (Pacek *et al.*, 1994) it was shown that the power of the Weber number equals 1 rather than -3/5. Thus it can be seen that this empirical approach tends to be highly scale-dependent.

It appears that Kolmogorov-Hinze theory does not account for the dispersed phase viscosity. Therefore, equation 2.10 and, consequently, equation 2.11 are only valid for emulsions with a dispersed phase viscosity that is close to that of water. Various researchers have further developed the Kolmogorov-Hinze theory for these cases. One of the most acknowledged studies is that of Davies (1985), who considered the viscous stresses, τ_d, inside the deforming droplet (equation 2.13) in the context of the overall stress balance:

$$\tau_d = \frac{\mu_d \overline{U^2}^{1/2}}{d} \tag{2.13}$$

$$\overline{\Delta P(d)} \approx P_{cap} + \tau_d \tag{2.14}$$

where d is the droplet diameter, $\overline{U^2}$ is the velocity of eddies calculated from equation 2.6, μ_d is the viscosity of the dispersed phase and P_{cap} is the capillary pressure of the droplets calculated by equation 2.9. By employing equation 2.14 the universal form of the equation 2.10 is determined and is given by:

$$d_{max,I,visc} = C_4\left(1 + C_5\frac{\mu_d\varepsilon^{1/3}d_{max,I,visc}^{1/3}}{\sigma}\right)^{3/5}\sigma^{3/5}\varepsilon^{-2/5}\rho_c^{-3/5} \quad (2.15)$$

where C_4 and C_5 are constants related to capillary pressure and the relative effect of droplet viscosity, respectively. The second term in equation 2.15 exhibits the viscous energy dissipation normalised by surface tension. If μ_d is low (close to that of water) then equation 2.15 reduces to equation 2.10. A different approach was employed in studies by Calabrese *et al.* (1986a, 1986b), Wang and Calabrese (1986) and Lagisetty *et al.* (1986), in which the droplet deformation energy was compared with kinetic energies of eddies. They also considered emulsions that contain dispersed phases with significantly different densities to that of water. They proposed a generalised form of equation 2.15, which can be referred in their respective publications.

2.3.2.2 Predicting droplet size in non-dilute emulsions (φ>5%)

It can be seen from section 2.3.2.1 that emulsification in dilute systems has received considerable attention and a large number of publications can be found in the literature. However, in practical terms, conditions induced by dilute emulsions are rather restrictive, and since much industrial experience of concentrated emulsions is not published, there is a need to investigate these systems (Leng and Calabrese, 2004). Emulsification in the presence of a high volume fraction of the dispersed phase often involves droplet break-up, coalescence and rheological complexities. In addition, the relationship between eddies and droplets remains to be fully understood. In these systems, the inter-relation between droplets is often different to that with dilute systems. Data presented in the literature are often conflicting and case-dependent. This section attempts to represent some of the more accepted and conventional proposed approaches.

One of the first experimental studies on non-dilute emulsions was conducted by Laats and Frishman (1973) who studied jet flows. They showed that the mean-square of eddy velocity ($\overline{U^2}$) depends on the volume fraction according to:

$$\overline{U_\varphi^2} = (1 + C_6\varphi)^{C_7}\overline{U^2} \tag{2.16}$$

Where φ is the dispersed phase volume fraction, $\overline{U^2}$ and $\overline{U_\varphi^2}$ are the mean square velocities of eddies in the absence and presence of dispersed phase and C_6 and C_7 are adjustable parameters; C_6 is related to the experimental set-up and C_7 was determined to be -2 in their studies. This approach has been extended by other researchers. It has been proposed that equation 2.11 should be modified by equation 2.16 to include the effect of volume fraction (Doulah, 1975; Kumar *et al.*, 1991; Desnoyer *et al.*, 2003). Therefore, it reads:

$$\frac{d_{32}}{D} = C_8(1 + C_9\varphi)^{C_{10}}We^{-3/5} \tag{2.17}$$

In addition, it has been suggested that instead of including the effect of dispersed phase volume fraction into equation 2.11, it would be more convenient to define a correction factor for impeller speed (Coulaloglou and Tavlarides, 1977), as expressed by:

$$N_{eff} = \frac{N}{1+\varphi} \tag{2.18}$$

where N_{eff} is the corrected impeller rotational speed. Nonetheless, it can be seen that, according to equations 2.17 and 2.18, increasing the volume fraction of the dispersed phase increases the droplet size; a trend that has been observed by all the above-mentioned researchers. In addition, it has been observed that, in some experimental cases, the maximum droplet size increases by increasing the dispersed phase volume fraction, however, maximum droplet sizes decrease by further increasing the volume fraction (φ>50%) of the dispersed phase (Kumar *et al.*, 1991). Their observation was related to the changing of the inertial sub-

range droplet break-up mechanism by capillary breakage on the impeller. The reason for this change in the droplet break-up mechanism was, however, not elucidated.

As considering the effect of dispersed phase volume fraction as velocity correction factor is highly dependent on scaling laws and the fact that this approach might be an over simplification of the actual phenomena (Walstra and Smulders, 1998), a different approach must be considered. In light of this, Doulah (1975) developed a new approach under the assumption that, by increasing the viscosity of the emulsion (as the dispersed phase volume fraction increases), the energy dissipation from the Kolmogorov microscale decreases. Therefore, the dampening effect of the dispersed phase is given by:

$$\frac{\varepsilon_e}{\varepsilon_c} = \left(\frac{\nu_c}{\nu_e}\right)^3 \tag{2.19}$$

where ε_e is the energy dissipation related to the emulsion, ε_c is the energy dissipation of the process in the absence of the dispersed phase, or in the other words, the one related to the continuous phase, and ν_e and ν_c are the kinematic viscosities of the emulsion and continuous phase, respectively. Equation 2.19 is justified by the fact that in turbulent regimes an increase in the volume fraction of the dispersed phase induces turbulent depression, since some of the energy input is consumed by droplet convection, surface modulations and so on. This has been shown to be a more practical approach and it has been employed by number of researchers (Coulaloglou and Tavlarides, 1977; Tsouris and Tavlarides, 1994; Liu and Li, 1999).

Aside from these described studies, the effect of volume fraction on emulsification should be studied in more detail. In particular, the microscopic effect of the dispersed phase volume fraction on the hydrodynamic condition should be studied, in contrast to the macroscopic approach taken by Doulah (1975).

2.3.2.3 Kinetic studies of droplet size

Several studies have been conducted on the time needed for droplet size evolution to reach the final equilibrium size. Chen and Middleman (1967), Arai *et al.* (1977) and Lam *et al.* (1996) observed that it takes several hours in mixing tanks to reach the steady state droplet size. These observations were made on systems with low dispersed phase volume fractions. the above-mentioned authors argued that as droplet size decreases and approaches $d_{I,max}$ there is a considerable increase in the energy required to break the droplets, and therefore it takes a long time (several hours) to reach equilibrium. This hypothesis however was further extended experimentally by Lam *et al.* (1996) who argued that, due to turbulent intermittency, the system never reaches the equilibrium droplet size.

The observations made by Chen and Middleman (1967), Arai *et al.* (1977) and Lam *et al.* (1996) have little practical significance since the time to reach equilibrium droplet size decreases significantly at higher volume fractions. Experimental studies using online light transmittance undertaken by Hong and Lee (1983) show that it takes less than ten minutes to reach the steady state value for emulsification systems with a dispersed phase volume fraction of between 5% and 20%. This value increases when larger mixing vessels are employed. They argued that this is a consequence of droplet coalescence. They employed a reaction kinetics analogy to model their droplet size evolution data, leading to the model expressed by:

$$\frac{d(d_{32,t}-d_{32,eq})}{dNt} = -C_{11}(d_{32,t} - d_{32,eq})^{C_{12}} \tag{2.20}$$

where $d_{32,t}$ and $d_{32,eq}$ are the droplet size at different times and equilibrium droplet sizes, respectively. They found that C_{12} equals 1, therefore in their system, the droplet size reduced exponentially.

2.3.2.4 Final droplet size with respect to emulsifier type and concentration

It can be seen that most of the studies that have been performed to date have focused on emulsification with respect to the hydrodynamic condition of a system by employing high concentration of stabilisers. Therefore, the effect of emulsifier type and concentration did not absorb similar attention. The studies that have been performed in this regard have mostly been conducted to investigate droplet sizes in the obtained samples. As these samples may not be good representatives of the actual processes (specifically when low emulsifier concentrations are used), the effect of emulsifiers remains to be thoroughly studied.

One of the first discussions of the effect of emulsifiers on final droplet size is reported by Walstra (1993). Droplets in a turbulent system deform, emulsifiers are adsorbed on the interface and droplets collide. These phenomena occur simultaneously at very short timescales. At sufficiently high emulsifier concentration it can be assumed that there is an abundance of emulsifier and therefore the rate of emulsifier adsorption can be completely ignored. Consequently, the droplet size is only affected by the hydrodynamic condition of the process (effectively ε of the system) and emulsifiers only affect the process through reducing interfacial tension (Djakovic *et al.*, 1987; Das and Kinsella, 1993; Euston *et al.*, 1999; Tcholakova *et al.*, 2003; Tcholakova *et al.*, 2004). All experimental studies conducted by these researchers confirm this hypothesis.

On the other hand, it has been observed that at lower emulsifier concentration the equilibrium droplet size only depends on the quantity of surfactant and type of the stability mechanism induced (as opposed to droplet coalescence) (Das and Kinsella, 1993; Tcholakova *et al.*, 2004). It has been stated that there is a threshold emulsifiers' surface concentration (Γ^*) above which excess emulsifier does not affect the final droplet size. This value is shown to be independent of the dispersed phase volume fraction; hence it is a characteristic of each

emulsifier. Below this threshold, droplet sizes can be estimated simply by employing a mass balance of emulsifier, assuming that all emulsifier would be used to cover the droplets:

$$d_{32} \approx \frac{6\varphi\Gamma^*}{(1-\varphi)C_{ini}} \tag{2.21}$$

Where Γ^* is the threshold emulsifier concentration on the droplet's interface, φ is the dispersed phase volume fraction and C_{ini} is the initial concentration of the emulsifiers. It should be noted that equation 2.21 only holds for systems containing emulsifiers that stabilise droplets by purely steric repulsive forces; this is true regardless of emulsifier type (protein, surfactant or solid particles). This expression (equation 2.21) holds specifically for emulsifications containing solid particles (Tcholakova *et al.*, 2008).

In contrast, for systems containing an anionic surfactant, which induces an electrostatic barrier, no threshold surface concentration has been found and it has been shown that the final droplet size depends also on the hydrodynamic condition at low emulsifier concentration (Taisne *et al.*, 1996; Narsimhan and Goel, 2001; Tcholakova *et al.*, 2004).

These conclusions are based on the hypothesis that droplets continue to coalesce until sufficient surfactant is adsorbed on the interface to suppress droplet coalescence. At the concentration at which the threshold is attained, it has been observed that the timescales of droplet deformation and collision are comparable with the timescales of surfactant adsorption. Therefore above the threshold droplet collision occurs between droplets for which interfaces are already covered by surfactant.

In contrast with the above hypothesis, Walstra (1993) argued that emulsifier adsorption rate is always longer than the droplet deformation rate in turbulent systems. Additionally, at high dispersed phase volume fractions, the collision timescales are significantly smaller than emulsifier adsorption times. Thus, droplets deform and break into several daughter droplets which then subsequently collide with each other (since they are

already in close proximity) before emulsifiers adsorb onto the newly made interfaces. Consequently, the important parameter is surfactant adsorption rather than surface coverage.

Previous studies have mostly been conducted on surfactants, and studies on emulsification in the presence of proteins have employed only globular proteins (for example, Whey protein isolate). When random-coil proteins (such as sodium caseinate) are employed, it has been observed that final droplet size decreases with increasing sodium caseinate concentration and then, after a certain point, remains constant with further increase in concentration (Britten and Groux 1990; Dickinson, 2001). Furthermore, it has been observed that at low concentrations of sodium caseinate droplet coalescence is enhanced by bridging of the protein molecule between droplets, thus bringing them into close proximity and increasing the droplet flocculation.

Apart from afore-mentioned studies, the effect of solid particles on droplet size has been studied. It has been shown that, in the presence of solid particles, although the stability of these emulsions is enhanced when compared with surfactants, the resultant emulsions contain larger droplets (Aveyard *et al.*, 2003; Binks and Lumsdon, 2000a; Binks, 2002; Pichot *et al.*, 2009). This is related to the fact that solid particles are not surface active and hence they do not reduce interfacial tension.

Studies on emulsions with mixed-emulsifier systems generally show that employing nonionic surfactants (Midmore, 1998; Ghouchi Eskandar, 2007), cationic surfactants (Lan *et al.*, 2007), anionic surfactants (Vashisth *et al.*, 2010) or proteins (Murray *et al.*, 2011) in conjunction with particles, emulsions with smaller droplets are produced when compared to using only solid particles. This is related to the beneficial attributes of both particles and emulsifiers. Adsorption of emulsifiers onto interfaces reduces the interfacial tension, thus decreases droplet size. The resultant droplets are then stabilised against coalescence by

particle adsorption at later stages. Similar observations have been reported in cases when oil soluble emulsifiers are used with particles (Pichot *et al.*, 2009; Wang *et al.*, 2009). It should be noted there is little information regarding the effect of relative ratios of the amount of particles to emulsifiers on droplet size. Nonetheless, it has been shown that the smallest droplet size in the specific cases can be achieved by using larger quantities of surfactants compared with particles (Pichot *et al.*, 2009; Wang *et al.*, 2009; Whitby *et al.*, 2009).

2.3.3 Droplet break-up rate in the turbulent regime

Apart from the vast number of studies that have been conducted in order to determine the final droplet size, the kinetic aspect of droplet break-up is another important parameter which must be investigated. This is an important problem from a practical viewpoint since the emulsification process might require a long time to reach steady state. Most of the studies to date employ population balances to investigate the parameters affecting droplet break-up rate. In this framework, either theoretical expressions have been employed or numerical values have been experimentally determined. Therefore, this section is divided into two sub-sections of mathematical expressions and experimental studies on the droplet break-up frequency.

2.3.3.1 Theoretical expressions of droplet break-up rate in turbulent systems

The mechanism of droplet break-up is fully addressed in section 2.3.2.1. A number of theoretical approaches have been proposed for determining the droplet break-up rate, which have been critically reviewed by Lasheras *et al.* (2002). Here, the theoretical expression that has attracted the most attention is explained, and other expressions are briefly introduced. The model proposed by Prince and Blanch (1990) which was later modified by Tsouris and Tavlarides (1994) considers that the break-up rate consists of a droplet-eddy collision term and a collision efficiency given by:

$$Break-up\ rate = (droplet - eddy\ collision) \times (breakage\ efficiency) \quad (2.22)$$

The droplet-eddy collision rate is determined by analogy with the molecular theory of gases. The collision rate (h_d) between droplet size, d, and eddy size, d_e, can be calculated by equation 2.23. It should be noted that, in development of equation 2.23, it was assumed that eddies of the same size or smaller than the droplet size can cause droplet break-up and larger eddies only transport the droplets.

$$h_d = \int_{n_e} S_{d,e}(\overline{U_d}^2 + \overline{U}^2)^{1/2} n_d dn_e \quad (2.23)$$

where n_d is number concentration of droplets with size d, $\overline{U_d}$ is the mean velocity of droplet, $\overline{U}$ is the mean velocity of the eddy and dn_e is the number concentration of eddies between size d_e and $\lambda+\delta\lambda$. $S_{d,e}$ is the cross-section of the collision and is defined by:

$$S_{d,e} = \frac{\pi}{4}(d+\lambda)^2 \quad (2.24)$$

In equation (2.23), dn_e is determined according:

$$dn_{e(\kappa)} = \frac{0.1\kappa^2}{\rho_c} d\kappa \quad (2.25)$$

where $n_{e(\kappa)}$ is the number concentration of eddies with wave number κ, which equals half of the eddy size per unit mass of fluid. Moreover, the breakage efficiency term (Y_d) on the right hand side of equation 2.22 is defined by:

$$Y_d = \exp\left(-\frac{surface\ energy\ of\ droplets}{Kinetic\ energy\ of\ eddies}\right) \quad (2.26)$$

It should be noted that the exponential behaviour of collision efficiency is an arbitrary choice (Tsouris and Tavlarides, 1994; Vankova *et al.*, 2007b). The surface energy of droplets (E_σ) and kinetic energy of eddies (E_{kin}) can be expressed by equations (Tsouris and Tavlarides, 1994):

$$E_\sigma \sim \pi d^2 \sigma \quad (2.27)$$

$$E_{kin} = 0.43\pi\rho_c\left(\frac{2}{\kappa}\right)^{11/3}\varepsilon^{2/3} \quad (2.28)$$

Now, by substituting equations 2.23-2.28 into equation 2.22 the expression for droplet break-up rate is determined. In addition, the most efficient break-up phenomena are caused by the eddies with the same size as the droplets, therefore the break-up rate (B) expression can be estimated by:

$$B \sim \frac{\varepsilon^{1/3}}{d^{2/3}} \exp\left(-\frac{\sigma}{\rho_c \varepsilon^{2/3} d^{5/3}}\right) \tag{2.29}$$

where ε is the energy dissipation, d is the droplet diameter, σ is the interfacial tension between dispersed and continuous phases and ρ_c is the density of the continuous phase. This equation was later modified to account for the dispersed phases with high viscosity by Vankova *et al.* (2007b).

Apart from this approach, another framework was proposed by Coulaloglou and Tavlarides (1977) which assumes that the break-up rate is the product of the droplets that contain sufficiently high energy to undergo the break-up process and the reciprocal of the required time for droplet break-up. In this approach the break-up time is assumed to be equal to the droplet deformation time, which is itself determined by comparing the dynamic turbulent stresses on the droplets by the acceleration of the fluid inside the droplets. Moreover, Alopaeus *et al.* (1999) employed a similar approach to that proposed by Tsouris and Tavlarides (1994) with the difference that they assumed that the eddy-droplet collision behaves as a Poisson process. Their approach leads to an empirical expression for droplet break-up rate. Additionally, Nambiar *et al.* (1994) and Martinez-Bazan *et al.* (1999) developed so-called 'kinetic' models in which the break-up rate is assumed to be the reciprocal of droplet break-up time, which in turn is determined from the stress balance across the droplet. In another approach an empirical model based on the decrease in the mean droplet size of an emulsion is determined which includes several adjustable parameters (Sis and

Chander, 2004; Sis *et al.*, 2005). Finally, Narsimhan *et al.* (1980) developed a semi-empirical model based on experimentally determined break-up rates.

It can be seen that a number of different droplet break-up rate modelling frameworks have been proposed in the literature. However, as the droplet break-up rate is a complex phenomenon, different models lead to different outcomes. Therefore, it is advisable, where possible, to determine droplet break-up rates experimentally.

2.3.3.2 Experimental studies on droplet break-up rate

In contrast to studies that have been conducted on the final droplet size of emulsification, the subject of the droplet break-up rate still lacks adequate experimental study (Liao and Lucas, 2009). It should be noted that, in this section, experiments that have been performed to validate the mathematical models that were presented in previous section are not included, since they are not sufficiently thorough studies.

Most experiments in this regard are performed in so-called 'non-coalescing' systems. The volume fractions of the dispersed phase in these experiments were very low (φ<1%) and/or in the presence of high concentrations of surfactants. Narsimhan *et al.* (1980) studied the break-up rate by employing dispersed phases (oil) with different interfacial tensions at various impeller speeds in mixing systems in the absence of any emulsifier. They concluded that droplet break-up rate increases with increasing impeller speed and decreasing interfacial tension. Similar results were obtained by Vankova *et al.* (2007b) who determined droplet break-up rates by using population balances for a series of experiments. The emulsions in their study contained low dispersed phase volume fraction in the presence of a relatively high emulsifier concentration. They employed a nonionic surfactant (Brij 58) and a random coil protein (sodium caseinate) as emulsifiers. The emulsification was performed in a homogeniser under different pressures in order to induce a range of energy dissipation rates. They also

employed a mono-dispersed pre-emulsion (produced by membrane process) as a feed for the homogeniser in order to study the effect of droplet size. Their study concluded that the droplet break-up rate increases with increasing energy dissipation rate and decreasing interfacial tension (the experiments in the presence of sodium caseinate in this case showed lower interfacial tension than Brij 58). They also showed that the droplet break-up rate is high for larger droplets and significantly decreases as the droplet size reduces to the Kolmogorov microscale. The mentioned dependency of droplet break-up rate on the energy input or interfacial tension and droplet size has been observed in a number of other studies (Sanchez *et al.*, 2001; Lasheras *et al.*, 2002; Sis *et al.*, 2005; Liao and Lucas 2009).

Studies that attempt to observe the effect of emulsifier type and concentration are mostly based on non-food emulsions in the presence of surfactants. Sanchez *et al.* (2001) employed poly(ethylene glycol) nonylphenyl ether as a nonionic surfactant. They related the decrease in droplet break-up rate with decreasing surfactant concentration to the lowering of the adsorption rate of the surfactant. Additionally, Sis and Chander (2004) studied the effect of poly(ethylene glycol) nonylphenyl ether and Pluronic L-61 (nonionic surfactants) concentration on droplet break-up rate. They reported that droplet break-up rate increases with increasing emulsifier concentration due to the higher reduction in interfacial tension. On the other hand, the decrease in droplet break-up rate by an increase in concentration of PVA reported by Chatzi and Kiparssides (1995) were related to the emulsifier's conformational changes at the interface of the droplets after adsorption.

Finally, to the best of author's knowledge, there is no thorough study on the effect of dispersed phase volume fraction on the droplet break-up rate. From all these experimental studies it can be concluded that there is a need of further experimental investigation of the droplet break-up rate in the presence of food-grade materials.

2.3.4 Droplet coalescence rate in the turbulent regime

In comparison with droplet break-up, droplet coalescence is often considered a more complex phenomenon (Chesters, 1991; Liao and Lucas, 2010) due to the fact that droplets are not only engaged with the surrounding liquid, but also with other droplets in the system. Various studies have been conducted on droplet coalescence in which either theoretical expressions have been developed or experimental studies have been performed. The mechanism of droplet coalescence can be summarised as follows. When two droplets collide, a layer of continuous phase is entrapped between them (Figure 2.8). The force that squeezes the droplets is caused by continuous fluid fluctuations and is referred to as a 'turbulent force'. A turbulent force acting on the droplets results in the entrapment of a layer of continuous phase between them, the thickness of which is a consequence of the strength of the turbulent force and the size of droplets. The continuous phase between droplets then drains to a critical thickness at which the two droplets then coalesce. Emulsifiers are able to influence the above-described phenomena by providing repulsive forces to induce a barrier which opposes turbulent forces. However, emulsifiers should first be adsorbed on the interface, which, according to the emulsifier type, are able to influence these phenomena via a number of mechanisms.

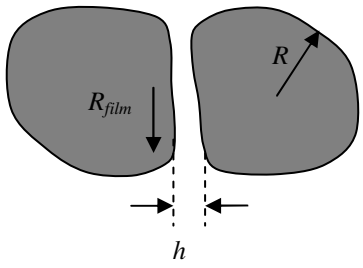

2.9. Schematic representation of droplet coalescence mechanism.

2.3.4.1 Theoretical expressions of droplet coalescence rate in the turbulent regime

A number of empirical and mechanistic models have been developed in order to estimate droplet coalescence rate, which are reviewed by Liao and Lucas (2010). However, the most acknowledged approach is now described here. The droplet coalescence rate can be defined as a product of collision rate and a collision efficiency, since not all collisions result in coalescence, as given in (Coulaloglou and Tavlarides, 1977; Chesters, 1991; Tsouris and Tavlarides 1994; Liu and Li, 1999; Narsimhan, 2004):

$$A = \chi \times \xi \tag{2.30}$$

where A is the coalescence rate, χ is the collision rate and ξ is collision efficiency. The collision rate and efficiency are individually developed in the following sub-sections.

2.3.4.1.1 Collision rate

A number of approaches have been used to estimate the droplet collision rate; however most of these approaches result in similar expressions with minor differences in the constants. Therefore, the well accepted approach that was proposed by Chesters (1991) and Tsouris and Tavlarides (1994) is employed herein. In this approach, it is considered that droplet collisions are caused by turbulent random motion which, in turn, is assumed to behave similar to the random movements of gas molecules as described in kinetic gas theory (Liao and Lucas, 2010). This phenomenon is expressed by:

$$\chi = S_{12} U_{relative} \tag{2.31}$$

where S_{12} is the cross sectional area of colliding drops and $U_{relative}$ is the approach velocity. By assuming equal droplet size and the fact that droplet collision occurs in the inertial sub-range of the turbulent regime, it reads:

$$\chi = \frac{28\sqrt{2}\pi}{3} \varepsilon^{1/3} d^{7/3} n^2 \tag{2.32}$$

where ε is the energy dissipation, d is the droplet size and n is the number concentration of droplets. Although this approach is used widely, a number of modifications have been suggested which can be divided into two groups. The first group is characterised by the inclusion of the effect of the dispersed phase volume fraction on the increase of the collision rate. Different expressions for this factor have been proposed (Wu *et al.*, 1998; Lehr *et al.*, 2002; Wang *et al.*, 2005a-b) and all of them show that until a dispersed phase volume fraction of 70% the collision rate should be multiplied by a factor of between 1 and 2. The second group introduces a decreasing factor that is related to the ratio of the mean distance between droplets and the turbulent path length (Wang *et al.*, 2005a-b). However, as these modifications are mostly selected arbitrarily or are empirical (Liao and Lucas, 2010), they are not introduced here.

2.3.4.1.2 Collision efficiency

Three different approaches have been proposed for modelling the collision efficiency. The first approach proposed that the molecular composition of the interface does not affect the collision process and the droplet coalescence is only a function of collision energy (Howarth, 1967). The second approach relates this phenomenon to the velocity of approach, such that, when droplets reach a critical velocity, coalescence occurs spontaneously (Lehr *et al.*, 2002). The last approach, which is the most developed and accepted of all three, relates the collision efficiency to the drainage of the entrapped continuous phase. However, as the phenomena occurring at the interfaces during collisions are not well understood, and the fact that behaviour of interfaces may vary depending on the emulsifier type, a number of approaches have been developed, all of which have questionable validity. As an example, the dependencies on the operational parameters of a number of different approaches are summarised below.

Howarth (1964) proposed a model in which collision efficiency increases with increasing droplet size and energy input. In contrast, the model of Coulaloglou and Tavlarides (1977) shows a decrease in collision efficiency as droplet size and energy input increase and when interfacial tension decreases. Muralidhar and Ramkrishna (1986) reported contradictory dependencies. In the case of static droplet deformation, collision efficiency increases with droplet size and energy input and decreasing interfacial tension. However, when dynamic deformation of a droplet is considered, collision efficiency decreases with droplet size and energy input and decreasing interfacial tension. In another report, Muralidhar *et al.* (1988) proposed that collision efficiency also depends on force fluctuations. In the case of small force fluctuations, the collision efficiency decreases with increasing droplet size and energy input. An inverse dependency has been observed for large force fluctuations. Tobin and Ramkrishna (1999) proposed that collision efficiency decreases with increasing droplet size. Kumar *et al.* (1993) generated a model for collision efficiency and their expression showed a minimum value when droplet size and energy input are increasing. Liu and Li (1999) proposed an expression that shows that collision efficiency decreases with increasing energy input and droplet size and increases with increasing volume fraction. Narsimhan (2004) proposed a model for the case of rigid droplets in the presence of an electrostatic double layer. This model shows that the coalescence time does not depend on the initial distance between the droplets upon collision. It further indicates that coalescence time decreases with decreasing droplet size and energy dissipation. In conclusion, contradicting dependencies are predicted from various models and there is no thorough experimental study to prove or favour any of the above models. Therefore, none of the above-mentioned models are introduced in this section.

2.3.4.2 Experimental studies on the droplet coalescence rate

Unlike the low numbers of existing studies on the break-up rate, a large number of studies can be found on droplet coalescence rate. This is partly caused due to the newly available experimental techniques to investigate droplet coalescence individually (section 2.2.2). In this section, regardless of the experimental method used, the results regarding the dependency of droplet coalescence rate on the operational and formulation parameters are summarised.

It has been shown in a number of studies (Wright and Ramkrishna, 1994; Taisne *et al.* 1996; Mohan and Narsimhan, 1997; Narsimhan and Goel, 2001; Lobo and Svereika, 2003) that an increase in homogeniser pressure or impeller speed, which both result in higher energy dissipation, leads to an increase in droplet coalescence regardless of the emulsifier that is employed. This dependency has been related to the fact that, at higher energy input, larger turbulent forces affect the droplets; hence the continuous film drains more rapidly to the critical thickness.

Studies on the effect of volume fraction of the dispersed phase on the droplet coalescence rate show an increase in droplet coalescence by increasing φ (Mohan and Narsimhan 1997; Narsimhan and Goel, 2001; Lobo and Svereika, 2003). However, it should be noted that these studies are all performed in homogenisers and they are limited to 15% dispersed phase volume fractions. These investigators have concluded that the increase in the dispersed phase volume fraction effectively increases the collision rate and therefore increases the droplet coalescence probability.

Apart from aforementioned studies, a number of studies have been performed to observe the effect of emulsifier type and concentration. Taisne *et al.* (1996), Narsimhan and Goel (2001) and Lobo and Svereika (2003) employed an anionic surfactant (SDS) in their experiments with a homogeniser and observed that the droplet coalescence rate decreases with

increasing surfactant concentration. They justified their findings by the presence of SDS on the interfaces of the droplets, which causes electrostatic repulsion forces, hence suppressing continuous phase film drainage. A similar dependency of droplet coalescence on surfactant concentration was observed for nonionic surfactants (Brij 58 and Tween 20) (Lobo and Svereika 2003; Henry *et al.*, 2009). In these cases, the reduction in droplet coalescence due to an increase in surfactant concentration was related to the interfacial coverage of droplets by nonionic surfactant. This results in the steric stabilisation of droplets against droplet coalescence.

Unlike surfactants, droplet coalescence in the presence of proteins has not attracted much attention. Mohan and Narsimhan (1997) studied droplet coalescence in the presence of random coil (sodium caseinate) and globular (whey protein isolate) proteins. Using a homogeniser as the emulsification apparatus, they varied protein concentrations, ionic strength and the pH of the aqueous phase. Their experiments showed that increasing protein concentration leads to a reduction in droplet coalescence rate due to the higher interfacial coverage of proteins. On the other hand, increasing ionic strength or reducing the pH increases droplet coalescence rate. This is justified by the reduction in electrostatic repulsive force that is induced by proteins by screening (increasing ionic strength) or by approaching the iso-electric point of the proteins (decreasing pH). As has been mentioned, these experiments were performed in a homogeniser. The study of bubble coalescence in a mixing tank however shows that an increase in sodium caseinate does not reduce droplet coalescence (Hu *et al.*, 2003). However, the reasons behind their observation were not described in their publication.

Chapter 3

Materials and Methods

This chapter details the experimental works and procedures undertaken for this thesis.

3.1 Materials

This section introduces the chemical compounds used throughout this work. It should be noted that all the concentrations of the materials are given in "%" and they are the percent by weight of the total emulsion, unless stated otherwise.

3.1.1 Continuous phase

Water was used as the continuous phase in all emulsion preparations. Water was de-ionised and double distilled by passing through an Aquatron de-ionising filter followed by an Aquatron A4D double distillation unit (supplied by Bibby Sterillin Ltd., Staffordshire, England). Subsequently the water was stored in the reservoir tanks. The density of water was 998.23 $kg.m^{-3}$ and the viscosity was 0.001 Pa.s at 25 °C.

3.1.2 Dispersed phase

Edible rapeseed oil was employed in this work as the dispersed phase. The rapeseed oil was purchased in bulk from the local market and used without any modification. Throughout this work, the oil was kept away from light in order to prevent degradation. Density and viscosity of the rapeseed oil were 920 $kg.m^{-3}$and 0.05 Pa.s at 25 °C, respectively.

3.1.3 Emulsifiers

A range of emulsifier types were used in this work, each of them are individually described in the following sections.

3.1.3.1 Nonionic surfactants

Tween 20 (polyoxyethylene (20) sorbitan monolaurate) was supplied by Sigma Aldrich LTD. (UK), and Brij 97 (polyethylene glycol (10) monooleyl ether) was purchased from Fluka Chemie (GmbH). The *HLB* value of Tween 20 and Brij 97 were reported by the

manufacturers to be 16 and 12.4, respectively. Therefore both of the surfactants were hydrophilic.

3.1.3.2 Proteins

In order to investigate the effect of different types of proteins and their concentration on the emulsification processes, two types of globular and random coil proteins were selected. Whey protein isolate (WPI) and sodium caseinate were used as globular and random coil proteins in these studies.

The food grade WPI was kindly provided by DAVISCO (Geneva, Switzerland). The specifications of WPI were provided by the manufacturer and they can be seen in Table 3.1. The product is in dry powder form and it is fully soluble in water with pH range between 2 and 9. The WPI powder contains more than 95% whey proteins consisting of beta-lactoglobulin and alpha-lactalbumin.

Table 3.1-The specification of WPI provided by the manufacturer.

Component	Portion/value
Moisture	Maximum 5%
Protein (dry basis)	Minimum 95%
Fat	Maximum 1%
Ash	Maximum 3%
Lactose	Maximum 1%
pH	6.7-7.5
Scorched particles	Maximum 0.015/25 gram weight of total powder

Sodium caseinate was kindly provided by DMV International (Veghel, The Netherlands). It was provided as dry powder and was fully soluble in water. It contained more

than 92% caseins.

3.1.3.3 Solid particles

In this thesis, the effect of solid particles on emulsification was studied when used individually and as part of mixed-emulsifier system with surfactants. Hydrophilic fumed silica particles (Aerosil® 200) were selected as solid particles in these studies and they were kindly provided by Degussa (UK). The particles were in the dry powder form with a primary particle size of 12 nm diameter. After dispersion in water, particle aggregates were reported to have diameter of 150 nm at pH 2 (Pichot *et al.*, 2009). They were used without any modifications.

3.2 Experimental devices and procedures

The devices that were employed for the purpose of the characterisation of emulsions are presented in this section. In addition, the procedures followed for each of the experimental works are explained.

3.2.1 Preparation of the aqueous phase

Prior to the emulsification experiments, the aqueous phase was prepared by dissolving the desired amount of emulsifier in water as the used emulsifiers were all hydrophilic. This was carried out by adding the emulsifier in water and mixing the solution with a magnetic stirrer. In the cases where the emulsifiers were not readily soluble in water (for example Brij 97 and sodium caseinate), the mixtures were heated during mixing in order to enhance their dissolution. This was conducted by adjusting the temperature of the magnetic stirrer hotplate surface. Care was taken to avoid denaturation of sodium caseinate (~80 °C at pH 6.5) and WPI (~72°C) (Brown, 1999) in the solutions by heating the aqueous phases at 50 °C.

The dispersions of silica particles were prepared by adding the required amount to the water. Subsequently, the pH of the dispersions was adjusted at 2, since the best long-term stability against droplet coalescence was observed at this pH where particles are neutralised from electric charge (Pichot *et al.*, 2009). This was carried out by adjusting the pH (measured by Mettler Toledo pH meter, Beaumont Leys Leicester, UK) by adding the required amount of HCl (1 M) to the solution. Finally, the silica particles were dispersed in the water by an intensity Ultrasonic Vibracell processor (Jencons-PLs, operating at 20 *Hz* and 700 *W*).

3.2.2 Emulsification process

The emulsification was carried out in a mixing vessel, during which, the reflectance of emulsions was measured in order to determine the droplet size of the emulsion. Here, the mixing vessel and the apparatus used for the purpose of the emulsions' reflectance

measurement are described. The detail description of the developed method and the experimental procedure are detailed in Chapter 4.

3.2.2.1 Emulsion Reflectance measurement

The light reflectance of the process was measured by using a Colorimeter (CR-410, Konica Minolta, Japan). This device is originally employed for colour detection of various surfaces. The principle of the measurement is as follows. Firstly, light generated by a pulsed Xenon lamp illuminated the surface; subsequently the amount of light reflected from the surface was measured using a Silicon photocell detector. This measurement was conducted in the wide-area illumination system with the diameter of 50 mm. The least acquisition time that can be used is 3 s which is significantly lower than the acquisition time during the experiments (30 s). The sensitivity of the device was provided by the manufacturer and was reported to have 0.07 standard deviation (in ΔE*ab system) within the range of 0.01% and 160% of the reflectance (*Y*). This device (measuring head) was connected to the data processor which provides further analysis to determine the colour of the specimen in various colour-spaces. After measurement, the obtained data could be exported from the data processor for further processing. The employed colorimeter can be seen in Figure 3.1.

Figure 3.1. Colorimeter employed in the experiments for the measurement of the reflectance during processing.

3.2.2.2 Mixing vessel set-up

All emulsification experiments were performed in the same cylindrical glass vessel with an internal diameter of 70 mm. The fact that the Colorimeter device records reflectance data within a circular 'measuring window' of 50 mm in diameter and the bottom of the cylindrical vessel chosen to have a diameter, D_T, of 70 mm, ensure, to a great extent, that the obtained droplet size data fully represent the structure of the system under processing in the vessel as a whole. An illustrative diagram of the vessel with dimensions is shown in Figure 3.2. The vessel was constructed specifically for the purpose of this study from glass by the glass blower provided by the University of Birmingham. Four equally spaced stainless steel baffles attached to the external ring were constructed. The baffles were fitted into the vessel and the width of the baffles was chosen to be 1/10th (W_b=7 mm) of the vessel diameter.

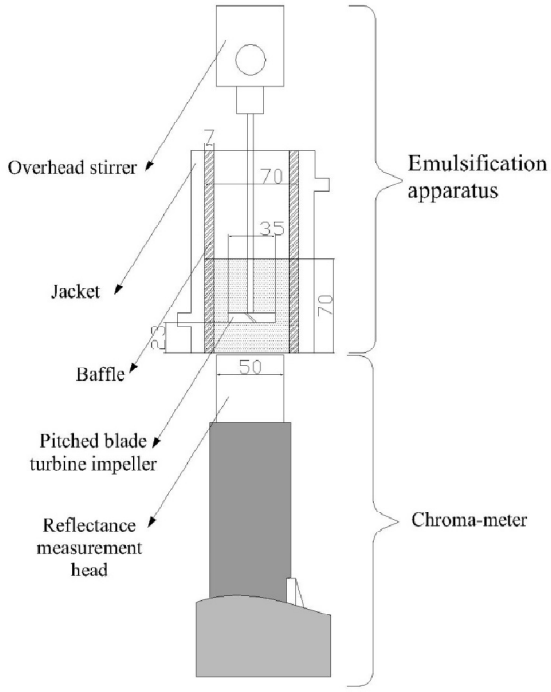

Figure 3.2. Emulsification system: a mixing vessel and a chroma-meter positioned underneath the vessel for reflectance measurements. The dimensions are reported in mm.

The impeller used in all of the experiments was a standard pitched blade turbine (PBT) with four blades and a diameter of 35 mm, half that of the vessel diameter ($D = D_T/2$). The impeller was centred axially but adjusted to have 23 mm clearance, C_T, from the bottom of vessel ($C_T = D_T/3$). The vessel was positioned in a rig constructed to allow the mounting of a variable speed motor, a Eurostar overhead stirrer (IKA, Germany), above the vessel. The speed control unit was calibrated in revolutions per minute (rpm). The impeller shaft was connected to the motor through a locking collar on the underside of the motor.

The volume of material to be processed was carefully controlled to always result in a height, H, of material in the vessel that was equivalent to the diameter of the vessel ($H = D_T =$ 70 mm). The temperature of the process was controlled by pumping water from temperature-controlled water bath (Tempette TE 7, Tecam) by rotating pump to the jacket around the vessel. The Jacket was designed to cover around the vessel and not the underside where the colorimeter device was placed. This design was implemented in order to ensure that the reflectance measurement is not interfered by the extra layer of glass. The reflectance of the system was measured at 30 s intervals during processing.

The average energy dissipation inside the mixing vessel was calculated and used in this work as information regarding the flow behaviour in the mixing vessels is often difficult to determine. It should be noted that a number of expressions (Zhou and Kresta, 1996) have been suggested to estimate the maximum energy dissipation rate which occurs in the regions around the impeller. However, as these estimations depend on the scaling laws, it is appropriate to use average energy dissipation in data analysis. The general form of the expression to estimate the average energy dissipation can be defined by:

$$\bar{\varepsilon} = \frac{PoN^3D^5}{\frac{\pi}{4}D_T{}^3} \tag{3.1}$$

where D is the impeller diameter, N is rotational speed of the impeller, D_T is the diameter of the tank and Po is the power number (1.35 for pitched blade turbine impeller with 4 blades used in this work). By employing the rig's dimensions in equation 3.1, it reduces to:

$$\bar{\varepsilon} = \frac{PoN^3D^2}{2\pi} \tag{3.2}$$

3.2.2.3 Experimental procedure

In order to ensure the reflectance measurement from the early stages of the emulsification, the processing was initiated by adding the required amount of the continuous phase into the mixing vessel. The impeller speed was adjusted and the first light reflectance measurement with the data acquisition time of 30 s was conducted, which was effectively from processing of only the continuous phase. Subsequently, the required amount of dispersed phase was rapidly (~10 s) added to the impeller vicinity. This ensures that the full amount of the dispersed phase was dispersed throughout the process. By this methodology, the second reflectance measurement (after 30 s) conducted on the processing in the presence of emulsion, and the value was reported as the "initial droplet size".

3.2.3 Droplet size measurement

Droplet size measurements were performed offline by laser scattering technique. The device and the experimental procedures are presented herein.

3.2.3.1 Device description

The Mastersizer 2000 (Malvern, UK) has been found to be suitable for oil-in-water emulsions' droplet size characterisation. Mastersizer 2000 (Figure 3.3) employs the light scattering method for droplet size distribution determination. The principle of the light scattering technique is as follows. When a monochromic light such as laser hits small particles, the light scatters in all directions. This phenomenon is referred to as the "Rayleigh

scattering principle". Subsequently, one observes a time-dependent fluctuation in the scattering intensity. The scattered light can undergo either constructive or destructive interference by the surrounding particles and within this intensity fluctuation. The particle size (or droplet size in emulsion-based samples) can be determined by employing suitable scattering theories. It should be noted that the dispersed phase volume fraction of the samples should be less than 0.05% to avoid the hard to implement multiple-scattering of the light.

The samples were introduced to the "dispersion unit", which is a mixing tank with low impeller speed (Figure 3.3). The dispersion unit then pumps the emulsions to the "measurement cell" where the scattered laser light is measured. The data were reported by the computer attached to the device.

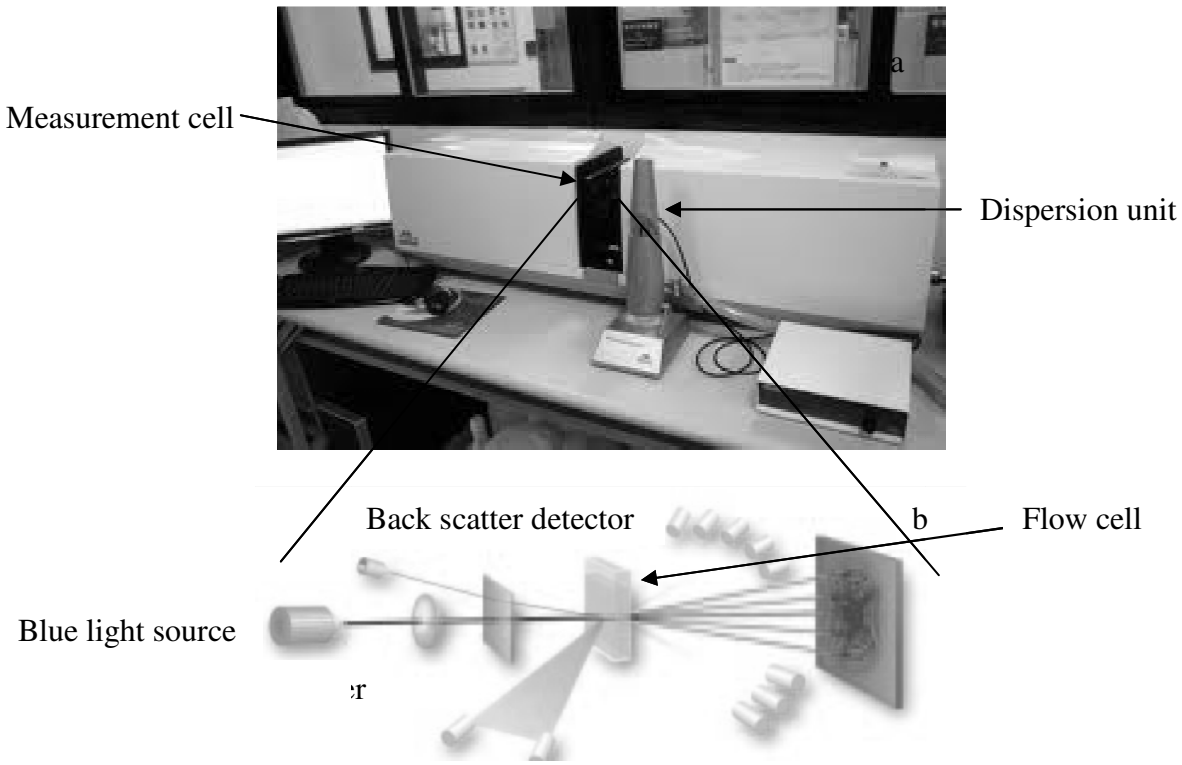

Figure 3.3. Dispersion unit (a) and inside themeasurement cell (b) of the Mastersizer 2000 device are shown (Malvern Instruments, 2009).

3.2.3.2 Experimental procedure

After the emulsification processes, samples were obtained in order to measure their droplet size by Mastersizer device. In order that samples represent the process, they should be stable until the measurement. The obtained samples were either stable in natural condition (due to the high concentration of emulsifiers), or they were introduced to the solution of high concentration (2% to the weight of water) of Tween 20 to ensure their stability.

The calculation of the droplet size from the light scattering data requires knowledge of the refractive indices of the continuous and the dispersed phases. The refractive indices were selected from the database of refractive indices of materials embedded in the software provided by the manufacturer. The refractive indices of 1.33 and 1.46 were selected for aqueous phase and the oil phase, respectively. The stirrer speed of the dispersion unit was adjusted at 500 rpm, and the emulsions were added drop-wise by pipette until the laser obscuration reached ~15% of its total value. Three measurements were performed per sample, and the droplet size distribution was determined by using log-normal model.

3.2.4 Rheological studies

The experimental methods involved the rheological studies of emulsions are presented in this section. The emulsion samples were obtained after the emulsification experiments. In rheological studies, only stable emulsions (prior to the measurement) were used.

3.2.4.1 Device description and experimental procedure

The rheological studies were carried out by a stress-controlled Bohlin Gemini Nano Rheometer (Malvern, UK). A 60 mm acrylic parallel plate was employed for rheological measurements. All measurements were carried out at 25 °C.

In order to determine the viscosity of the emulsions at various shear rates, the shear stress was determined by inducing a range of shear rates between 0.1 and 1000 s^{-1}. Each

experiment was performed at least in triplicate on each different sample. The data obtained were fitted to either Newtonian viscosity model or power law model (shear thinning fluids) given by:

$$\tau = \mu_e \dot{\gamma} \quad (3.3)$$

$$\mu_e = K\dot{\gamma}^{j-1} \quad (3.4)$$

where μ_e is the viscosity of the emulsion, τ is the shear stress, $\dot{\gamma}$ is the shear rate, K is the consistency constant and j is the power-law index.

3.2.5 Interfacial tension measurement

The experimental devices and procedure of the interfacial tension measurement between water and oil phases in the presence of various emulsifiers are presented in this section.

3.2.5.1 Device description

The interfacial tension measurement was carried out by plate method using a K100 tensiometer (KRUSS, Germany). An abraded platinum plate (height 10 mm, width 19.9 mm and thickness 0.2 mm) was employed. The principle behind the interfacial tension measurement is as follows (Figure 3.4). The plate is positioned on the interface between water and oil phases. Subsequently, it is raised until the contact angle between interface and the plate equals zero. The maximum tension on the plate is measured by a micro-balance connected to the plate by the plate's anchor. This value is recorded as the interfacial tension between two phases. The schematic representation of the measurement is shown in Figure 3.4.

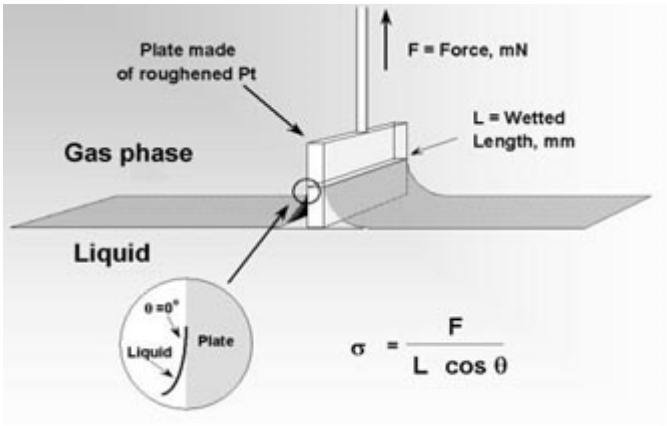

Figure 3.4. Schematic illustration of the plate method is shown (Kruss, 2011).

The plate should be optimally wetted that the contact angle of the interface with plate would be virtually zero, consequently the term *cos(θ)* equals 1. This results in the fact that only the measured force and plate length are then considered in the measurement. The plate method is performed in static conditions; meaning that after positioning the plate with zero contact angle, it is not moved and the force is measured in time.

3.2.5.2 Sample preparation and experimental procedure

Prior to the measurement, the sampling vessel (provided by manufacturer) and the platinum plate were both thoroughly cleaned and heated in order to remove any remaining emulsifiers on the surfaces. The aqueous phase is separately prepared as discussed in section 3.2.1, with the similar emulsifier concentration as the aqueous phase used in emulsification studies. Subsequently, the prepared aqueous phase was added into the sampling vessel which is positioned in the device. The plate was adjusted at the surface of the aqueous phase. The balance was locked at this moment, and the oil phase was added into the sampling vessel. Due to the lower density, the oil phase 'sits' on top of the aqueous phase. The balance was unlocked and the sampling vessel was lowered to zero contact angle with the plate. Finally, the measurement was conducted and the results were reported as the interfacial tension with respect to time. The measurement was carried out until the equilibrium value was reached,

where there would be no further changes in the interfacial tension with time. Each measurement was performed at least three times on samples to ensure their reproducibility.

3.2.6 Zeta potential measurement

The device and the procedures for measurement of the zeta potential of the interface of droplets due to the adsorption of proteins are presented in this section.

3.2.6.1 Device description

The zeta potential of the emulsions in the presence of proteins was measured using Delsa^{TM} Nano C (Beckman Coulter, Brea, CA, USA). The principle of the measurement is as follows. The sample (emulsion) in the measurement cell is exposed to an electric field. Charged particles move towards the opposite electrode. Since the velocity of droplets is a function of the electric potential, the zeta potential is calculated by measuring the velocity of droplets. The velocities of droplets are measured by electrophoretic light scattering method (Figure 3.5). The droplets are irradiated by laser light and the scattered light emitted is detected. The frequency difference between incident light and scattered light is related to the velocity of droplets. The device can measure the zeta potential of the emulsions with dispersed phase volume fractions as high as 40%. This is the main advantage of this device that the emulsions do not require dilution. This device is fully automated and calculates the zeta potential automatically based on the droplet size and ionic strength.

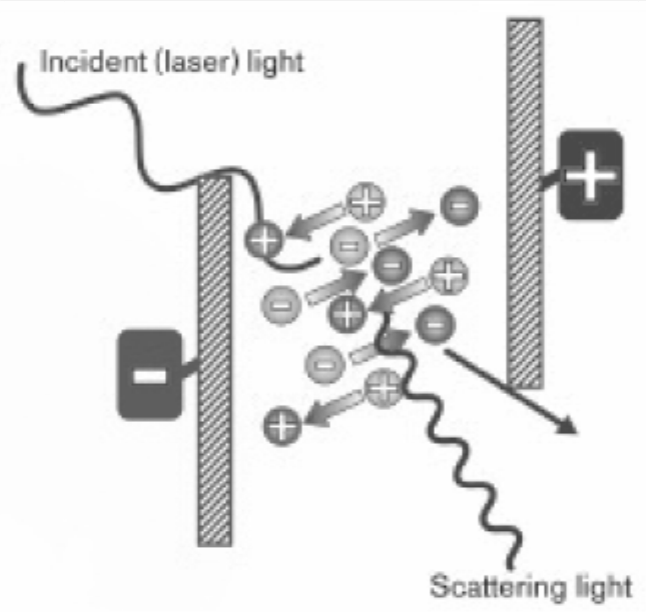

Figure 3.5. The schematic representation of the electrophoretic light scattering method is shown (Bechman Coulter, 2010).

3.2.6.2 Sample preparation and experimental procedure

The emulsions in the presence of protein (either WPI or sodium caseinate) were prepared by the mixing system introduced in section 3.2.2. Subsequently, the "high concentrated zeta cell" was filled with the emulsion samples, and it was placed inside the device. The measurement was carried out automatically by the device and the results were reported in the form of mobility and the surface potential. The experiments were performed in triplicate for each sample in order to ensure reproducibility.

Chapter 4

Development of a new technique for real-time droplet size measurement

This chapter focuses on the development of a new reflectance technique that in the subsequent result chapters is used to determine real-time droplet sizes during emulsification processes.

4.1 Framework

The aim of this thesis was to monitor and study the emulsion formation during processing. In order to achieve this aim, there is a need to observe the evolution of droplet sizes in real-time during the process. As it has been stated in section 2.2, a number of techniques have been developed to determine the droplet size evolution data for emulsification processes. With the intention of selecting the most suitable technique for the purpose of this study, the following requirements have been considered:

- *Preferably, physical sampling should be avoided.*

Emulsion microstructure development during processing could be different to that characterised after sampling and could result in an inaccurate representation of droplet size. In order to observe the behaviour of the emulsion under varying hydrodynamic conditions an online technique is needed.

- *It should be possible to investigate emulsification in the presence of high ($\varphi \geq 2\%$) dispersed phase volume fractions.*

This is an important requirement since there is little existing information about the emulsification behaviour of concentrated emulsions.

- *The technique should have the capability to investigate fast-occurring processes.*

The data acquisition time of the measurement technique should be less than the time scale of the droplet size variation, since the detailed events that occur during the processes are still not well understood.

- *The technique should be simple to implement.*

This is an important attribute since one should be able to study, with relative ease, various processes occurring under different conditions.

Most of the current techniques are not capable of online monitoring of droplet sizes during emulsification processes in the presence of high dispersed phase volume fractions. Therefore, the search to develop the most suitable technique was carried out by considering the above-mentioned requirements. The colouring, ultra-sonic spectroscopy and reflectance techniques were all investigated. Of these three, the reflectance technique was shown to be the best to use in the current study. The detailed experimentation using the colouring and ultra-sonic spectroscopy techniques, and the reasons for not selecting these are given in Appendix A.

4.2 Development of the reflectance technique

4.2.1 Relationship between droplet size and reflectance of the emulsion

There have been long-standing difficulties in the objective definition of the colour of materials (McClements, 2002a), and therefore the colour of objects is normally quantified by measurement devices in 'tristimulus coordinates', such as the most common colour space "$L^*a^*b^*$" defined by the "International Commission on Illumination" (CIE) in 1976. Other coordinate systems have been also defined but those are not considered in this thesis. The main reason for defining in tristimulus values is that all colours can be described by just three variables. For example, in $L^*a^*b^*$ coordinates, L^* is an indication of lightness (which reflects the subjective brightness perception of a human's observation) and a^* and b^* are colour coordinates.

A number of studies have been conducted in order to determine the relationship between emulsion colour and its physical properties (Walstra, 1968; Dickinson, 1994; Chantrapornchai *et al.*, 1999). These studies have shown that L^* depends on the volume fraction, droplet size and relative refractive index (the refractive index of the dispersed phase

divided by the refractive index of the continuous phase). In addition, theoretical expressions of the colour of emulsions have been presented (McClements, 2002a), in which it is assumed that the colour of dilute emulsions is determined by the light that is transmitted through them, whereas for concentrated emulsions (opaque appearance), the colour is determined by the light reflected from the surface of the emulsion. The work of this thesis focuses on systems with high volume fractions and therefore discussion is limited to concentrated emulsions.

The theoretical method of estimating the colour from the emulsions' characteristics is now summarised. Firstly, the scattering characteristics of individual droplets are calculated from their size and refractive index. Secondly, by using the droplet concentration and scattering characteristics, the scattering and absorption coefficients for an emulsion are calculated in the visible region of the electromagnetic spectrum. Thirdly, the reflectance spectrum of the emulsion is calculated, and finally, the tristimulus coordinates ($L^*a^*b^*$) of the emulsion are estimated. In all steps the appropriate models and theories are implemented. A full mathematical description of this approach has been given elsewhere (McClements, 2002b). It should be noted that the theoretical predictions obtained through such an approach do not wholly agree with experimental measurements, since the models fail to take into account the existence of the emulsion container. Nonetheless, there is qualitative agreement between theoretical predictions and experimental results. The theoretical predictions of the colour coordinates of emulsions in relation to their properties can be seen in Figure 4.1.

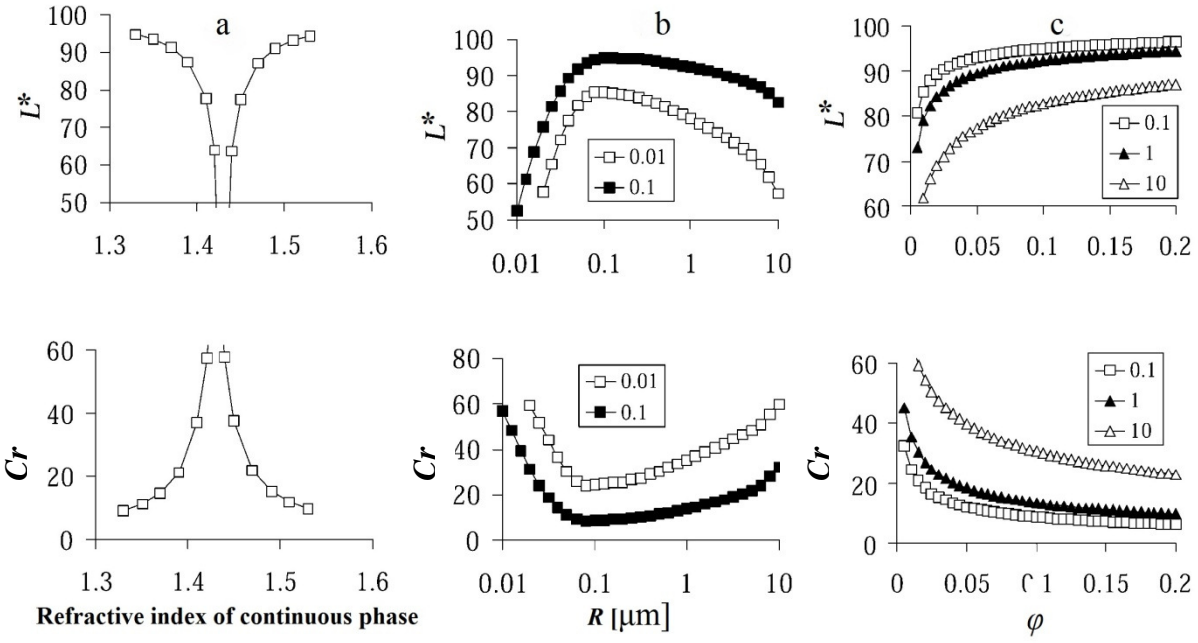

Figure 4.1.Theoretical predictions of the influence of relative refractive index of the continuous phase (a), emulsion's droplet sizes (b) and volume fractions (c) on the colour coordinates of emulsions are shown (McClements, 2002a).

In Figure 4.1 the influence of emulsion properties on L^* and colour coordinate Cr is represented. The colour coordinate or Chroma (Cr) is defined as:

$$Cr = \sqrt{(a^*)^2 + (b^*)^2} \tag{4.1}$$

It should be noted that, Figure 4.1-a shows various values of L^* and C when the refractive index of the continuous phase was varied from lower to higher values than the dispersed phase refractive index (refractive index of dispersed phase was taken to be 1.43). This results in the generation of various relative refractive indices. It can be seen that, L^* is decreasing when the relative refractive index approaches unity (for example a continuous phase refractive index of 1.43). Subsequently, it increases when the relative refractive index increases above unity. The value of L^* when the refractive index of the continuous phase is equal to that of the dispersed phase depends on the background colour of the emulsion during measurement (Chantrapornchai *et al.*, 2001b). When the background colour was white, a peak was determined, whereas with the black colour background a through in the graph of L^* was observed.

Figure 4.1-b also clearly demonstrates that L^* increases rapidly with droplet size until it reaches a maximum at droplet radius of 0.1 μm, and then decreases slowly at higher droplet sizes. It should be noted that the growth of individual droplets (for example due to droplet coalescence or Ostwald ripening phenomena) is responsible for the change in L^*, and not the formation of flocs or clumps of droplets (Chantrapornchai *et al.*, 2001a; Weiss and McClements, 2001).

Furthermore, it is shown that L^* increases with increasing volume fraction (Figure 4.1-c), rapidly at first, and then at a slower rate at higher volume fractions. As can be seen in Figure 4.1, there is a reverse trend but a similar dependency of the Chroma parameter on the emulsion properties. It should be noted that the validity of theoretical expressions is limited to volume fractions up to 20 %; this is a result of the lack of predictive scattering theories for volume fractions above 20 %.

These dependencies form the basis of the reflectance method. If volume fractions and relative refractive index of emulsions are similar, then the colour of various emulsions is determined solely by reflectance which, in turn, is a function of droplet size only. In order to achieve this methodology, droplet sizes of systems with the same volume fractions and relative refractive indices are calibrated experimentally in order to find the relationship between mean droplet size and L^*.

As previously mentioned, the amount of light reflected from the sample is the main parameter in the determination of colour or tristimulus coordinates of concentrated emulsions. In colour theories, the reflectance is defined in the *XYZ* colour space as the value *Y* and is an indication of light reflectance of the specimen. *Y* has been measured and used in calibration studies, since a simple relationship exists between L^* and *Y*:

$$L^* = 116\left(\frac{Y}{Y_n}\right)^{1/3} - 16 \qquad (4.2)$$

where Y_n is the tristimulus value for a perfect reflecting diffuser. In this study the relation between Y and droplet size was determined through calibration curves for emulsions of different dispersed phase volume fractions and of known droplet sizes.

4.2.2 Calibrating reflectance of emulsions with their droplet sizes

In order to use the reflectance of an emulsion as a measure of its mean droplet size, a series of calibration experiments were designed and performed. A set of stable emulsions with different droplet sizes were prepared in the presence of either Tween 20 or sodium caseinate or silica particles as emulsifiers. In addition, emulsions with a wide range of droplet sizes (10 to 300 μm) were prepared, with varying dispersed phase volume fractions. The properties of the emulsions (for example droplet size and volume fraction) selected for the calibration studies matched the properties of the emulsions studied throughout this thesis. For Tween 20, a set of stabilised emulsions with dispersed phase volume fractions of 5 %, 10 %, 20 % and 50 % were prepared. For systems containing sodium caseinate and silica particles only a dispersed phase volume fraction of 10 % was used. Calibration curves were determined for each of these systems.

A mixing tank, as described previously, was used to produce emulsions. The mean droplet size (d_{32}) was measured using a Mastersizer device and the reflectance of the emulsions placed in a stirred tank was measured using a Chroma-meter device. Emulsions were prepared with high concentrations of emulsifiers in order to ensure their stability. Calibration curves were determined using 2 % Tween 20 and 1.5 % sodium caseinate.

Moreover, since silica particles were used on their own as well as with Tween 20 as part of a mixed-emulsifier system (Chapter 7), the emulsions (containing either only silica particles or mixed-emulsifier system) that were stable during the assigned stability check period were used to construct the calibration curve. Furthermore, it should be noted that, as

only two concentrations (1 % and 0.02 %) of silica particles were used for preparation of emulsions in this thesis, the calibration curves were produced only for emulsions in the presence of 1 % silica particles (either on its own or as part of a mixed-emulsifier system). Droplet sizes determined from emulsions in the presence of lower concentration (0.02%) of silica particle were shown to be best predicted using the calibration curve constructed for emulsions in the presence of Tween 20. This is probably a consequence of similar refractive indices of solutions of 0.02 % silica particles and the ones related to Tween 20, since the low concentration of silica particles does not affect the refractive index of water (Malvern Instruments, 2011).

The stability and the reflectance of all emulsions were monitored for over a month, except in the case of silica particles where the emulsion was monitored for one week. In all cases, both droplet size and reflectance remain unchanged over the monitoring period. The obtained calibration curves are shown in Figures 4.2, 4.3 and 4.4 for Tween 20, sodium caseinate and silica particles, respectively.

It should be noted that, Brij 97 and WPI were also used in this study. A number of emulsions were produced and their experimentally determined droplet sizes were compared to those predicted from the calibration curves. Good agreement was shown between the measured droplet sizes and the predicted droplet sizes, confirming that those calibration curves were also appropriate for use in these systems. Therefore, in the cases of emulsions stabilised by Brij 97 and WPI no new calibration curves were constructed.

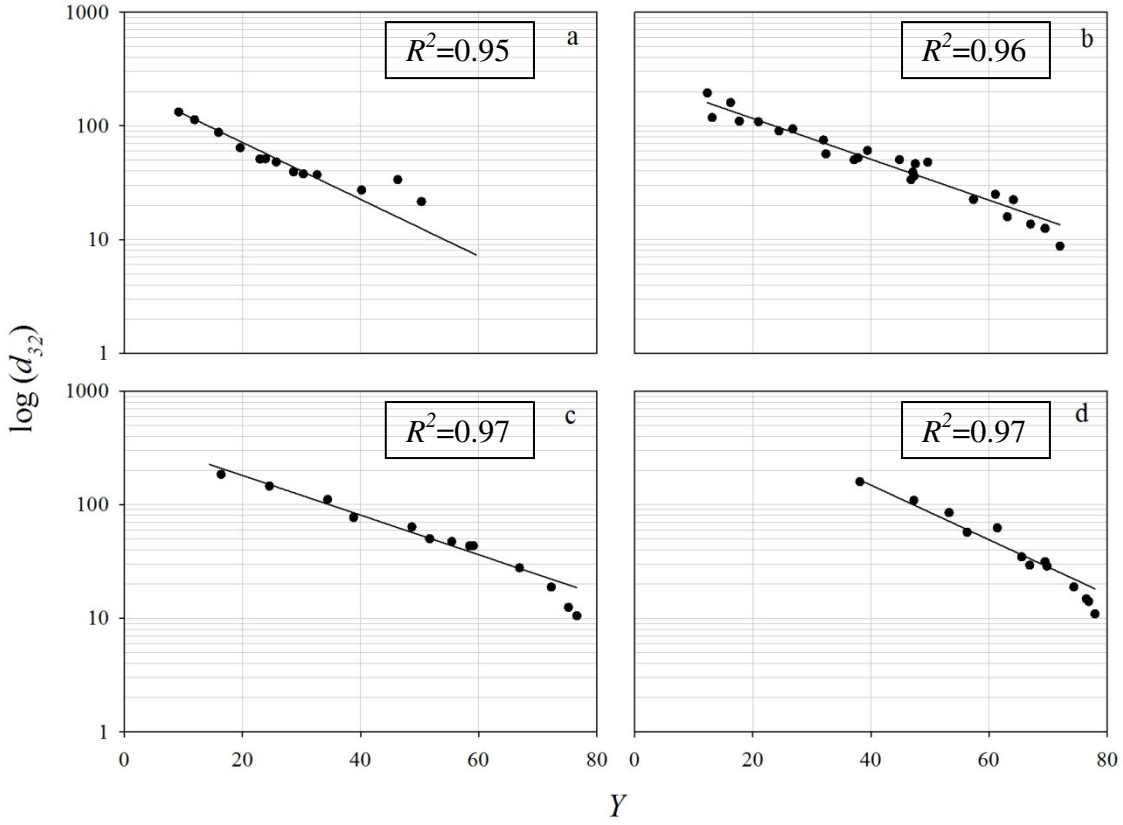

Figure 4.2. Calibration Curves of reflectance (*Y*) as a function of mean droplet diameter (d_{32}) for oil-in-water emulsions of 5% (a), 10% (b), 20% (c) and 50% (d) dispersed phase volume fractions stabilised by Tween 20.

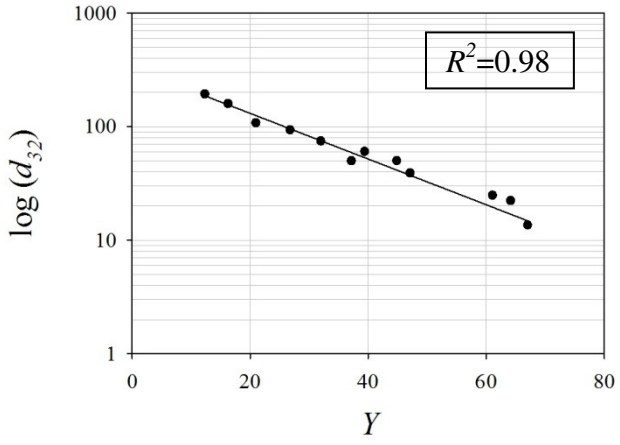

Figure 4.3. Calibration Curves of reflectance (*Y*) as a function of mean droplet diameter (d_{32}) for oil-in-water emulsions of 10% dispersed phase volume fraction stabilised by sodium caseinate.

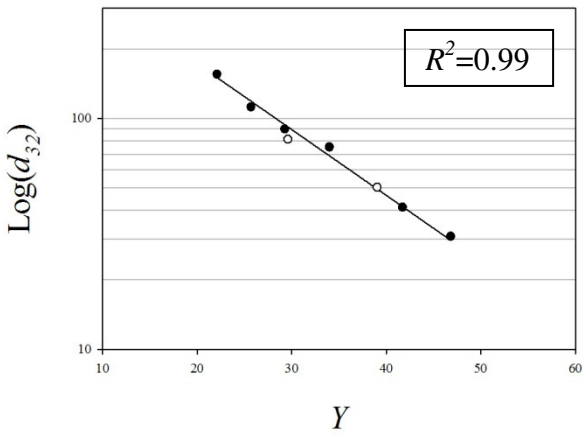

Figure 4.4. Calibration Curves of reflectance (*Y*) as a function of mean droplet diameter (d_{32}) for oil-in-water emulsions of 10% dispersed phase volume fraction stabilised by silica particles (●) and mixture of silica particles and Tween 20 (○).

As demonstrated in Figures 4.2-4.4, a linear relationship ($R^2 > 0.9$, for all systems studied) exists between the log(d_{32}) and *Y*. It should be stressed that the proposed relationship should only hold for systems within the size range used in the calibration tests and for processing in agitated vessels as the one used in this study.

4.2.2.1 Determining the droplet size of emulsions in the absence of added emulsifier

The calibration curves shown in Figures 4.2-4.4 were obtained only for systems in the presence of emulsifiers. Since the oil phase, and consequently the refractive index of the dispersed phase used, is the same for all studied systems, the difference between the relative refractive indices arises from the various refractive indices that result from using aqueous phases of different surfactants. Therefore, care must be taken in the use of these calibration curves for estimating the droplet size evolution of the oil-in-water emulsion formation in the absence of added emulsifiers.

The calibration curve determined for Tween 20 (Figure 4.2) is employed for cases where no emulsifier was present. The amount of Tween 20 used does not significantly affect

the refractive index of water since the highest employed concentration was 2%. In order to show the effect of Tween 20 on the refractive index of its solution, the refractive indices of pure water and Tween 20 are considered to be 1.33 (Mastersizer 2000, 2009) and 1.46 (Anon, 2007), respectively. This results in the refractive index of solution to be as follows (Malvern Instruments, 2011):

$$Refractive\ index\ of\ solution = 0.98 \times 1.3330 + 0.02 \times 1.4615 = 1.3326 \quad (4.3)$$

Equation 4.3 shows that the refractive index of the Tween 20 solution is not significantly different with that of pure water thus it is safe to consider the same calibration curves for cases with various Tween 20 concentrations and the ones without any added emulsifier.

4.2.2.2 Effect of droplet size distribution type/shape on calibration curves

It can be argued that the type/shape of droplet size distribution may affect the relationship between reflectance and mean droplet size and therefore, since varying surfactant concentrations were used in these studies, the reflectance of two different mean droplet sizes may be similar. This can be indeed true in the systems where two different types of droplet size distributions are generated, such as bimodal or log-normal distributions.

In order to demonstrate whether droplet size distribution affects reflectance measurements, droplet size distributions of emulsions with high concentration and low concentration of surfactants were determined for the studied systems. In the case where a high concentration of emulsifier was used and stable emulsions were obtained from the process, samples without further modification were used to determine droplet size distributions. However, in order to observe the droplet size distributions of emulsions produced with a lower concentration of emulsifier, which are not stable, samples obtained from the process were quickly introduced to a solution of high concentration (2%) of Tween 20.

Finally, it should be noted that these experiments were performed under the same hydrodynamic conditions to the performed experiments in emulsification studies (Chapters 5, 6 and 7) and the same experimental protocol was used. Initially, processing was initiated at a constant impeller speed (first processing step). After two hours of processing, the impeller speed was reduced to half of the initial speed (second processing step), also for two hours. The detailed experimental protocol is described in section 4.3. The droplet size distributions obtained from these experiments can be seen in Figures 4.5 and 4.6. The samples were obtained at three different times during processing: at the end of the first processing step, at the early stages of the second processing step and at the end of the second processing step. In the cases where there was no significant difference between the determined droplet size distributions from these three stages, only one of them is presented. Two different concentrations of Tween 20, high (1%) and low (0.01%), were used during emulsifications at different experimental processing modes of 1600-800 and 2000-1000 (where numbers indicate impeller speed in rpm) and for different dispersed phase volume fractions (5% and 50%). When sodium caseinate was employed, concentrations of 0.02% and 1% were chosen as the low and high emulsifier concentrations respectively, systems were processed at 1600-800 conditions and the dispersed phase volume fraction was 10%.

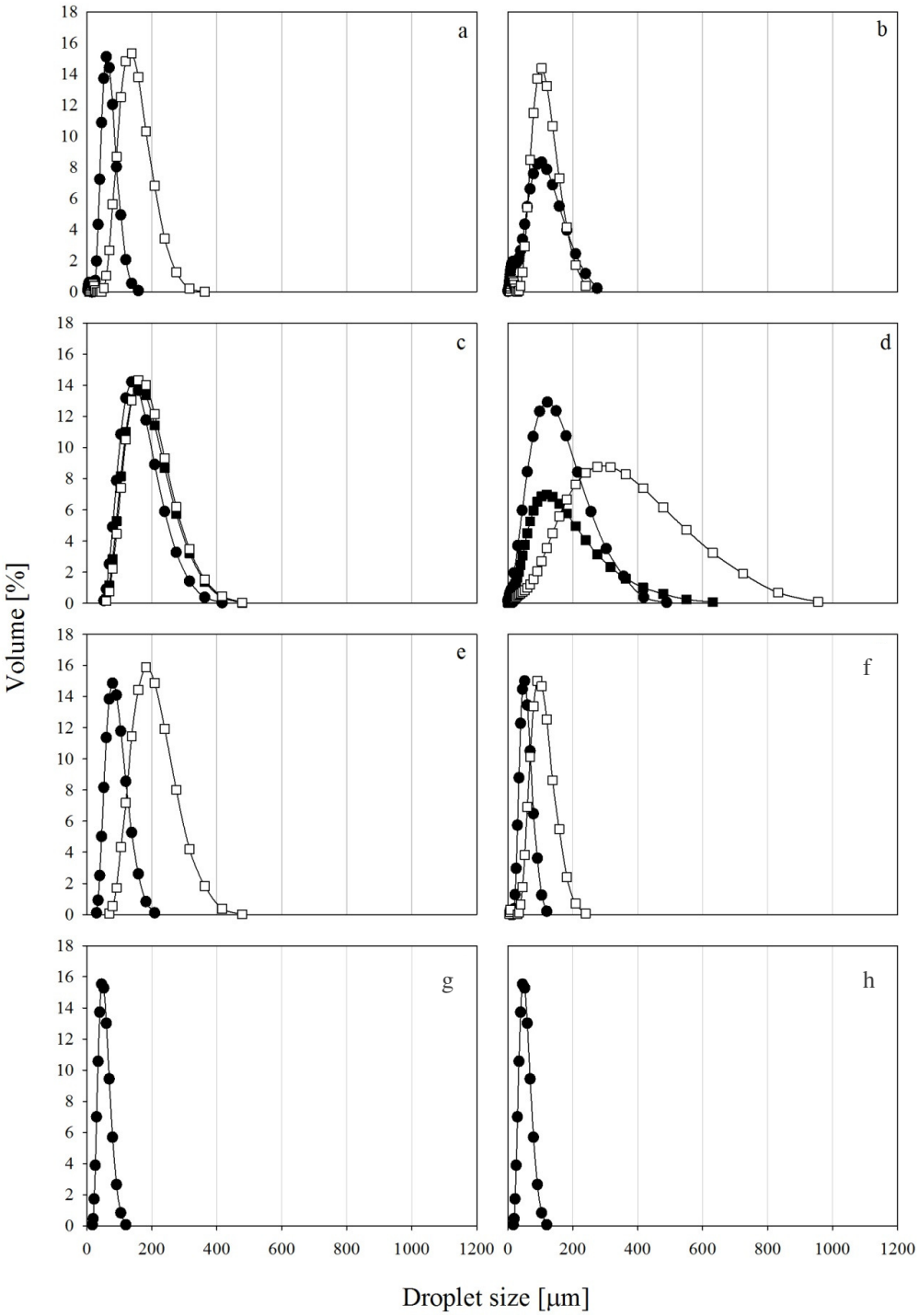

Figure 4.5. Droplet size distributions determined from emulsion samples in the presence of Tween 20 were obtained at the end of the first (●), at the early stages of the second (■) and at the end of the second processing step (□) for various experimental set-ups hydrodynamic conditions and dispersed phase volume fraction: (a) 5% oil-in-water emulsion processed at 1600-800 experiment containing 0.01% Tween 20, (b) 5% oil-in-water emulsion processed at 2000-1000 experiment containing 0.01% Tween 20, (c) 50% oil-in-water emulsions processed at 1600-800 experiment containing 0.01% Tween 20, (d) 50% oil-in-water emulsion processed at 2000-1000 experiment containing 0.01% Tween 20, (e) 5% oil-in-water emulsion processed at 1600-800 experiment containing 1% Tween 20, (f) 5% oil-in-water emulsion processed at 2000-1000 experiment containing 1% Tween 20, (g) 50% oil-in-water emulsion processed at 1600-800 experiment containing 1% Tween 20 and (h) 50% oil-in-water emulsion processed at 2000-1000 experiment containing 1% Tween 20.

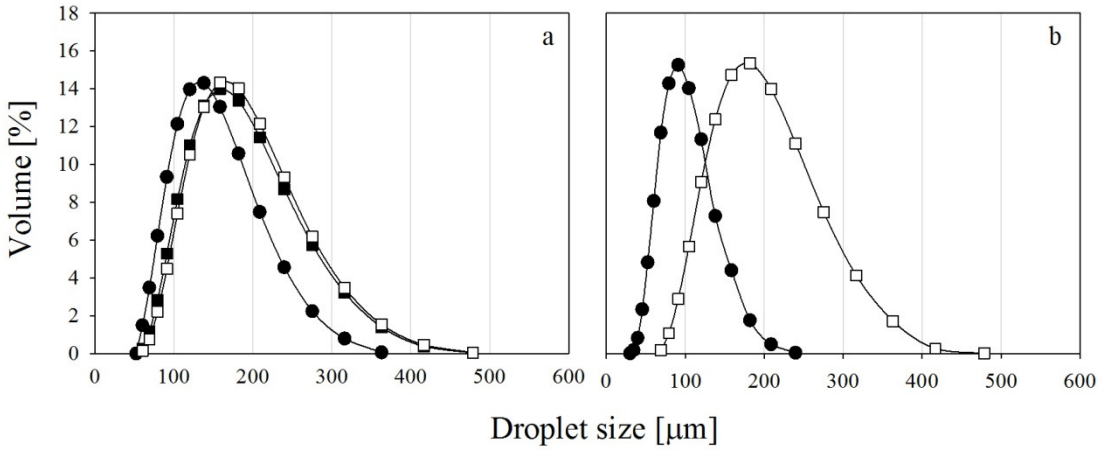

Figure 4.6. Droplet size distributions determined from emulsion samples in the presence of sodium caseinate were obtained at the end of the first (●), at the early stages of the second (■) and at the end of the second processing step (□) for various experimental set-ups hydrodynamic conditions and dispersed phase volume fractions: (a) 10% oil-in-water emulsion processed at 1600-800 experiment containing 0.02% sodium caseinate, (b) 10% oil-in-water emulsions processed at 1600-800 experiment containing 1% sodium caseinate.

As can be seen in Figures 4.5 and 4.6, representative droplet size distributions obtained at different stages in the process 'shift' to larger droplet sizes when the impeller speed is reduced, without any change in the type/shape of the distribution. Similar observations were previously reported by Narsimhan *et al.* (1980) and Sis and Chander (2004) with experimental work demonstrating that the droplet size distribution shape during mixing is 'self-preserving'; meaning that the droplet size distribution type/shape does not change although the mean droplet diameter is reduced with time.

The observations presented here show that the type/shape of droplet size distribution does not change due to variations in emulsifier concentration or the chosen experimental protocol. Therefore, the change in reflectance is a consequence of the change in mean diameter in any particular calibration curve.

4.3 Experimental procedure

Experiments were designed and carried out in order to study droplet break-up and coalescence phenomena independently. All experiments consist of three processing steps.

Initially, processing began at a constant impeller speed (first processing step). The very early stages of this step are dominated by droplet break-up events. After two hours of processing, the impeller speed was reduced (second processing step) to half of that in the first processing step, creating conditions where coalescence events dominate. This method was first proposed by Howarth (1967), while Wright and Ramkrishna (1994) calculated that the impeller speed should be reduce by at least a factor of 1.78 in order to generate a coalescence dominant regime. Processing during this second step was also allowed to take place for two hours, and subsequently the impeller speed was again increased (third processing step) to that in the first processing step and kept constant for one hour, to induce a further droplet break-up dominant regime and investigate the response of the system. Throughout this thesis experiments are denoted using "impeller speed of the first - the second - and the third processing step" as a descriptor. For example the '1600-800-1600' experiment denotes that impeller speed was varied from 1600 rpm (first processing step) to 800 rpm (second processing step) and finally increased to 1600 rpm (third processing step). It should be noted that due to the high number of data points obtained from each emulsification experiment, one every fifteen data point is shown in droplet size evolution diagrams.

4.4 Analysis of experimental data

Theoretical expressions suitable for analysis of the experimental data obtained by the reflectance technique were employed. Some of these expressions were fully developed according to phenomena that occurred during processing, and others are modifications of well established expressions in the literature. These expressions are presented in this section.

4.4.1 Hydrodynamic conditions during processing

Knowledge of the hydrodynamic conditions during processing is of major importance in order to understand the mechanism of emulsification. This is because the hydrodynamic condition will affect all the sub-processes that determine droplet sizes, which include droplet break-up, droplet coalescence, rate of surfactant adsorption and many more.

Hydrodynamic conditions can be determined from the Reynolds number (*Re*); the ratio of inertial and viscous forces. The Reynolds number related to the mixing in the vessels is determined according to:

$$Re = \frac{\rho N D^2}{\mu} \tag{4.4}$$

where ρ is the density of fluid, N is the impeller rotational speed, D is the impeller diameter and μ is the viscosity of the fluid. It has been shown that systems of similar design to the mixing vessel employed in this study can be considered to operate in fully turbulent regime when the respective Reynolds number is above 10^4 (Leng and Calabrese, 2004; Hall *et al.*, 2005a). In the case where the fluid is an emulsion the literature is 'divided' into two groups of opinions. In the first group (Hong and Lee, 1985; Walstra and Smulders, 1998), the authors believe that the Reynolds number in emulsification should be calculated using the density and viscosity of the continuous phase. In the second group, however, the authors (Leng and Calabrese, 2004) believe that the so-called 'effective' density and viscosity (which are the density and viscosity of the emulsion) should be used instead.

Nonetheless, in mixing systems, as the energy is transferred to the system by an impeller, it is expected that dispersed (oil) and continuous (water) phases experience similar agitations. It has been observed (Kumar *et al.*, 1991) that at volume fractions below 50% (the maximum volume fraction that was used in this study), even though low Reynolds numbers can be determined (if the properties of the emulsion are considered in the calculation), the

process of break-up and coalescence can be best defined by the theories related to the inertial sub-range of the turbulent regime. Therefore, in this work the first approach is employed. This is a consequence of the fact that the energy is similarly experienced by both continuous and dispersed phase in the impeller region, thus at that instance, where droplet break-up occurs, the dispersed phase does not affect the turbulent fluctuations of the continuous phase, and hence only the properties of the continuous phase should be considered. Consequently, the Reynolds numbers for all experimental conditions that are employed in this study are calculated herein. Table 4.1 shows the calculated Reynolds numbers for various experimental conditions.

Table 4.1. Reynolds numbers calculated for various experimental conditions employed in this study.

Impeller speed [rpm]	Reynolds number
400	8,000
800	16,000
1000	20,000
1600	32,000
2000	41,000

It can be seen that, the Reynolds numbers related to the most impeller speeds indicate that the experiments operate in the fully turbulent regime. However, the experiment performed with impeller speed of 400 rpm shows Reynolds number of 8,129 which is lower than 10^4; suggesting that the process operates in the higher transitional regime. However, as most of the studies on mixing systems were performed on the agitated mixers of the diameter of 15 cm and above, and the fact that the agitated mixer employed in this study is 7 cm, the behaviour of fluid may well not be as expected. Therefore, a number of studies have been

performed on the hydrodynamic condition of so-called 'high throughput' mixers (Hall *et al.*, 2005a; Hall *et al.*, 2005b; Chung *et al.*, 2007; Chung *et al.*, 2008). These studies show that, although these processes result in Reynolds numbers related to the higher transitional regime, they behave as though they operate in the turbulent regime. For example, the study by Hall *et al.* (2005a), which used an experimental set-up similar to the system employed in this work, reports that even at Reynolds numbers as low as 4000, the behaviour is that of a fully turbulent system. For these reasons the system processed at the lowest impeller speed (400 *rpm*) will be taken to operate in turbulent regime.

4.4.2 Energy dissipation of the process

Emulsification processes are highly dependent on the energy input to the system (by the action of the impeller in this work), which is itself defined in the form of energy dissipation of eddies. The energy dissipation affects the droplet size evolution by influencing droplet break-up and coalescence rates and therefore, it is vitally important to be estimated. The expression for estimating the average energy dissipation ($\bar{\varepsilon}$) in mixing systems is already given in section 3.2.2.2 and it is defined by:

$$\bar{\varepsilon} = \frac{PoN^3D^2}{2\pi} \tag{3.2}$$

where N is the impeller speed, D is the impeller diameter and Po is the power number of mixing set-up and equals to 1.35 for the experimental set-up in this work. In turbulent regimes an increase in volume fraction induces turbulent depression since some of the energy input is consumed on droplet convection, surface modulations and so on (Colaloglou and Tavlarides, 1977). Doulah (1975) developed an approach in which it was assumed that by increasing the viscosity (as dispersed phase volume fraction increases) the energy dissipation from the Kolmogorov microscale decreases (refer to section 2.3.2.2). Therefore, the dampening effect of the dispersed phase is given by:

$$\frac{\varepsilon_e}{\varepsilon_c} = (\frac{\nu_c}{\nu_e})^3 \quad (2.19)$$

where ε_e is the energy dissipation related to the emulsion, ε_c is the energy dissipation in the absence of a dispersed phase, or in the other words, that of the continuous phase, and ν_e and ν_c are the kinematic viscosities of the emulsion and continuous phase, respectively. Throughout this study, equation 2.19 is used to calculate energy dissipation of the emulsification as in number of previous studies (Tsouris and Tavlarides, 1994; Liu and Li, 1999).

4.4.3 The kinematic viscosity of an emulsion

The kinematic viscosity of an emulsion (ν_e) is determined from:

$$\nu_e = \frac{\mu_e}{\rho_e} \quad (4.6)$$

where, μ_e is the effective viscosity and ρ_e is the effective density of the emulsion, estimated according to:

$$\rho_e = \rho_d \varphi + \rho_c (1 - \varphi) \quad (4.7)$$

where ρ_d and ρ_c are the densities of the dispersed and continuous phases, respectively, and φ is the volume fraction of the dispersed phase. A number of studies have been conducted on the viscosity of emulsions, since viscosity not only plays a major role when choosing the operating conditions of industrial processes, but also provides information regarding the rheological behaviour of these systems. A number of predictive models have been proposed which are mostly based on the theory regarding the packing of hard spheres in the continuous phase. A full review has been given by Dickinson (1998).

Despite the existence of a number of predictive means to calculate the viscosity of emulsions, in the present work this parameter was experimentally determined. However, as the rheometer device used for these studies is not suitable for dilute emulsions (φ = 5%), and since very noisy data were determined, the widely used semi-empirical equation suggested by Krieger and Dougherty was employed to estimate the viscosity of these types of emulsions.

$$\mu_r = \left(1 - K_\varphi \varphi\right)^{-2.5/K_\varphi} \quad (4.8)$$

where K_φ is the crowding factor equal to the reciprocal of packing fraction of droplets (~85% in the case of emulsions) and μ_r is the relative viscosity defined as:

$$\mu_r = \frac{\mu_e}{\mu_c} \quad (4.9)$$

where μ_e and μ_c are the viscosities of the emulsions and continuous phase.

4.4.4 Droplet break-up frequency

The model proposed here for the calculation of the droplet break-up frequencies, during the stages of the process where droplet break-up is the dominant phenomenon, was developed assuming that: i) droplet break-up and droplet coalescence events are two independent processes and ii) at the very initial stages of the first and the third processing steps of the experiments droplet size evolution is dominated by break-up events. These reasonable assumptions suggest that the change in the number of droplets is a direct consequence of droplet break-up, thus the rate of change in the number of droplets is equal to the droplet break-up rate. This results in:

$$B = \frac{dn}{dt} \quad (4.10)$$

where B is the break-up rate per unit time and unit volume, n is the number of droplets per unit volume, which is defined by:

$$n = \frac{6\varphi}{\pi d_{32}^3} \quad (4.11)$$

Substituting equation 4.11 to equation 4.10 gives:

$$B = \frac{-18\varphi}{\pi (d_{32})_0^4} \left(\frac{d(d_{32})}{dt}\right)_0 \quad (4.12)$$

where $(d_{32})_0$ and $(\mathrm{d}(d_{32})/\mathrm{d}t)_0$ are the mean droplet diameter and mean droplet diameter evolution, respectively, during the very initial stages in the emulsification process where droplet break-up dominates. Equation 4.12 provides a tool to determine the droplet break-up

rate from experimental droplet size evolution data. Then, the break-up frequency β (the reciprocal of the droplet lifetime between break-up events) of a single droplet can be calculated from:

$$\beta = \frac{B}{n_0} \tag{4.13}$$

where n_0 is the initial number of droplets per unit volume. In this study, the droplet break-up dominant stage of the process was assumed to occur within the first three minutes of the first and the third processing steps. Droplet size evolution data within these selected droplet break-up dominant stages were used to calculate the $(d_{32})_0$ and $(\mathrm{d}(d_{32})/\mathrm{d}t)_0$ values and subsequently, using equations 4.12 and 4.13, the droplet break-up frequency β for each of these processing steps was calculated.

4.4.5 Droplet coalescence

Unlike droplet break-up, the droplet coalescence rate (A) can be defined as a product of collision rate (χ) and the ratio referred to as collision efficiency (ξ), according to the following relationship (Coulaloglou and Tavlarides, 1977; Chesters, 1991; Tsouris and Tavlarides, 1994; Liu and Li, 1999; Narsimhan, 2004):

$$A = \chi \times \xi \tag{4.14}$$

In this work, coalescence frequency and collision rate were determined as described in the following sections, and consequently, collision efficiency was calculated using equation 4.14.

4.4.5.1 Coalescence frequency

The approach described earlier for droplet break-up was also used to calculate the droplet coalescence frequencies, together with the additional assumption that only two droplets are involved in any of the coalescence events that occur in the system. Droplet coalescence would then cause the change in the number density of the droplets and thus the

droplet coalescence rate A (number of coalescence events per unit time and unit volume) can be calculated from:

$$A = \frac{-dn}{dt} \tag{4.15}$$

Employing equation 4.11 in conjunction with equation 4.15 results in:

$$A = \frac{18\varphi}{\pi(d_{32})_0^4}\left(\frac{d(d_{32})}{dt}\right)_0 \tag{4.16}$$

where $(d_{32})_0$ and $(\mathrm{d}(d_{32})/\mathrm{d}t)_0$, in this case, are calculated for the very initial stages in the process where droplet coalescence is dominant (second processing step). Then droplet coalescence frequency α (the reciprocal of the lifetime of the droplets between coalescence events) can be calculated from:

$$\alpha = \frac{\mathrm{A}}{n_0} \tag{4.17}$$

In this thesis, the droplet coalescence dominant stage of the process was taken to occur within the first three minutes of the second processing step. Droplet size evolution data within the selected droplet coalescence dominant stage were used to calculate the $(d_{32})_0$ and $(\mathrm{d}(d_{32})/\mathrm{d}t)_0$ values and subsequently, using equations 4.16 and 4.17, the droplet coalescence frequency α at the second processing step.

4.4.5.2 Collision rate

A number of approaches have been used to estimate the droplet collision rate (Coulaloglou and Tavlarides, 1977; Chesters, 1991; Tsouris and Tavlarides, 1994; Liu and Li, 1999; Narsimhan, 2004), however most of these result in rather similar expressions with minor differences, mainly in the constants used. The well accepted approach employed by Chesters (1991) and Tsouris and Tavlarides (1994) is used in this study. In this approach it is considered that droplets behave similar to gas molecules, therefore collision rates would be related to the characteristic velocity between two points of distance d apart. By assuming that

the system being processed is a mono-sized emulsion, for the inertial sub-range of the turbulent regime the collision rate can be calculated from:

$$\chi = \frac{28\sqrt{2}\pi}{3}\varepsilon^{1/3}d^{7/3}n^2 \tag{4.18}$$

where, the droplet diameter d can be assumed to be the mean droplet diameter (d_{32}), n can be determined according to equation 4.11 and also the average energy dissipation $\bar{\varepsilon}$ can be used instead of ε. Thus, equation 4.19 reduces to:

$$\chi = \frac{336\sqrt{2}\varphi^2}{\pi}\bar{\varepsilon}^{1/3}(d_{32})_0^{-11/3} \tag{4.19}$$

4.4.6 Collision efficiency

After the coalescence and collision rates have been obtained, the collision efficiency can be calculated using equation 4.14. Collision efficiency is a consequence of a number of parameters existing simultaneously. Numerous models have been developed to characterise the collision efficiency, however, they result in contradictory conclusions. Therefore, the behaviour of collision efficiency was investigated in this work by identifying the parameters that mainly affect droplet collisions.

When two droplets collide, a layer of continuous phase is entrapped between them. The force that 'squeezes' the droplets together is caused by continuous fluid fluctuations and is referred to as a 'turbulent force'. Turbulent force acting on the droplets results in the entrapment of a layer of continuous phase between them, the thickness of which is a consequence of the amount of the turbulent force and the size of the droplets. The continuous phase between droplets then drains as the droplets approach each other further. The two droplets coalesce when the entrapped continuous film thickness reaches a critical value. In addition, emulsifiers can influence the above-described phenomena by providing repulsive forces to induce a barrier opposing the turbulent force. One of the most important phenomena

that is rather difficult to describe mathematically is the drainage of the continuous phase entrapped between the colliding droplets, specially when emulsifiers are present on the interface. Thus, in order to be able to compare between various experimental results, each of the previously mentioned steps (in drainage phenomena) was individually determined.

4.4.6.1 Turbulent force

Due to the stochastic nature of turbulence, the force acting on droplets is also a stochastic parameter. Therefore, in this work, the mean turbulent force was used as an indication of the external force pushing droplets together. Since eddies larger than the droplet size are in fact responsible for movement (convective transport) of droplets (Narsimhan, 2004; Tcholakova *et al.*, 2004), and that eddies with a similar size to droplets contain higher energy than eddies with smaller sizes, the eddies with similar size to that of droplets are the only eddies that are considered in the estimation of the turbulent force (Narsimhan, 2004; Tcholakova *et al.*, 2004; Vankova *et al.*, 2007b). According to the assumptions given above, the mean turbulent force ($\bar{F}$) can be given (Narsimhan, 2004):

$$\bar{F} = \frac{\pi\rho}{4} d^2 \overline{U^2}_d \tag{4.20}$$

where $\overline{U^2}_d$ is the characteristic velocity between two points separated by distance d. Therefore, the mean turbulent force acting on droplets can be, for the inertial sub-range of the turbulent regime, given by:

$$\bar{F} = \frac{\pi\rho}{2} \bar{\varepsilon}^{2/3} {d_{32}}^{8/3} \tag{4.21}$$

4.4.6.2 Emulsifier adsorption

In order to estimate the time needed for emulsifier to adsorb on the interface, the approach proposed by Levich (1962) was considered. The mechanism that describes emulsifiers' transport to the interface can be summarised as follows. When the dispersed

phase is introduced into the continuous phase, emulsifiers are already present. Thus, as the turbulent regime increases the interfacial area, the emulsifiers are adsorbed almost instantaneously. Therefore, the limiting step in emulsifier adsorption would be their transport onto the naked interfaces. In the turbulent regime diffusion is negligible in comparison to convective transport. Thus, the time required for emulsifier convective transport (t_A) in the inertial sub-range of the turbulent regime can be defined from (Walstra and Smulders, 1998; Tcholakova *et al.*, 2004):

$$t_A = \frac{\Gamma \rho^{1/3}}{m_s \bar{\varepsilon}^{1/3} d_{32}{}^{1/3}} \tag{4.22}$$

where Γ is the surface excess when the interface is fully covered by the emulsifier and m_s is the amount of emulsifier in the aqueous phase. It should be noted that equation 4.22 is only valid for rapid adsorption of emulsifiers, and therefore, after adsorption of the emulsifiers on the interface, the expression cannot be used. As an estimation, full coverage of the interfaces are considered to be 10 times of the t_A (Walstra and Smulders, 1998). In addition, these expressions are mostly employed in the cases where surfactants are used, since larger amphiphilic molecules (such as proteins) would require longer times to adsorb on the interface. Attempts have been made to incorporate this effect in the adsorption time, however, due to the complexity they have not been considered; examples of such expressions can be found elsewhere (Hsu *et al.*, 1997; Hsu *et al.*, 2000). Nonetheless, equations 4.22 provide useful values for comparison purposes in the case of surfactants.

4.4.6.3 Dimensions of the entrapped continuous film

In order to determine the amount of continuous liquid or planar film captured between two droplets due to collision, the film thickness and the radius of the film are needed. According to thin liquid film theories (Ivanov, 1988) the thickness of the film between approaching droplets under external force can be determined when the dynamic capillary

pressure in the gap would be comparable to the capillary pressure of the droplets. This film thickness is referred to as the 'inversion thickness' (h_{inv}) and is defined as (Ivanov, 1988):

$$h_{inv} = \frac{\bar{F}}{2\pi\sigma} \tag{4.23}$$

where the external force can be determined from equation 4.21 and σ is the interfacial tension between the dispersed and continuous phases. Moreover, the radius of the flattened area (R_{film}) can be estimated by equalising the hydrodynamic force and the external force that is created by viscous dissipation of the film (Ivanov, 1988). The viscous dissipation of the film can be estimated as a product of the droplet capillary pressure and the film area, therefore it can be given from (Ivanov, 1988):

$$R_{film}{}^2 = \frac{d_{32}\bar{F}}{4\pi\sigma} \tag{4.24}$$

It should be noted that equations 4.23 and 4.24 can only be used in systems that do not display long-range strong repulsive force (for example electrostatic double layer) or those having rigid interfaces (for example in Pickering emulsions). Therefore throughout this thesis equation 4.23 and 4.24 were used only for systems with short-range repulsive forces (for example steric repulsive forces). The nature and description of these repulsive forces is presented in the following section.

4.4.6.4 Colloidal interactions

As previously mentioned, the dimension of the captured thin film can be estimated. This film needs be drained in order for the two droplets to coalesce. In addition, when the interfaces of two droplets are in close proximity, van der Waals attractive forces also contribute to droplet coalescence. However, the presence of emulsifiers on the interface can stabilise the film and suppress droplet coalescence.

Various colloidal interactions are induced when droplets approach each other. Depending on the nature of the force and separation distance, the interactions can be attractive

(for example van der Waals forces) or repulsive (for example electrostatic double layer or steric interactions). In order to determine the stability of the droplets against coalescence, the interaction forces between them are determined, in respect to their separation distance, and consequently, compared to turbulent forces. The attractive and repulsive forces are presented individually, and as a layer of molecules exist on the surface of the droplets, these forces are presented in the form of energy per unit area. Consequently the colloidal forces can be determined according to the Derjaguin approximation (Israelachvili, 1997; Kralchevsky *et al.*, 2009). For similar size spherical droplets, the interaction force ($F_{droplet}$) can be expressed by:

$$F_{droplet} = \pi R W_{planar} \tag{4.25}$$

where R is the radius of the droplet and W_{planar} is the interaction energy relating to two planar surfaces. Equation 4.25 states that the force related to colloidal interactions of two droplets can be determined from the interaction energy of two planar surfaces possessing similar physicochemical properties.

4.4.6.4.1 Van der Waals attractive interactions

The intermolecular van der Waals forces arise due to the attraction between molecules that are orientationally polarised (McClements, 2005), and therefore, they can act between two nearby surfaces that contain a large number of polarised molecules. The surface energy density (W_{vw}) induced by the van der Waals interaction of two planar surfaces of distance h apart can be given by (Israelachvili 1997; Kralchevsky *et al.*, 2009):

$$W_{vw} = \frac{-A_H}{12\pi h^2} \tag{4.26}$$

where A_H is the Hamaker constant of combination of the aqueous phase and droplets. Since two phases are involved, the following approximation of the Hamaker constant can be used (Yang *et al.*, 1999):

$$A_H = (A_{water} - A_{oil})^2 \tag{4.27}$$

in which A_{water} and A_{oil} are the Hamaker constants of water and oil, respectively, and reported to be 3.7×10^{-20} and 4.5×10^{-20} J (employed in this study) (Yang *et al.*, 1999). The interaction force (F_{vw}) can be determined from combining equations (4.26) and (4.25) to get:

$$F_{vw} = -\frac{A_H R}{12h^2} \tag{4.28}$$

4.4.6.4.2 Electrostatic double layer interactions

One of the most effective and long-range stabilisation mechanisms is induced by to the adsorption of the ionic emulsifiers on the interfaces (Israelachvili, 1997; McClements, 2005; Kralchevsky *et al.*, 2009). These emulsifiers alter the electric charge on the interfaces, thus resulting in electrostatic repulsive forces between two approaching droplets. Consequently, electrostatic double layer interactions are a function of the pH and ionic strength of the solution (continuous phase). Therefore, it is vitally important to adjust these parameters in cases where ionic emulsifiers are employed (for example proteins). The induced interaction energy (W_{ele}) for two planar surfaces can be given by (Israelachvili, 1997; Kralchevsky *et al.*, 2009):

$$W_{ele} = \frac{64 n_0 K_B T}{\kappa} \left[\tanh\left(\frac{Ze\Psi_s}{4K_B T}\right)\right]^2 \exp\left(-\kappa_D h\right) \tag{4.29}$$

where n_0 is the electrolyte number concentration, K_B is the Boltzmann constant, T is temperature, Z is the ionic valency, e is the elementary charge, Ψ_s is the electrical surface potential of droplets (approximated by the measured ζ potential, Tcholakova *et al.*, 2004) and κ_D is the reciprocal of Debye screening length, which can be estimated by:

$$\kappa_D = \left[\frac{2000 e^2 N_A c Z^2}{\varepsilon_r \varepsilon_0 K_B T}\right]^{1/2} \tag{4.30}$$

where N_A is the Avogadro constant, c is the concentration of the electrolyte in moles per litre, ε_0 is the permitivity of the vacuum and ε_r is the factor that determines the permittivity of the

liquid medium. The repulsive force (F_{ele}) induced by electrostatic double layer interactions can be determined from equations 4.25 and 4.29:

$$F_{ele} = \frac{64\pi}{\kappa} n_0 K_B T R \left[\tanh\left(\frac{Ze\Psi_s}{4K_B T}\right)\right]^2 \exp(-\kappa h) \quad (4.31)$$

4.4.6.4.3 Steric interaction

Emulsifiers that are not electrically charged induce a repulsive force against attractive forces (for example van der Waals forces) referred to as steric forces (McClements, 2005). Steric repulsive forces become effective when the proximity between droplets is such that the molecular segments of the emulsifiers from the different interfaces overlap. This mechanism is unaffected by the ionic strength or pH of the continuous phase. The range of influence of steric interactions is short (approximately up to twice the size of the molecules) and they are mostly effective at high emulsifier concentrations and only when the entire droplet interface is covered (McClements, 2005). Some models have been proposed to estimate the repulsive force induced by this mechanism (McClements, 2005; Kralchevsky *et al.*, 2009), however due to the complex nature of some parameters, determination of the exact value requires precise measurement of the forces acting when two emulsifier-coated interfaces are brought into close proximity (McClements, 2005). Nonetheless, in this thesis the amount of emulsifier on the droplet's interface (surface coverage) was used as an indication of the steric repulsive forces (Tcholakova *et al.*, 2004; McClements, 2005). In the cases where emulsifiers covered the entire interface of the droplets, it is considered that the droplets should in fact be stabilised through steric repulsion, otherwise, weak stabilisation is considered to be induced.

4.4.6.4.4 Magnitude of total interaction

As stated in the previous section, the steric repulsive interaction has been analysed qualitatively, thus, the total interaction forces are only determined for systems which induce stability through electrostatic repulsive forces. In order to incorporate both van der Waals and

electrostatic double layer forces, the Derjaguin-Landau-Verwey-Overbeek (DLVO) theory has been employed. In this theory the total interaction energy (W_{total}) is assumed to be expressed as:

$$W_{total} = W_{ele} + W_{vw} \tag{4.32}$$

where, W_{ele} and W_{vw} can be determined from equations 4.30 and 4.27, respectively. The colloidal forces between the interfaces of droplets can be determined as the superposition of interaction energies as described by equations 4.28 and 4.31.

$$F_{total} = \frac{64\pi}{\kappa} n_0 K_B T R \left[\tanh\left(\frac{Ze\Psi_s}{4K_B T}\right)\right]^2 \exp(-\kappa h) - \frac{A_H R}{12h^2} \tag{4.33}$$

Equation 4.33 results in the total colloidal force induced when two droplets are brought into close proximity. It should be noted that, in these equations two spherical droplets are considered rather than the flat surfaces that occur when droplets are pushed toward each other. However, as the size of the flattened area is significantly smaller than the droplet radius and the fact that the colloidal interactions are not only effective at the flattened area, but also on the spherical areas that are not flattened, the assumption that the droplets are spherical, even at close proximity is a valid one (Narsimhan, 2004; Tcholakova *et al.*, 2004).

4.5 Concluding remarks

The focus of this chapter was on the development of a methodology to examine emulsion formation during processing. Firstly, a technique based on the relationship between light reflected (Y) from the process and emulsion's properties was developed to determine the droplet size evolution in real-time. The mean droplet size showed linear dependency on the light reflectance in the semi-logarithmic diagram. Calibration curves were produced for all the dispersed phase volume fractions and emulsifier used. Owing to the fact that the presence of Tween 20 does not affect the refractive index of water, the droplet size in the absence of

added emulsifier can be determined from that of Tween 20. Additionally, since the shape/type of droplet size distributions are self-preserving in the mixing processes, they do not influence the calibration curves.

The reflectance technique benefits from its online and non-invasive nature (it does not influence the process or formulation), fast data acquisition rate and simplicity (can be used with relative ease). However, one of the main drawbacks of the technique is related to the fact that it does not provide any information regarding the droplet size distribution during processing.

An experimental procedure was designed to be able to examine droplet break-up, droplet coalescence and the equilibrium droplet size achieved by selected formulations and processing conditions. Although, a number of other methodologies were published that may provide an environment to study emulsification phenomena, the selected procedure is shown to be the most suitable to this study since not only droplet break-up and equilibrium droplet sizes can be examined, but also droplet coalescence can be solely investigated. In addition, the droplet coalescence can be directly related to the process in the first processing step. Consequently, although three steps exist in experimental procedure, all of them can be analysed in relation to each other.

In order to analyse the experimentally obtained data, using the phenomena occurring during the process, mathematical expressions were developed in order to determine the droplet break-up and coalescence rates. These expressions are particularly useful since they do not depend on the hydrodynamic condition of the system. Therefore, the uncertainties related the hydrodynamic regime of the emulsification do not influence the values.

Chapter 5

Mechanistic understanding of emulsion formation during processing: The emulsions with 50 % dispersed phase volume fraction in the presence of nonionic surfactants

This chapter describes experiments designed and performed in order to study the influence of operating parameters on emulsification when nonionic surfactants are used with 50 % dispersed phase volume fraction.

5.1 Introduction

Experiments were designed and carried out in order to investigate the oil-in-water emulsion formation containing 50 % dispersed phase volume fraction. The experimental procedure (presented in Section 4.3) was performed in the presence of a range of nonionic surfactants and processing conditions. The experimental conditions carried out in this chapter are summarised in Table 5.1.

Table 5.1. Emulsifier type and concentration used and the experimental conditions carried out in Chapter 5.

Dispersed phase volume fraction	50 %		
Emulsifier	**Type**	**Concentration**	
	Tween 20	0 %, 0.01 %, 0.02 %, 0.2 %, 0.6 % and 1 %	
	Brij 97	0 %, 0.005 %, 0.01 %, 0.02 %, 0.2 %, 0.6 % and 1 %	
Impeller speed [rpm]	**First processing step**	**Second processing step**	**Third processing step**
	800	400	800
	1600	800	1600
	2000	1000	2000

Each experiment was performed at least three times in order to establish data reproducibility, with the reported droplet sizes being the mean values from the three runs. Each of these experimental steps is interpreted individually. In order to fully analyse the data obtained from the processing experiments, a series of interfacial tension measurement and rheological studies were carried out.

It should be noted that similar results were obtained from experiments in the presence of Brij 97 to those related to Tween 20. Therefore, the experimental data are not shown in this chapter; instead they are presented in Appendix B.

5.2 Rheological studies

The importance of the influence of the viscosity of emulsion was pointed out in Section 2.3.2.2. It was shown that, the viscosity of the emulsion during processing affects the energy dissipation of the mixing system. Therefore, it is of major importance to measure the viscosities of studied systems. This was achieved by performing a series of rheological studies on the emulsions. Sampling took place at the end of the emulsification experiments. In order to examine the effect of dispersed phase volume fraction, emulsions were prepared with dispersed phase volume fractions of 10 %, 20 % and 50 %. Samples were subjected to a wide range of shear rates (0.1-1000 s^{-1}) applicable to emulsification processes. In order to investigate whether the size of the emulsions' droplets affected the viscosity of the systems, samples with 50 % dispersed phase volume fraction were repeated for two impeller speeds (800 and 2000 rpm). All emulsions were prepared with 1 % Tween 20. Samples were stable until the measurement at this concentration of Tween 20. Figure 5.1 shows the rheological results, namely the shear stress with respect to the given shear rates.

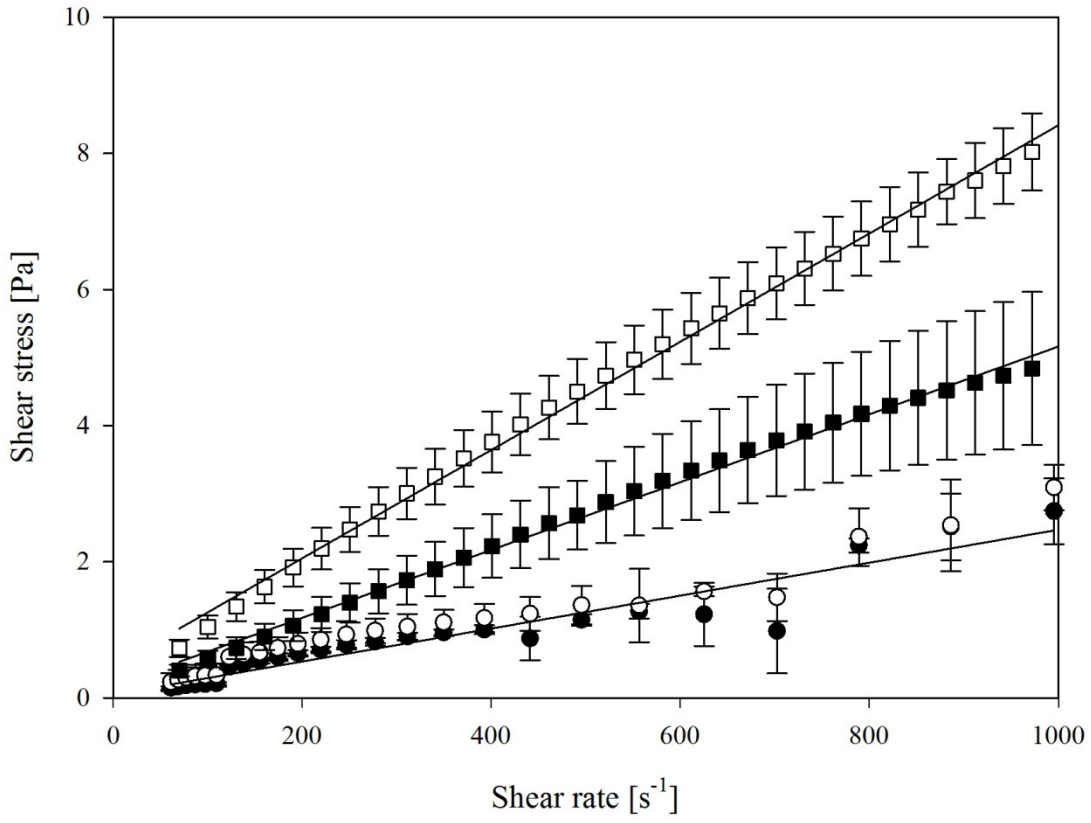

Figure 5.1. The flow-curves of shear stress in respect with shear rate are shown for oil-in-water emulsions containing various dispersed phase volume fractions produced under different processing conditions for emulsion with 10 % dispersed phase volume fraction containing 1 % Tween 20 produced under 2000 rpm impeller speed (●), emulsion with 20 % dispersed phase volume fraction containing 1 % Tween 20 produced under 2000 rpm impeller speed (○), emulsion with 50 % dispersed phase volume fraction containing 1 % Tween 20 produced under 800 rpm impeller speed (■) and emulsion with 50 % dispersed phase volume fraction containing 1 % Tween 20 produced under 2000 rpm impeller speed (□).

It can be seen that the shear stress increased with the shear rate for all measurements. Data related to the emulsions with 10 % and 20 % dispersed phase volume fraction showed a notable level of noise for shear rates of about 100 s^{-1}. This was due to the low viscosity of these emulsions which were close to the lower limit of the resolution of the rheometer; hence noisy results were generated for these emulsions. Nonetheless, these emulsions were showing a Newtonian behaviour, thus, the flow curves were fitted well by linear equations with viscosity of ~0.002 Pa.s for both cases ($R^2 \approx 0.98$).

Emulsions with 50 % dispersed phase volume fraction, on the other hand, show a weak shear thinning behaviour. Due to the determination of a high power-law index (j=0.91, R^2=0.978), when a power-law equation (equation 3.2) is fitted to the data, in these studies it is assumed that they behave as Newtonian fluids. Therefore, a linear (related to Newtonian fluids) was fitted to the data (R^2=0.976) and viscosity of ~0.0085 Pa.s was determined

In addition, the emulsions with 50 % dispersed phase volume fraction were processed at different impeller speeds, thus having different droplet sizes. The impeller speeds of 800 rpm resulted in emulsions with droplet sizes of 100 μm and the impeller speeds of 2000 rpm resulted in 30 μm droplet sizes. The emulsions with larger droplets resulted in lower viscosity than the ones related to emulsions with lower droplet sizes. Similar dependency was previously observed by Chanami and McClements (2000) and Krynnke *et al.* (2004). This is a consequence of the transmission of the tangential stress from the continuous phase across the interface of droplets. This results in a circulation in the droplets which was opposed by viscous stresses inside the droplets. Therefore, in the case of smaller droplets, a more packed structure is adopted, which increases the interfacial area and hence higher viscous dissipation, resulting in a higher observed viscosity. It should be noted that, the viscosities of the emulsions with smaller droplet sizes were used to consider the effect of viscosity on the energy dissipation of the system, since they resulted in higher viscosities and hence the extreme case is assumed.

5.3 Interfacial tension studies

One of the most important parameters affecting droplet break-up and coalescence is the interfacial tension. Therefore, in order to determine the influence of the surfactant on the interfacial tension, it was measured for oil and water phase interfaces containing the same

components as the ones used in emulsification studies. Figure 5.2 shows the interfacial tension between oil and aqueous phase containing varying concentrations of Tween 20.

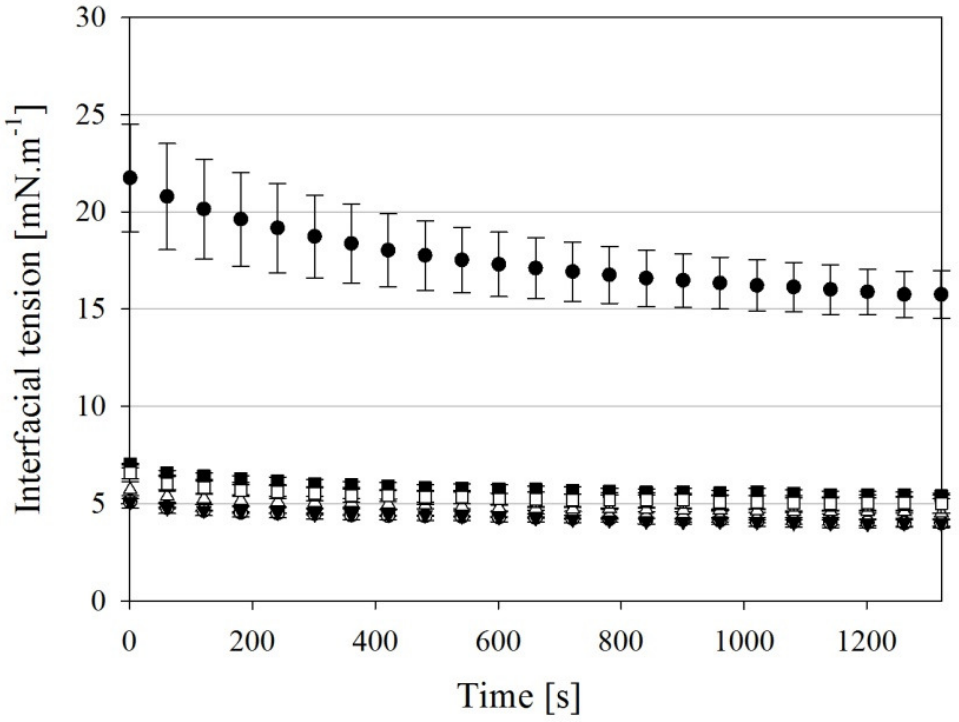

Figure 5.2. Interfacial tension measured at the oil and water interface in the absence of added emulsifier 0 % (●) and in presence of 0.01 % (□), 0.02 % (■), 0.2 % (Δ), 0.6 % (▼) and 1 % (○) concentrations of Tween 20.

The interfacial tensions measured in the presence of varying concentrations of Tween 20 are given in Figure 5.2. The high value of interfacial tension is reported in the absence of added emulsifier; subsequently it decreases up to a Tween 20 concentration of 0.01 % and remains constant by further increase in Tween 20 concentration (up to 1 %). This is as expected since the concentrations used in these experiments are all above the *cmc* value of Tween 20 (~0.006 %). It should be noted that, the interfacial tensions measured with the tensiometer are different to the ones during processing. The interfacial area during these experiments is constant, whereas it is markedly higher during processing. The higher interfacial area produced during processing of the emulsions with higher volume fractions of

the dispersed phase results in higher adsorption times, a lower amount of 'free' Tween 20 in the aqueous phase and hence higher interfacial tensions. This was previously demonstrated by measuring the 'dynamic' interfacial tension. For example, Fainerman *et al.* (1994) showed that a nonionic surfactant at a concentration of five times its *cmc* value had an interfacial tension closer to that of pure water than the equilibrium value after 30 ms. Moreover, it has been stated that the interfacial tension during processing can be as low as half the respective equilibrium interfacial tension (Walstra and Smulders, 1998).

5.4 Emulsification experiments

5.4.1 First processing step

The experimental data related to the first processing step are presented and analysed in this section.

5.4.1.1 Droplet size evolution data

Figure 5.3 shows the droplet size evolution data obtained from the first processing step of the emulsification experiments with 50 % dispersed phase volume fraction in the presence of varying concentrations of Tween 20 processed under a range of impeller speeds of 800 rpm (5.3-a), 1600 rpm (5.3-b) and 2000 rpm (5.3-c).

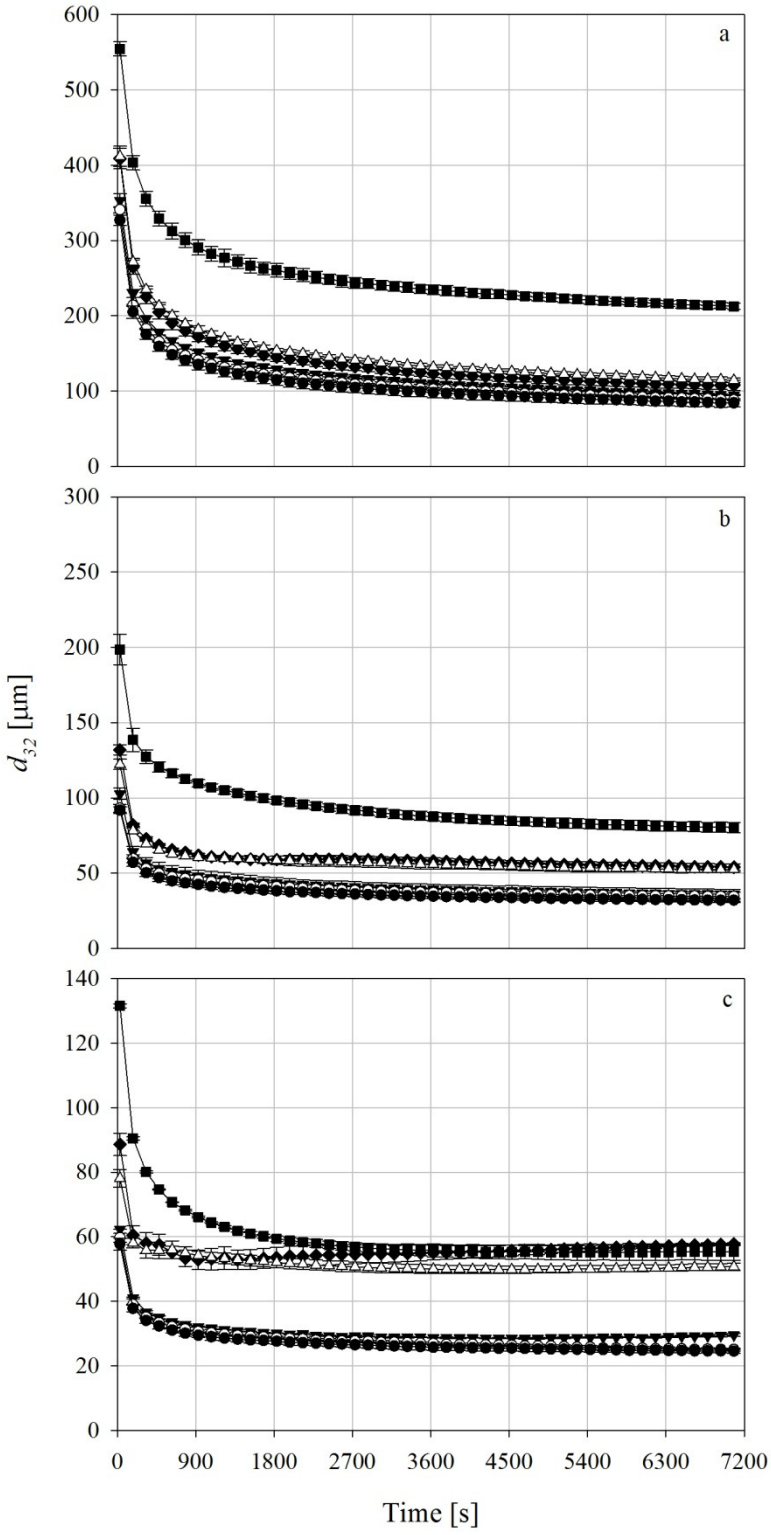

Figure 5.3. Droplet size evolution data obtained from the first processing step of emulsification experiments with 50 % dispersed phase volume fraction in the absence of added emulsifier (■) and in the presence of 0.01 % (▲), 0.02 % (Δ), 0.2 % (▼), 0.6 % (○) and 1 % (●) concentrations of Tween 20 under different impeller speeds of (a) 800 rpm, (b) 1600 rpm and (c) 2000 rpm.

As can be seen in Figure 5.3, this processing step can be characterised by three distinct regions in all experimental cases; a rapid decrease of the droplet size, where droplet break-up is dominant, which is followed by the plateau region caused by the dynamic balance between droplet break-up and coalescence events. Moreover, a region can be observed which forms the transition between the rapid decrease and the plateau regions. Each of these regions are analysed individually in the following sections.

5.4.1.1.1 Rapid decrease region

In the first part of the droplet size evolution, droplet sizes rapidly decrease due to the high number of droplet break-up events in the initial stages of the process. Therefore, the droplet break-up can be studied individually at this stage. In the other stages the droplet size is also affected by droplet coalescence. The phenomenon of droplet break-up depends on the droplet size at the initial stage of the first processing step, since it is likely that break-up events continue until the size of droplet is small enough for flow fluctuations to have minimal effect on droplet break-up. Thus, Figure 5.4 shows the initial droplet sizes and break-up frequencies with respect to concentration for various experimental cases. The droplet break-up frequencies of all experimental conditions are calculated using equation 4.12.

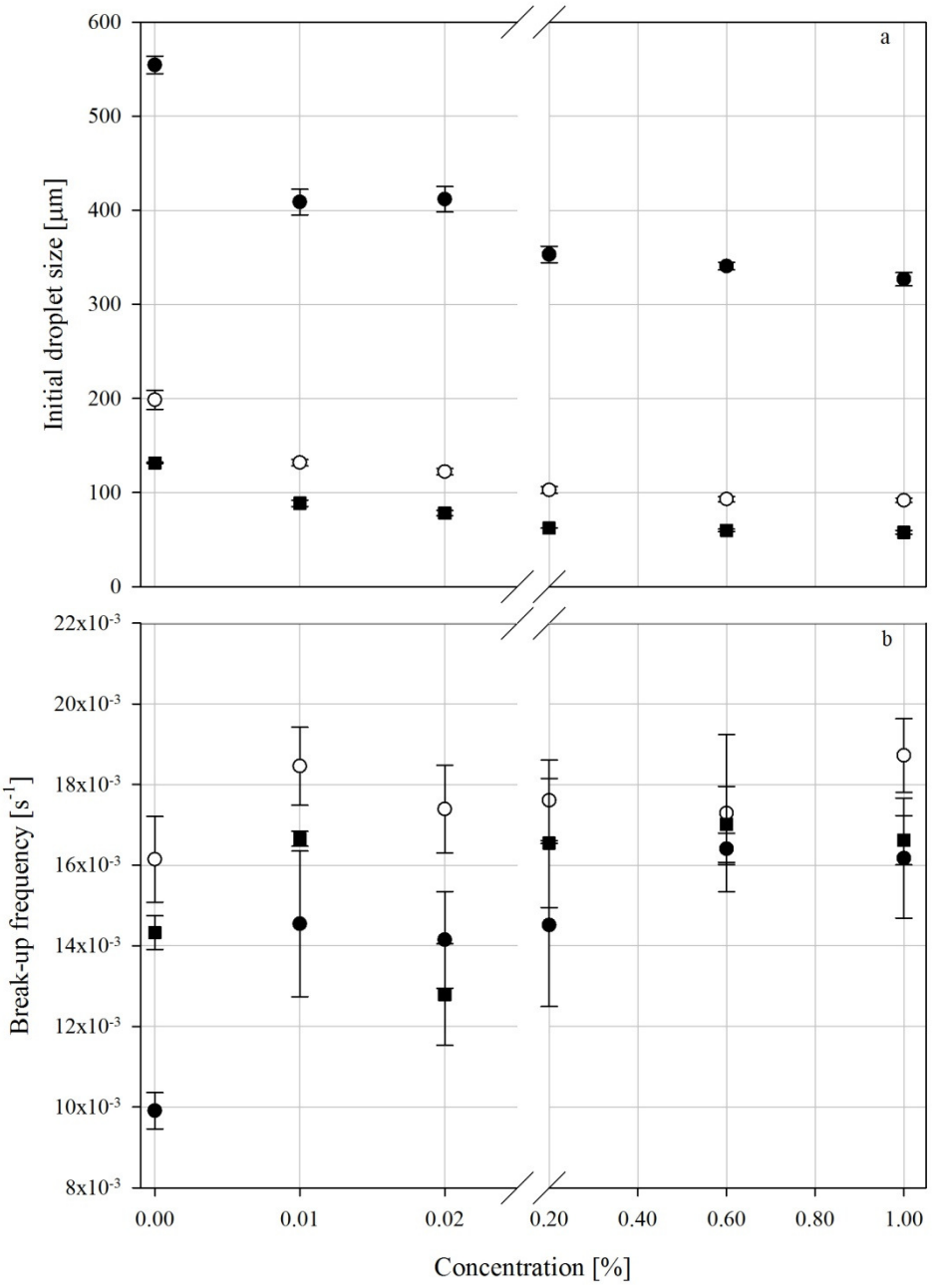

Figure 5.4. Initial droplet size (a) and break-up frequencies (b) calculated at the initial stages of the first processing step of experiments with respect to concentration of Tween 20 for impeller speeds of 800 rpm (●), 1600 rpm (○) and 2000 rpm (■).

It can be seen in Figure 5.4-a that the initial droplet sizes are lower when the surfactant concentration is increased to ~0.02 %, and this is followed by a plateau section where no significant changes are observed by a further increase in surfactant concentration. However, Figure 5.4-b shows that the break-up frequency is low when no emulsifier is used,

and then it increases marginally by increasing surfactant concentration until a threshold value (0.02 % in both cases), which then does not change to any further extent with surfactant concentration.

As it has been previously mentioned, the droplets break down when the inertial stresses overcome the capillary pressure of the droplets. Therefore, similar droplet break-up frequencies with respect to Tween 20 concentration at any given impeller speed might be caused by the similar capillary pressures induced by those systems. Assuming two cases of Tween 20 concentration of 0.01 and 1 % processed under 800 rpm impeller speed, inducing similar capillary pressure by these systems results in:

$$P_{cap}{}_{0.01\,\%} = P_{cap}{}_{1\,\%} \rightarrow \frac{d_{32}{}_{0.01\,\%}}{d_{32}{}_{1\,\%}} = \frac{\sigma_{0.01\,\%}}{\sigma_{1\,\%}} \quad (5.1)$$

where $P_{cap}{}_{0.01\,\%}$ and $P_{cap}{}_{1\,\%}$ are the capillary pressures, $\frac{d_{32}{}_{0.01\,\%}}{d_{32}{}_{1\,\%}}$ is the ratio of the initial droplet sizes and $\frac{\sigma_{0.01\,\%}}{\sigma_{1\,\%}}$ is the ratio of the interfacial tensions on the droplets when 0.01 % and 1 % Tween 20 is employed. By using the values in Figure 5.4-a, $\frac{d_{32}{}_{0.01\,\%}}{d_{32}{}_{1\,\%}}$ results in ~1.2 which is more or less the same as experimentally determined $\frac{\sigma_{0.01\,\%}}{\sigma_{1\,\%}}$ (from Figure 5.2 it results ~1.12). This dependency can be observed by all the experiments under varying impeller speeds. This indicates that the similar capillary pressure is the cause of the observed dependency.

Figure 5.4-b shows that the increase in impeller speed does not significantly affect the droplet break-up rate, although the initial droplet size is lower at higher impeller speeds (Figure 5.4-a). It can be deduced that although higher inertial stresses are expected at higher impeller speeds, the higher capillary pressure induced by smaller droplets at higher impeller speeds results in similar break-up frequencies. Considering experiments with 1 % Tween 20

processed under 800 and 2000 rpm, if their respective interfacial tensions are similar, then $\frac{P_{cap_{800\,rpm}}}{P_{cap_{2000\,rpm}}}$ results in ~6.4 showing the increase in capillary pressure.

A question arises regarding the observation of lower initial droplet sizes at higher impeller speeds. As previously mentioned, the observed initial droplet size is the first measurement obtained from experiments after dispersed phase was added to the mixing tank. Therefore, the initial droplet size is a result of daughter droplet size production. The number and size of daughter droplets resulting from droplet break-up is a function of energy experienced by the droplets (Tsouris and Tavlarides, 1994; Tcholakova *et al.*, 2007c). Therefore, higher impeller speed results in higher energy dissipation which consequently results in smaller and more daughter droplets from breaking a mother droplet.

5.4.1.1.2 Transitional region

The droplet size evolution data, presented in Figure 5.3, shows that in most cases there is a smooth transition between the rapid decrease and plateau regions. However, a peculiar behaviour can be seen for some experimental conditions, more specifically, in cases with low emulsifier concentration processed at higher impeller speeds. Systems of higher emulsifier concentrations, under the same processing conditions, but also those systems processed at 800 rpm, regardless of emulsifier content, were seen to enter the plateau region, with droplet sizes decreasing until the completion of the first processing step. In contrast, the droplet size in systems with 0.01 % and 0.02 % Tween 20 processed at 1600 rpm, after an initial rapid decrease, appears at first to increase slightly and to then remain constant (Figures 5.3-b and 5.3-c). This is more evident for systems with 0.01 % and 0.02 % Tween 20 processed at 2000 rpm, where the droplet size, after again an initial rapid decrease, exhibits a gradual increase, which is maintained until the end of the first processing step.

The reason is hypothesised to relate to the intense processing conditions involved, which act to decrease the emulsion's droplet size rapidly. This results in a considerable increase in the interfacial area of the system, which in turn significantly 'depletes' this low concentration of emulsifier (for example 0.01 % Tween 20) and decreases the rate of adsorption of Tween 20. Under these conditions, coalescence events are promoted and the droplet size is increased. This increase is only temporary for some cases, as equilibrium between droplet break-up and coalescence is eventually reached. On the other hand, the droplet size in the other cases is increased permanently as equilibrium between the two sub-processes is not reached within the time scale of the experiment; as seen in, for example, Figure 5.3-c, where the droplets that form the emulsion at such low emulsifier concentration even reach, at the end of the processing step, the size of the droplets in those experiments where no emulsifier is used.

In order to test the proposed hypothesis, the following experiment was performed. An emulsion, again with a dispersed phase volume fraction of 50 %, containing 0.01 % Tween 20 was processed at 400 rpm for five hours. The impeller speed was subsequently increased to 800 rpm for a further five hours and finally it was increased again to 1600 rpm for two hours (Figure 5.5). The specific experiment was designed to gradually increase the hydrodynamic conditions experienced by the system, thus providing enough time for surfactant adsorption and configuration at the interface; the obtained droplet size evolution data are shown in Figure 5.5. What is demonstrated is that, by progressively (and not directly as in the first processing step) introducing the system to the hydrodynamic conditions induced by the 1600 rpm impeller speed, the local coalescence region that was previously observed (for the case with 0.01 % Tween 20) is no longer present, although the final droplet size in both cases is more or less the same. By increasing the impeller speed in stages, the excess of interfacial area,

created in the case of the intense hydrodynamic conditions is never reached and the equilibrium droplet size is, in this case, gradually approached (Figure 5.5).

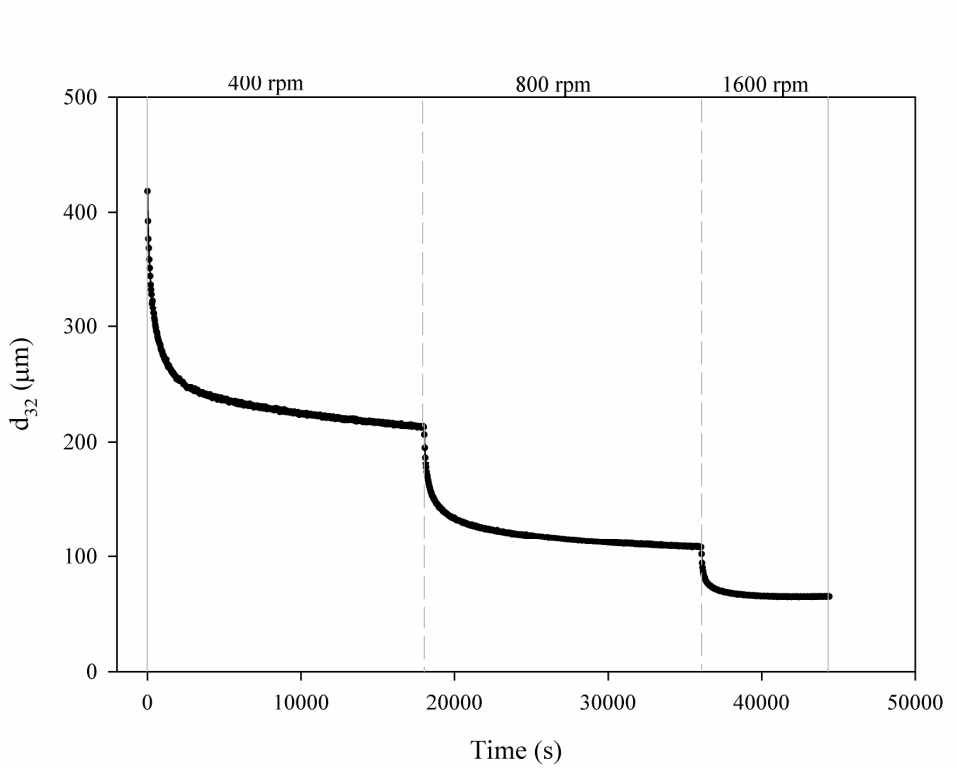

Figure 5.5. Oil-in-water emulsion containing 0.01 % Tween 20 subjected to a gradual impeller speed increase (400 rpm → 800 rpm → 1600 rpm).

5.4.1.1.3 Plateau region

After the initial stages and as the processing proceeds in time, the rate of change in droplet size evolution is reduced (Figure 5.3), since the droplets break down to a smaller size so that they are less affected by fluid fluctuations, resulting in a decrease in droplet break-up frequency. This is a direct result of the droplet break-up mechanism in the turbulent regime. This mechanism is fully explained in Section 2.3.2.1. When droplet sizes are reduced, their respective capillary pressure increases and smaller eddies containing lower energy would affect them. Therefore, the rate of droplet break-up reduces. On the other hand, a decrease in the size of the droplets increases the number of droplets thus resulting in an increased probability of droplet coalescence. As emulsification proceeds, the effect of droplet

coalescence on the mean droplet size increases and tends to increase the droplet size in opposition to droplet break-up. The dynamic equilibrium between these two phenomena results in the final droplet size that is produced at the end of the first processing step. The final droplet sizes achieved with different experimental conditions are presented in Figure 5.6.

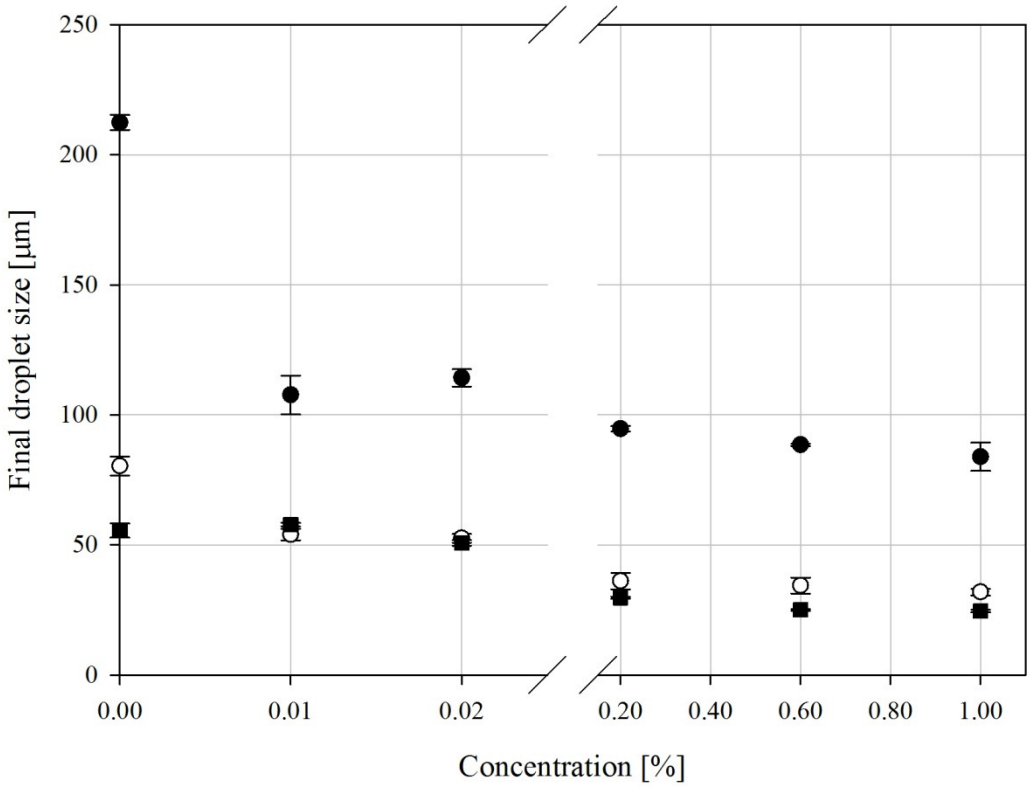

Figure 5.6. Droplet sizes determined at the end of the first processing step of experiments with respect to concentrations of Tween 20 for varying impeller speeds of 800 rpm (●), 1600 rpm (○) and 2000 rpm (■).

The equilibrium droplet size is affected by both the hydrodynamic conditions of the process as well as the emulsifier concentration used (Figure 5.6). As the concentration of Tween 20 is progressively increased (< 0.2 %), the equilibrium droplet size decreases, but when the emulsifier concentration is increased further (≥ 0.2 %) the droplet size does not change significantly.

It is generally believed (Walstra, 1993; Tsouris and Tavlarides, 1994; Windhab *et al.*, 2005) that Tween 20 would affect the final droplet size through two different processes. When a new droplet is formed due to the droplet break-up, Tween 20 is adsorbed on the interface. Upon adsorption, Tween 20 would suppress the droplet coalescence caused by the probable collision of droplets and, in addition, it would reduce the interfacial tension, which in turn would increase the rate of droplet break-up. In order to thoroughly investigate the effect of Tween 20 and to understand which surfactant role is more significant in the process, Table 5.2 given below shows the amount of Tween 20 remaining in the solution, the interfacial area of droplets and the time required for surfactant to adsorb on the naked interface of the droplet. These parameters are estimated using the equations given in Chapter 4.

Table 5.2. Interfacial area produced in various conditions, amount of Tween 20 remaining in the solution and the time needed for Tween 20 to be adsorbed on the newly made droplet.

Impeller speed [rpm]	Tween 20 concentration [%]	d_{32} [µm]	Interfacial area of the droplets [m^2]	Tween 20 remaining in the solution [%]	Adsorption time [s]
800	0.00	211.99	3.80	0.000	NA
	0.01	107.60	7.49	0.002	14.867
	0.02	114.03	7.06	0.013	1.953
	0.20	94.61	8.52	0.187	0.168
	0.60	88.47	9.12	0.562	0.060
	1.00	83.84	9.62	0.993	0.036
1600	0.00	80.30	10.05	0.000	NA
	0.01	53.97	14.95	0.000	NA
	0.02	52.52	15.36	0.007	2.794
	0.20	36.06	22.37	0.177	0.165
	0.60	34.36	23.48	0.551	0.056
	1.00	31.87	25.32	0.981	0.034
2000	0.00	55.45	14.55	0.000	NA
	0.01	57.91	13.95	0.000	NA
	0.02	50.72	15.91	0.007	2.194
	0.20	29.62	27.23	0.173	0.147
	0.60	24.98	32.31	0.545	0.055
	1.00	24.54	32.88	0.976	0.031

Table 5.2 shows that the interfacial area produced by each experiment increases with Tween 20 concentration and impeller speed. This is a consequence of higher break-up rates, which is expected at higher impeller speed and/or Tween 20 concentrations. When higher impeller speeds are employed (for example 2000 rpm), higher energy dissipation results, which, in turn, results in smaller droplet sizes. On the other hand, when a higher concentration of Tween 20 is used, more surfactant is available for droplets and less energy is needed for them to break. It can be seen that in comparison with the initial concentration, a high amount of surfactant still remains in the aqueous phase.

Table 5.2 further shows that for experiments with concentrations of 0.01 % and 0.02 % Tween 20 processed at 1600 rpm and 2000 rpm, almost all the surfactant in the systems is adsorbed. This indeed demonstrates that there would be no surfactant left at lower droplet sizes to cover their interfaces and hence higher droplet coalescence is expected. In addition, this dependency further demonstrates the depletion effect observed in these experiments in the transitional region of the droplet size evolution data. On the other hand, it can be seen that not only Tween 20 is depleted at above-mentioned experiments, but also significantly larger adsorption times are observed.

From Table 5.2 it can be deducted that depletion of the surfactant acts to decrease the break-up rate and to increase the droplet coalescence rate, and the high adsorption rates are responsible for the behaviour observed in Figure 5.6. Furthermore, Table 5.2 shows that, at low concentration and intense hydrodynamic conditions, the final droplet sizes are a function of the surfactant's concentration alone and not the hydrodynamic condition. This phenomenon has been previously reported by Tcholakova *et al.* (2004) in which it was indicated that at

lower concentrations of Tween 20 the droplet size is determined by the interfacial area that can be covered by emulsifier, regardless of the hydrodynamic condition of the process.

Nonetheless, Figure 5.6 further shows that the final droplet sizes are not significantly changed by increasing the impeller speed from 1600 rpm to 2000 rpm. This may be a consequence of the dampening effect of the dispersed phase, which reduces the effect of the energy dissipation rate. Moreover, similar droplet sizes are observed in Figure 5.6 for lower concentrations of Tween 20 and the experiment in the absence of added emulsifier (for example experiments in the absence of added emulsifier and 0.01 % of Tween 20 processed at 1600 rpm). This is, once more, a consequence of the depletion of the Tween 20 under the intense hydrodynamic condition, which is fully addressed in Section 5.5.1.2.

5.4.2 Second processing step

In the second processing step, the impeller speed is reduced to half of that in the first step in order to create processing conditions where droplet coalescence, rather than droplet break-up, is now the dominant phenomenon. The data obtained from the second step of experiments and subsequent analyses are presented in this section.

5.4.2.1 Droplet size evolution data

The droplet size evolution data obtained from the second processing step of experiments are presented in Figure 5.7. It shows the droplet size evolution of experiments with various concentrations of Tween 20 processed under different impeller speeds of 800-400 rpm (5.7-a), 1600-800 rpm (5.7-b) and 2000-1000 rpm (5.7-c).

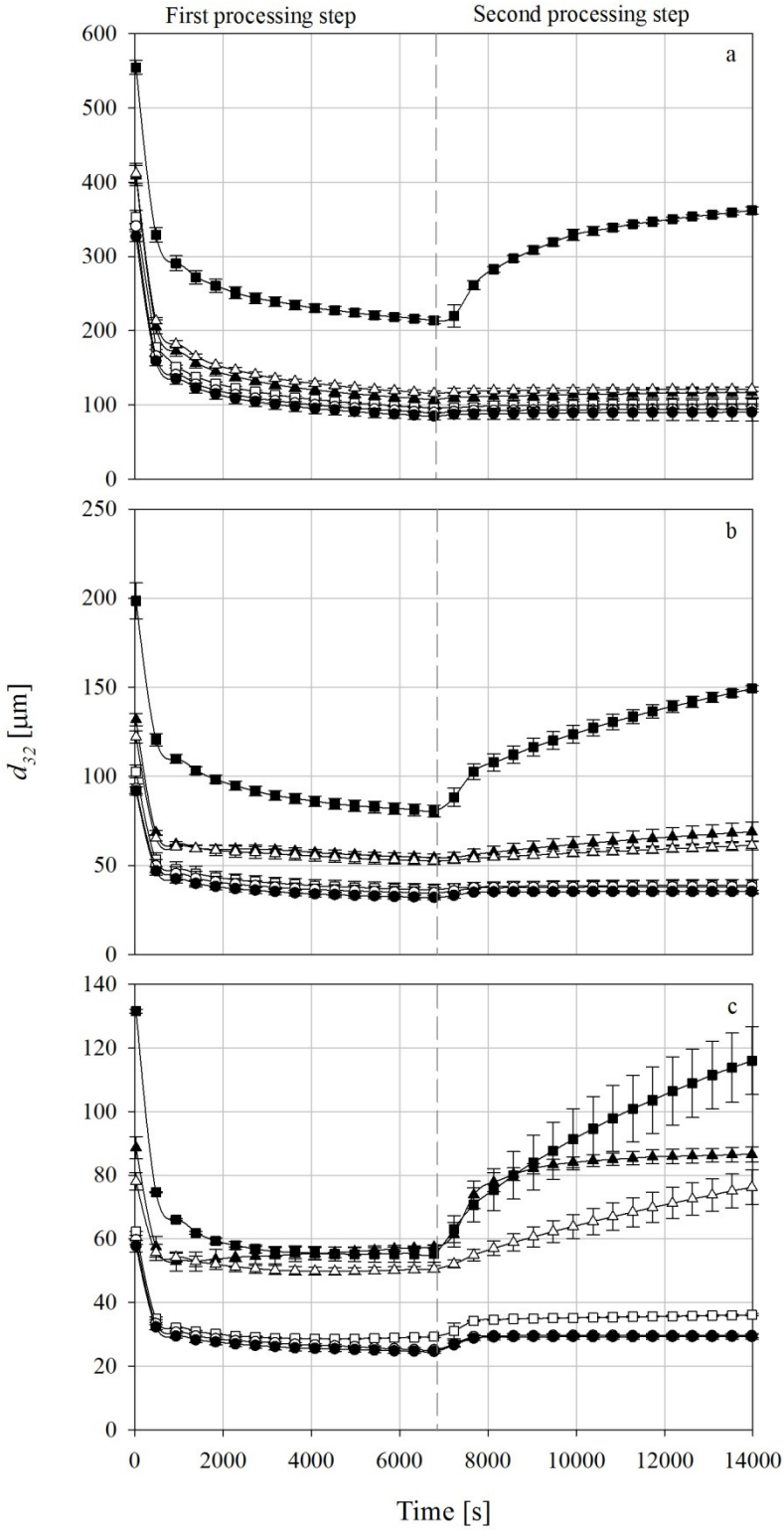

Figure 5.7. Droplet size evolution data obtained from the first and the second processing steps of emulsification experiments with 50 % dispersed phase volume fraction in the absence of added emulsifier (■) and in the presence of 0.01 % (▲), 0.02 % (Δ), 0.2 % (▼), 0.6 % (○) and 1 % (●) concentrations of Tween 20 under different impeller speeds of (a) 800-400 rpm, (b) 1600-800 rpm and (c) 2000-1000 rpm.

The behaviour displayed in Figure 5.7 (for all experimental conditions) is highly dependent not only on the emulsifier concentration in the system, but also on the hydrodynamic conditions involved. For the lower emulsifier concentration systems (≤ 0.02 % of surfactant) the droplet size evolution increases considerably and is affected by the induced processing conditions (impeller speed). On the other hand, for the higher emulsifier concentration systems (≥ 0.2 % of surfactant), the droplet size at the beginning and the end of the step is unaffected by the emulsifier content and the changes in hydrodynamic conditions.

Moreover, emulsions prepared with low concentrations of surfactant show different behaviour, where the droplet size evolution data (at the initial stages of the second processing step) demonstrate an increase in the droplet sizes that are larger than those determined by emulsion without added surfactant. However, these experiments quickly reach an equilibrium value which is lower than equilibrium values that are obtained in experiments in the absence of added surfactant. This behaviour is more evident for lower concentrations of surfactant processed under higher impeller speeds. For example, the emulsions processed under 2000-1000 rpm with 0.01 % Tween 20 (Figure 5.7-c) exhibit such behaviour. These behaviours relate directly to the occurrence of coalescence in the system in the early stages of the second processing step.

5.4.2.2 Droplet coalescence

In order to further investigate these observed behaviours, droplet coalescence frequencies during the second processing step were calculated from the obtained droplet size evolution data by equations 4.16. Figure 5.8 shows the calculated coalescence frequencies with respect to Tween 20 concentration for experiments performed under varying impeller speeds.

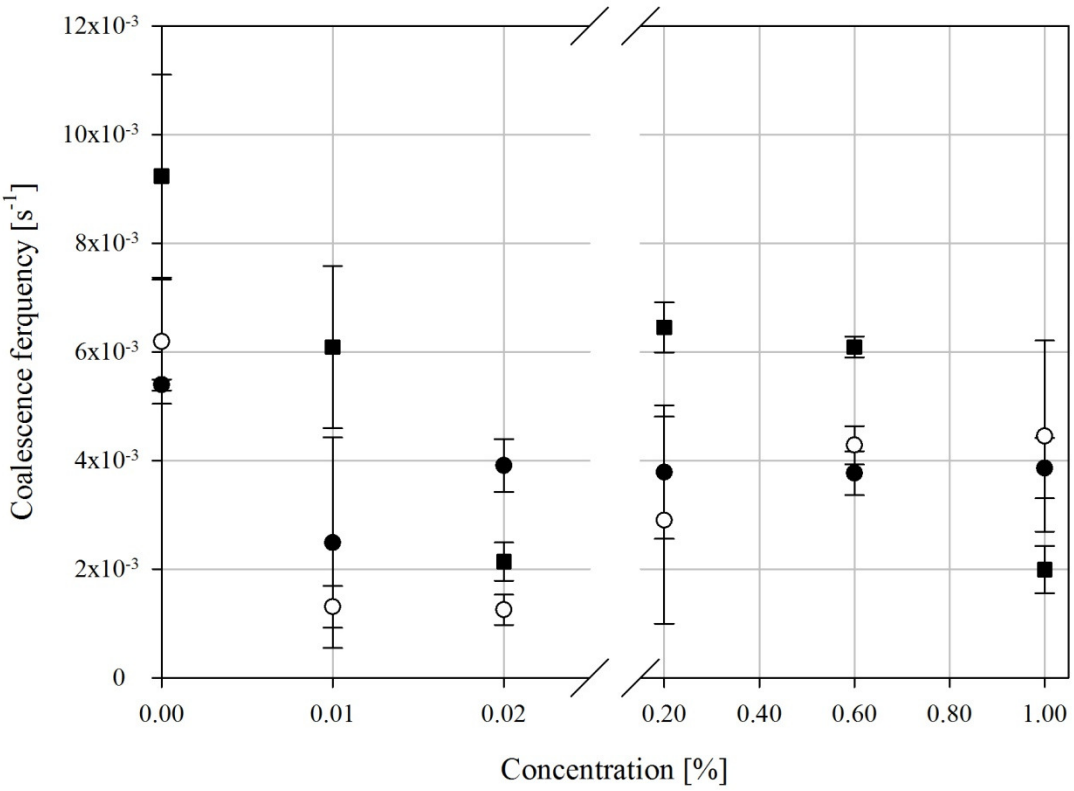

Figure 5.8. Coalescence frequencies at the initial stages of the second processing step of experiments with respect to varying concentrations of Tween 20 for varying impeller speeds of 800-400 rpm (●), 1600-800 rpm (○) and 2000-1000 rpm (■).

It can be seen in Figure 5.8 that the coalescence frequencies calculated for experiments in the absence of added surfactant are higher than the experiments in the presence of Tween 20. Moreover, Figure 5.8 shows that the coalescence frequency related to the experiments with impeller speed of 800-400 rpm decreases with increasing surfactant concentration, until a concentration of 0.02 %, after which it then remains unchanged. However, although similar behaviour is observed for experiments related to 1600-800 rpm impeller speeds, and droplet coalescence frequency reduces by increasing surfactant concentration up to a concentration of 0.02 %, the coalescence frequency increases and then remains more or less the same for higher surfactant concentrations (≤0.2 %). The same can be observed for the experiments performed with impeller speeds of 2000-1000 rpm. In addition,

it can be seen in Figure 5.8 that coalescence frequency increases with higher impeller speeds (except for concentration of 0.02 % Tween 20). In order to understand the effect of energy input and surfactant concentration on the observed behaviour of droplet coalescence, the behaviour of collision rates as well as the collision efficiency for the systems in this study should be investigated.

5.4.2.2.1 Collision rate and collision efficiency

Collision rates corresponding to each experiment were calculated by equation 4.19 and collision efficiencies were subsequently determined by employing equation 4.14. Figure 5.9 presents the calculated collision rates in respect of Tween 20 concentration for various hydrodynamic conditions.

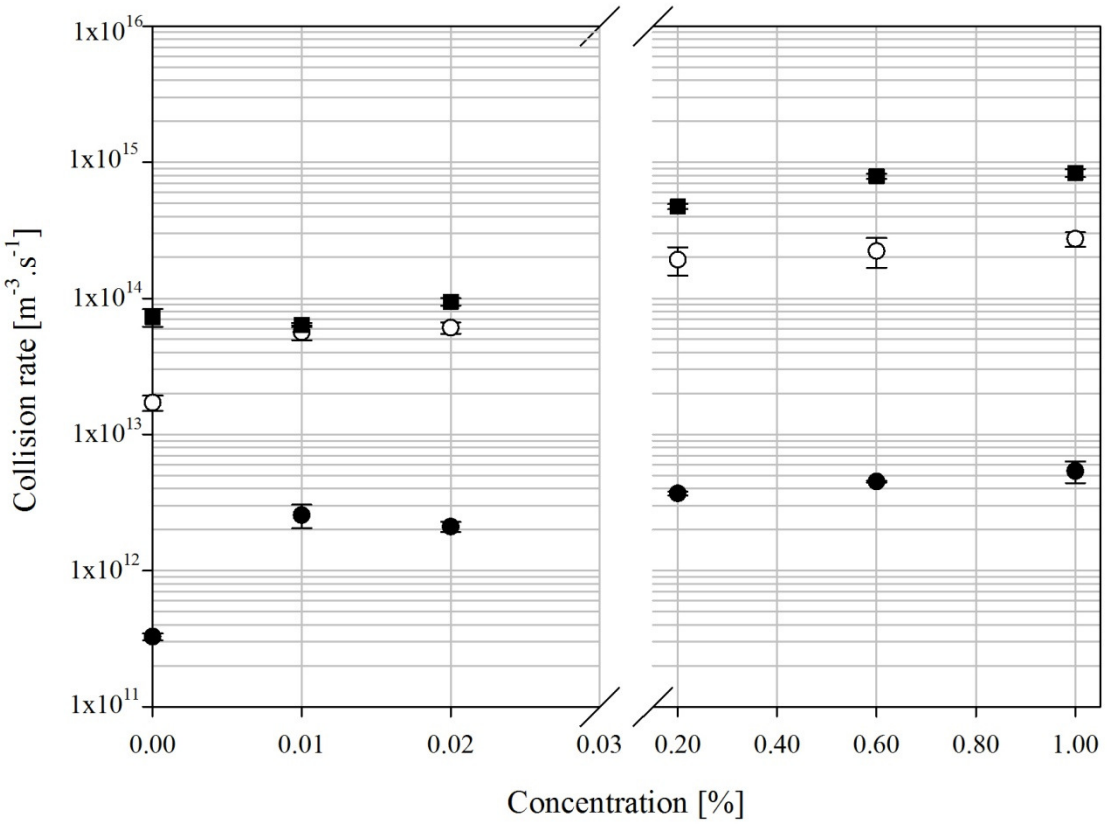

Figure 5.9. Collision rates calculated at the initial stages of the second processing step of experiments with respect to varying concentrations of Tween 20 for varying impeller speeds of 800-400 rpm (●), 1600-800 rpm (○) and 2000-1000 rpm (■).

Figure 5.9 shows that the collision rates progressively increase with increasing surfactant concentration. This is more evident in the experiments carried out under 800-400 rpm impeller speeds. In addition, it can be seen that the collision frequencies at higher impeller speeds (1600-800 and 2000-1000 rpm) are similar and lower values are reported for the ones related to experiments with 800-400 rpm impeller speeds. The reason for the increase in collision rate is related to the batch operating mode of the process. As a higher Tween 20 concentration and/or impeller speed is employed, smaller droplet sizes are produced, which in turn increases the number of droplets, consequently, the collision rate increases. It should be noted that the collision rates determined at lower concentrations of surfactants (≤ 0.02 %) are one order of magnitude smaller than those determined at higher concentrations. This may be one of the reasons for the above mentioned sudden increase in coalescence frequency observed in Figure 5.8, by increasing surfactant concentration from 0.02 % to 0.2 %.

Nonetheless, interestingly, the data presented in Figure 5.9 suggest that the droplet coalescence should in fact increase by increasing Tween 20 concentration and impeller speed, especially as the collision rate of 1 % Tween 20 is one order of magnitude larger than that in the absence of Tween 20. Investigating collision efficiency may result in an understanding of the reasons for the observed dependency. Figure 5.10 shows the calculated collision efficiencies with respect to employed concentrations of Tween 20 for experiments performed under varying impeller speeds.

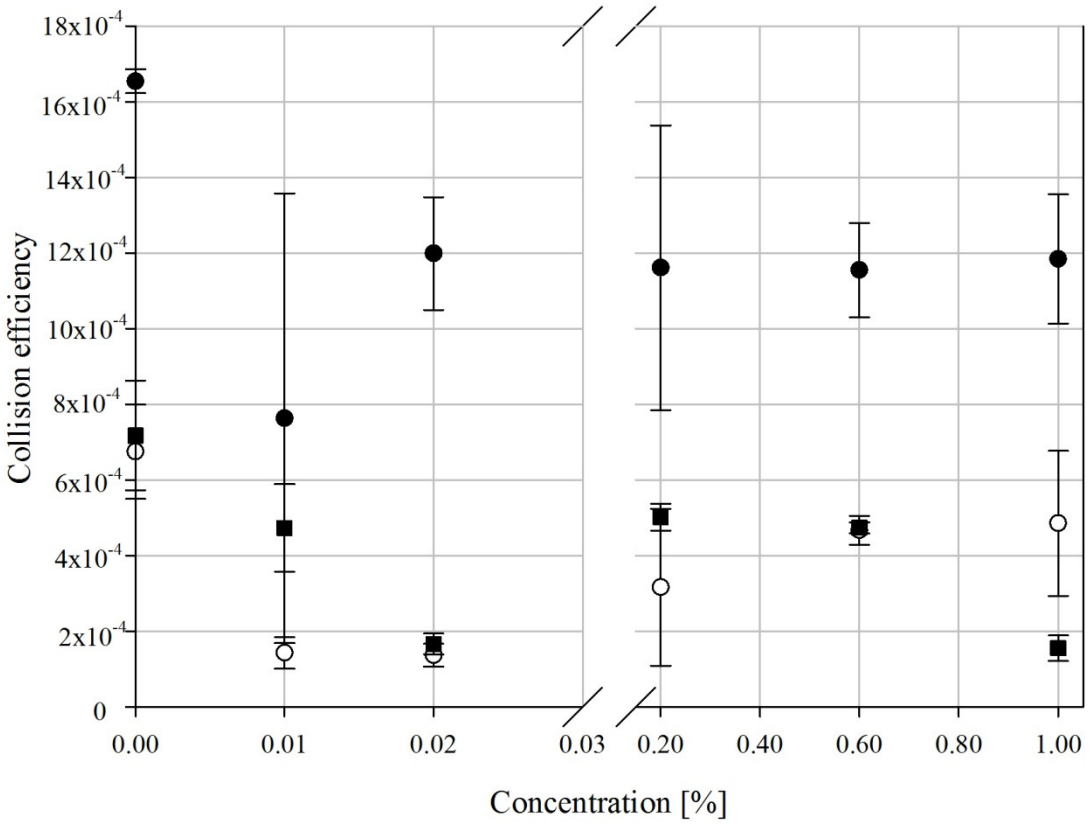

Figure 5.10. Collision efficiencies calculated at the initial stages of the second processing step of experiments with respect to varying concentrations of Tween 20 for varying impeller speeds of 800-400 rpm (●), 1600-800 rpm (○) and 2000-1000 rpm (■).

It can be seen in Figure 5.10 that the experiments with impeller speeds of 1600-800 and 2000-1000 rpm show a decrease in collision efficiency with a further increase in surfactant concentration up to 0.02 %, and then it remains unchanged with increasing concentration but at the higher value of collision efficiency (surfactant concentration ≥ 0.2 %). However, this is not the case for experiments performed at an impeller speed of 800-400 rpm. In these experiments a high value is reported when no emulsifier is employed, then a lower value at 0.01 % Tween 20, which then increases at 0.02 % Tween 20. Subsequently, the collision efficiency remains constant with further increase in surfactant concentration.

In order to investigate the dependencies of collision efficiency with impeller speed and Tween 20 concentration, the physical mechanism that collision efficiency represents,

which is given in section 4.4.5, should be considered. In order to investigate the effect of each parameter individually, the mean turbulent force, continuous film thickness and the radius of flattened area are determined, all of which are given in Table 5.3 with respect to surfactant concentrations at all the experimental conditions.

Table 5.3. Estimated parameters responsible for collision efficiency.

Impeller speed [rpm]	Tween 20 Concentration [%]	d_{32} [µm]	Capillary pressure [Pa]	Turbulent force [x10^{-10} N]	Film thickness [x10^{-9} m]	Film radius [x10^{-13} m]
400	0.00	211.99	376.72	8.30	6.6	7.0
	0.01	107.60	204.45	1.40	3.9	2.1
	0.02	114.03	192.63	1.60	4.6E	2.6
	0.20	94.61	190.24	0.96	3.4	1.6
	0.60	88.47	180.83	0.80	3.2	1.4
	1.00	83.84	190.84	0.70	2.8	1.2
800	0.00	80.30	996.16	2.50	2.0	7.9x10^{-1}
	0.01	53.97	407.61	8.50	2.5	6.7 x10^{-1}
	0.02	52.52	418.84	0.79	2.3	6.0 x10^{-1}
	0.20	36.06	499.09	0.29	1.0	1.9 x10^{-1}
	0.60	34.36	465.62	0.26	1.0	1.8 x10^{-1}
	1.00	31.87	502.03	0.21	0.8	1.3 x10^{-1}
1000	0.00	55.45	1442.55	1.40	1.1	3.2 x10^{-1}
	0.01	57.91	380.57	1.60	4.7	1.3
	0.02	50.72	433.70	1.10	3.3	8.4 x10^{-1}
	0.20	29.62	607.35	0.27	0.9	1.4 x10^{-1}
	0.60	24.98	640.52	0.17	0.7	8.6 x10^{-2}
	1.00	24.54	651.91	0.16	0.6	8.0 x10^{-2}

It can be seen that by increasing surfactant concentration, the mean turbulent force, thickness of entrapped continuous phase and the radius of flattened area of droplets all decrease as a consequence of smaller droplet size at higher surfactant concentrations. It is expected that the amount of continuous film captured between colliding droplets would play the major role on collision efficiency dependency on surfactant concentration. This hypothesis cannot be used to interpret the data observed in Figure 5.10. For example, high collision

efficiency is observed in experiments in the absence of added surfactant, even though a higher amount of continuous phase is captured. This can best be justified by the fact that, in these experiments there is no surfactant on the interface of droplets and as a result higher collision efficiency is observed. This hypothesis can be used to justify other cases as well. For example, similar collision efficiencies are observed when lower (0.01 % and 0.02 %) and higher (0.2 %, 0.6 % and 1 %) concentrations of surfactant are used, since similar droplet sizes are produced and the amount of captured continuous phase is similar and hence the existence of surfactant on the interface then plays the major role.

In addition, despite the fact that a higher collision rate is obtained when the impeller speed is increased the collision efficiency is decreased, which can be related to the higher capillary pressures of droplets at higher impeller speeds (lower droplet size) and smaller shear stresses on the smaller droplets. These parameters reduce the probability of drainage rate despite the smaller amount of continuous phase captured between two colliding droplets.

5.4.2.3 Emulsion response to coalescence dominant regime

Now that droplet coalescence is thoroughly analysed, it is worth investigating the reasons behind the droplet size evolution behaviour observed in Figure 5.8, as droplet coalescence observed in the initial stages of the second processing step may be responsible for the rapid increase in droplet sizes seen in the absence of added emulsifier or low (0.01 % and 0.02 %) concentration of Tween 20. In order to aid the analysis, the droplet size increase caused by impeller speed change in the second processing step is shown in Figure 5.11. Droplet coalescence continues to dominate until a ‘new’ equilibrium between coalescence and break-up, under the changed hydrodynamic conditions, is established and changes in the droplet size of the system are minimised. In the observed peculiar cases, such as the ones observed by experiments with low concentrations of surfactant processed at higher impeller

speeds (where Tween 20 is depleted in the first processing step), the droplet size evolution increases rapidly to values above that which is determined by the experiments in the absence of added surfactant. These cases establish the new equilibrium value sooner than those without added surfactant at lower droplet size. This is a consequence of existing surfactant on the interface which reduces the interfacial tension, causing droplet break-up to influence droplet size evolution data at lower droplet sizes. The reason that the droplet size increases faster than when no surfactant is used is related to the high collision rate observed for those cases which induces coalescence frequency.

This hypothesis can be employed to understand the droplet size evolution data corresponding to a high surfactant concentration (≤ 0.2 %). Figure 5.8 shows similar and/or higher coalescence frequency in comparison with that at lower concentrations of surfactant. However, it can be seen that (Figure 5.12) there is no significant difference between droplet sizes determined at the initial stages of the second processing step and those determined at the end of this processing step. This demonstrates that the presence of a high surfactant concentration in the emulsion results in a break-up frequency at a lower value of droplet size which eventually reaches equilibrium at lower droplet sizes with droplet coalescence.

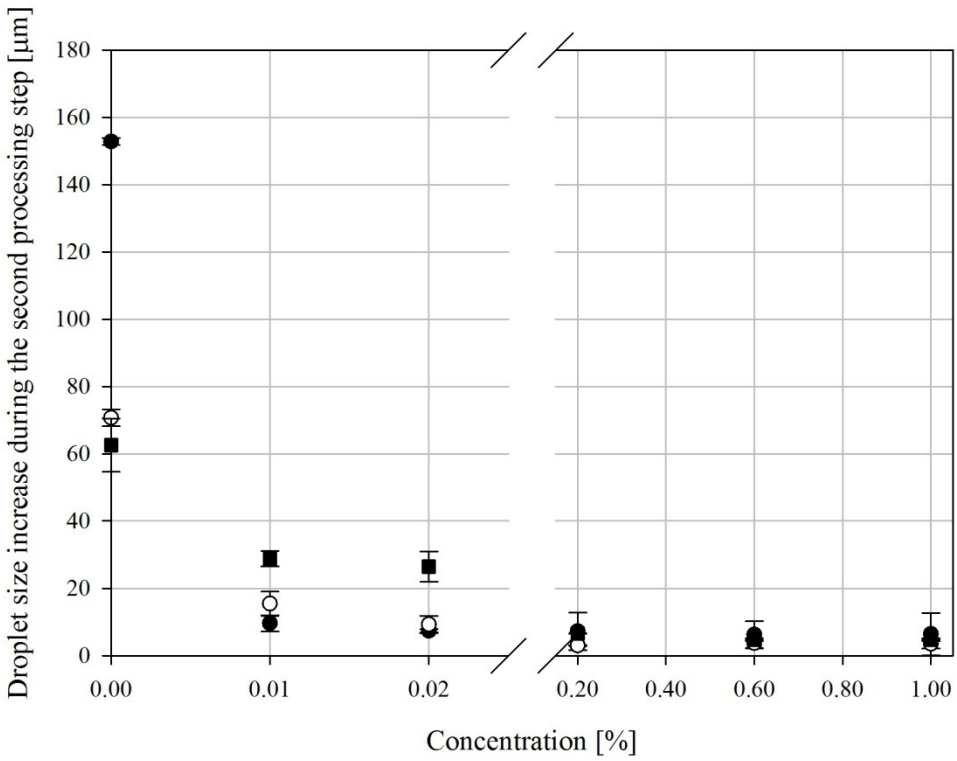

Figure 5.11. Droplet size increase by inducing step-change in the impeller speed is shown with respect to varying concentrations of Tween 20 at varying impeller speeds of 800-400 rpm (●), 1600-800 rpm (○) and 2000-1000 rpm (■).

5.4.3 Third processing step

In the third and final processing step of the experiments, the impeller speed was once again increased to that of the first step in order to test the response of the systems to this additional droplet break-up dominant environment. The experimental data and induced droplet break-up analysis are now presented.

5.4.3.1 Droplet size evolution data

The droplet size evolution data regarding this processing step is shown for various experimental conditions and in the presence of Tween 20 (Figure 5.12).

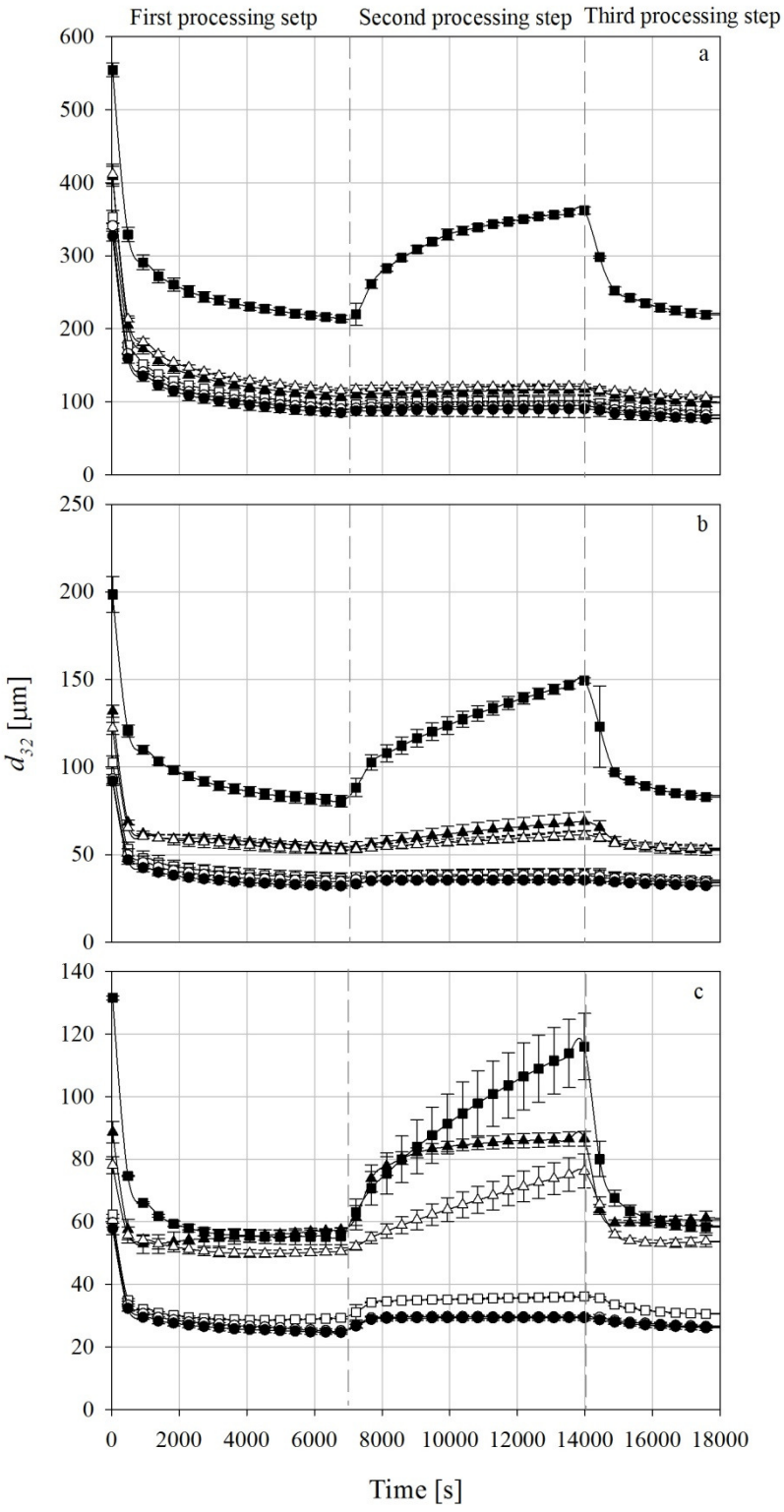

Figure 5.12. Droplet size evolution data obtained from the first, the second and the third processing steps of emulsification experiments with 50 % dispersed phase volume fraction in the absence of added emulsifier (■) and in the presence of 0.01 % (▲), 0.02 % (Δ), 0.2 % (▼), 0.6 % (○) and 1 % (●) concentrations of Tween 20 under different impeller speeds of (a) 800-400-800 rpm, (b) 1600-800-1600 rpm and (c) 2000-1000-2000 rpm.

It can be seen that the droplet size evolution data show different behaviours depending on the surfactant concentration. As an example, it can be seen that the droplet size evolution data related to lower concentrations of surfactant (≤ 0.02 %) show a rapid and significant reduction in droplet size which is followed by either a plateau section, or, after the rapid initial reduction, an increase. On the other hand, the droplet size evolution data related to the high concentration of surfactant (≥ 0.2 %) show no significant changes related to the step-change in impeller speed. This behaviour is caused by the fact that, in the third processing step, the droplet size returns to that achieved by the end of the first processing step. Therefore, if droplet sizes change significantly during the second processing step (since the droplet sizes at the end of the second processing step enter the third processing step) then the droplet size undergoes a rapid reduction. Otherwise, the droplet size evolution data does not show any changes. This can best be demonstrated by calculating break-up frequencies in the initial stages of the third processing step. In this experimental step, the size of the droplets that enter the break-up dominant regime is much smaller than that in the first processing step. The break-up frequencies related to experiments in the presence of Tween 20 are shown in Figure 5.13.

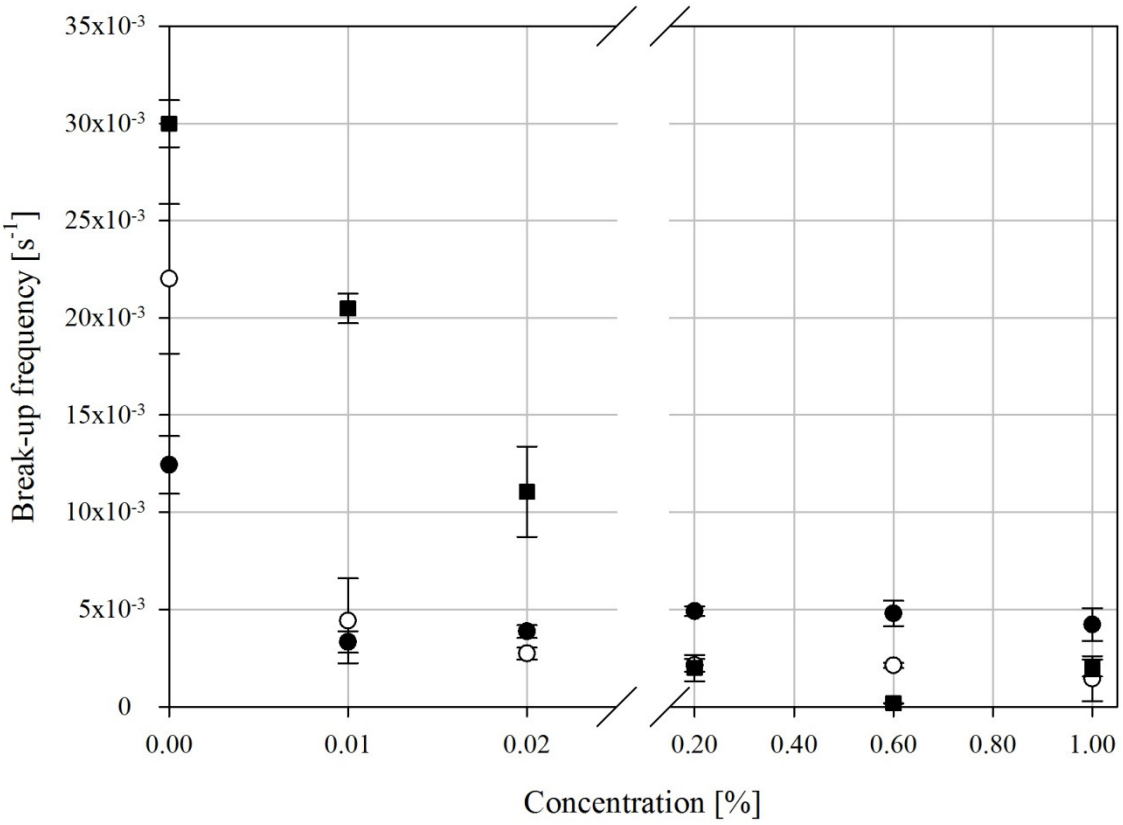

Figure 5.13. Break-up frequencies calculated at the initial stages of the third processing step of experiments with respect to varying concentrations of Tween 20 at varying impeller speeds of 800-400-800 rpm (●), 1600-800-1600 rpm (○) and 2000-1000-2000 rpm (■).

Figure 5.13 shows that the break-up frequencies determined at the initial stages of the third processing step are higher at lower concentrations of surfactant. In addition, it can be seen that the break-up frequency at lower concentrations of Tween 20 are greater for higher impeller speeds. This is true even though the droplet size difference between the initial and final stages (Figure 5.13) of the third processing step is higher for lower impeller speeds than the ones related to the higher impeller speeds. This means that droplet size reduces more at lower impeller speeds but with lower break-up frequency. Furthermore, it indicates that the break-up frequency is higher at higher energy input, even though it is initiated at lower droplet sizes and ought to reach a lower droplet size at the end of the process. This observed behaviour can best be analysed by investigating the emulsion response. In order to investigate

the emulsion response to the impeller speed change at the third processing step, the droplet size difference between the initial and final stages of the third processing step is shown in Figure 5.14.

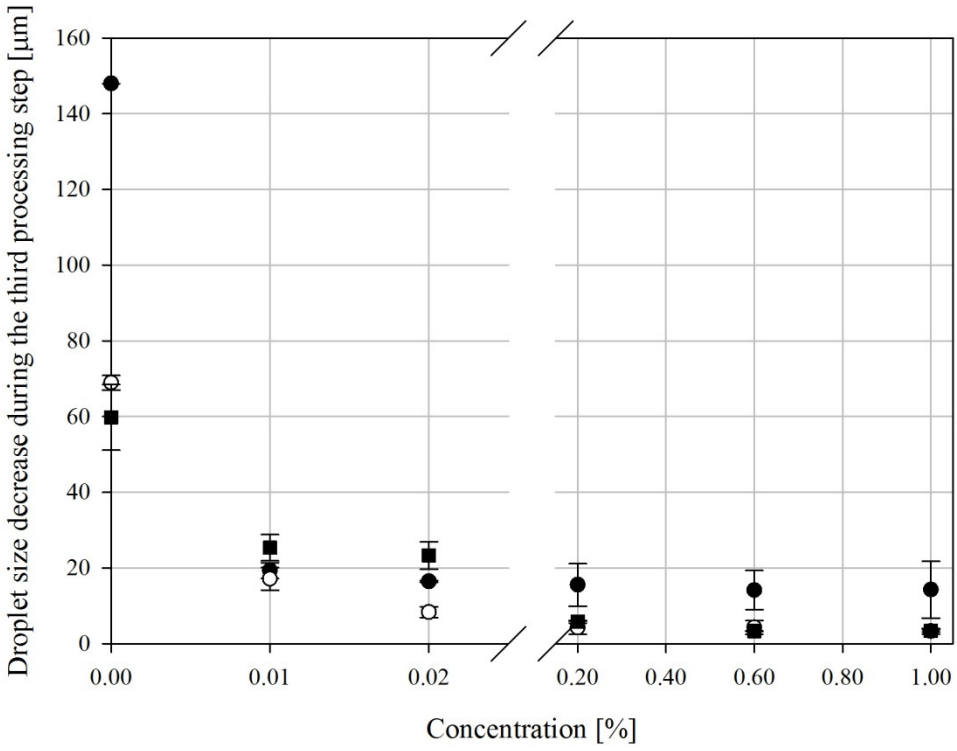

Figure 5.14. Difference in droplet sizes at the initial stages and the final stages of the third processing step are shown with respect to varying concentrations of Tween 20 at varying impeller speeds of 800-400-800 rpm (●), 1600-800-1600 rpm (○) and 2000-1000-2000 rpm (■).

The behaviour observed for the droplet size evolution data is the consequence of the fact that at the end of the first processing step, systems have already established a dynamic equilibrium, and any further minor reduction in droplet size is subject to 'aging' in the process (the emulsions should be processed for longer times). This reduction in droplet size continues gradually until the rate of emulsifier adsorption becomes small and the rate of droplet break-up and coalescence equilibriates.

The above mentioned phenomenon is also the cause of the dependencies observed for droplet break-up frequencies. Since the droplet sizes return to the pre-determined droplet sizes

(the droplet sizes reached at the end of the first processing step), the droplet break-up would be a function of the droplet size differences between droplet sizes at the end of the second and the first processing steps. Therefore, in cases where emulsfier is not employed, a large change in droplet size is expected, which results in a high break-up frequency. However, in the cases where there was not a significant change in the droplet size (experiments in which a high Tween 20 concentration was employed), a lower break-up frequency is observed.

An interesting observation that further confirms the above mentioned hypothesis is the droplet size evolution observed for lower concetrations of surfactant processed under higher impeller speed (Figures 5.12-b and 5.12-c). As has been previously mentioned (first processing step), the droplet sizes behave in a peculiar manner in the first processing step due to the depletion of the surfactant in the system. Figure 5.13 shows that, as the equilibrium between droplet break-up and coalescence has not been reached in the time scale of the first processing step, this phenomenon (high coalescence due to the depletion in surfactant) continues until equilibrium is reached. This shows that by allocating enough time (thus aging in the process), the local high coalescence phenomenon can eventually reach the plateau value where surfactant adsorption rate and droplet break-up and coalescence are all in equilibrium.

5.5 Concluding remarks

The experimental works in this chapter examined the effect of nonionic surfactant concentration and hydrodynamic conditions of the process on the oil-in-water emulsion formation containing 50 % dispersed phase volume fraction. The concluding remarks are summarised by considering the experiments in the presence of Brij 97 (Appendix B). The first processing step was characterised by 3 regions; namely, rapid decrease, transitional and plateau regions. It was shown that similar droplet break-up frequencies are determined at the early stages of the rapid decrease region at all used impeller speeds and Tween 20

concentrations. Since all Tween 20 concentrations used showed similar interfacial tension, therefore induced similar capillary pressure. Consequently similar droplet break-up frequencies were calculated at any given impeller speeds. The reason that similar droplet break-up frequencies were determined when impeller speeds were varied is related to two opposing parameters. The energy input which is higher at higher impeller speeds and capillary pressure, which is higher at higher impeller speeds (owing to the smaller droplets). Therefore the resulting break-up frequency at higher impeller speeds was similar to that calculated at lower impeller speeds.

The transition between rapid decrease region and the plateau region occurred smoothly in most cases. However, the droplet size evolution of some experimental cases, namely the ones in the presence of low (0.01 %, 0.02 %) Tween 20 concentration processed under intense hydrodynamic conditions (2000 rpm), were shown to first increase, and then decrease. This is related to the depletion of Tween 20 when there is a high rate of increase in interfacial area, which results in a locally higher droplet coalescence dominant regime.

The final droplet size (plateau region) was decreasing when higher impeller speeds and Tween 20 concentrations were employed. The increase in turbulent stresses decreases droplet sizes due to the higher droplet break-up rate operating on smaller droplets, due to a decrease in Kolmogorov microscale. High Tween 20 concentration results in higher adsorption rate which can further induce droplet break-up, thus decreasing droplet size.

In the second processing step the droplet coalescence was calculated. A consistent trend of droplet coalescence frequency's dependency on Tween 20 concentration and impeller speed was not observed; therefore the reasons were further elucidated by analysing collision rate and collision efficiency. Collision rate was shown to increase significantly by an increase in Tween 20 concentration and/or impeller speed. This may significantly increase the

likelihood of droplet coalescence. However, it was shown that collision efficiency decreases by increasing Tween 20 concentration and impeller speed. This was related to better surface coverage of droplets at higher Tween 20 concentrations which provides a steric repulsive force against turbulent stresses. The decrease in collision efficiency by an increase in the impeller speed was caused by the higher capillary pressure of smaller droplets which opposes the breakage of droplets for coalescence, although less amount of continuous phase was captured between two droplets.

At the final processing step, the droplet size evolution returns to the value determined previously in the first processing step. This was related to the 'ageing' of the droplets during processing. Therefore, the droplet break-up frequencies at this stage of the process were highly dependent on the droplet size increase during the second processing step, hence, higher at lower Tween 20 concentrations and in contrast, lower for higher Tween 20 concentrations.

Chapter 6

Mechanistic understanding of emulsion formation during processing: The effect of the dispersed phase volume fraction

This chapter describes experiments designed and performed in order to study the influence of the dispersed phase volume fraction on emulsification processes.

6.1 Introduction

The experimental works in this chapter were focused on the examination of the influence of the dispersed phase volume fraction on the droplet size evolution during processing, droplet break-up and coalescence. The experimental procedure is presented in Section 4.3. Each experiment was performed at least three times in order to obtain reproducible data and the results are reported as mean ± standard deviation of the three runs. Oil-in-water emulsions were subjected to various processing conditions whilst the dispersed phase volume fraction was varied. The experimental conditions and emulsifier concentrations are listed in Table 6.1.

Table 6.1. Emulsifier type and concentration used and the experimental conditions carried out in Chapter 6.

Dispersed phase volume fraction	5 %, 10 %, 20 % and 50 %		
Emulsifier	**Type**	**Concentration**	
	Tween 20	0 %, 0.02 % and 1 %	
Impeller speed [rpm]	**First processing step**	**Second processing step**	**Third processing step**
	1600	800	1600
	2000	1000	2000

In order to fully analyse the data obtained from the experiments, a series of interfacial tension measurements and rheological studies were carried out. All the interfacial tension data needed for this chapter is presented in Section 5.3. It was demonstrated that in the presence of varying concentrations of Tween 20, similar interfacial tensions were measured between oil and aqueous phases.

Rheological studies were carried out on the samples obtained after emulsification experiments. Emulsions contained a range of dispersed phase volume fractions of 10 %, 20 % and 50 %. It was shown that these emulsions behave as Newtonian fluids and their viscosity is

constant with respect to the shear they experience. Nonetheless, in this study the viscosity of emulsions with dispersed phase volume fraction of 5 % could not be experimentally determined, since it is very close to that of water and, thus, it is beyond the detectible range of the rheometer. Therefore, the viscosity of emulsions with 5 % dispersed phase volume fraction was calculated using the Krieger-Dougherty equation (equation 4.8).

6.2 Emulsification studies

6.2.1 First processing step

6.2.1.1 Droplet size evolution data

All the droplet size evolution data related to the first processing step is shown in Figures 6.1 and 6.2. Specifically, the figures show the droplet size evolution data of the emulsification processes with impeller speeds of 1600 rpm (Figure 6.1) and 2000 rpm (Figure 6.2), when different Tween 20 concentrations and dispersed phase volume fractions are employed, namely 5 % (a), 10 % (b), 20 % (c) and 50 % (d).

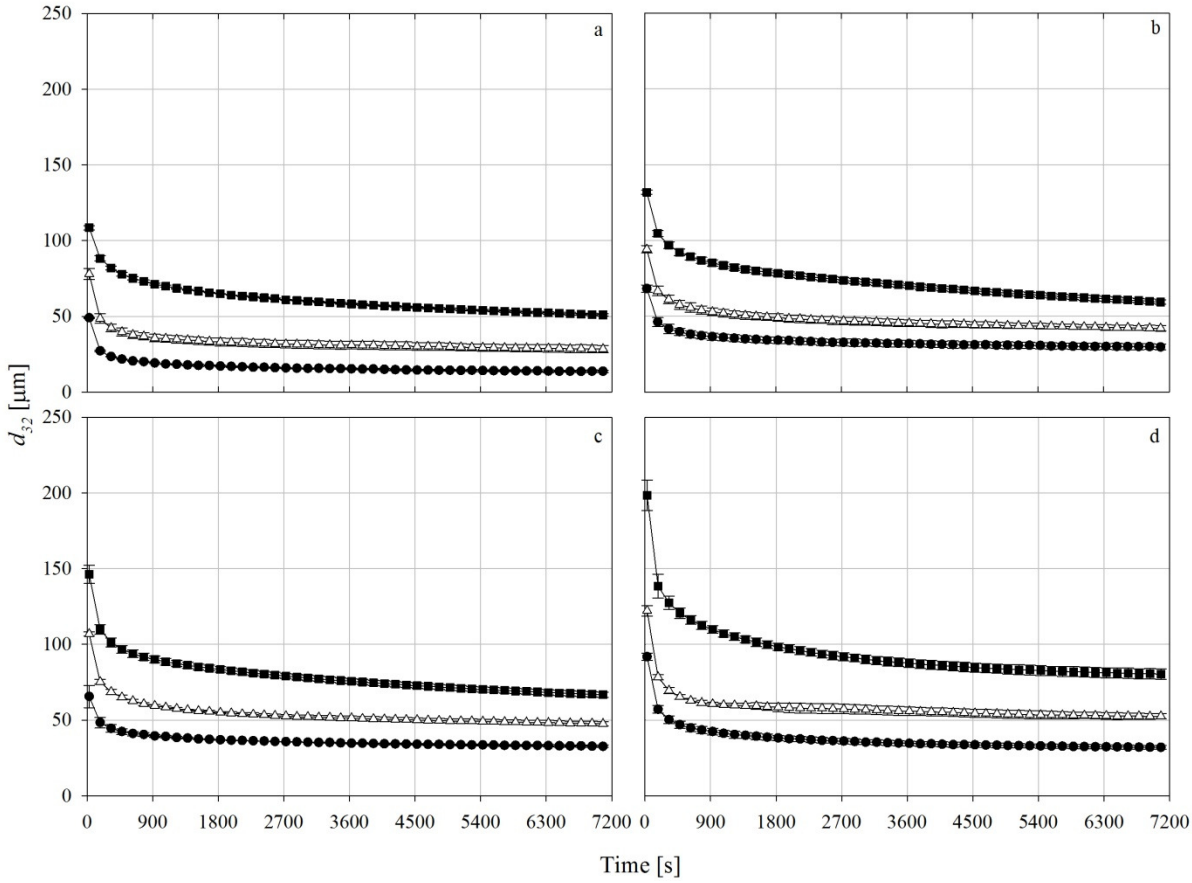

Figure 6.1. Droplet size evolution data obtained from the first processing step of emulsification experiments with impeller speed of 1600 rpm in the absence of added emulsifier (■) and in the presence of 0.02 % (Δ) and 1 % (●) concentrations of Tween 20 are shown for oil-in-water emulsions containing varying dispersed phase volume fractions of (a) 5 %, (b) 10 %, (c) 20 % and (d) 50 %.

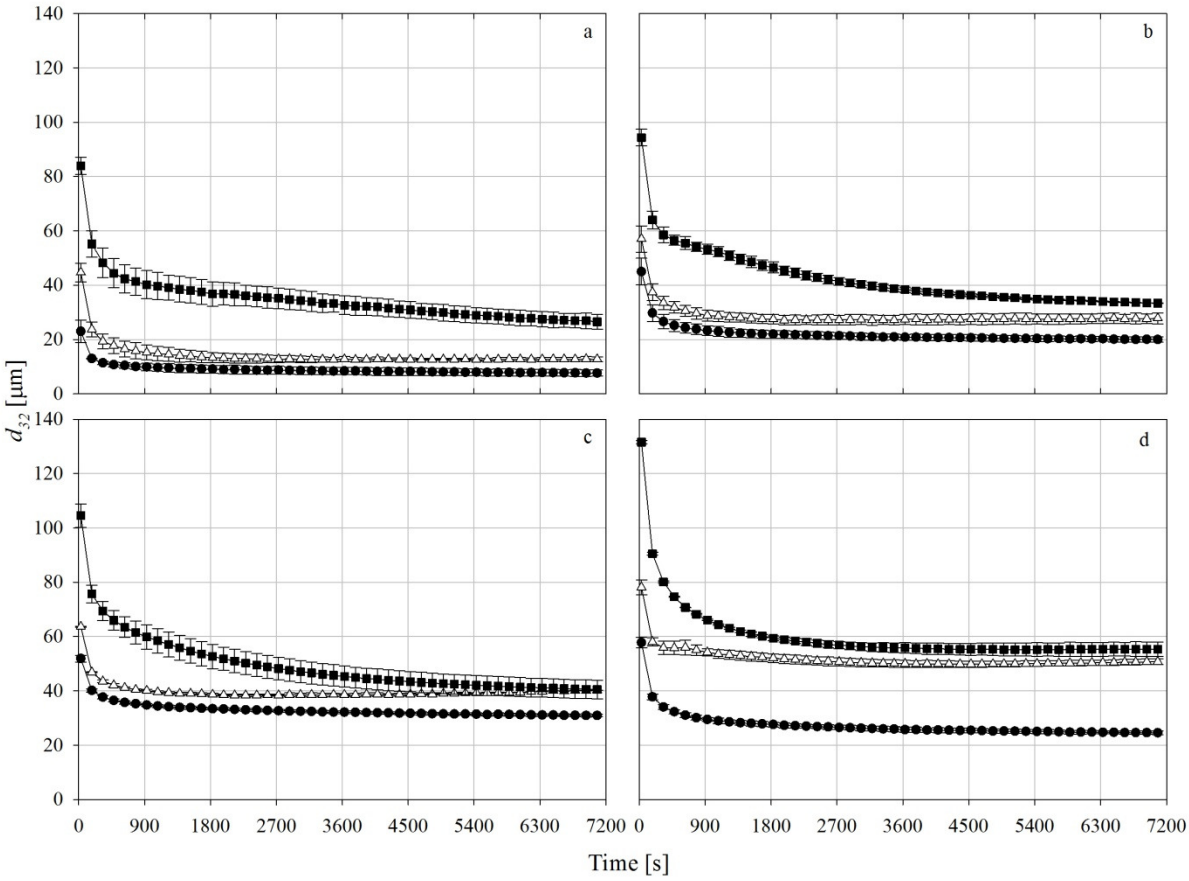

Figure 6.2. Droplet size evolution data obtained from the first processing step of emulsification experiments with impeller speed of 2000 rpm in the absence of added emulsifier (■) and in the presence of 0.02 % (Δ) and 1 % (●) concentrations of Tween 20 are shown for oil-in-water emulsions containing varying dispersed phase volume fractions of (a) 5 %, (b) 10 %, (c) 20 % and (d) 50 %.

Similar to the data of Chapter 5, three regions can be identified in each graph. The first region is the rapid decrease of droplet size where droplet break-up is the dominant phenomenon. This region is then gradually changing (transitional region) to the region where droplet size plateaus. Each of these regions is analysed separately.

6.2.1.1.1 Rapid decrease region

This stage of the process is only affected by droplet break-up and in comparison; droplet coalescence is negligible. Droplet break-up phenomena depend on the energy dissipation and initial droplet size of the first processing step, since it is likely that this phenomenon continues until the droplet size is too small for inertial stresses to have a

significant effect on droplet size. Figure 6.3 shows the initial droplet sizes and their respective break-up frequencies (equation 4.12) determined with respect to the dispersed phase volume fraction for varying concentrations of Tween 20 and impeller speeds, namely 1600 rpm in (6.3-a, c) and 2000 rpm in (6.3-b, d). The lines shown in Figure 6.3 do not have any mathematical meaning and are just shown as an eye-guide to follow each dataset.

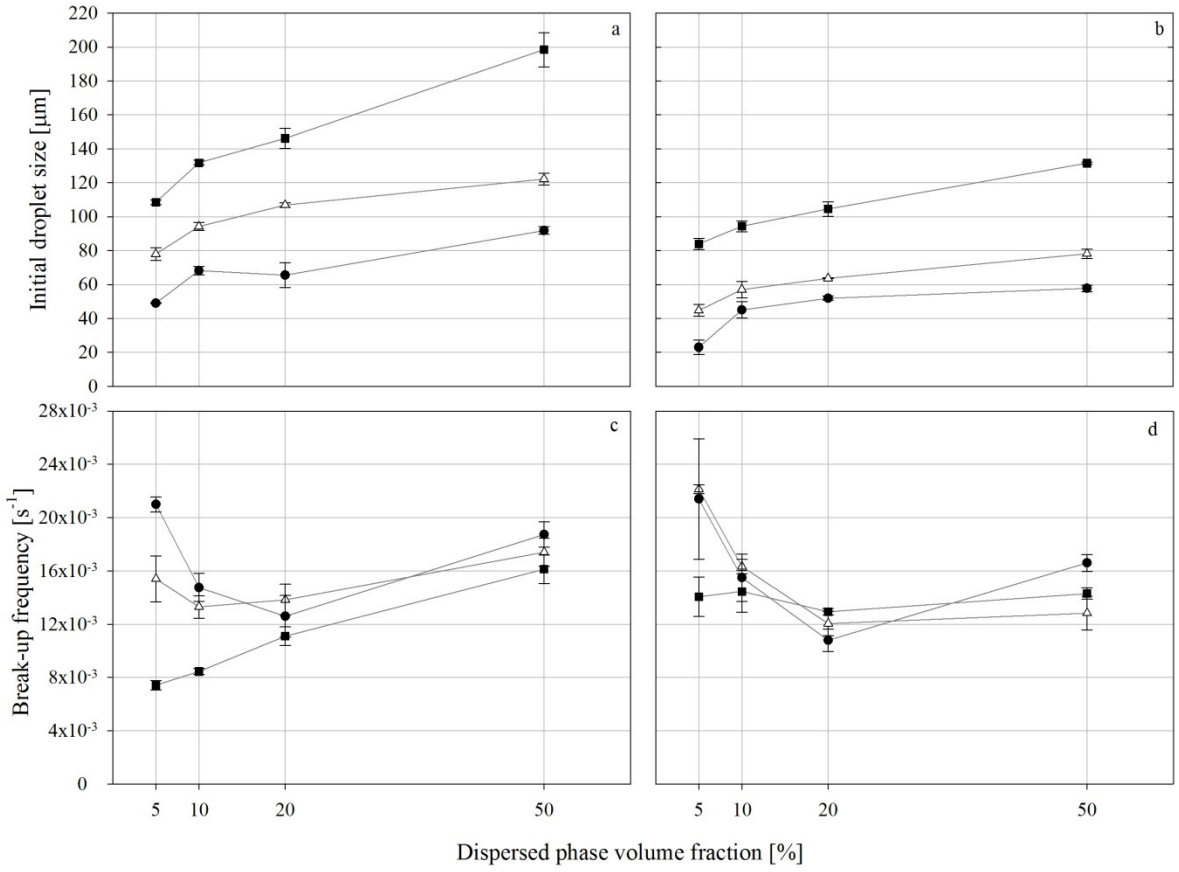

Figure 6.3. Initial droplet size (a, b) and droplet break-up frequencies (c, d) at the initial stages of the first processing step are shown with respect to the dispersed phase volume fraction in the absence of added emulsifier (■) and in the presence of 0.02 % (Δ) and 1 % (●) concentrations of Tween 20 corresponding to the first processing step with impeller speed of (a, c) 1600 rpm and (b, d) 2000 rpm.

Figures 6.3-a and b demonstrate that the initial droplet sizes are higher at higher volume fractions. However, the initial droplet sizes are lower at 2000 rpm and higher Tween 20 concentrations. As it has been stated in Chapter 5, the number and size of daughter droplets resulting from droplet break-up (at this stage) is a function of the energy experienced

by the droplets (Tsouris and Tavlarides, 1994; Tcholakova *et al.*, 2007). Thus, the dependency of the initial droplet size on dispersed phase volume fraction may be explained by the fact that at higher volume fractions, less energy is experienced by the droplets (due to the dampening effect of the dispersed phase); therefore, larger droplets are produced by break-up. Moreover, Tween 20 adsorption at the interface decreases the interfacial tension on the droplets, resulting in higher number of daughter droplets and, hence, lower droplet sizes. Furthermore, increasing the impeller speed increases the inertial stresses thus decreases the initial droplet sizes.

In the absence of Tween 20, as it can be seen in Figure 6.3-c and d, the break-up frequency gradually increases with respect to volume fraction when the impeller speed is 1600 rpm. However, when the impeller speed is 2000 rpm the break-up frequencies show a minimum at volume fraction of 20 %. The minimum droplet break-up frequency at 20 % dispersed phase volume fraction can be observed in all other experiments performed in the presence of varying Tween 20 concentrations and impeller speeds. The observation of a minimum is a consequence of two opposing factors; The capillary pressure, which reduces at higher volume fractions due to the larger droplets thus increasing droplet break-up frequencies, and the magnitude of inertial stresses. The latter decreases with increasing dispersed phase volume fraction as a consequence of the dampening effect of the dispersed phase. Considering similar interfacial tension at any given Tween 20 concentration at various dispersed phase volume fractions, it can be shown that the ratio of capillary pressures from 5 % to 50 % over 20 % dispersed phase volume fraction changes from 1.3 to 0.72, showing reduction in capillary pressure. On the other hand, the dampening effect ratio to that of 20 % (using the measured emulsions viscosities shown in Chapter 5) increases from 8 to 0.125. The reason that similar droplet break-up frequencies are reported at 10 % and 20 % dispersed

phase volume fraction is a consequence of similar capillary pressures and dampening effects. In order to find the influence of each parameter for determining the numerical condition which results in the minimum at 20 % dispersed phase volume fraction, a detailed analysis of the hydrodynamic condition of the mixing system is required which could form the basis for further investigation.

Figure 6.3-c and d demonstrate that the break-up frequencies are higher when an impeller speed of 2000 rpm is employed as a consequence of higher magnitude of inertial stresses. It should be noted that, in most experimental conditions at the same level of dispersed phase volume fraction and impeller speed, the break-up frequencies show similar values when 0.02 % and 1 % Tween 20 is used, while they are lower in the absence of added emulsifier. However, this observed difference between droplet break-up frequencies is less significant at higher volume fractions (20 % and 50 %) where the break-up frequencies are similar for all experiments. The dependency of the droplet break-up on Tween 20 concentration might stem from the fact that at higher volume fractions, a higher dampening effect is expected thus droplets experience similar inertial stresses therefore reducing the influence of the interfacial tension. For example, at 5 % dispersed phase volume fraction it can be seen that the difference between break-up frequencies at varying Tween 20 concentrations increases, owing to less dampening effect of the dispersed phase, at which interfacial tension effect on droplet break-up is more pronounced.

6.2.1.1.2 Transitional region

It can be seen in Figures 6.1 and 6.2 that the droplet size in most experimental studies decreases smoothly and enters the plateau region. However, some different behaviour is observed. This unusual behaviour is more obvious for the experiments performed with 0.02 % of Tween 20; for example, the experiments containing 0.02 % of Tween 20 in the cases where

emulsions with 10 %, 20 % and 50 % dispersed phase were processed at 2000 rpm impeller speed (Figures 6.2-b, c and d) and those with 50 % volume fraction were processed at 1600 rpm impeller speed (Figure 6.1-d). Systems of higher emulsifier concentrations subjected to the same processing conditions and also systems with the same volume fractions processed at lower impeller speeds appear to enter a nearly plateau region, with droplet sizes only marginally decreasing until the first processing step is completed. In contrast, after an initial rapid decrease, the droplet size in the systems with 0.02 % Tween 20 appear, at first, to increase slightly only to remain constant afterwards. This is more evident for cases where the droplet size, after an initial rapid decrease, exhibits a gradual increase, which is maintained until the end of the first processing step; for example, the emulsion with 20 % dispersed phase volume fraction processed at 2000 rpm shown in Figure 6.2-c.

This behaviour can be explained by the hypothesis described in the previous chapter, regarding the intense processing conditions involved, which attempt to decrease the emulsion's droplet size rapidly. This results in a considerable increase in the interfacial area of the system, which, in turn, significantly 'depletes' the low concentration of emulsifier (0.02 % Tween 20) and decreases the rate of adsorption of Tween 20. Under these conditions, coalescence events are dominant and the droplet size is increased. This increase is only temporary for some cases, as equilibrium between droplet break-up and coalescence is eventually reached. In contrast, the droplet size in the other cases is permanently increased as equilibrium between the two sub-processes is not reached within the time scale of the experiment. For example, this is seen in Figure 6.2-d, where the emulsion's droplets at such low emulsifier concentration reach, at the end of the processing step, the size of the droplets in the systems in the absence of added emulsifier.

The experiment performed in the previous chapters further confirmed this hypothesis, which indicates that, by progressively introducing the system to the hydrodynamic conditions induced by high impeller speed (for example, 2000 rpm impeller speed), the local coalescence region can be avoided. By increasing the impeller speed in stages, the excess of interfacial area, created in the case of the intense hydrodynamic conditions is never reached and the equilibrium droplet size is gradually approached.

6.2.1.1.3 Plateau region

After the initial stages and when the process proceeds in time, the speed of change in the droplet size evolution is reduced (Figures 6.1 and 6.2), since the droplets break down to smaller sizes so that they are less affected by fluid fluctuations and, hence, the droplet break-up frequency decreases. This is a direct result of the droplet break-up mechanism in the turbulent regime. When droplet sizes are reduced, not only does their capillary pressure increase, but also smaller eddies containing less energy are able to affect them. Therefore, the rate of droplet break-up is reduced. In contrast, the decrease in the size of the droplets, increases the number of droplets, resulting in an increase in the probability of droplet collision. At longer times in the process, the droplet coalescence effect on the mean droplet size increases and tends to increase the droplet size in opposition to the droplet break-up. The dynamic equilibrium of these two phenomena results in the final droplet size produced at the end of the first processing step. The final droplet size is affected by a number of parameters such as the dispersed phase volume fraction, the hydrodynamic condition, which itself is affected by the dispersed phase volume fraction (due to the dampening effect) and the rate of adsorption of Tween 20 on the newly made interfaces. Figure 6.4 shows the final droplet size corresponding to the first processing step for varying dispersed phase volume fractions and Tween 20 concentrations when the impeller speeds are 1600 rpm (a) and 2000 rpm (b).

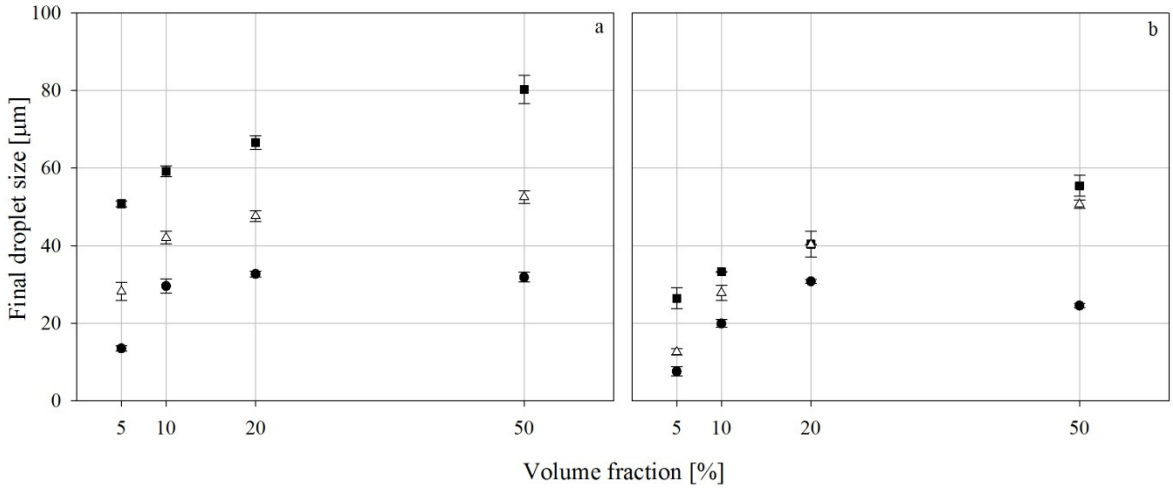

Figure 6.4. The final droplet sizes with respect to the dispersed phase volume fraction are shown in the absence of added emulsifier (■) and in the presence of 0.02 % (Δ) and 1 % (●) concentrations of Tween 20 corresponding to the first processing step with impeller speed of (a) 1600 rpm and (b) 2000 rpm.

Figure 6.4 demonstrates that, at any given impeller speed and Tween 20 concentration, the final droplet sizes are increasing by employing higher dispersed phase volume fractions. In addition, the experiments with higher impeller speeds and/or higher Tween 20 concentrations show lower droplet sizes.

All the above findings result from droplet break-up and coalescence mechanisms involved in the processes. When higher volume fractions are employed, not only is less energy experienced by the droplets (due to the dampening effect of the dispersed phase) but also, because of the existence of higher numbers of droplets at higher volume fractions, higher droplet coalescence frequencies are expected. In addition, higher impeller speed results in higher energy dissipation, hence the droplet break-up increases. However, at higher impeller speeds, higher numbers of droplets are produced; this should increase the droplet coalescence frequency. Clearly, this is not the case for these experiments and the droplet break-up, in fact, reduces the final droplet sizes.

Tween 20 is thought to affect the final droplet size through two different processes. When a new droplet is formed due to the droplet break-up, Tween 20 is adsorbed on the interface. Upon adsorption, Tween 20 prevents the droplet coalescence caused by the probable collision and, in addition, it reduces the interfacial tension, which, in turn, increases the droplet break-up frequency. In order to investigate the effect of Tween 20 thoroughly and to understand which role of surfactant is more significant on the process, Table 6.2 shows the amount of remaining Tween 20, the interfacial area of the droplets and the time required for surfactant adsorption when a new droplet is produced by droplet break-up. These parameters were estimated using equations given in Chapter 4.

Table 6.2. The interfacial area produced in various conditions, the amount of Tween 20 remaining in the solution and the time needed for Tween 20 to be adsorbed on the newly made droplet (NA: not applicable).

Volume fraction [%]	Impeller speed [rpm]	Tween 20 concentration [%]	d_{32} [µm]	Interfacial area [m^2]	Amount remaining Tween 20 [%]	Adsorption time [ms]
5	1600	**0.00**	50.81	1.59	0.000	NA
		0.02	28.20	2.87	0.018	2.33
		1.00	13.51	5.98	0.995	5.45×10^{-2}
	2000	**0.00**	26.41	3.07	0.000	NA
		0.02	12.63	6.41	0.015	2.87
		1.00	7.59	10.76	0.992	5.30×10^{-2}
10	1600	**0.00**	59.19	2.73	0.000	NA
		0.02	42.07	3.84	0.017	2.53
		1.00	29.59	5.47	0.996	4.97×10^{-2}
	2000	**0.00**	33.29	4.85	0.000	NA
		0.02	27.88	5.81	0.016	2.54
		1.00	19.93	8.11	0.994	4.55×10^{-2}
20	1600	**0.00**	66.58	4.85	0.000	NA
		0.02	47.62	6.79	0.015	3.89
		1.00	32.73	9.87	0.992	6.74×10^{-2}
	2000	**0.00**	40.41	8.03	0.000	NA
		0.02	40.28	8.02	0.014	3.51
		1.00	30.81	10.49	0.992	5.50×10^{-2}
50	1600	**0.00**	80.30	10.07	0.000	NA
		0.02	53.34	15.39	0.009	25.95
		1.00	31.87	25.38	0.981	2.74×10^{-1}
	2000	**0.00**	55.45	14.5	0.000	NA
		0.02	50.72	15.93	0.008	22.67
		1.00	24.54	32.93	0.975	2.41×10^{-1}

Table 6.2 shows that the interfacial area produced by the various experimental conditions increases when higher dispersed phase volume fractions are employed. For example, emulsification with 5 % dispersed phase volume under 2000 rpm impeller speed after two hours of processing produces ~10 m^2 of interfacial area; in contrast, the same experimental condition with 50 % dispersed phase volume produces ~32 m^2, which is significantly higher. As a result, Tween 20 is depleted in the aqueous phase in the latter case which is shown in Table 6.2. For 50 % dispersed phase volume fraction, more or less all Tween 20 is adsorbed at lower concentrations, whereas at higher concentrations, although a significant amount of Tween 20 remains in the system, a longer time is needed to fully adsorb on the interface of a newly made droplet when 50 % volume fraction is employed. The difference in the adsorption times between higher and lower volume fractions is significant (one order of magnitude difference between similar experiments with 5 % and 50 % dispersed phase volume fractions), although a similar amount of Tween 20 remains in the system for both cases. These observations demonstrate that, when the emulsifier is in excess, the droplet size is controlled by the hydrodynamic condition of the process and droplet coalescence. At higher volume fractions (for example, 50 %) there is less Tween 20 in the aqueous phase, resulting in lower adsorption rates, which, in turn, causes higher droplet coalescence. In addition, droplet coalescence is increased due to the existence of a higher number of droplets in the emulsion with 50 % volume fraction. In contrast, at lower concentrations of Tween 20, the droplet size is mainly controlled by the amount of Tween 20 in the system as it has been previously observed by Tcholakova *et al.* (2004).

Further, it is shown that, for example, in the cases with 5 % dispersed phase and 0.02 % Tween 20, although still more or less the same amount of Tween 20 remains in the system, compared with its initial value, still there is a significant difference in droplet sizes produced

in comparison to the case employing 1 % Tween 20 and otherwise identical experimental conditions. It should be noted that the hydrodynamic condition of these two processes are similar. This demonstrates that, the main parameter affecting the final droplet sizes, when the same amount of volume fraction is employed, is not the amount of Tween 20, but the rate at which Tween 20 can reach the newly made interface to further promote droplet break-up. In the following section it will be shown that droplet coalescence is not suppressed by the existence of Tween 20 on the interface. Therefore, the rate of adsorption is an important parameter determining the final droplet size and, hence, the extent of droplet break-up.

It should be noted that, there are some unexpected data in Figure 6.4-b; for example, the experiments with no Tween 20 and 0.02 % of Tween 20 processed under 2000 rpm impeller speed with 50 % volume fraction show similar final droplet sizes. This is related to the behaviour shown in the transitional region. Since Tween 20 is depleted, droplet coalescence dominates the process and, due to the intense hydrodynamic condition, the droplet size cannot reach the equilibrium during the first processing step. Therefore, similar droplets are reported for both experimental conditions.

6.2.2 Second processing step

The second processing step is characterised by abrupt reduction in the impeller speed, which induces a hydrodynamic condition promoting droplet coalescence. The coalescence in this process is related to the droplet sizes determined at the end of the first processing step in the hydrodynamic regime of the second processing step. It should be stressed that, the droplet coalescence in this stage is different from that observed at the end of the first processing step since there is negligible droplet break-up events to affect the process. Consequently, the findings presented in this section may be useful for understanding the mechanism of droplet

coalescence individually. The experimental data obtained and the analyses applied to them are presented in the following sections.

6.2.2.1 Droplet size evolution data

All droplet size evolution data obtained from the experiments performed is shown in Figures 6.5 and 6.6. Specifically, the figures show the droplet size evolution data of the second processing step of emulsification processes with impeller speeds of 800 rpm (Figure 6.5; a 1600 rpm impeller speed was used at the first processing step) and 1000 rpm (Figure 6.6; a 2000 rpm impeller speed was used at the first processing step), for different Tween 20 concentrations and dispersed phase volume fractions of 5 % (a), 10 % (b), 20 % (c) and 50 % (d).

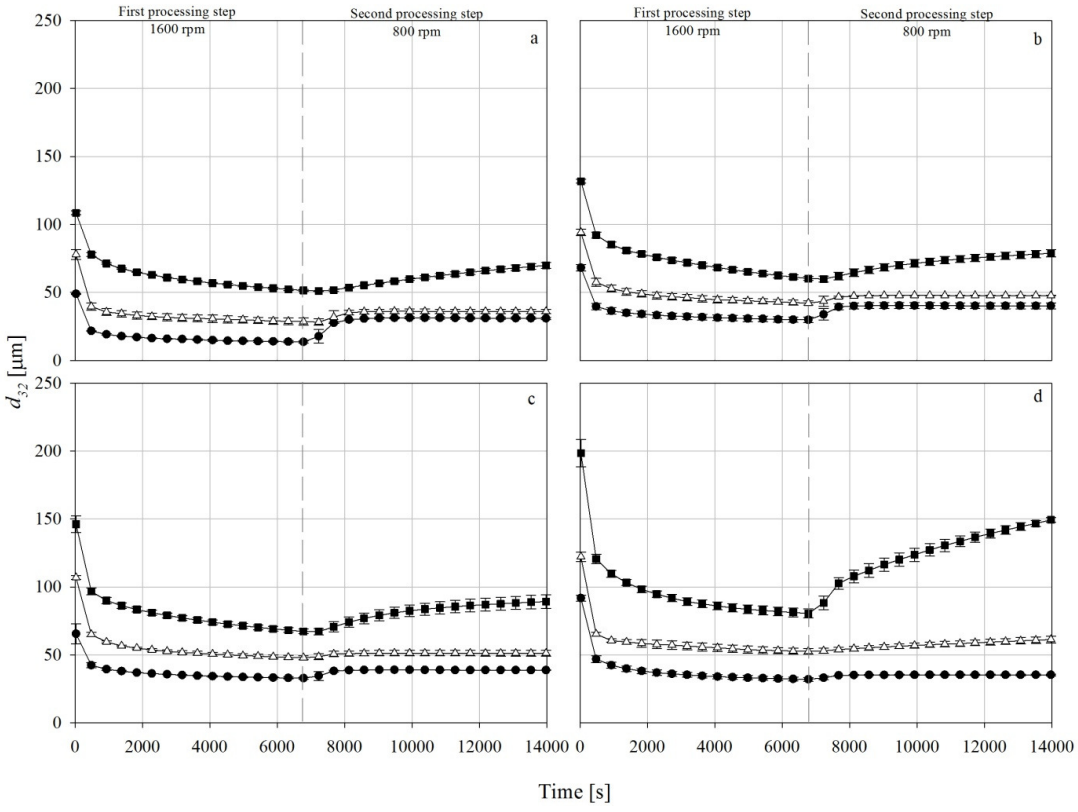

Figure 6.5. Droplet size evolution data obtained from the first and the second processing steps of emulsification experiments with impeller speed of 1600-800 rpm in the absence of added emulsifier (■) and in the presence of 0.02 % (Δ) and 1 % (●) concentrations of Tween 20 are shown for oil-in-water emulsions containing varying dispersed phase volume fractions of (a) 5 %, (b) 10 %, (c) 20 % and (d) 50 %.

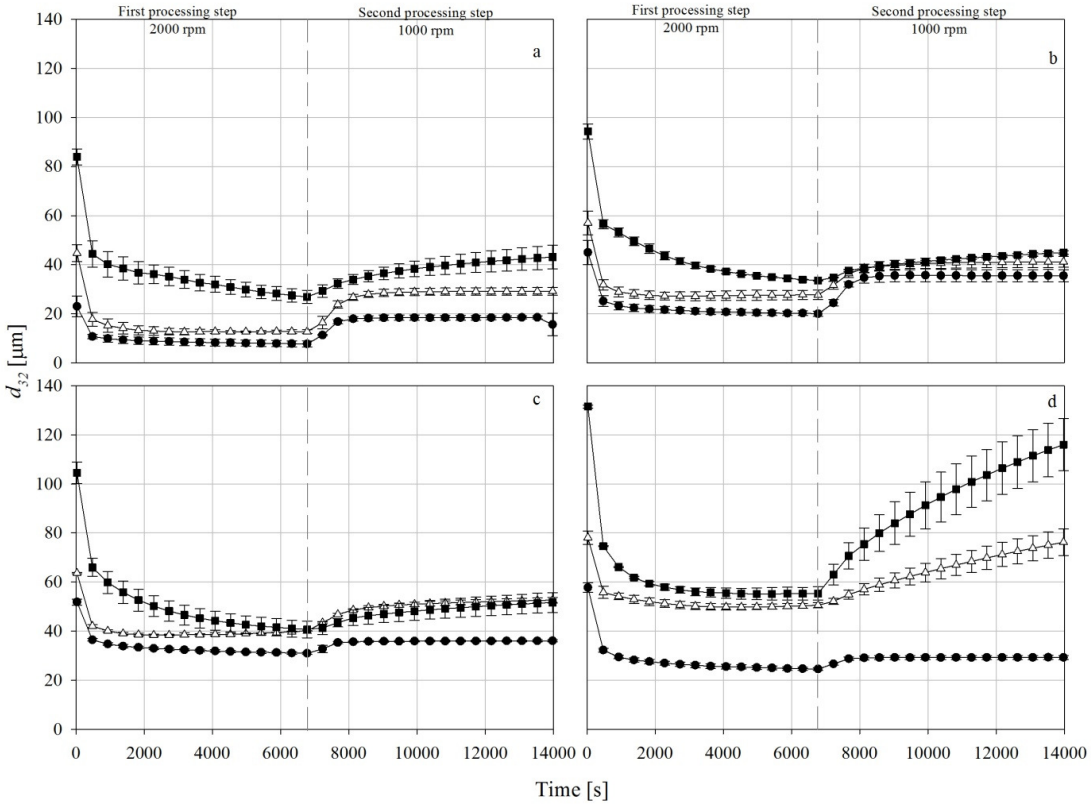

Figure 6.6. Droplet size evolution data obtained from the first and the second processing steps of emulsification experiments with impeller speed of 2000-1000 rpm in the absence of added emulsifier (■) and in presence of 0.02 % (Δ) and 1 % (●) concentrations of Tween 20 are shown for oil-in-water emulsions containing varying dispersed phase volume fractions of (a) 5 %, (b) 10 %, (c) 20 % and (d) 50 %.

Figures 6.5 and 6.6 show that the droplet size evolution data in this processing step are characterised by two regions. The first region that can be seen in all experiments is the rapid increase in droplet size. This region follows by either a less steep increase in droplet size (observed in the experiments with no Tween 20) or a plateau region (observed in the experiments with 0.02 % and 1 % Tween 20). The rapid increase in droplet size is caused by the high number of droplet coalescence events as a consequence of the reduction in droplet break-up induced by the step-change in the impeller speed. The duration of this increase varies among the various experimental conditions due to the diverse effects of operating parameters on droplet coalescence.

6.2.2.2 Droplet coalescence

The droplet coalescence frequency at this processing step was calculated by using equation 4.16. Figure 6.7 shows the droplet coalescence frequencies corresponding to the initial stages of the second processing step for varying dispersed phase volume fractions and Tween 20 concentrations when the impeller speed is 1600-800 rpm (a) and 2000-1000 rpm (b). The lines in Figure 6.8 connect the data points and are used as an eye-guide to follow each dataset.

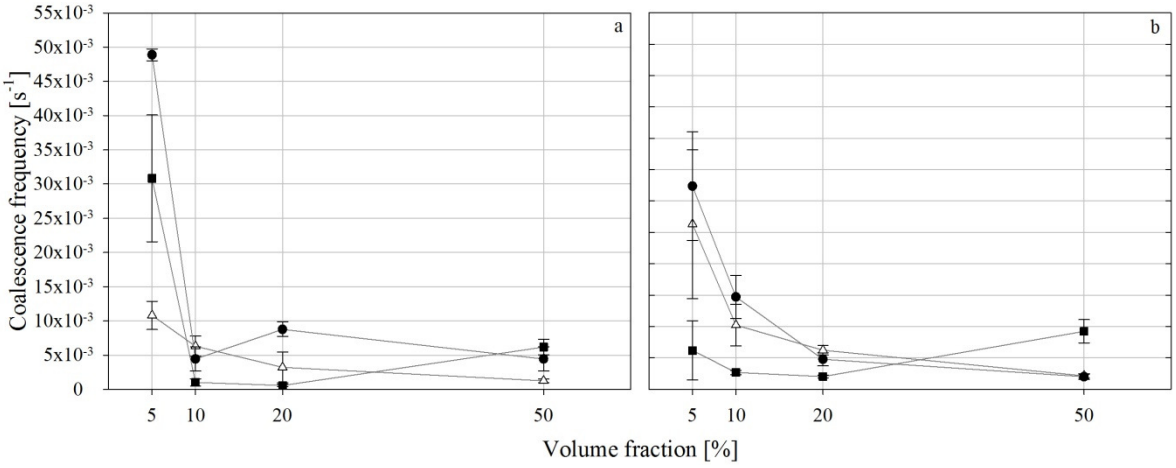

Figure 6.7. Droplet coalescence frequencies calculated at the initial stages of the second processing step are shown with respect to the dispersed phase volume fraction in the absence of added emulsifier (■) and in the presence of 0.02 % (Δ) and 1 % (●) concentrations of Tween 20 corresponding to the first processing step with impeller speed of (a) 1600-800 rpm and (b) 2000-1000 rpm.

Figure 6.7 shows that at the initial stages of the second processing step, when higher dispersed volume fractions are used, lower droplet coalescence frequencies are observed. There are few published studies on the effect of high dispersed phase volume fractions on coalescence frequency, but the recent studies have shown an increase in coalescence frequency upon an increase in volume fraction. For example, Lobo and Svereika (2003) conducted experiments on dispersed phase volume fractions between 2 % and 5 % which were notably lower than those employed in the present study. Narsimhan and Goel (2001)

performed experiments with volume fractions of 5 %, 10 % and 15 % which showed similar trends.

Figure 6.7 shows no consistent dependency of droplet coalescence frequency on Tween 20 concentration. For example, when 5 % dispersed phase volume fraction is used with impeller speed of 1600-800 rpm, the coalescence frequency derived from the experiment in the absence of Tween 20 is higher than that calculated for the experiment with 0.02 % Tween 20. However, when the same experimental conditions are used under 2000-1000 rpm impeller speed, the droplet coalescence frequency is higher for 0.02 % Tween 20 than when Tween 20 was not used. In both cases, 1 % Tween 20 shows the highest coalescence frequency. Moreover, in the experiments with 10 % volume fraction, the highest coalescence frequency under impeller speed of 1600-800 rpm is observed for 0.02 % Tween 20, while under impeller speed of 2000-1000 rpm, 1 % Tween 20 shows the highest coalescence frequency. These inconsistencies are observed at higher volume fractions as well. At a volume fraction of 20 %, the highest coalescence frequency is observed for 1 % Tween 20 with an impeller speed of 1600-800 rpm, while, with an impeller speed of 2000-1000 rpm, it is observed for 0.02 % and 1 % Tween 20. It should be noted that the experiments in the absence of Tween 20 show the lowest coalescence frequency for volume fractions less than 20 % (except for the afore-mentioned experiment with 5 % dispersed phase volume fraction and an impeller speed of 1600-800 rpm). However, this is not the case when a 50 % dispersed phase volume fraction is employed, where the highest coalescence frequency is observed when Tween 20 was not used. Therefore, the afore-mentioned observations indicate that droplet coalescence frequency does not depend on Tween 20 concentration alone.

It can be seen that when higher volume fractions are employed, the difference between droplet coalescence frequencies decreases. For example, at volume fraction of 5 % and

impeller speed of 1600-800 rpm, the coalescence frequencies are 0.03, 0.01 and 0.05 s^{-1} in the absence of Tween 20, and in the presence of 0.02 % and 1 % of Tween 20, respectively. In contrast, for the same experimental condition but with a 50 % dispersed phase volume fraction, similar coalescence frequencies are observed for all Tween 20 concentrations (all coalescence frequencies are lower than 0.01 s^{-1}).

Figure 6.7 further indicates that the higher impeller speed (2000-1000 rpm) or higher energy dissipations result in higher droplet coalescence frequencies. However, there are some exceptions to this observation. For example, the increase in the impeller speed (from 1600-800 to 2000-1000 rpm) in experiments with 5 % dispersed phase volume fractions results in a lower coalescence frequency. It should be noted that Taisne *et al.* (1996), Lobo and Svereika (2003) and Narsimhan and Goel (2001) observed that the increase in energy dissipation increases the coalescence frequency.

The reasons for the observed dependencies of droplet coalescence on operating parameters can be investigated through examining the collision rate and efficiency.

6.2.2.2.1 Collision rate and collision efficiency

Collision rates (a, b) and collision efficiency (c, d) were calculated using equation 4.19 and 4.14, respectively, and shown in Figure 6.8 with respect to varying concentrations of Tween 20 and dispersed phase volume fractions for experiments with impeller speeds of 1600-800 rpm (a, c) and 2000-1000 rpm (b, d).

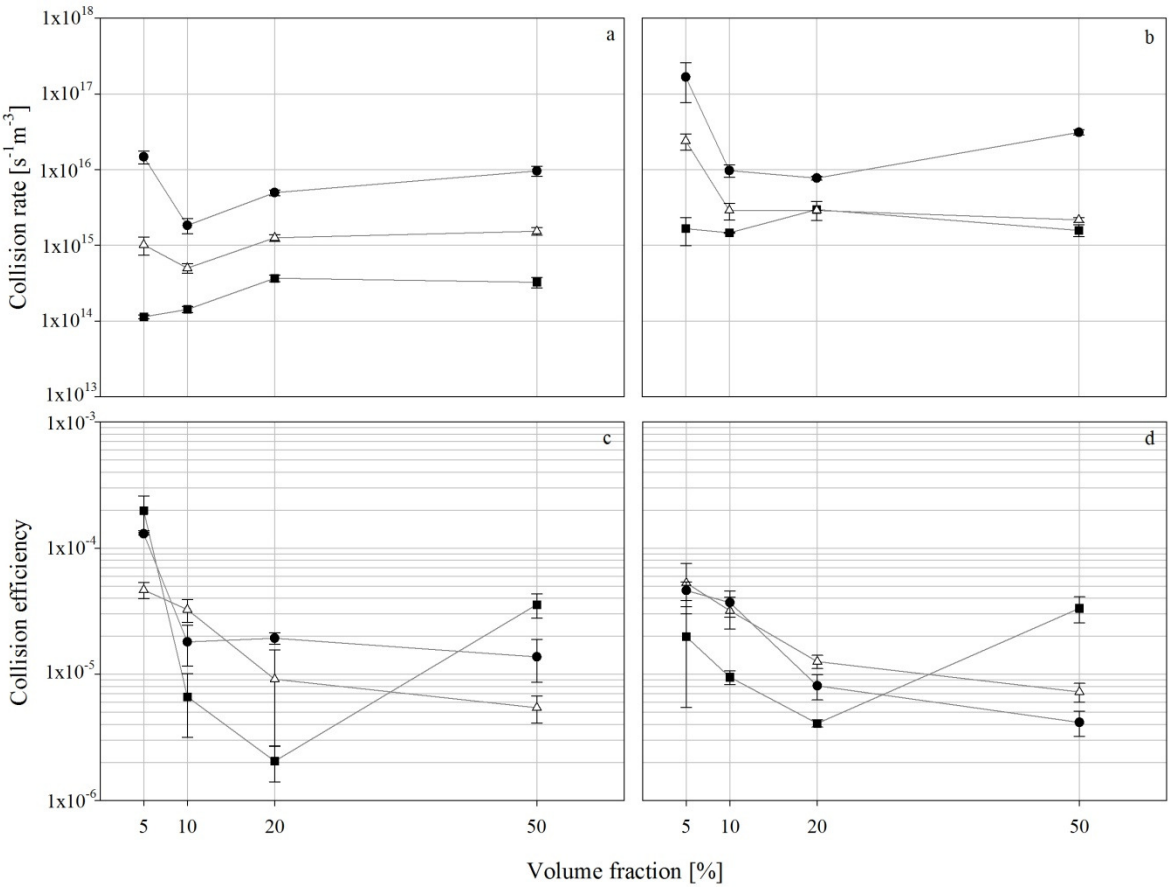

Figure 6.8. Collision rates (a, b) and collision efficiencies (c, d) corresponding to the initial stages of the second processing steps with respect to the dispersed phase volume fraction in the absence of added emulsifier (■) and in the presence of 0.02 % (Δ) and 1 % (●) concentrations of Tween 20 are shown for impeller speeds of 1600-800 rpm (a, c) and 2000-1000 rpm (b, d) (the lines connecting the data points are used merely for visual guidance).

It can be seen from Figures 6.8-a and b that the highest collision rates are observed in the experiments with 1 % Tween 20, while the lowest collision rates are observed in those in the absence of Tween 20. This is a consequence of the initial size of the droplets involved in the coalescence phenomena. The experiments with 1 % Tween 20 concentration enter the second processing step with lower droplet sizes, which results in a higher number of droplets in the system and, hence, higher collision rates. Furthermore, it can be seen that using a higher impeller speed (2000-1000 rpm) results in a higher collision rate. This is expected, since increasing the impeller speed, increases the energy dissipation rate of the process.

An unexpected observation with regard to the dispersed phase volume fraction is that the minimum collision rate happens at a volume fraction of 10 % in all studied experiments (Figures 6.8-a and b). For example the collision rates for experiment in the presence of 1 % Tween 20 with dispersed phase volume fractions of 5 %, 10 %, 20 % and 50 % are $2x10^{16}$, $3x10^{15}$, $7x10^{15}$ and $1x10^{16}$, respectively. In addition it can be seen that there is not much difference between the collision rates of experiments with volume fractions of 20 % and 50 %. These observations are in contrast with the widespread view that, by increasing the volume fraction, the collision rate should increase. In fact in the experiments with an impeller speed of 1600-800 rpm, the highest collision rate is demonstrated by the experiment in the absence of Tween 20. This is caused by a two-fold effect of the dispersed phase volume fraction. Not only does increasing the volume fraction increase the number of the droplets, but also it increases the dampening effect of the dispersed phase.

It should be stressed, once more, that the collision efficiency refers to the fraction of droplets that coalesce upon collision. Investigation of the collision efficiency may provide an explanation why a higher number of droplets coalesced. Figures 6.8-c and d show no apparent pattern in collision efficiency variations arising from changes in Tween 20 concentration. This demonstrates that the effect of Tween 20 concentration on collision efficiency is complex and may be more fully determined by considering the mutual effect of number of parameters and Tween 20 concentration, since each individual factor is not a determinant parameter. For example, in the experiments with a 5 % dispersed phase volume fraction and an impeller speed of 1600-800 rpm, although the collision rate significantly increases with increasing Tween 20 concentration (the collision rate for 1 % Tween 20 is one order of magnitude higher than that corresponding to 0.02 % Tween 20, which itself is one order of magnitude higher than the rate in the absence of Tween 20), the collision efficiency when Tween 20 is not used

is the highest among the collision efficiencies related to all examined Tween 20 concentrations under the same experimental conditions. In addition, it can be seen that the collision efficiency for 1 % Tween 20 is higher than that for 0.02 %. This is an interesting observation since it is a common view that increasing the amount of Tween 20 suppresses the coalescence phenomenon. This peculiar behaviour is also observed for other experiments. For example, the experiments with a dispersed phase volume fraction of 20 % and an impeller speed of 1600-800 rpm show that the collision efficiency for 1 % Tween 20 is the highest among the collision efficiencies related to all examined Tween 20 concentrations under the same experimental conditions.

Figures 6.8-c and d show an increase in collision efficiency when a higher impeller speed is used. Moreover, it can be seen that an increase in dispersed phase volume fraction results in a reduction in collision efficiency, except for the case of 50 % dispersed phase volume fraction in the absence of Tween 20, which shows an increase in collision efficiency in comparison with 20 % dispersed phase volume fraction at either impeller speeds (1600-800 or 2000-1000 rpm).

As mentioned earlier (Section 2.3.4.1), there is no consistent collision model described in the published literature. Therefore, the phenomena occurring during the collision are characterised by a number of fundamental parameters and the effect of each parameter has been investigated individually. These parameters are the mean turbulent force, the entrapped film thickness, the radius of the flattened area, the eddy life time and the time scale of the collisions. The values of the flattened area as well as the continuous film thickness determine the amount of the continuous phase trapped between the droplets. All these parameters were calculated by using equations given in Chapter 4.

Table 6.3. Calculated parameters responsible for collision efficiency.

Volume fraction [%]	Impeller speed [rpm]	Tween 20 concentration [%]	d_{32} [µm]	Mean turbulent force x10^{-10} [N]	Film thickness x10^{-9} [m]	Radius of flattened area x10^{-14} [m]	eddy life time x10^{-2} [s]	Time scale of collision x10^{-12} [s]
5	800	0.00	50.81	34.198	27.227	69.172	1.77	32.74
		0.02	28.20	6.220	16.508	23.284	1.20	3.65
		1.00	13.51	1.071	3.483	2.354	0.73	0.25
	1000	0.00	26.41	6.607	5.260	6.954	0.91	2.24
		0.02	12.63	1.274	3.380	2.135	0.56	0.15
		1.00	7.59	0.240	0.779	0.296	0.39	0.02
10	800	0.00	59.19	37.223	29.636	87.721	2.33	16.96
		0.02	42.07	15.338	40.705	85.624	1.85	4.83
		1.00	29.59	4.949	16.084	23.799	1.47	1.31
	1000	0.00	33.29	11.973	9.532	15.867	1.27	1.65
		0.02	27.88	6.214	16.490	22.990	1.13	0.83
		1.00	19.93	2.665	8.660	8.634	0.90	0.25
20	800	0.00	66.58	25.339	20.174	67.159	3.51	9.10
		0.02	47.62	9.505	25.227	60.072	2.81	2.66
		1.00	32.73	3.916	12.727	20.829	2.19	0.67
	1000	0.00	40.41	9.425	7.504	15.166	2.01	1.13
		0.02	40.28	10.211	27.100	54.591	2.01	1.16
		1.00	30.81	5.139	16.702	25.736	1.68	0.43
50	800	0.00	80.30	2.965	2.361	9.481	15.90	11.45
		0.02	53.34	0.907	2.409	6.326	11.90	2.42
		1.00	31.87	0.223	0.724	1.155	8.56	0.38
	1000	0.00	55.45	1.649	1.313	3.642	9.91	2.36
		0.02	50.72	1.138	3.022	7.665	9.34	1.71
		1.00	24.54	0.160	0.521	0.639	5.76	0.12

Table 6.3 shows the values of the parameters affecting the collision efficiency. It can be seen that in all experimental conditions, the droplets' collision time scale (the reciprocal of the collision rate in the process) is significantly lower than the eddies' life time, meaning that the droplets are under constant turbulent force before colliding with another droplet (so-called "third droplet") which may be either disrupting or enhancing the on-going droplet coalescence. If the "third droplet" collides in any direction other than the direction of the centre-line of droplets, it may separate the two attached droplets, consequently terminating the continuous film drainage. However, if the "third droplet" collides in-line with the centre-lines of the attached droplets, it may well amplify the drainage rate.

It can also be seen in Table 6.3 that when a higher concentration of Tween 20 is used, smaller droplets enter the coalescence dominant region, resulting in a smaller amount of continuous phase entrapped between the droplets, thus, reducing the drainage time. At the same time, the turbulent force decreases, due to the smaller droplet sizes, which appears to be a less important factor in comparison with the amount of captured continuous phase affecting collision efficiency. It should be noted that at the beginning of the second processing step the droplets are fully covered by Tween 20. Therefore, this trend is caused by the smaller size of the colliding droplets generated as a result of employing a higher concentration of Tween 20. It can be argued that, since there is no emulsifier on the interface, in experiments where no Tween 20 is used, any collision should result in coalescence. This is not the case for these experiments where the time scale of droplets in contact is much higher than the time scale of collisions. It is suggested that the continuous film drainage is disrupted by colliding with the "third droplet", which separates the two droplets in contact.

The collision efficiency shows a direct dependency on energy. This can be explained by the fact that, at higher levels of energy input, a planar film of smaller thickness is entrapped between droplets, which decreases the drainage time. At the same time, the radius of the flattened area is reduced, which has a two-fold effect. A large radius of the flattened area increases the amount of continuous phase entrapped and, as a result, increases the drainage time. However, it increases the likelihood for surface modulations, raising the probability of a contact generation between two parallel planar surfaces. In addition to these effects, the turbulent force magnitude is reduced by increasing the energy input, which, in turn, may reduce the collision efficiency. It can be deduced from Table 6.3 that the drainage time plays the most important role on this dependency.

The same analysis can be employed to explain the inverse dependency of the collision efficiency on the dispersed phase volume fraction. It can be seen that the turbulent force is reduced by an increase in the dispersed phase volume fraction, although there are several exceptions; for example when no emulsifier is used in the experiments where emulsions are processed at 1600-800 rpm with dispersed phase volume fractions of 5 % or 10 %. The thickness of the continuous phase captured between droplets decreases by increasing the dispersed phase volume fraction. In contrast, the calculated radius of the flattened area increases by increasing the volume fraction when Tween 20 is used (at 0.02 % and 1 % concentrations) and decreases when no emulsifier is used. These trends would have opposing effects on the collision efficiency. For example, larger droplets (a consequence of employing a higher dispersed phase volume fraction) collide with a planar film of smaller thickness which promotes coalescence and with a flattened area of larger diameter which tends to reduce the collision efficiency. Nonetheless, in these experiments the turbulent force appears to be the important parameter determining the effect of dispersed phase volume fraction on collision efficiency, which is also highly affected by the dampening effect of the dispersed phase on the energy experienced by the droplets.

It is now worth investigating the high collision efficiency observed in the experiment with 50 % dispersed phase volume fraction in the absence of Tween 20. This may have been caused either by the large size of the droplets observed at this experiment or by a strong dampening effect due to the high internal phase,. This results in a significant reduction in turbulent forces acting on the droplets. The short-range steric repulsive forces may be comparable to turbulent forces when 50 % dispersed phase volume fraction is used; therefore, the droplets that are covered by Tween 20 show lower droplet coalescence, hence, having lower collision efficiency.

From all the dependencies of the operating parameters on collision efficiency it can be deduced that the amount of continuous phase captured between two colliding droplets is the main parameter affecting the collision efficiency at the same dispersed phase volume fraction. Consequently, the droplet coalescence frequency at the second processing step is mostly affected by the size of the droplets and, hence, number of droplets and the collision rate. If the collision efficiency is investigated with regard to the dispersed phase volume fraction, the dampening effect plays the most important role on the variations of the collision efficiency. Nonetheless, still the collision rate will determine the droplet coalescence rate which, in turn, is highly influenced by the dampening effect of the dispersed phase volume fraction.

6.2.2.3 Response of the emulsions to the coalescence dominant regime

Apart from investigating the droplet coalescence corresponding to the initial stages of the second processing step, it is worth analysing the data on the droplet size evolution. It can be seen from Figures 6.7 and 6.8 that the droplet size increases gradually throughout the second processing step in the experiments when surfactants are not employed. However, in the experiments where Tween 20 is used, the droplet size reaches equilibrium after a rapid increase. This is demonstrated in Table 6.3 which shows the droplet sizes that are achieved at the end of two hours of processing after the impeller speed change in the second processing step. In addition, in order to investigate the extent of the influence of the droplet coalescence dominant regime on the droplet size evolution, the droplet size increase (or the droplet size difference) during the second processing step is also shown in Table 6.4.

Table 6.4. The final droplet size reached at the end of the second processing step and the droplet size difference between the final droplet sizes produced at the end of the first and second processing steps of the experiments.

Volume fraction [%]	Impeller speed [rpm]	Tween 20 concentration [%]	d_{32} [µm]	Droplet size difference [µm]
5	800	0.00	70.57	19.76
		0.02	35.95	7.74
		1.00	30.91	17.39
	1000	0.00	42.94	16.50
		0.02	29.13	16.50
		1.00	18.52	10.92
10	800	0.00	78.92	19.72
		0.02	47.69	5.62
		1.00	40.09	10.50
	1000	0.00	45.06	11.77
		0.02	41.17	13.29
		1.00	35.56	15.62
20	800	0.00	89.41	22.83
		0.02	51.18	3.56
		1.00	38.79	6.07
	1000	0.00	51.73	11.31
		0.02	52.68	12.40
		1.00	36.06	5.25
50	800	0.00	149.76	69.46
		0.02	61.42	8.90
		1.00	35.36	3.49
	1000	0.00	116.84	61.38
		0.02	76.51	25.79
		1.00	29.29	4.75

It can be seen that, in the experiments where 0.02 % Tween 20 is employed and emulsions in the absence of added emulsifier, the increase in the mean droplet size increases by employing higher dispersed phase volume fractions. However, this is not the case for emulsions containing 1 % Tween 20, where the difference in mean droplet sizes decreases. In addition, the droplet size difference decreases by increasing the Tween 20 concentration at each volume fraction and impeller speed, except for the case with a dispersed phase volume fraction of 5 % which shows an opposite trend; the increase in droplet size is the highest for emulsions containing 1 % Tween 20. This observation demonstrates that when Tween 20 is employed, the droplet break-up occurs at lower droplet sizes in comparison with experiments

in the absence of added emulsifier. This is caused by the lower interfacial tension induced by adsorption of Tween 20. In the case with 1 % Tween 20 processed with 5 % dispersed phase volume fraction, the effect of high concentration of Tween 20 is less significant due to the high coalescence frequencies and the high collision rates observed at the initial stages of the second processing step.

6.2.2.4 Discussion on the differences between the experimental observations and the published literature

The results presented in the previous section are partly in contradiction with results reported in the literature. Taisne *et al.* (1996) investigated the coalescence occurrence during emulsification by employing SDS as a surfactant. They showed that, at higher concentrations of SDS, the coalescence is completely suppressed. Their emulsions were prepared with 10 % dispersed phase volume fraction. The same results were observed by Lobo and Svereika (2003) and Narsimhan and Goel (2001) when SDS was employed. In the present study, the results of the same volume fraction (10 %) show the opposite trend (Figure 6.8). Henry *et al.* (2009) investigated coalescence in the presence of Tween 20 using the same method proposed by Lobo *et al.* (2002). They determined that coalescence is suppressed at a concentration above a certain value. Their experiments were conducted in a homogeniser and on nano-sized droplets with a volume fraction of 10 %.

The reasons for different trends observed by published literature are related to the different experimental conditions employed in the present study in comparison to those of the published studies. For example Taisne *et al.* (1996), Lobo and Svereika (2003) and Narsimhan and Goel (2001) performed their experiments using SDS which is an anionic surfactant. The difference between SDS and Tween 20 is due to the fact that Tween 20 is a nonionic surfactant and does not stabilise droplets against coalescence by generating an

electrostatic double layer, which generates a high repulsive force. Colloidal repulsive forces attributed to Tween 20 are steric repulsion (which is considered as a short-range force).

Nonetheless, the main difference between the present study and the published ones concerns the choice of the emulsification process. The published studies performed their experiments with homogeniser which operated as a continuous process, as opposed to the batch process employed in the present study. The difference between the results of the present study and those in the published studies may be caused by the fact that, in homogenisers, the damping effect may not be as important as it is in the stirrer tanks as the residence time of emulsion in the homogeniser's chamber is significantly lower in comparison with a batch stirred system. These methodological differences may also explain the discrepancy noted between the results of the present study and those reported by Henry *et al.* (2009) since they used Tween 20 as well in their study. In addition, the work of Lobo and Svereika (2003) and Henry *et al.* (2009) is comparable only with the first processing step of the present study, where droplet coalescence and break-up occurred simultaneously and not with the second processing step where droplet coalescence was solely responsible for the droplet size variations.

6.2.3 Third processing step

6.2.3.1 Droplet size evolution data

In this processing step, the size of the droplets entering the break-up dominant regime was notably smaller than the respective size in the first processing step. This induces droplet break-up on the already formed interfaces. The droplet size evolution data corresponding to the third processing step of the experiments performed is shown in Figures 6.9 and 6.10. Specifically, the figures show the droplet size evolution data of the third processing step of emulsification processes with impeller speeds of 1600-800-1600 rpm and 2000-1000-2000

rpm, for varying Tween 20 concentrations and dispersed phase volume fractions of 5 % (a), 10 % (b), 20 % (c) and 50 % (d).

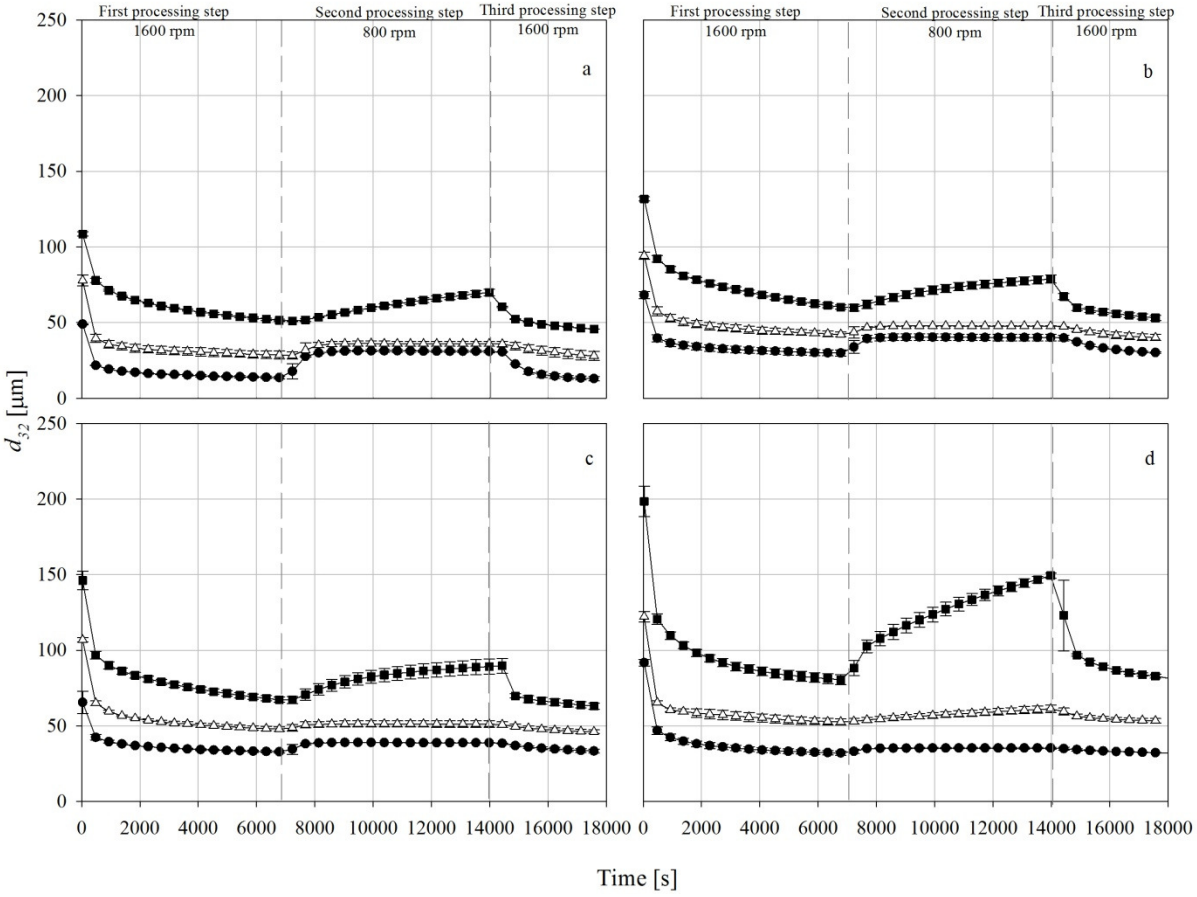

Figure 6.9. Droplet size evolution data obtained from the first, the second and the third processing steps of emulsification experiments with impeller speed of 1600-800-1600 rpm in the absence of added emulsifier (■) and in the presence of 0.02 % (Δ) and 1 % (●) concentrations of Tween 20 are shown for oil-in-water emulsions containing varying dispersed phase volume fractions of (a) 5 %, (b) 10 %, (c) 20 % and (d) 50 %.

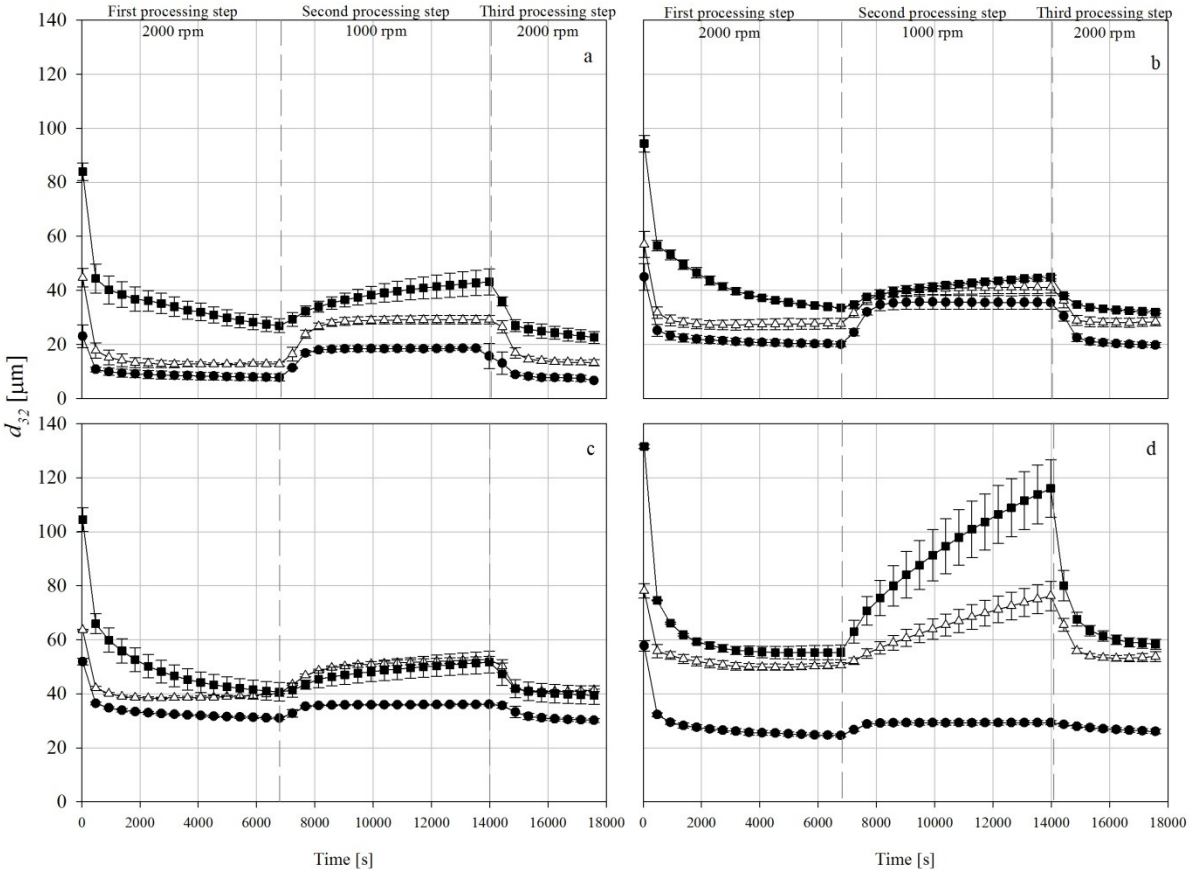

Figure 6.10. Droplet size evolution data obtained from the first, the second and the third processing steps of emulsification experiments with impeller speed of 2000-1000-2000 rpm in the absence of added emulsifier (■) and in the presence of 0.02 % (Δ) and 1 % (●) concentrations of Tween 20 are shown for oil-in-water emulsions containing varying dispersed phase volume fractions of (a) 5 %, (b) 10 %, (c) 20 % and (d) 50 %.

It can be seen from Figures 6.9 and 6.10 that the behaviour of the droplet size evolution depends on the Tween 20 concentration. For example, the experiments with 50 % dispersed phase volume fraction in the absence of Tween 20 and processed under 1600-800-1600 rpm impeller speed (Figure 6.9-d) show a rapid reduction which is followed by the plateau region. However, the same experimental condition using 1 % Tween 20 (Figure 6.9-d) shows no significant changes of the droplet size from the initial value during the third processing step. These behaviours are due to the fact that, in the third processing step, the droplet size evolution data returns to the droplet size achieved by the end of the first processing step. Therefore, if there was a significant change in droplet size during the second

processing step (since the droplets at the end of the second processing step enter the third processing step) then there would be a rapid reduction in droplet size during the third processing step. This can be demonstrated by calculating the droplet break-up frequencies at this processing step.

6.2.3.2 Droplet break-up and the response of the emulsions to the third processing step

The break-up frequency calculations assume that the droplet coalescence is negligible at the very early stages of the third processing step. These frequency values, together with the droplet sizes at the end of the first and third processing steps are shown in Table 6.5.

Table 6.5. Break-up frequencies calculated at the early stages of the third processing step and final droplet sizes determined at the end of the first and third processing steps for various experimental conditions employed.

Volume fraction [%]	Impeller speed [rpm]	Tween 20 concentration [%]	Break-up frequency x10^{-3} [s^{-1}]	Final droplet size at the end of the first processing step [μm]	Final droplet size at the end of the third processing step [μm]
5	1600	0.00	10.60	50.81	45.09
		0.02	0.63	28.20	27.45
		1.00	1.66	13.51	12.69
	2000	0.00	15.90	26.44	22.32
		0.02	5.10	12.63	13.32
		1.00	6.51	7.59	7.38
10	1600	0.00	11.10	59.19	52.51
		0.02	0.51	42.07	39.86
		1.00	0.58	29.59	29.98
	2000	0.00	12.90	33.29	31.88
		0.02	6.37	27.88	28.53
		1.00	7.91	19.93	19.75
20	1600	0.00	11.40	66.58	62.52
		0.02	0.47	47.62	45.89
		1.00	0.71	32.73	33.15
	2000	0.00	10.90	40.41	39.30
		0.02	4.16	40.28	41.38
		1.00	0.90	30.81	30.07
50	1600	0.00	22.00	80.30	82.07
		0.02	2.73	52.52	53.45
		1.00	1.44	31.87	32.06
	2000	0.00	30.00	55.45	58.24
		0.02	11.1	50.72	53.91
		1.00	1.99	24.54	25.92

Table 6.5 shows that, in contrast to the droplet break-up frequencies of the first processing step, higher break-up frequencies are observed for systems without any added emulsifier, while using Tween 20 reduces the break-up frequencies. It should be noted that there is no clear pattern indicating the effect of dispersed phase volume fraction and energy input on the break-up frequency in this step. In fact, all these dependencies result from the behaviour of droplet size evolution at the second processing step. This can be seen in Table 6.5, which reports similar values of the final droplet sizes for the first and third processing steps.

Figures 6.9 and 6.10 demonstrate that the droplet size evolution continues the path of the first processing step. In other words, when the droplet size at the third processing step reaches the plateau region, it behaves as if the second processing step had not been carried out. This is due to the fact that at the end of the first processing step, the system has already established a dynamic equilibrium and a further minor reduction in the droplet size is subject to 'aging' in the process (the emulsion should be processed for longer times). This reduction in droplet size continues gradually until the rate of emulsifier adsorption becomes small and the rates of droplet break-up and coalescence equilibrate. This phenomenon causes the behaviour observed for the droplet break-up frequencies. Since the droplet sizes are reduced to their predetermined values (droplet sizes reached at the end of the first processing step), the droplet break-up frequency will be a function of the droplet size differences between the droplet sizes at the end of the second and the first processing steps. Therefore, in the cases where an emulsifier is not employed, a big change in droplet size is observed, resulting in a high droplet break-up frequency. However, in the cases where there is not a significant change in the droplet size (experiments with Tween 20) a lower break-up frequency is observed.

6.3 Concluding remarks

This chapter focused on the investigation of the influence of the dispersed phase volume fraction on the underlining processes affecting droplet size of emulsions. It can be concluded that the final droplet sizes decreased with increasing Tween 20 concentration, impeller speeds and reduction in the dispersed phase volume fraction. The high droplet coalescence events are commonly assumed to be responsible. However, it was shown that this is caused by the low droplet break-up rate caused by the low adsorption rate of Tween 20 at lower concentrations.

A minimum was observed in droplet break-up frequency with respect to volume fraction of the dispersed phase. This was a consequence of the competitive effect of dampening effect of the dispersed phase and the capillary pressure of the droplets. An increase in impeller speed increased the droplet break-up frequency. This was a consequence of the fact that higher turbulent stress resulted in breaking smaller droplets. The droplet break-up frequency was more affected by Tween 20 concentration at lower dispersed phase volume fractions. This was due to the fact that at higher volume fractions higher interfacial area was produced which resulted in inducing similar interfacial tension at all Tween 20 concentrations.

The collision rate showed a minimum at dispersed phase volume fraction of 10 % at all used Tween 20 concentrations and impeller speeds. This was a consequence of the competing effects of the dampening effect and higher number of droplets in the processes. Furthermore, an increase in Tween 20 concentration and impeller speed showed to cause an increase in collision rate.

Collision efficiency did not have any consistent dependency on Tween 20 concentration. An increase in volume fraction of the dispersed phase caused a decrease in

collision efficiency. Finally, increasing impeller speed increased the collision efficiency. It can be concluded that the amount of continuous phase captured between two colliding droplets is the main parameter affecting the collision efficiency at the same dispersed phase volume fraction. Consequently, the droplet coalescence frequency is affected by the size of the droplets and, hence, number of droplets, demonstrated in the collision rate. If the collision efficiency is investigated with regard to the dispersed phase volume fraction, the dampening effect plays the most important role on the variations of the collision efficiency.

As to conclude the analysis of the first and the second processing steps, it can be deduced that the droplet coalescence cannot be suppressed completely in these experiments by presence of Tween 20 on the interface. This can be justified by the fact that in batch processes a high collision rate is expected and since Tween 20 can be desorbed from the interface, a high colaescence frequency is observed. It can be further concluded that the final droplet size is the result of the equilibrium of droplet break-up, droplet coalesnce and the rate of adsorption of Tween 20.

The droplet size evolution data of the third processing step at all experiments returned to their respective values determined at the first processing step. This was due to the fact that at the end of the first processing step, the system has already established a dynamic equilibrium and a further minor reduction in the droplet size is subject to ‘aging’ in the process.

Chapter 7

Mechanistic understanding of emulsion formation during processing: The effect of emulsifier type and concentration

This chapter focuses on the investigation of emulsion formation during processing in the presence of various emulsifier Types and concentrations.

7.1 Introduction

The aim of this chapter was to study the influence of operating parameters on emulsification in the presence of varying emulsifier types and concentrations. The experiments were designed such that droplet break-up and/or coalescence would be the dominant phenomenon, allowing the investigation of each of these phenomena. The experimental procedure is given in section 4.3. The selected emulsifiers and their concentration are listed in Table 7.1.

Table 7.1. Emulsifier type and concentration used and the experimental conditions carried out in Chapter 7.

Dispersed phase volume fraction	10 %		
Emulsifier	**Type**	**Concentration**	
	Tween 20	0 %, 0.02 % and 1 %	
	Silica particles	0 %, 0.02 % and 1 %	
	Sodium caseinate	0 %, 0.02 % and 1 %	
	WPI	0 %, 0.02 % and 1 %	
	Mixed-emulsifier	Combinations of Tween 20 and silica particles	
Impeller speed [rpm]	**First processing step**	**Second processing step**	**Third processing step**
	1600	800	1600

The experimental protocol was performed on emulsions in the presence the emulsifiers listed in Table 7.1. It should be noted that mixed-emulsifier systems consisted of low concentrations (0.02 %) of silica particles and Tween 20, low concentrations (0.02 %) of silica particles with high concentration (1 %) of Tween 20, high concentration (1 %) of silica particles and Tween 20 and high concentration of silica particles (1 %) with low concentration of Tween 20 (0.02 %). It should be noted that, since the environment of the process affects the physical structure of proteins in the solution, the pH and ionic strength of solutions were adjusted to 7 and 0.01 M, respectively. Each experiment was performed at least three times in

order to obtain reproducible data and the results are reported as mean ± standard deviation of the mean of the three runs. Each of these experimental steps was interpreted individually.

In order to fully analyse the data obtained from the experiments, additional experiments were carried out. After emulsification experiments, samples were obtained and their flow curves were determined in order to evaluate the rheological behaviour of the emulsions during the processes. Additionally, equilibrium interfacial tension was determined in order to obtain information regarding the interfaces between the dispersed and the continuous phases.

7.2 Rheological behaviour of the emulsions

The viscosities of a number of stable emulsions with different concentrations of Tween 20, silica particles, sodium caseinate and WPI were measured. The rheological studies were carried out under a range of shear rates (0.1-1000 s^{-1}). Five different samples were prepared with varying emulsifier concentrations. Emulsions were prepared with 1 % silica particles alone, 0.02 % silica particles in conjunction with 1 % Tween 20, 1 % of both silica particles and Tween 20 and 1 % sodium caseinate at pH 7 and ionic strength of 0.01 M. By this method, the effect of silica particles on emulsion viscosity, when they are employed individually or as part of a mixed-emulsifier system, can be investigated. The rheological data are shown in Figure 7.1; specifically, the measured shear stresses (a) and viscosities (b) are plotted with respect to the shear rate.

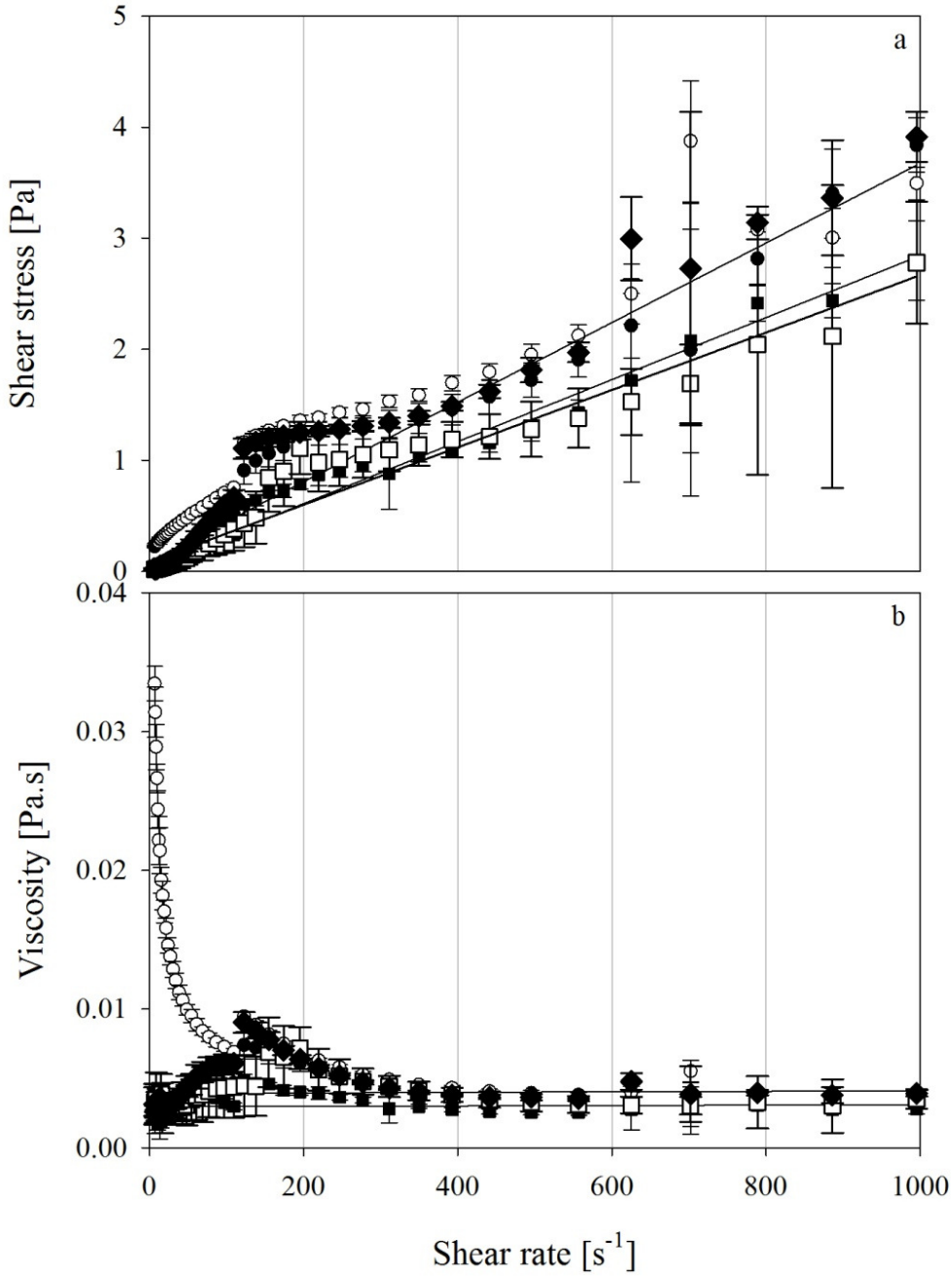

Figure 7.1. The flow curves of shear stress (a) and viscosity (b) with respect to the shear rate for oil-in-water emulsions with 10 % dispersed phase volume fraction and in the presence of 1 % silica particles alone (●), 1 % silica particles in conjunction with 1 % Tween 20 (○), 0.02 % silica particles and 1 % Tween 20 (■), 1 % sodium caseinate (□) and 1 % WPI (♦).

Figure 7.1 demonstrates that the emulsions stabilised with 1 % silica particles, mixed-emulsifier systems of 0.02 % silica particles and 1 % Tween 20, 1 % sodium caseinate

and 1 % WPI have the same behaviour as those stabilised solely with small molecule surfactants observed in Chapters 5 and 6. Overall, the data are noisy at shear rates smaller than 100 s^{-1}, while there is Newtonian behaviour at higher shear rates with viscosity of 0.002 or 0.003 Pa.s. This is expected due to the low volume fraction (φ = 10 %) of the dispersed phase, where the colloidal inter-droplet interactions are negligible. This behaviour was previously observed for emulsion systems with similar dispersed phase volume fractions in the presence of proteins and silica particles (Dickinson and Golding, 1997; Krynke and Sek, 2004; Morishita and Kawaguchi, 2009).

The emulsions in the presence of a mixed-emulsifier system with 1 % silica particles and 1 % Tween 20 show a yield stress. This behaviour has been previously observed by Nciri *et al.* (2010) and Simon *et al.* (2010) and is related to the presence of high concentration of silica particles in the aqueous phase, resulting in the formation of a 3D network in the continuous phase. By increasing the shear rate up to 50 s^{-1}, these networks break down resulting in the low viscosity observed at higher shear rates. It should be noted that, during the process, since the fluid is in motion and not stationary during these experiments, there is insufficient time for the silica particles to create 3D networks. Therefore, it may be assumed that these emulsions behave as Newtonian fluids, similar to their behaviour at higher shear rates where they show similar viscosity (~0.003 Pa.s) as the other emulsions in Figure 7.1.

7.3 Interfacial tension studies

One of the most important parameters affecting droplet break-up and coalescence is the interfacial tension between the oil and aqueous phases of an emulsion. The balance between the interfacial tension and the hydrodynamic forces determines the stability of the droplets during the process. Therefore, in order to determine the effect of the emulsifier on the interfacial tension between the oil and aqueous phases of an emulsion, the types and

concentrations of the emulsifiers tested were the same as those used in the emulsification experiments. Figure 7.2 plots the interfacial tension between the oil and aqueous phases of emulsions containing varying concentrations of silica particles and Tween 20.

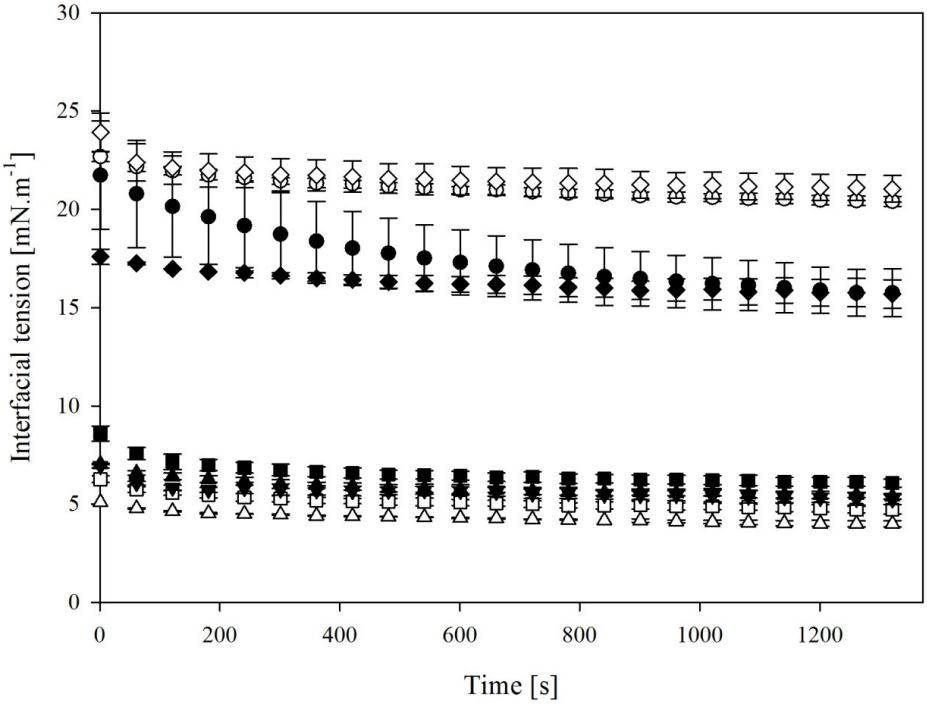

Figure 7.2. Interfacial tension measured between oil and water solutions in the absence of added emulsifiers (●), and in the presence of 0.02 % silica particles (○), 0.02 % silica particles and 0.02 % Tween 20 (■), 0.02 % silica particles and 1 % Tween 20 (□), 1 % silica particles (♦), 1 % silica particles and 0.02 % Tween 20 (◊), 1 % silica particles and 1 % Tween 20 (▼), 1 % Tween 20 (Δ), and 0.02 % Tween 20 (▲).

Figure 7.2 demonstrates that the presence of silica particles alone does not affect the interfacial tension between water and oil; thus, similar interfacial tension values are reported for oil and pure water and for oil and water with added silica particles (with less than 25 % relative difference at any time point). This has been previously reported by other studies (Morishita and Kawaguchi, 2009; Nciri *et al.*, 2010). The reason that the interfacial tension between oil and water in the absence of added emulsifier and the ones with silica particles (for example the solution with 0.02 % silica particles) does not change with time and, in some cases shows higher interfacial tension (namely, the solution with 0.02 % silica particles), is

that the rapeseed oil used in these studies was food grade and not pure, thus containing small amounts of surface active materials, which, by adsorption on the interface, can marginally decrease the interfacial tension. However, in the presence of silica particles, their adsorption rate decreases significantly due to the formation of a layer of silica particles on the interface.

In contrast, when Tween 20 was used with silica particles, the reported interfacial tension was similar to the values reported when only Tween 20 was employed. For example, the values of the interfacial tension reported for mixed-emulsifier systems of 0.02 % silica particles with 1 % Tween 20 are similar to those reported for the solution of 1 % Tween 20. The reason for this is that the silica particles in the aqueous phase do not compete with Tween 20 on adsorption on the interface. First, Tween 20 is adsorbed and subsequently, with their slower pace, silica particles 'fill' the empty spaces on the interface, as shown schematically in Figure 7.3-a.

Alternatively, the observed behaviour can be explained by adsorption of Tween 20 on the interface of silica particles. This is caused due to the hydrophilicity of the surfaces of the particles which attract the Tween 20 hydrophilic segments. This causes a drop in Tween 20 concentration (Figure 7.3-b). It should be noted that both of described hypotheses can explain the experimental data.

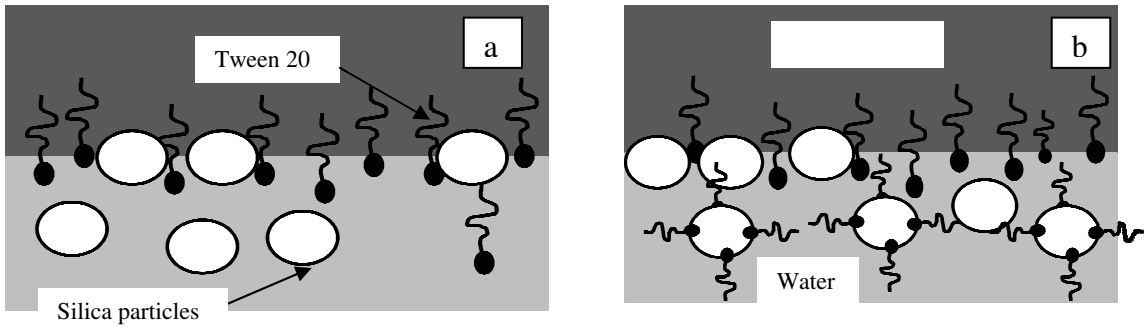

Figure 7.3. Schematic diagram of the positions of Tween 20 and silica particles at the interface between oil and water.

There is a case, however, which does not behave as the structure shown in Figure 7.3. As can be seen in Figure 7.2, the interfacial values reported for the system of 1 % silica particles with 0.02 % Tween 20 are similar (with less than 25 % relative difference at any time point) to those observed for the solution with 1 % silica particles, which is closer to pure water. This, in fact, further demonstrates that, since a high concentration of silica particles exists in the aqueous phase, the layer is formed on the interface faster than the time required for Tween 20 to be adsorbed. Thus the low amount of Tween 20 is hindered in reaching the interface and, hence, the resultant interfacial tension reported is close to that of pure water. However, this observation does not hold for the case of the solution of a 1 % silica particles and 1 % Tween 20, where the high concentration of Tween 20 results in the rapid formation of a layer on the interface. Alternatively, when 0.02 % of Tween 20 is used with 1 % of silica particles, the adsorption of Tween 20 on the surfaces of silica particles depletes Tween 20 in the aqueous phase, hence; the interfacial tension would be only affected by silica particles. This results in similar interfacial tension as when 1 % silica particles are employed.

The interfacial tension between the oil and aqueous phases in the presence of varying concentrations of sodium caseinate and WPI is plotted in Figure 7.4.

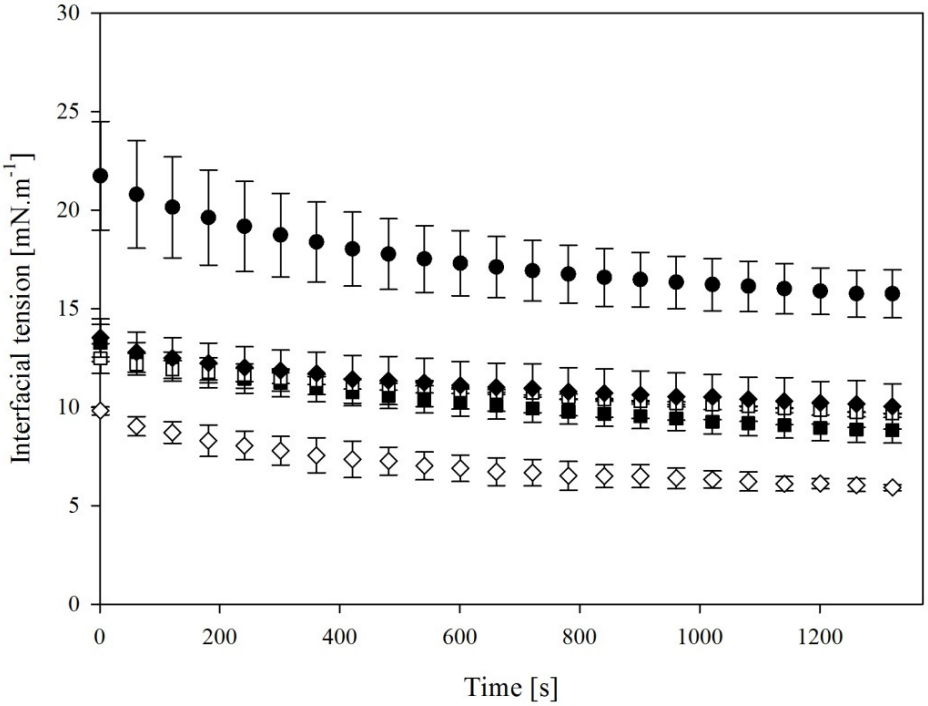

Figure 7.4. Interfacial tension measured between oil and water solutions in the absence of added emulsifier (●), and in the presence of 0.02 % sodium caseinate (■), 1 % sodium caseinate (□), 0.02 % WPI (♦), 1 % WPI (◊).

It can be seen in Figure 7.4 that similar interfacial tension values (~10 $mN.m^{-1}$) are reported for the cases of 0.02 % and 1 % of sodium caseinate. In contrast, although a similar interfacial tension (~10 $mN.m^{-1}$) is reported for 0.02 % WPI, a notably lower interfacial tension is observed for 1 % WPI (~6 $mN.m^{-1}$). This difference may be caused by the difference between the types of proteins. Sodium caseinate is considered to have disordered flexible structures whereas WPI remains as globules in the solution (Dickinson *et al.*, 1985a; Dickinson *et al.*, 1985b; Dickinson, 1997). The reason that similar interfacial tension values are reported for high and low concentrations of sodium caseinate relates to the adsorption layer on the interface. The interfacial layer of sodium caseinate is formed by the adsorption of long chains of molecules in the form of 'loops and tails'. Moreover, the casein molecules contain negative charge in the solution with natural pH (Dickinson, 2001). As a result of these phenomena, the formed interfacial layer prevents other molecules from reaching the interface,

inhibiting the formation of multi-layer molecules on the interface; thus, similar interfacial tension values are reported. It should be noted that the low concentration of sodium caseinate appears to be sufficient to form a layer on the interface. In contrast, as WPI molecules adsorb on the interface as globules and, subsequently, unfold on the interface, there will be more space for other molecules to reach the interface. Hence, a higher number of molecules in the solution will result in the adsorption of a higher number of molecules on the interface causing, subsequently, lower interfacial tension. In order to further investigate this hypothesis, the interfacial tension of a range of sodium caseinate concentrations was measured and the results are plotted in Figure 7.5. It can be seen that similar interfacial tension values are reported even with concentrations of sodium caseinate as low as 0.01 %. This observation further suggests that once a mono-layer of sodium caseinate is formed on the interface (0.01 % sodium caseinate was sufficient in this study) any excess of sodium caseinate does not affect interfacial tension.

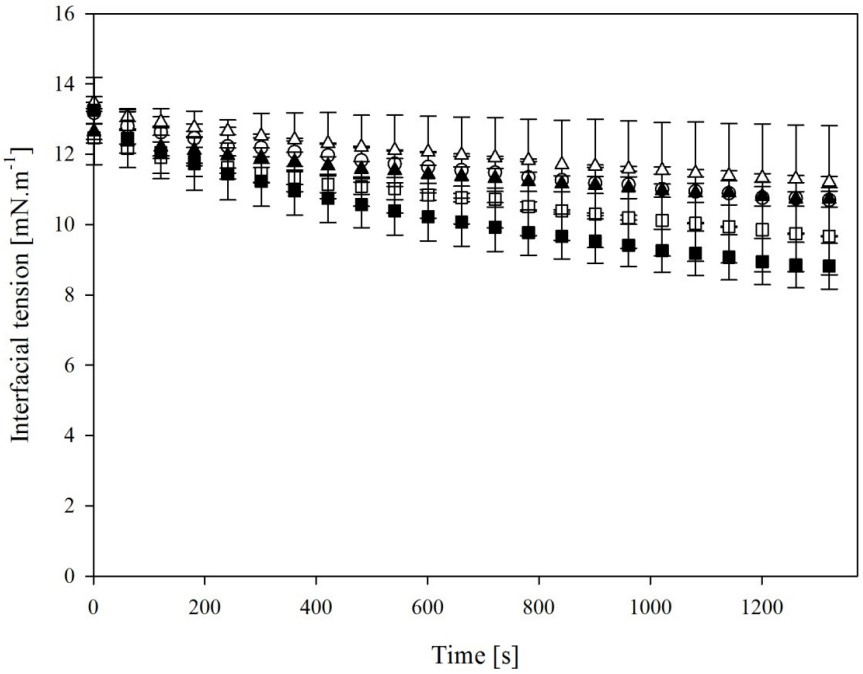

Figure 7.5. Interfacial tension measured between oil and water solutions in the presence of 0.01 % (Δ), 0.02 % (■), 0.2 % (▲), 0.6 % (○) and 1 % (□) of sodium caseinate.

Nonetheless, it should be noted that in the described studies the interfacial area remained constant whereas in the emulsification processes, due to the droplet break-up, it increases. Therefore, the similar interfacial tension values observed in the described studies most probably will not occur during processing and, consequently, they may be quite different in accordance to the time scale of the process and the interfacial area. However, the described studies showed that lower interfacial tension can be achieved by solutions of WPI in comparison with solutions of sodium caseinate at similar concentration; in addition, a higher interfacial tension is expected from solutions of proteins in comparison with solutions of Tween 20 or most of the mixed-emulsifier solutions.

7.4 Emulsification experiments

7.4.1 First processing step

7.4.1.1 Droplet size evolution data

The droplet size evolution data related to the first processing step (impeller speed of 1600 rpm) of the emulsification experiments are shown in Figures 7.6-7.8. The first graph contains the data related to experiments in the presence of varying concentrations of Tween 20 and silica particles used individually (Figure 7.6). The second graph contains data related to the emulsification experiments in the presence of the mixed-emulsifier systems (Figure 7.7). The third graph contains the data related to the emulsification experiments with solutions containing varying concentrations of milk proteins (Figure 7.8).

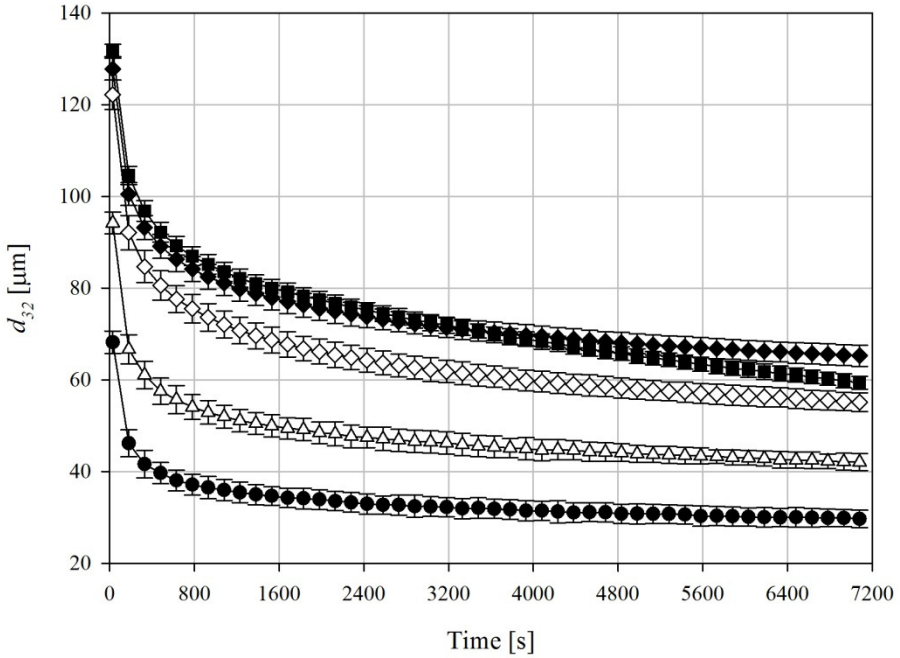

Figure 7.6. Droplet size evolution data related to the first processing step (impeller speed of 1600 rpm) of the emulsification experiments with solutions containing varying concentrations of silica particles and Tween 20, separately: (■) no silica particles or Tween 20 , (♦) 0.02 % Silica particles, (◊) 1 % Silica particles, (Δ) 0.02 % Tween 20 and (●) 1 % Tween 20.

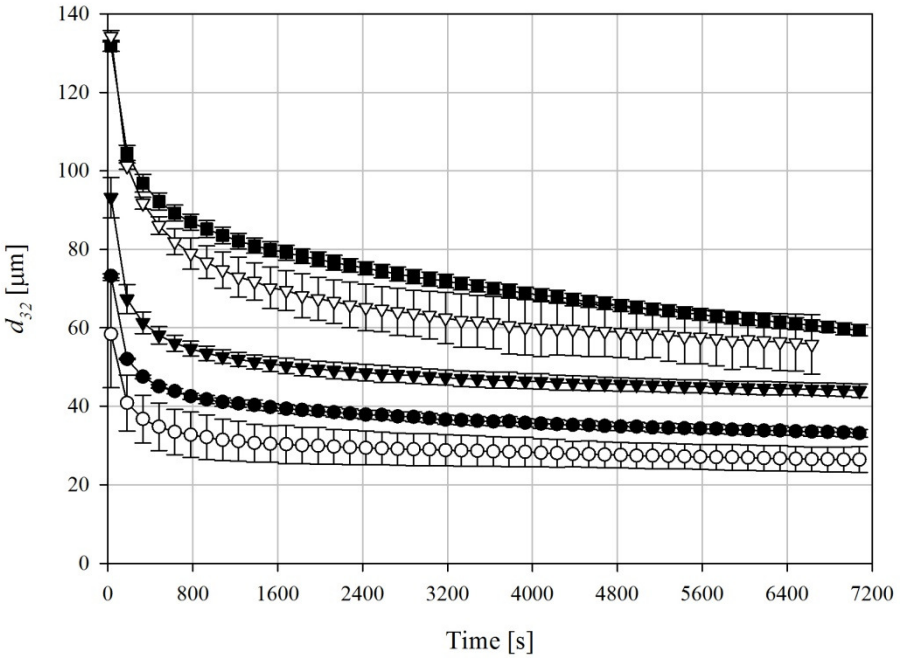

Figure 7.7. Droplet size evolution data related to the first processing step (impeller speed of 1600 rpm) of the emulsification experiments with solutions containing varying concentrations of silica particles and Tween 20 in combination: (■) no silica particles or Tween 20, (▼) 0.02 % Silica particles with 0.02 % Tween 20, (▽) 1 % Silica particles with 0.02 % Tween 20, (●) 0.02 % Silica particles with 1 % Tween 20 and (○) 1 % Silica particles with 1 % Tween 20.

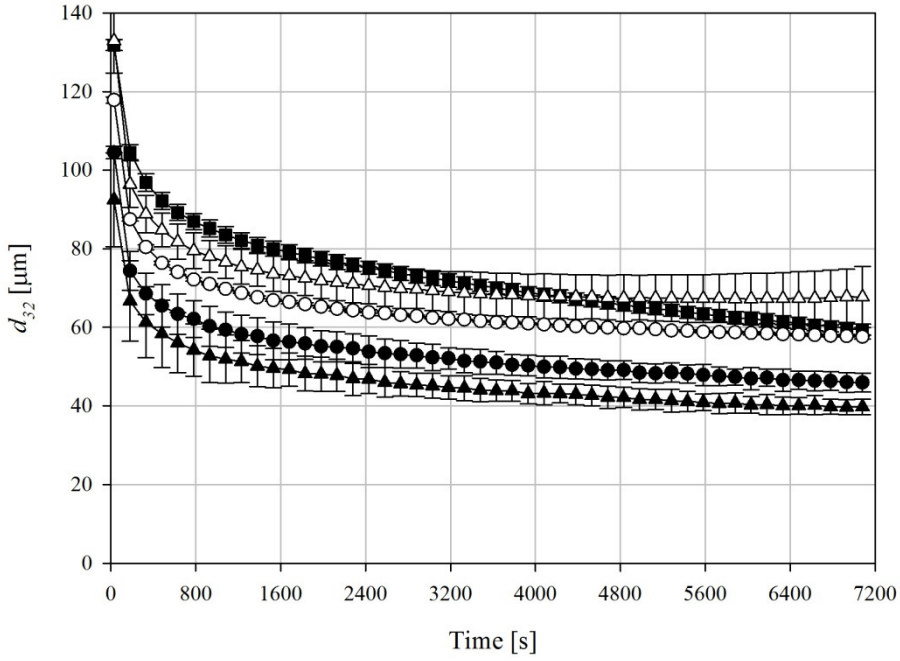

Figure 7.8. Droplet size evolution data related to the first processing step (impeller speed of 1600 rpm) of the emulsification experiments with solutions containing varying concentrations of sodium caseinate and WPI separately: (■) No sodium caseinate or WPI, (Δ) 0.02 % Sodium Caseinate, (▲) 1 % sodium caseinate and (○) 0.02 % WPI and (●) 1 % WPI.

It can be seen in Figures 7.6-7.8 that the behaviour of the droplet size evolution is similar to the trend observed in previous chapters.

7.4.1.1.1 Rapid decrease region

The droplet size at the initial stages of the process decreases rapidly due to the high droplet break-up frequency. The latter is observed since the droplets are unstable under the hydrodynamic conditions of the process. It should be stressed that the droplet coalescence frequency is negligible compared with the droplet break-up frequency during the initial stages of the process.

Droplet break-up frequency is a function of the droplet size at this stage and the composition of the interfaces of the droplets. Various emulsifier types may indeed affect the droplet break-up differently. In order to examine the emulsifier type and concentration, droplet break-up frequencies were calculated (equation 4.12). Each of the emulsifiers groups were analysed individually.

Tween 20 and silica particles

The initial droplet size and calculated droplet break-up frequencies are shown in Figure 7.9-a and b with respect to emulsifier concentration.

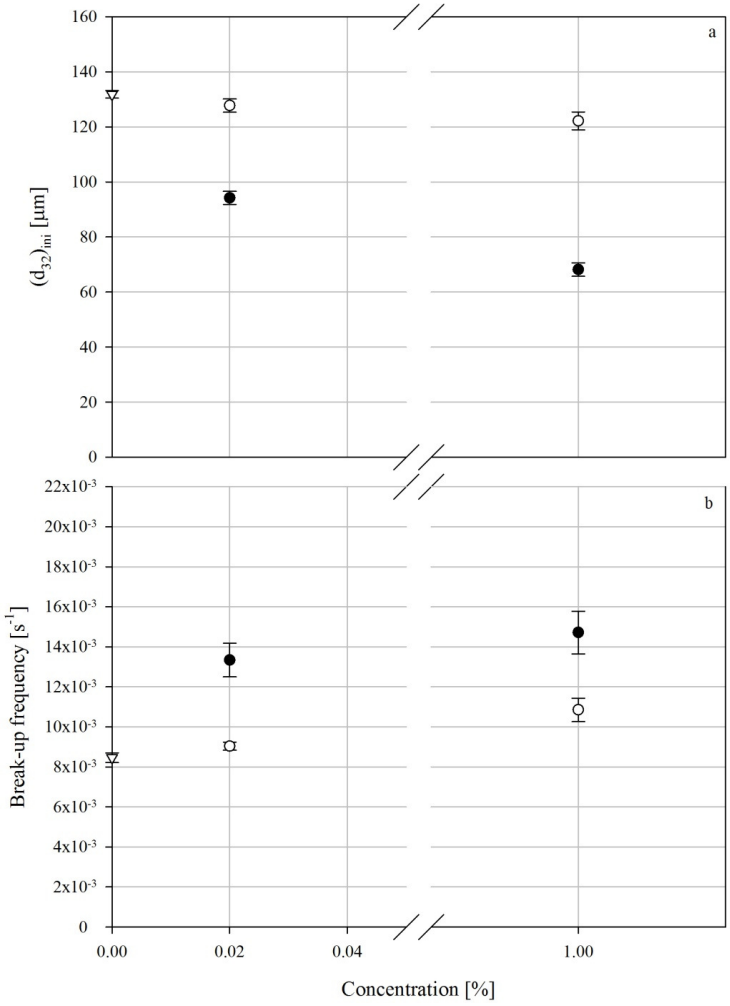

Figure 7.9. Initial droplet diameter (a) and break-up frequency (b) determined at the initial stages of the first processing step with respect to and varying concentrations of Tween 20 (●) and silica particles (○) and experiments in the absence of added emulsifier (▽).

It can be seen from Figure 7.9-a that the initial droplet sizes determined when only Tween 20 is used decreases when the concentration of Tween 20 increases. This observation has already been made and, subsequently, analysed in Chapter 6. Since the size and number of daughter droplets are a function of energy experienced by the mother droplet (Tsouris and Tavlarides, 1994; Tcholakova *et al.*, 2007), the size of the inital droplet size depends on the interfacial tension of the droplets. Hence, the experiment which shows lower interfacial tension (1 % Tween 20) would result in lower droplet sizes. In addition, Figure 7.9-b shows that the break-up frequencies when varying concentrations of Tween 20 are used are marginally increasing, even though the used concentrations are significantly different, and both values are higher than the break-up frequency of the experiment in the absence of added emulsifier. This observation has been explained in detail in Chapter 6 and it was related to the interfacial tension induced, hence capillary pressures (since droplet sizes are similar), at the early stages of the process.

In contrast, a different trend is observed when solely silica particles are used in the emulsification. In this case, the initial droplet size is not affected by increasing the concentration of silica particles up to 1 %, in fact they are similar to that determined in emulsions in the absence of emulsifiers. The reason that a similar initial droplet size is observed for a system in the absence of added emulsifier and for a system with silica particles only, is related to the fact that silica particles do not reduce the interfacial tension (Section 7.2); thus when the droplets experience similar inertial stresses, the daughter droplets are expected to show similar trend. Furthermore, the droplet break-up frequency increases marginally with silica particles concentration; nevertheless, it is similar to that corresponding in the absence of added emulsifiers and is much smaller than that corresponding to Tween 20.

The dependency of droplet break-up on silica particles concentration can be explained by the fact that silica particles adsorption on the interface does not influence the interfacial tension of the droplets. Their role in emulsification is merely to cover the droplets in order to suppress droplet coalescence (Binks and Kirkland, 2002; Aveyard *at al.*, 2003). Consequently, the capillary pressure of the droplets when silica particles are present will be similar to that in the absence of added emulsifier (since the droplet sizes are similar); this, in turn, results in similar droplet break-up frequencies, as observed in Figure 7.9-b. The slight increase in the break-up frequency caused by the increase in the concentration of silica particles may be a consequence of the improved stabilisation of the newly made droplets against coalescence. Although droplet coalescence frequency is negligible comparing with droplet break-up frequency, however, its value might be comparable when the comparison is made between various experiments.

Mixed-emulsifier systems

The initial droplet size and calculated droplet break-up frequencies of experiments in the presence of mixed-emulsifier systems are shown in Figure 7.10-a and b with respect to silica particles concentration.

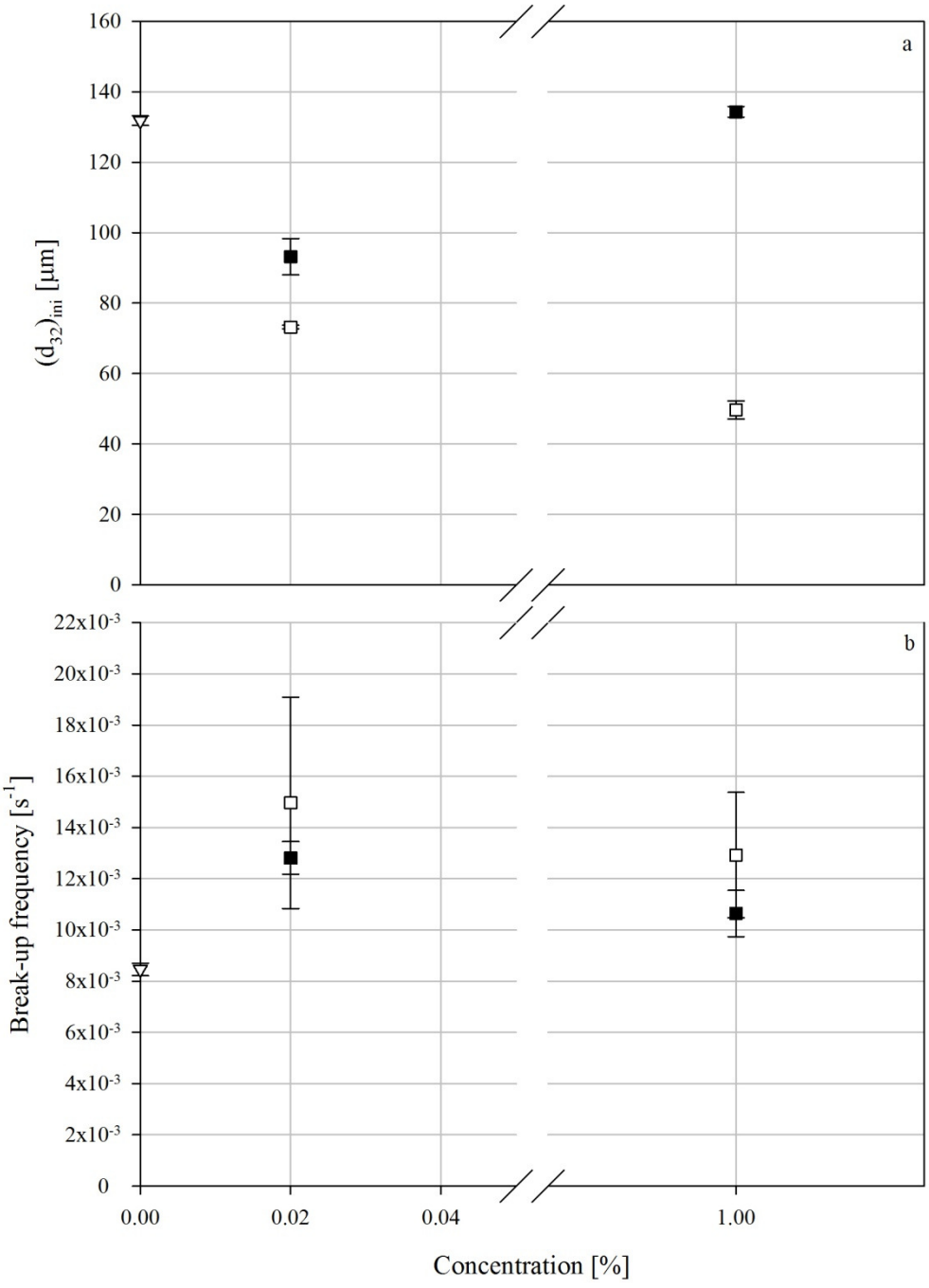

Figure 7.10. Initial droplet diameter (a) and break-up frequency (b) determined at the initial stages of the first processing step with respect to varying concentrations of silica particles with 0.02 % Tween 20 as mixed-emulsifier system (■) and silica particles with 1 % Tween 20 as mixed emulsifier system (□) and experiments in the absence of added emulsifier (▽).

Figure 7.10-a shows that the initial droplet sizes determined in the presence of mixed-emulsifier systems do not show similar trends to those determined when only silica particles are used. It can be seen that the initial droplet size of emulsions with

mixed-emulsifier systems containing 0.02 % silica particles and 0.02 % Tween 20 is similar to that observed when only 0.02 % Tween 20 is employed. Larger initial droplet size is observed in the emulsion of a mixed-emulsifier system containing 1 % silica particles and 0.02 % Tween 20. In addition, Figure 7.10-b shows that the droplet break-up frequency of system containing 0.02 % of both silica particles and Tween 20 is higher than the one related to the system containing 1 % silica particles and 0.02 % Tween 20. These observations might be the result of two competing phenomena. It has been previously shown that the rate of adsorption of silica particles is lower than surfactants such as Tween 20 (Binks, 2002; Tcholakova *et al.*, 2008). On the other hand, the adsorption rate of Tween 20 is a function of its concentration in the aqueous phase. When the same concentration (0.02 %) of both silica particles and Tween 20 is used, Tween 20 is adsorbed faster on the interface, hence reduces the interfacial tension. This results in the lower daughter droplet size hence initial droplet size (Figure 7.10-a) and lower capillary pressure hence higher droplet break-up frequency (Figure 7.10-b). However, when 1 % of silica particles and 0.02 % of Tween 20 are used, the higher amount of silica particles seems to result in faster adsorption of silica particles on the interface. When a layer of silica particles is formed on the interface, it acts as a barrier and suppresses the Tween 20 adsorption due to packed and rigid structure of the layer (Binks, 2002). Therefore the interfacial tension remains as the one in the absence of added emulsifier. In turn this causes the higher initial droplet size (Figure 7.10-a) and lower droplet break-up frequency (Figure 7.10-b).

Figure 7.10-a shows that the mixed-emulsifier system containing 0.02 % silica particles and 1 % Tween 20 shows an initial droplet size similar to that of an emulsion in the presence of 1 % Tween 20 only (Figure 7.9-a). However, a lower initial droplet size is observed for the system when 1 % of both silica particles and Tween 20 is employed (Figure

7.10-a). This is a result of the high concentration of silica particles which, to some extent, suppresses droplet coalescence. It should be noted that, as previously mentioned, although droplet coalescence may exist in the initial stages of the droplet size evolution, its amount is negligible in the presence of high rates of droplet break-up. However, the coalescence rate may be different in comparison with other systems.

Figure 7.10-b show that, both mixed-emulsifier systems containing 0.02 % and 1 % silica particles with 1 % Tween 20 show similar droplet break-up frequencies. These observations are a consequence of the fact that in the presence of high concentration of Tween 20, the adsorption rate of Tween 20 would be faster than silica particles, therefore, the interfacial tension is affected by Tween 20, hence a similar trend as systems in the absence of silica particles is observed.

It should be noted that the droplet break-up frequencies determined from the experiments with mixed-emulsifier systems of varying concentrations of silica particles with 1 % Tween 20 are higher than those corresponding to varying concentrations of silica particles and 0.02 % of Tween 20. This is clearly justifiable by the presence of a higher concentration of Tween 20 in the system which increases the droplet break-up by decreasing capillary pressure of droplets.

Proteins

The initial droplet size and calculated droplet break-up frequencies by equation 4.12 of experiments in the presence of sodium caseinate and WPI are shown in Figure 7.11-a and b with respect to proteins' concentration.

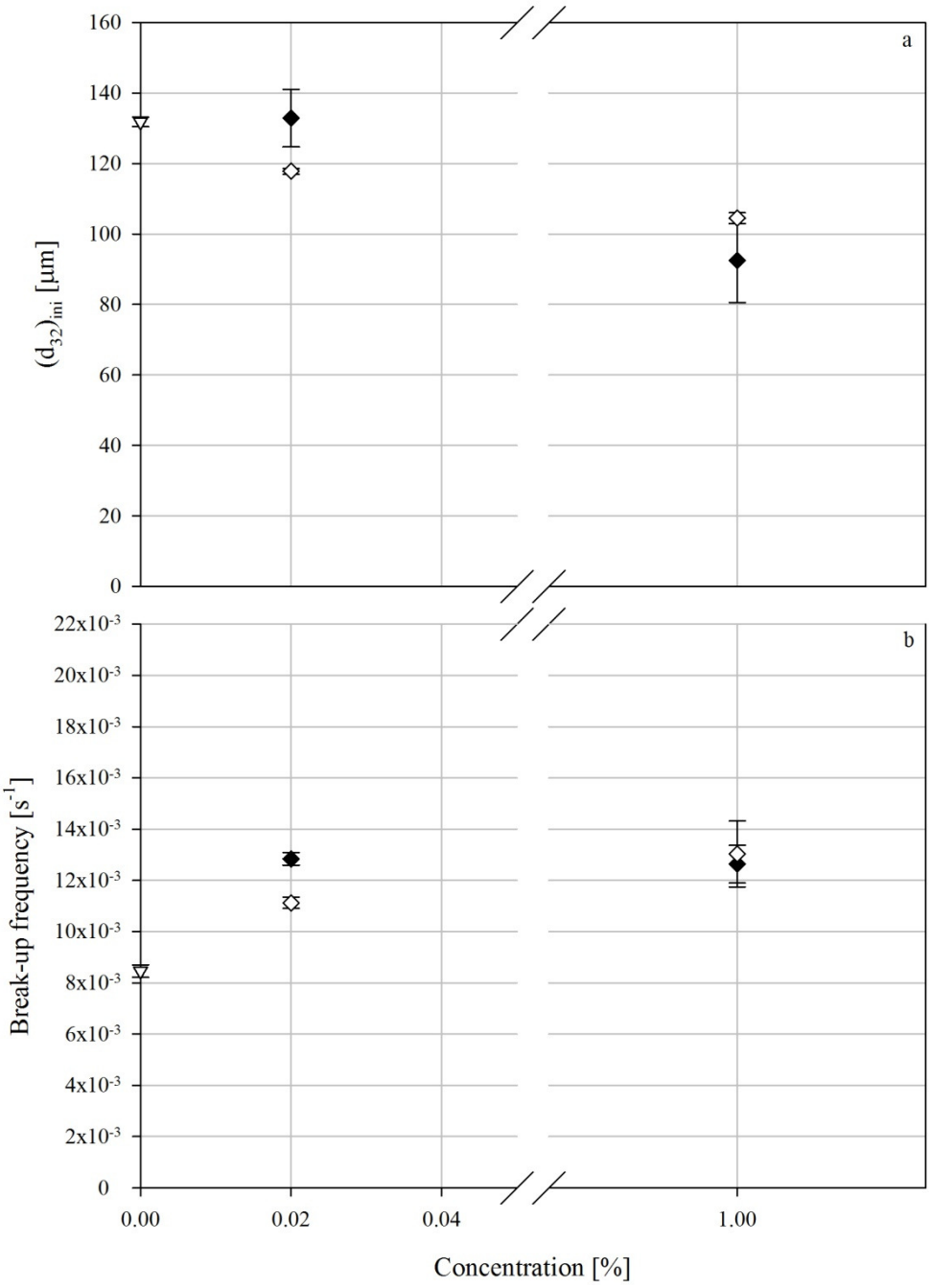

Figure 7.11. Initial droplet diameter (a) and break-up frequency (b) determined at the initial stages of the first processing step with respect to varying concentrations of sodium caseinate (♦) and WPI (◊) and experiments in the absence of added emulsifier (▽).

It can be seen from Figure 7.11-a that, in both cases (sodium caseinate and WPI) the initial droplet sizes are marginally lower than the experiments in the absence of added emulsifier. This is caused by the low adsorption rate at low concentrations of proteins on the

interface. A lower initial droplet size is reported by 1 % of sodium caseinate and WPI by inducing a lower interfacial tension; thus with a similar magnitude of inertial stresses, there are a higher number of smaller daughter droplets.

Figure 7.11-b shows that the droplet break-up frequencies corresponding to various concentrations of sodium caseinate are similar. This a consequence of the similar interfacial tension induced by both concentrations. Since the initial droplet sizes are similar, then so are capillary pressures, therefore similar break-up frequencies are determined. It should be noted that, droplet break-up frequencies for experiments in the presence of proteins are smaller than the ones reported in the case of surfactants (Figure 7.9-b). This is the result of either lower adsorption rate of proteins or higher interfacial tension they induce (Section 2.3).

7.4.1.1.2 Transitional region

As can be seen in Figures 7.6-7.8, unlike the behaviour observed at higher impeller speeds (Chapter 5 and 6), the droplet size evolution changes smoothly from the rapid decrease region into the plateau region. This shows that the intense hydrodynamic condition does not lead to the depletion of the emulsifiers and, therefore, a locally 'high coalescence' region is not observed.

7.4.1.1.3 Plateau region

The plateau region in all the droplet size evolution data (Figures 7.6-7.8) is characterised by the dynamic equilibrium between droplet break-up, coalescence and rate of adsorption of the emulsifiers onto the droplet interface.

Tween and silica particles

The silica particles are not surface-active and do not reduce the interfacial tension to enhance the break-up phenomenon. Thus, the break-up phenomenon, similar to the system in the absence of added emulsifiers is determined only by the hydrodynamic condition of the

system. However, silica particles, upon adsorption, provide an elastic layer on the interface which can reduce or suppress droplet coalescence. The final droplet size determined at the end of the first processing step of emulsions containing only Tween 20 or silica particles is shown in Figure 7.12.

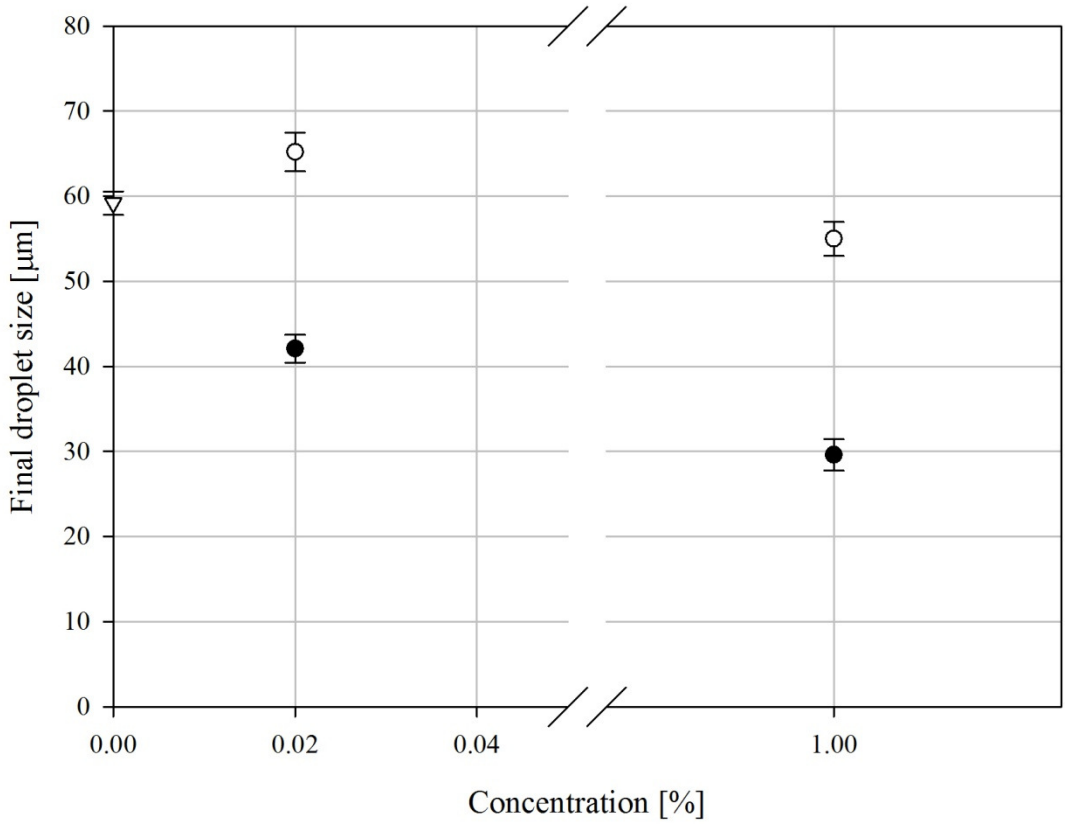

Figure 7.12. Final droplet size at the end of the first processing step with respect to varying concentrations of Tween 20 (●) and silica particles (○) and in the absence of added emulsifier (▽).

As can be seen in Figure 7.12, and in agreement with the observations made in Chapters 5 and 6, the addition of Tween 20, either at low (0.02 %) or high (1 %) concentrations, decreases the final droplet size. This results from the adsorption of Tween 20 on the interface of newly made droplets, which in turn increases the droplet break-up. The droplet break-up is lower at these stages in comparison with the initial stages of the process

(rapid decrease region) because the hydrodynamic fluctuations have a weaker effect on the droplets due to their small size.

In contrast, it can be seen from Figure 7.12 that in the presence of 0.02 % silica particles, the final droplet size is higher than that observed in the absence of added emulsifiers. However, the emulsion with 1 % silica particles shows a lower droplet size than the system with no added emulsifiers. It should be noted that these differences are small; nonetheless, it is worth investigating the causes of this behaviour since these differences also result in significant differences in the respective droplet size evolution data (Figure 7.6). As Figure 7.6 demonstrates, the droplet size evolution data related to emulsions in the absence of added emulsifier and 0.02 % silica particles are initially similarly (their respective data points overlap), however, precisely when the systems reach the plateau region, the droplet size evolution related to 0.02 % silica particle remains constant, while that related to the system without any added emulsifier decreases marginally. In addition, the system with 1 % silica particles shows similar behaviour as that with 0.02 % silica particles, but only at the smaller droplet sizes.

The smaller droplet size observed in systems with 1 % silica particles is due to the fact that lower droplet coalescence is expected when there is a high concentration of silica particles as they form a layer on the droplets interfaces (Binks, 2002; Binks and Kirkland, 2002). However, the existence of a layer of silica particles on the interface may in fact disrupt the droplet break-up at the final stages, where the break-up rate is lower. The same effect is observed in the case of 0.02 % silica particles due to the rigid interfacial structure, where the droplet size remains constant (it is larger than the droplet size with 1 % silica particles due to the lower amount of silica particles in the aqueous phase) and the droplet size related to emulsification in the absence of added emulsifiers decreases with time, though only slightly.

Mixed-emulsifier systems

The final droplet sizes generated by emulsions in the presence of mixed-emulsifier systems are plotted in Figure 7.13.

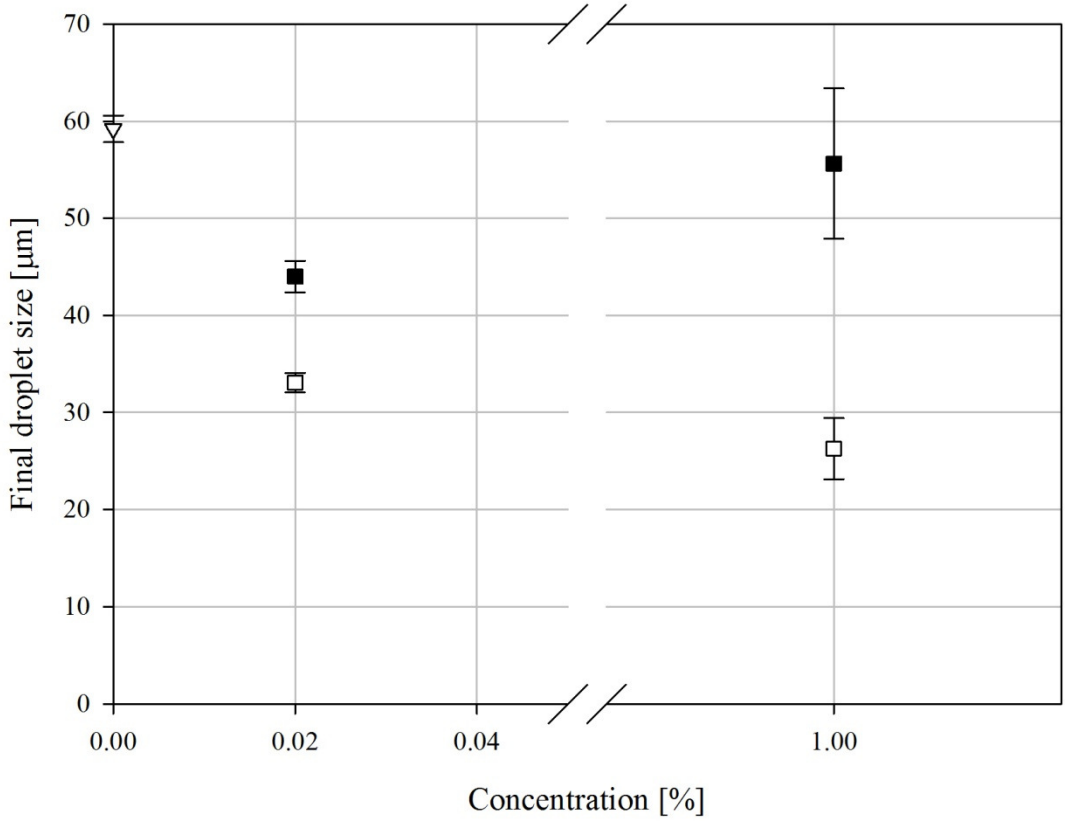

Figure 7.13. Final droplet size at the end of the first processing step with respect to varying concentrations of silica particles with 0.02 % Tween 20 as a mixed-emulsifier system (■) and silica particles with 1 % Tween 20 as a mixed emulsifier system (□) and in the absence of added emulsifier (▽).

It can be seen in Figure 7.13 that lower droplet sizes are observed in the mixed-emulsifier systems in comparison with the systems where only one type of emulsifier is employed. This was previously reported by Pichot *et al.* (2009). The lower droplet sizes observed in mixed-emulsifier systems is due to the fact that both beneficial features of these two types of emulsifiers affect droplet break-up and coalescence. The break-up in these cases is higher due to the reduced interfacial tension caused by Tween 20, while droplet coalescence

is suppressed by the existence of a layer of silica particles on the interface of newly made droplets.

When only Tween 20 is used, the break-up frequency is as high as, or even higher than, in the emulsion where Tween 20 is used as part of a mixed-emulsifier system. This is due to the fact that, in the presence of silica particles, the amount of Tween 20 on the interface (surface excess) may be lower; hence, a higher interfacial tension and a lower break-up frequency are expected in this case. Even though this may be true, the droplet size in the final stages of the first processing step will be affected by droplet coalescence since, as has been shown, Tween 20 cannot completely suppress droplet coalescence; in fact, the magnitude of droplet coalescence will be amplified at lower droplet sizes (Chapter 6). In contrast, the systems with only silica particles, although they may completely suppress droplet coalescence, do not affect interfacial tension; hence, large droplet sizes are produced. The mixed-emulsifier systems do not have these shortcomings and, therefore, they achieve smaller droplet sizes.

It should be noted that the experiment with 1 % silica particles and 0.02 % Tween 20 shows a different trend when compared with the other cases (Figure 7.13). This system, in fact, results in a droplet size similar to the system emulsified with solely 1 % silica particles. This is a result of two competing phenomena. Although, at similar concentrations, Tween 20 would be adsorbed faster than silica particles (Binks, 2002), however a low concentration (0.02 %) of Tween 20 results in lower adsorption rate compared with high (1 %) concentration of silica particles. Therefore, a layer of silica particles is formed on the interface which suppresses, to some extent, the adsorption of Tween 20. The interfacial tension of the droplets thus is not affected. Therefore, lower droplet break-up and higher final droplet size are achieved.

It should be noted that, the mixed-emulsifier systems containing 1 % Tween 20 and silica particles, at either low (0.02 %) or high (1 %) concentrations, produce largely similar final droplet sizes. This demonstrates that when silica particles are added to the aqueous phase containing Tween 20, the resultant droplet size is independent of the quantity of silica particles. This finding is explained by the fact that in the presence of a high concentration of Tween 20, the droplet surfaces are mostly covered by Tween 20 and not by silica particles, as observed in the interfacial tension studies (Section 7.3).

Proteins

The obtained droplet sizes at the plateau region of the first processing step of emulsification in the presence of proteins are shown in Figure 7.14.

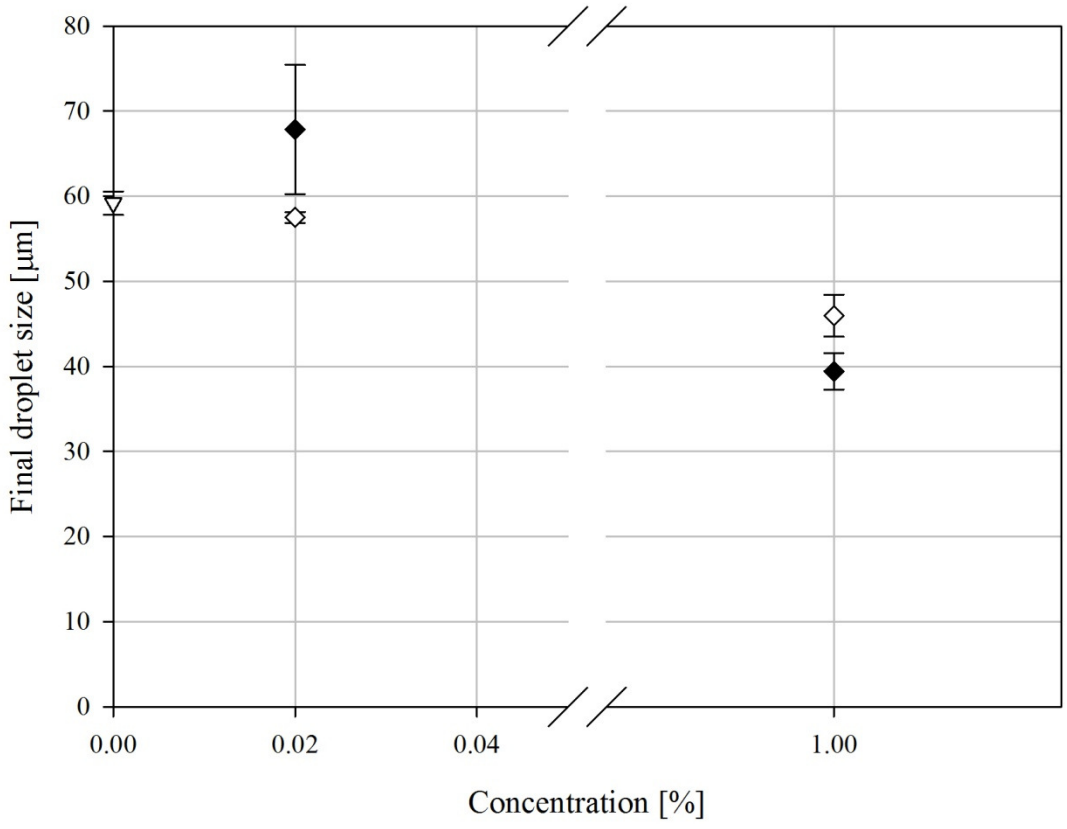

Figure 7.14. Final droplet size at the end of the first processing step with respect to varying concentrations of sodium caseinate (♦) and WPI (◊) and in the absence of added emulsifier (▽).

In the case of low concentration of sodium caseinate, although the 'rapid decrease' region occurs at droplet sizes smaller than those observed in the absence of added emulsifier, the final droplet size is larger. This finding can be explained by referring to the droplet size evolution data shown in Figure 7.8. It can be seen that the droplet size reduces rapidly, reaches the plateau region and, then, increases marginally until the end of the first processing step.

It should be noted that this peculiar behaviour is different from that observed for emulsifications of low concentrations of Tween 20 in intense hydrodynamic conditions (Chapters 5 and 6). In those experiments, an increase in droplet size was observed during the transition between the rapid decrease in droplet size and the plateau region. This observation is in marked contrast with the experiments herein, where the rise in droplet size occurs in the final stages of the process.

This behaviour can have several causes. Firstly, the casein molecules might break down during processing. The 'sequencing' of casein molecules to amino acids reduces the ability of molecules to suppress the droplet coalescence, hence droplet size increases. However, casein sequencing requires heat treatment of proteins at low pH and high temperatures around 110 °C (Holt, 1992). These conditions are not realised in these experiments since the temperature of the process is controlled at 25°C.

Another reason can be the crossover or 'bridging' of casein molecules. Previously it was observed that when low concentration of sodium caseinate is used in emulsification, the droplets flocculate due to crossing over the casein chains between several droplets (Dickinson, 1997 and 2002). Casein molecules at low concentrations cannot cover all the interfaces, and due to their surface activity they adsorbed on interfaces of several droplets. This might be the reason that droplet size is increasing toward the end of the process.

Production of high interfacial area during the process and low concentration (0.02 %) of sodium caseinate might lead to bridging of casein molecules. This results in the formation of flocs in the final stages of the process, which increases droplet coalescence. This is more probable cause of the observation as bridging was only observed when low concentrations of sodium caseinate were used (Dickinson, 1997 and 2002) and the fact that the above-mentioned trend is not observed by WPI or when higher concentration (1 %) of sodium caseinate is used.

In contrast, the final droplet size achieved when 0.02 % of WPI is used is lower; however not notably lower than the one related to the experiment in the absence of added emulsifier. This shows that, although WPI can indeed reduce the interfacial tension, the low rate of adsorption will result in a higher coalescence rate.

Moreover, it can be seen that lower droplet size is observed when sodium caseinate is used compared to WPI. This happens despite the fact that lower interfacial tension is induced by the same concentration of WPI. Possible causes for this behaviour are the better stability against coalescence achieved by sodium caseinate and the lack of sufficient time for WPI to reduce the interfacial tension down to the levels observed in the interfacial tension studies (Figure 7.4). Since WPI is a globular type protein, upon adsorption it unfolds on the interface (Dickinson, 2001) and the interfacial tension observed in Figure 7.4 results from molecular modifications at the interface. During the process and since there is not enough time for WPI molecules to change their shape, higher interfacial tension may be induced. In order to identify which of these parameters are responsible for the high droplet size observed, the droplet coalescence when 1 % WPI is used should be studied.

7.4.2 Second processing step

7.4.2.1 Droplet size evolution data

As has already been mentioned, data is grouped into the three sets of emulsifiers. The first graph (Figure 7.15) is related to the data obtained from experiments performed in the presence of Tween 20 or silica particles, when they were employed individually. Figure 7.16 plots the droplet size evolution data corresponding to the second processing step of the experiments performed with mixed-emulsifier systems. Finally, the droplet size evolution data corresponding to the experiments performed in the presence of proteins are shown in Figure 7.17.

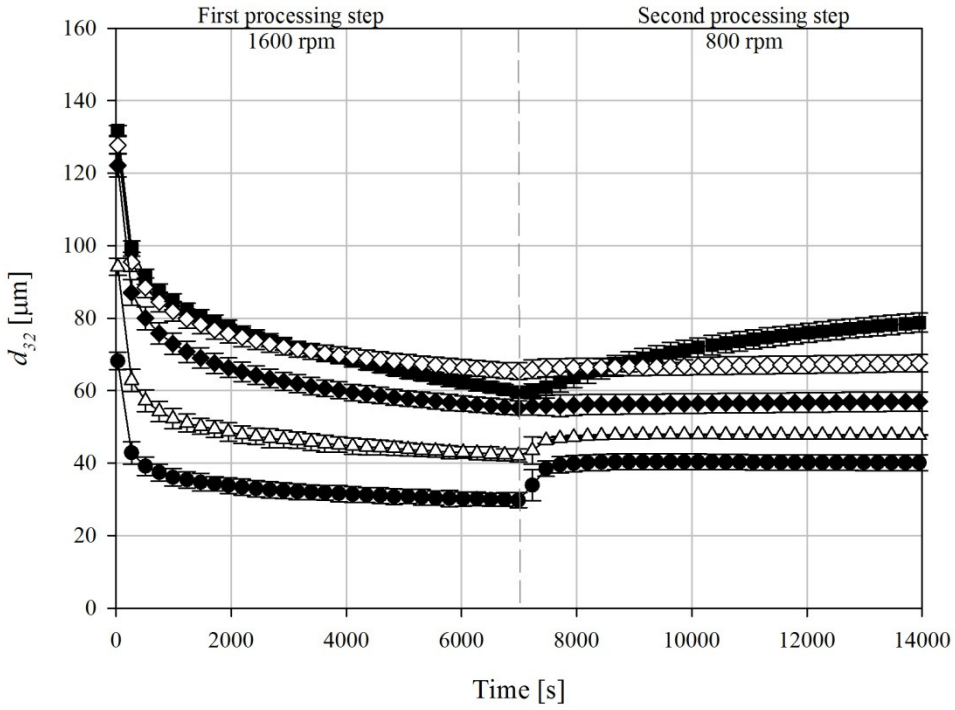

Figure 7.15. Droplet size evolution data corresponding to the first and second processing steps of the emulsification experiments with varying solutions containing 0.02 % silica particles (♦), 1 % silica particles and 0.02 % Tween 20 (Δ) and 1 % Tween 20 (●) and in the absence of added emulsifier (■).

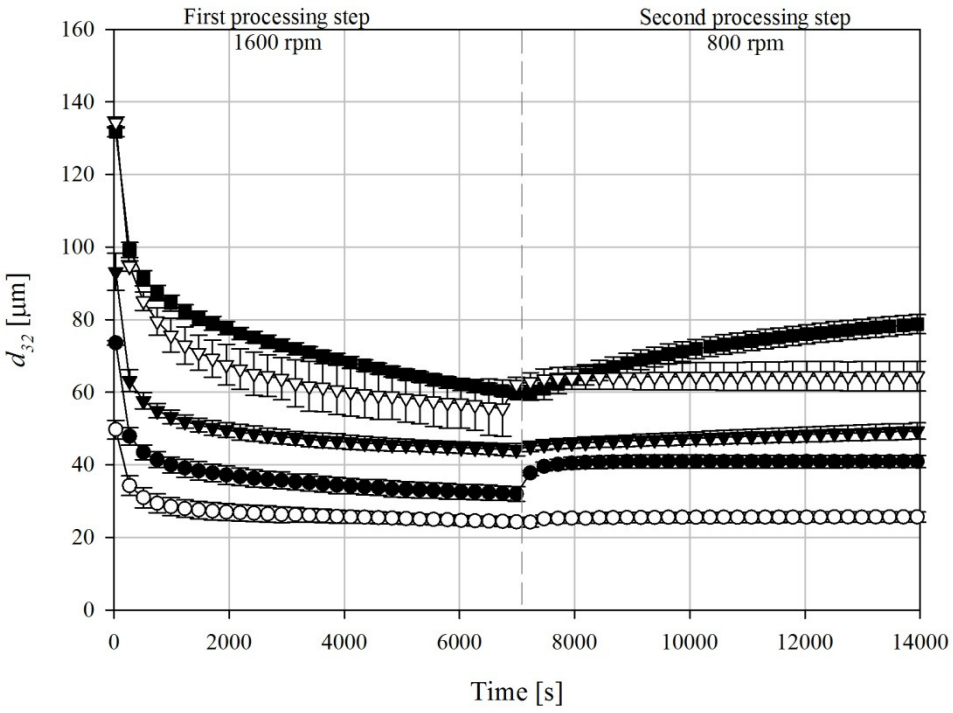

Figure 7.16. Droplet size evolution data corresponding to the first and second processing steps of the emulsification experiments with varying solutions containing 0.02 % silica particles with 0.02 % Tween 20 (▼), 1 % silica particles with 0.02 % Tween 20 (▽), 0.02 % silica particles with 1 % Tween 20 (●) and silica particles with 1 % Tween 20 (○) and in the absence of added emulsifier (■).

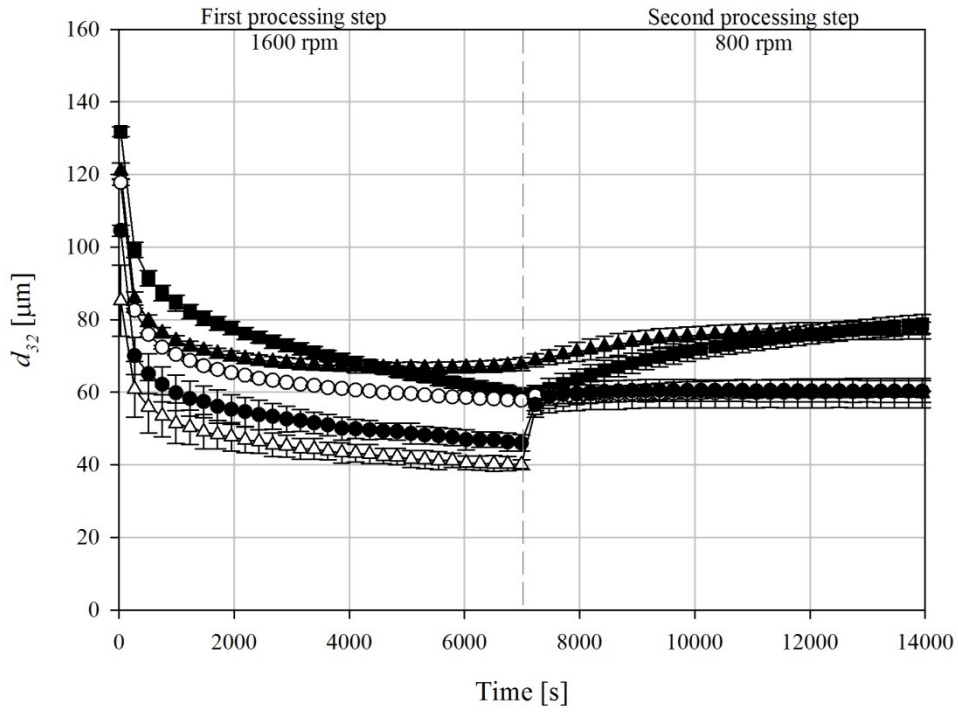

Figure 7.17. Droplet size evolution data corresponding to the first processing step of the emulsification experiments with varying solutions containing 0.02 % sodium caseinate (Δ), 1 % sodium caseinate (▲), 0.02 % WPI (○) and 1 % WPI (●) and in the absence of added emulsifier (■).

In all the plots of Figures 7.15-7.17 the droplet size evolution data corresponding to the first and then the second processing steps are shown. The dashed lines in each graph indicate the time-point where the impeller speed has been changed. As stated earlier, immediately after the impeller speed change, the droplet coalescence will be the dominant phenomenon which results in an increase in droplet size.

7.4.2.2 Droplet coalescence

The early stages of the second processing step are dominated by droplet coalescence. Therefore, droplet coalescence can be analysed individually at this stage. The droplet coalescence frequency has been calculated using equation 4.16.

7.4.2.2.1 Tween 20 and silica particles
Droplet coalescence frequency

The droplet coalescence frequency corresponding to the systems containing Tween 20 or silica particles are plotted in Figure 7.18.

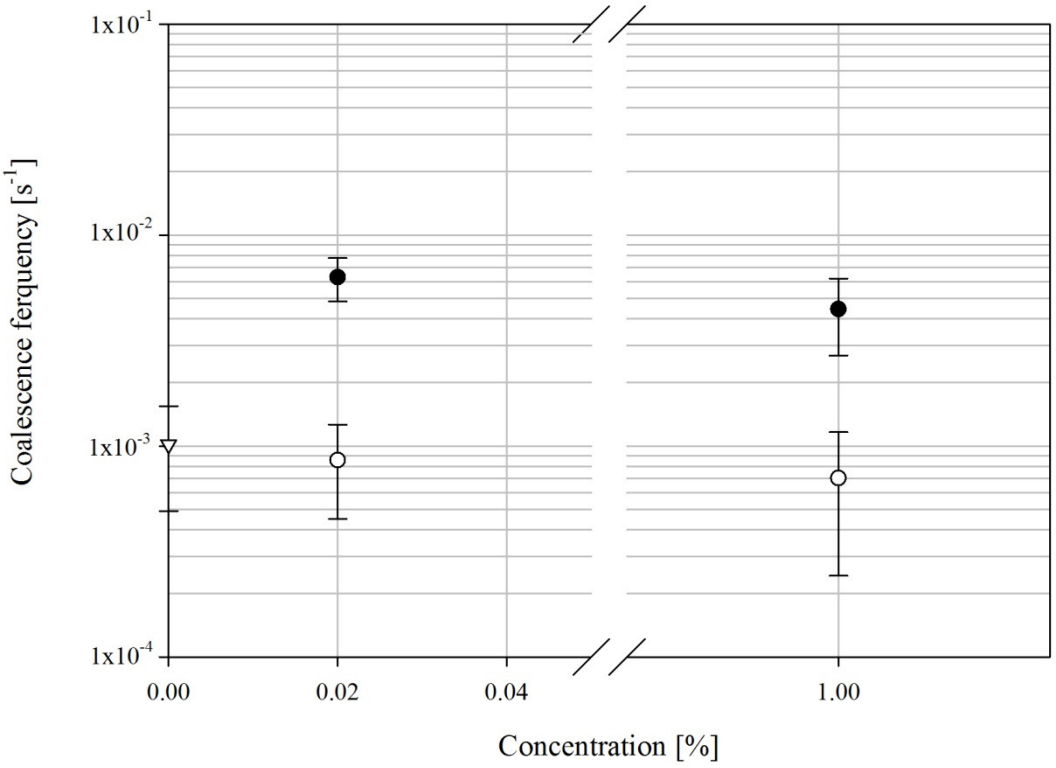

Figure 7.18. Droplet coalescence frequency determined at the initial stages of the second processing step with respect to varying concentrations of Tween 20 (●) and silica particles (○) and in the absence of added emulsifier (▽).

It can be seen in Figure 7.18 that the droplet coalescence frequency of the systems with Tween 20 is higher than that reported for systems with silica particles. Moreover, increasing the concentration of Tween 20 or silica particles only marginally decreases the droplet coalescence frequency. An interesting notion is that the droplet coalescence frequency of the systems containing Tween 20 is higher than that in the absence of added emulsifier. This has been thoroughly analysed in Chapter 6. In contrast, the droplet coalescence frequency of the systems containing silica particles is lower than that in the absence of added emulsifier. It should be noted that, to the extent of the author's knowledge, there have been no

published studies regarding coalescence during emulsification of systems containing silica particles.

The data reported in Figure 7.18 suggests that the stability against coalescence induced by the adsorption of silica particles is significantly better than that achieved by Tween 20. This finding has been previously reported by a number of studies through monitoring the produced emulsions stability (Binks, 2002; Aveyard *et al.*, 2003; Vermant *et al.*, 2004; Hunter *et al.*, 2008; Pichot *et al.*, 2009). However, it should be noted that the droplet coalescence for systems containing Tween 20 is related to droplets smaller than those corresponding to silica particles. In order to investigate thoroughly the droplet coalescence with regard to these parameters, the collision rate and collision efficiency are analysed separately.

Collision rate and collision efficiency

As has been mentioned in Section 2.3, the collision rate and collision efficiency depend on the droplet size and the energy dissipation of the system. Additionally, the collision efficiency is a function of the mechanism of droplet coalescence during emulsification. In order to investigate each of these dependencies separately, the collision rate and collision efficiency are calculated (equations 4.19 and 4.14, respectively) and plotted with respect to emulsifier concentration in Figures 7.20-a and b, respectively.

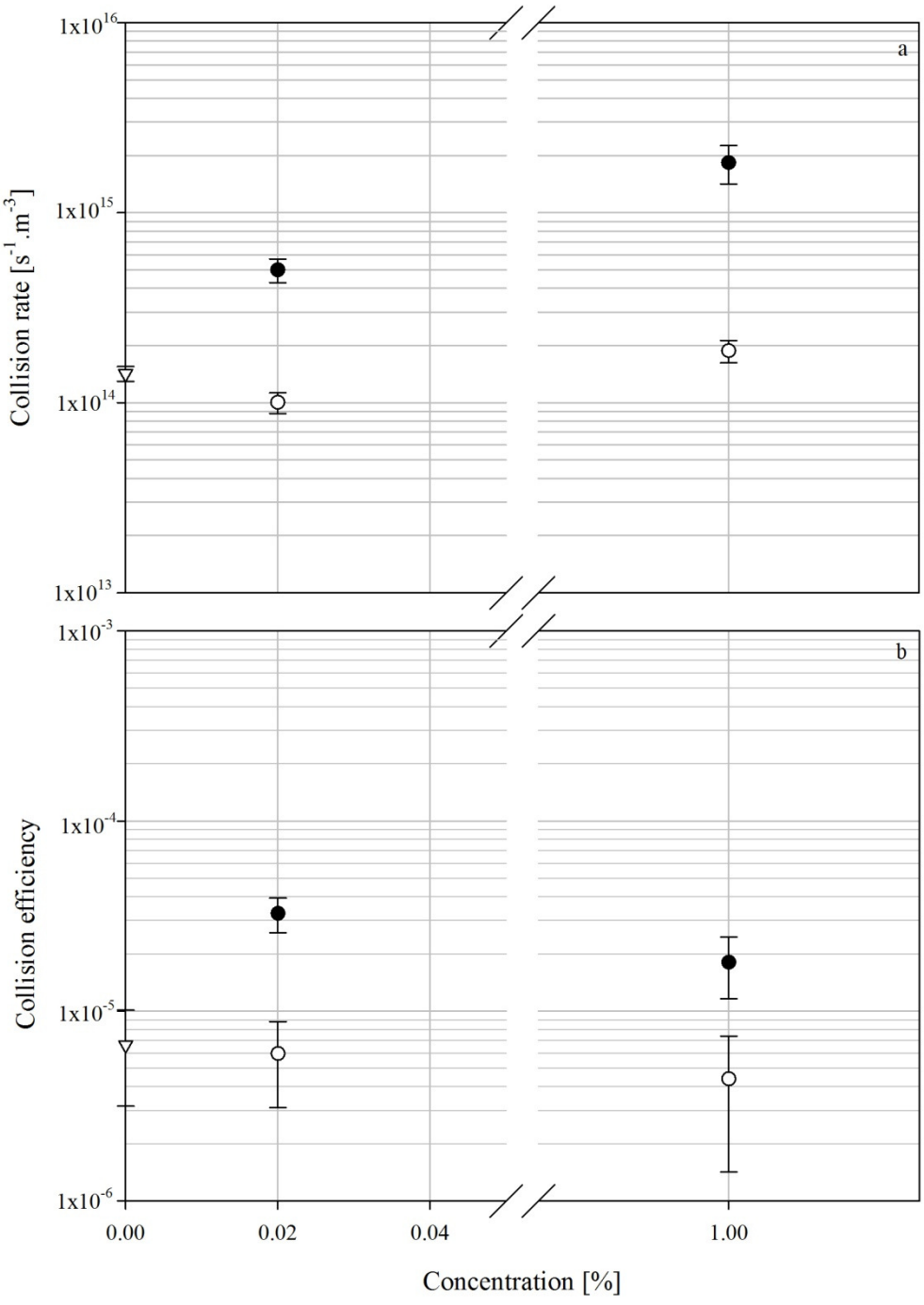

Figure 7.19. Collision rate (a) and collision efficiency (b) of experiments in the presence of varying concentrations of Tween 20 (●) or silica particles (○) and in the absence of added emulsifier (▽).

Figure 7.19-a demonstrates that increasing Tween 20, results in lower droplet sizes thus higher number of droplets, leading to an increase in the collision rate. However, the collision rate at a silica concentration of 0.02 % is lower than in the absence of added

emulsifiers but similar to the system with 1 % silica particles. This behaviour is not surprising, since the damped energy dissipation is similar in all cases and, hence, the collision rate is a function of the droplet size only. As a lower droplet size is reported in the systems containing Tween 20, the higher collision rate is expected. The same rationale applies for the case of systems with 0.02 % silica particles where a higher droplet size is reported than in the systems without added emulsifiers and, therefore, a lower collision rate is expected and reported for the former systems. It should be noted that the collision rate for the systems containing Tween 20 is one order of magnitude larger than the collision rate for the systems with silica particles. Since it has been shown that the collision rate increases the coalescence frequency, the high coalescence frequency of the systems containing Tween 20 can be explained by their higher collision rate (Chapter 6).

Figure 7.19-b shows that in both system types with silica particles and Tween 20, the collision efficiency of 1 % concentration of emulsifiers is lower than that of 0.02 % concentration of emulsifiers, even though a higher collision rate is observed for the former (Figure 7.19-a). In the systems containing Tween 20, this behaviour was analysed previously and was explained by the higher surface coverage of Tween 20 induced by its higher concentrations. Although Tween 20 at higher concentrations is able to stabilise the emulsion during shelf-life, it cannot fully stabilise the droplets during the process due to the short-range nature of their stabilisation mechanism (steric stabilisation) and the fact that they can be desorbed from the surface of droplets.

In marked contrast, this is not the case for silica particles. It has been reported that the adsorption of silica particles can be considered as an irreversible phenomenon (Binks, 2002). This means that the corresponding activation energy of desorption is high enough for the probability of its occurrence to be close to zero. Previous studies found little or no droplet

coalescence in the presence of solid particles (Binks, 2002; Pichot *et al.*, 2009). However, not only does droplet coalescence occur, but also, although a lower collision rate is observed at systems with 0.02 % silica particles than in the systems without any added emulsifier, a similar collision efficiencies to the experiment in the absence of added emulsifier is reported.

The mechanism of droplet coalescence in the presence of surfactants involves the drainage of the layer of continuous phase trapped between two colliding droplets. During the drainage stage, the Tween 20 desorption plays the decisive role. However, as this is not the case for silica particles, the droplet coalescence mechanism should, indeed, be different.

Droplet coalescence is completely suppressed if a mono-layer of close-packed silica particles forms on the interface. This is expected when 1 % silica particles are employed, since they are enough to cover all the interfaces. However, due to turbulent fluctuations, when two droplets collide, the droplets might deform, causing flattening of droplets. This surface expansion results in the creation of spots deprived from particles (Figure 7.20). During this phenomenon the surface of droplets in these spots form a curvature due to the capillary pressure across the surfaces. This results in the proximity of the two interfaces from opposite droplets, which, in turn, can indeed reduce the continuous film thickness to the critical value, at which coalescence occurs. This mechanism is fully shown by Tcholakova *et al.* (2008).

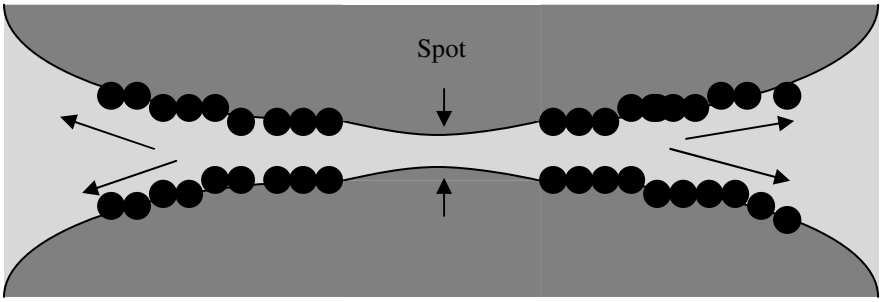

Figure 7.20. Droplet coalescence mechanism in presence of solid particles is shown.

Nonetheless, although it is clear that droplet coalescence is not completely suppressed by silica particles, it can be seen that the droplet coalescence mechanism for silica particles is less efficient than the droplet coalescence mechanism for Tween 20.

7.4.2.2.2 Mixed-emulsifier systems
Droplet coalescence frequency

The coalescence frequencies determined for mixed-emulsifier systems are plotted in Figure 7.21.

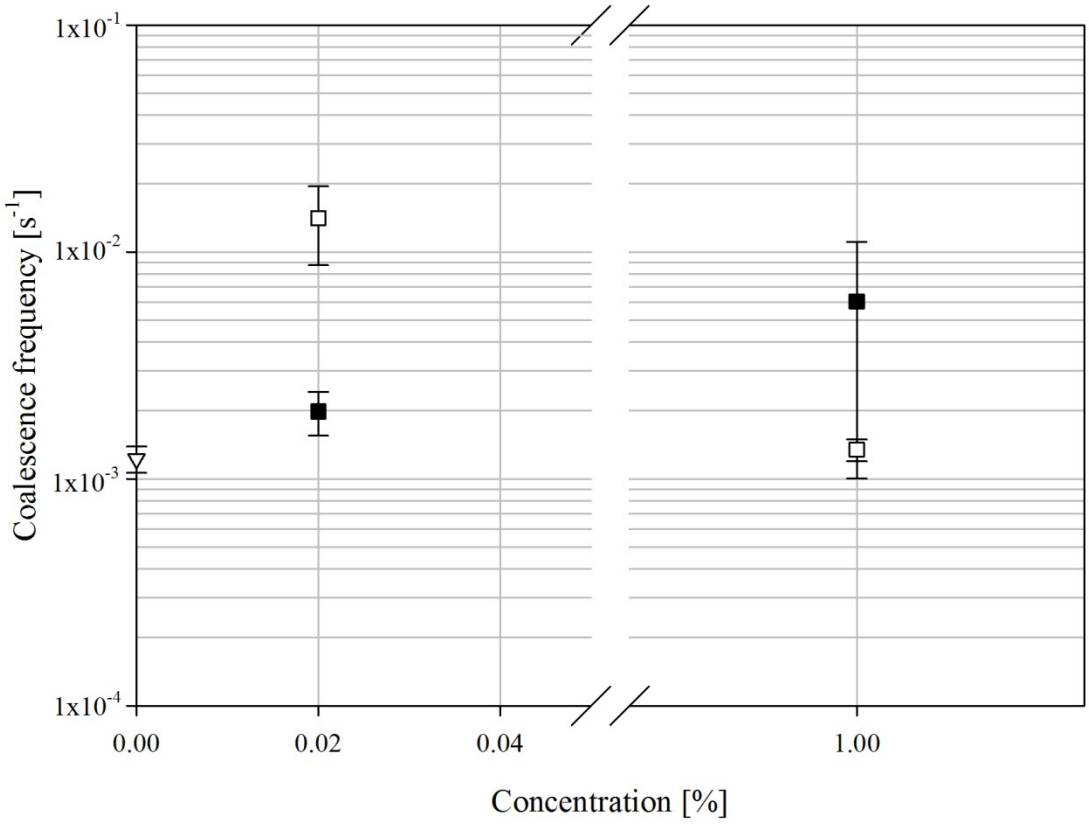

Figure 7.21. Droplet coalescence frequency determined at initial stages of the second processing step with respect to mixed-emulsifier systems containing silica particles with 0.02 % (■) or 1 % (□) Tween 20 and in the absence of added emulsifier (▽).

Two different trends can be observed in Figure 7.21. The systems containing varying concentrations of silica particles with 0.02 % Tween 20 show an increase in the droplet coalescence frequency when the concentration of silica particles increases.

Contrary to the aforementioned trend, the emulsions containing varying concentrations of silica particles with 1 % Tween 20 show a decrease in coalescence frequency when the concentration of silica particles increases. Additionally, it should be noted that the droplet coalescence frequency reported for all the mixed-emulsifier systems is similar or higher to that corresponding to emulsification in the absence of added emulsifiers. In order to investigate these trends, the collision rate and the collision efficiency of these systems are analysed.

Collision rate and collision efficiency

The collision rate and the collision efficiency for mixed-emulsifier systems are plotted in Figure 7.22.

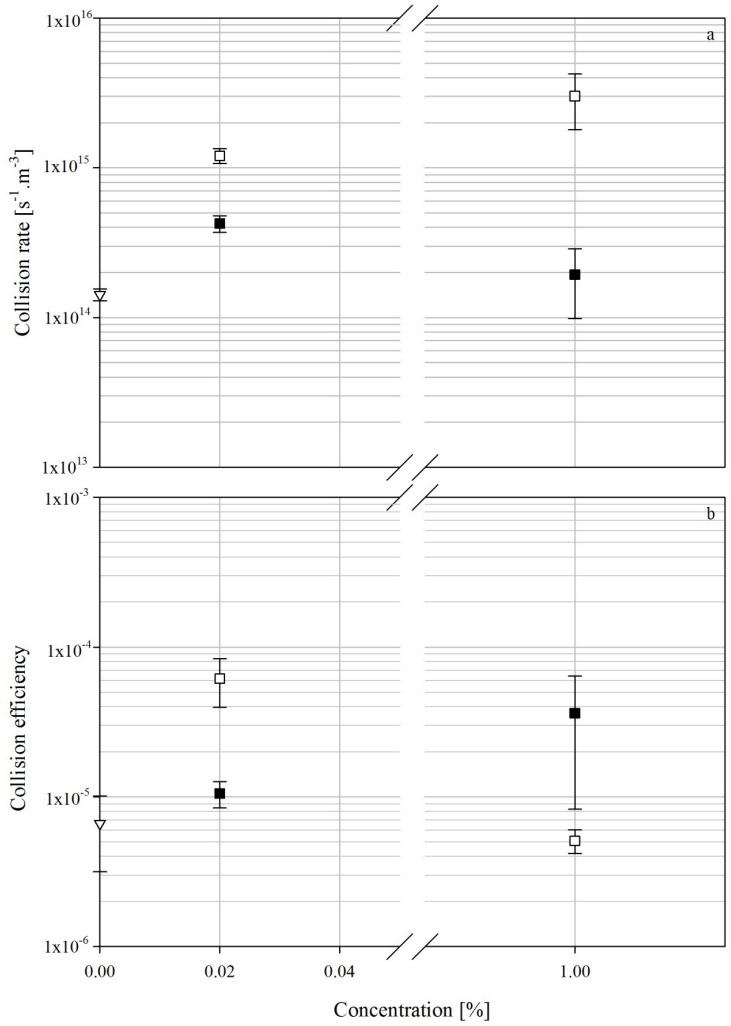

Figure 7.22. Collision rate (a) and collision efficiency (b) of experiments in the presence of mixed-emulsifier systems containing varying concentrations of silica particles with 0.02 % (■) and 1 % (□) Tween 20 and in the absence of added emulsifier (▽).

Figure 7.22-a shows that the collision rate in the mixed-emulsifier system containing 0.02 % silica particles and 0.02 % Tween 20 is higher than that in the mixed-emulsifier system with 1 % silica particles and 0.02 % Tween 20. As mentioned earlier, since the emulsification is carried out in similar hydrodynamic conditions, the droplet size is the only parameter influencing the collision rate. As a higher droplet size is observed for mixed-emulsifier systems with 1 % silica particles and 0.02 % Tween 20, a lower collision rate is observed. Although the low collision rate decreases the probability of droplet coalescence, Figure 7.22-b shows that collision efficiency of this system is indeed higher than that of the

system with 0.02 % silica particles and 0.02 % Tween 20. At varying concentrations of silica particles and a lower concentration (0.02 %) of Tween 20, the Tween 20 molecules and silica particles are 'sitting' on the interface side by side. As two droplets approach, Tween 20 might be desorbed from the interface resulting in droplet coalescence. A higher collision efficiency with high standard deviation is observed, since droplet coalescence depends on the arrangement of silica particles and Tween 20 molecules on the interface of the droplets. It can be seen that the amount of Tween 20 is markedly lower than that of silica particles; however, the adsorption rate of Tween 20 is higher than that of silica particles. If Tween 20 is adsorbed faster than the silica particles, then the silica particles will in fact sit on the side of Tween 20 molecules and the collision of the droplets will result in coalescence. However, if silica particles are adsorbed first on the interface (due to the high amount of silica particles in the aqueous phase) they will form a layer which suppresses the adsorption of Tween 20 on the interface. This results in the formation of a layer of silica particles on the interface.

In contrast, the mixed-emulsifier systems containing varying concentrations of silica particles with 1 % Tween 20 show a different trend. Figure 7.22 shows that, although the collision rate increases by increasing the concentration of silica particles in the mixed-emulsifier system, the collision efficiency decreases. This demonstrates that, when a low concentration of silica particles is used with a high concentration of Tween 20, the fast adsorption of Tween 20 and the low amount of silica particles in the aqueous phase, the stability against coalescence that is expected by the silica particles does not occur and the system actually behaves similar to a system containing only Tween 20. In contrast, when a high concentration of both silica particles and Tween 20 is present, a multi-layer is formed, where Tween 20 covers the interface and a layer of silica particles form a layer on top of the Tween 20 layer. In these systems, although a high collision rate is observed due to the small

droplet size, the droplet coalescence is completely suppressed by the multilayer on the interface. A similar argument can be used for the trend observed in experiments containing 0.02 % silica particles and varying concentrations of Tween 20, where a higher collision rate and a higher collision efficiency are observed for systems containing higher concentration of Tween 20.

7.4.2.2.3 Proteins
Droplet coalescence frequency

The coalescence frequencies for systems containing proteins (sodium caseinate and WPI) are plotted with respect to protein concentration in Figure 7.23.

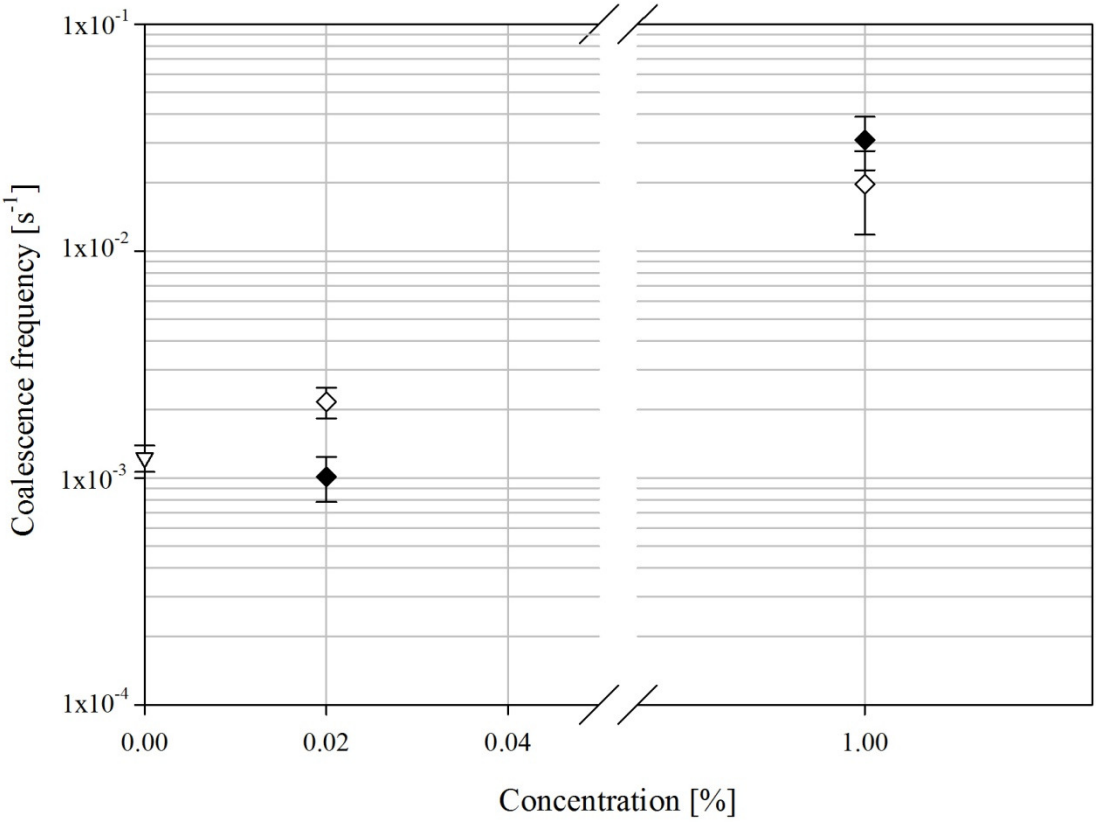

Figure 7.23. Droplet coalescence frequency determined at the initial stages of the second processing step with respect to varying concentrations of sodium caseinate (♦) and WPI (◊) and in the absence of added emulsifier (▽).

Figure 7.23 shows that, for both cases where sodium caseinate and WPI are employed, the droplet coalescence frequency increases with increasing concentration. It should be noted

that a low coalescence frequency is observed for the system containing 0.02 % sodium caseinate. This is a consequence of the droplet size behaviour before the step-change in the impeller speed. As can be seen in Figure 7.17, notable droplet coalescence is observed in the final stages of the first processing step due to the bridging effect of casein molecules which increases the droplet coalescence. Therefore, at the point of the impeller speed change, the increase in droplet size will be lower due to the increase in droplet size that has already occurred.

The existence of droplet coalescence in systems containing sodium caseinate was previously observed by Hu *et al.* (2003). They employed a method similar to that used in this work. They induced a droplet coalescence regime by a step-change in the impeller speed. They observed that bubble coalescence cannot be suppressed even at high concentrations of sodium caseinate, although no explanation for the observed behaviour was given. However, these observations are in contrast to the data presented by Tcholakova *et al.* (2003). They performed some experiments with systems containing Whey Protein Concentrate (WPC). They found that at higher concentrations of WPC the droplet size can be estimated with the assumption that coalescence is completely suppressed. They employed a homogeniser device. It should be noted that they did not study droplet coalescence and, therefore, their study can be best compared with the first processing step. Nonetheless, they relate their assumptions to their studies on the amount of WPC on the interface (surface excess). They found that multi-layer WPC is adsorbed on the droplets and that the WPC adsorption can be considered to be an irreversible phenomenon.

Mohan and Narsimhan (1997) performed some experiments on the coalescence of emulsions in the presence of varying concentrations of WPI and sodium caseinate with dispersed phase volume fraction of 10 % using a homogeniser. They generated a coalescence-

dominant regime by employing the same methodology as that used throughout this report. They suddenly decreased the homogeniser pressure, which induced a droplet coalescence-dominant regime. They reported that increasing the concentration of proteins (either WPI or sodium caseinate) will decrease droplet coalescence. However, they only studied protein concentrations in the range 0.01 %-0.05 % and they did not report a complete suppression of coalescence in their systems. This trend may be explained by the use of the emulsification device. As previously mentioned, homogenisers can be considered to be continuous processes, where the emulsion is passed through a valve. The residence time of emulsions at the point where actual droplet coalescence should occur is significantly lower than for agitated vessels. In agitated vessels a higher collision rate is expected and, as a result, a greater coalescence frequency is expected.

In order to provide an explanation for the observations presented in this section, the collision rate and collision efficiency are analysed.

Collision rate and collision efficiency

Collision rates and collision efficiencies corresponding to droplet coalescence of systems containing varying concentrations of sodium caseinate and WPI are plotted in Figures 7.24-a and b, respectively.

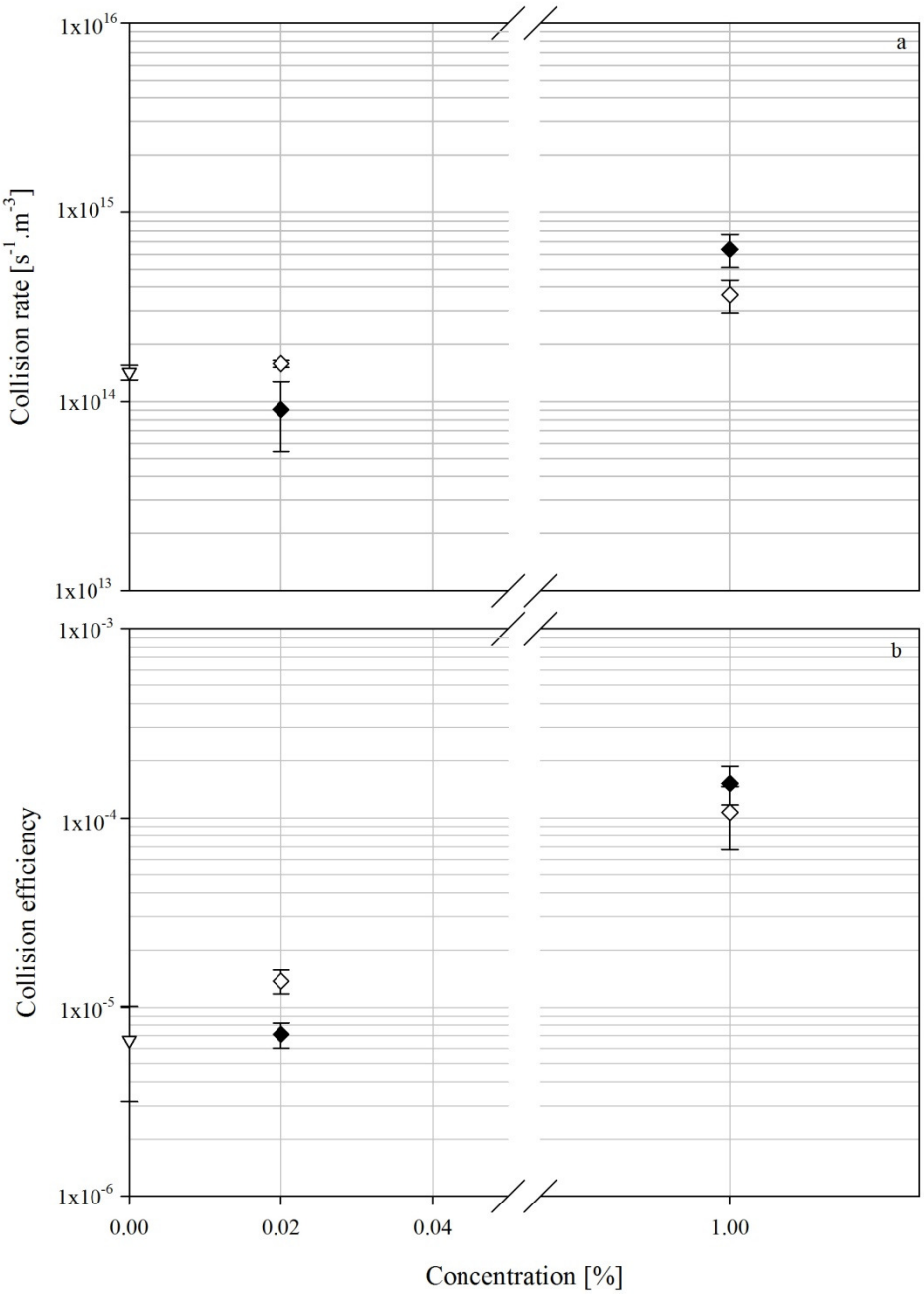

Figure 7.24. Collision rate (a) and collision efficiency (b) of experiments in the presence of varying concentrations of sodium caseinate (♦) and WPI (◊) and in the absence of added emulsifier (▽).

As expected, due to the smaller droplet sizes, the collision rate increases with increasing protein concentrations (Figure 7.24-a). However, according to the explanations outlined earlier, a low collision rate is observed at the systems containing 0.02 % sodium caseinate. Figure 7.24-b shows the same trend regarding protein concentrations. As sodium

caseinate and WPI concentrations increase, the collision efficiencies also increase, leading to higher numbers of coalesced droplets.

It can be seen that at lower concentrations (0.02 %) of sodium caseinate, better stability against coalescence is observed in comparison with the use of WPI. This observation is in agreement with data reported by Mohan and Narsimhan (1997). This observation, however, can be considered to be somewhat biased, as the system is already coalescing before the step-change in the impeller speed. Nevertheless, this is not the case for the use of high concentration of proteins where better stability is observed by WPI, although similar collision efficiencies are reported (Figure 7.24-b).

The stabilisation mechanism of WPI and sodium caseinate molecules is different from that using nonionic surfactants. Not only do proteins (both sodium caseinate and WPI) stabilise the droplets via a repulsive steric force, but also they induce an electrostatic barrier with a range larger than the former mechanism. Therefore, it is expected that the droplet coalescence will be smaller than that induced by other emulsifier types. As can be seen in Figures 7.23 and 7.24 this is not the case. In order to investigate the effect of the electrostatic repulsive force, the zeta potential of the emulsions was measured and the results are presented in Table 7.1. Employing the zeta potential and using equation 4.33, colloidal forces induced by various systems can be determined. Figure 7.25 plots the repulsive force induced by various systems with respect to the distance from the charged surface.

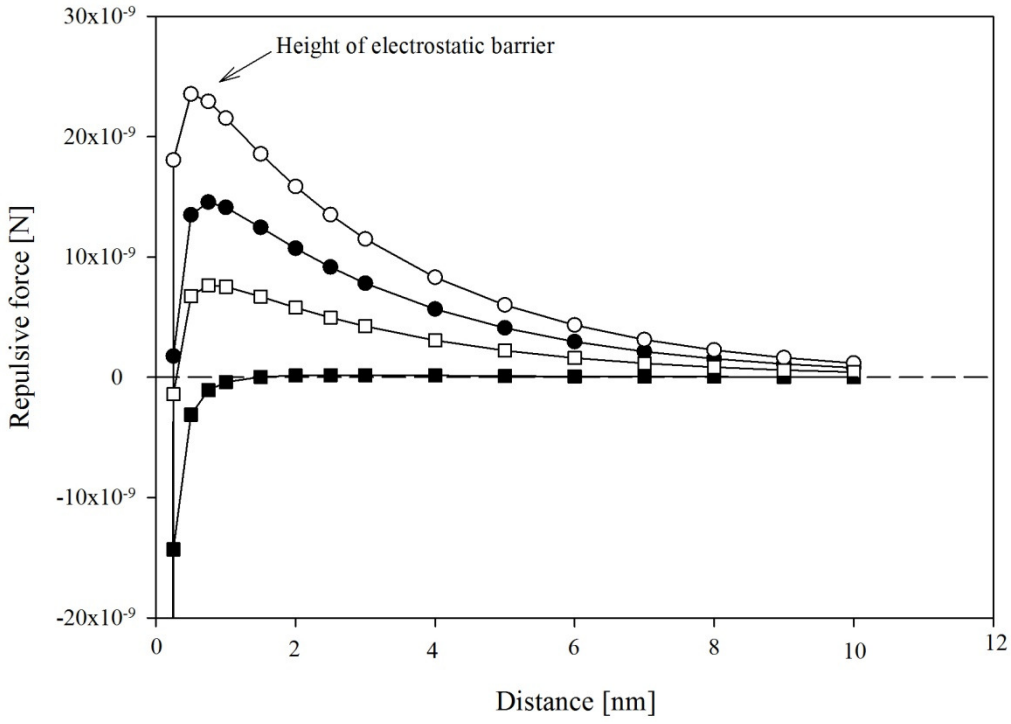

Figure 7.25. Overall colloidal force with respect to the distance from the surface of the droplets for systems containing 0.02 % sodium caseinate (●), 1 % sodium caseinate (○), 0.02 % WPI (■) and 1 % WPI (□).

It can be seen that the emulsion containing 1 % sodium caseinate shows the highest electrostatic barrier. This is reduced at 0.02 % sodium caseinate. The systems containing WPI show a lower electrostatic barrier than those containing sodium caseinate, to the extent that no electrostatic barrier will be observed for the system containing 0.02 % WPI, which results in the stabilisation being related to only the steric repulsion. This has been previously observed by Tcholakova *et al.* (2006), where it was reported that the electrostatic stabilisation is practically absent when Whey protein concentrate (WPC) is employed.

Table 7.2 gives the values of the electrostatic repulsive force and the mean turbulent force acting on the droplets.

Table7.2. Zeta potential, electrostatic force and mean turbulent force for various emulsions containing sodium caseinate and WPI.

Protein type	Concentration [%]	ζ potential [mV]	Maximum electrostatic repulsive force [N]	Mean turbulent force [N]
Sodium caseinate	0.02	-21	1.45e-8	2.15e-9
	1.00	-34	2.35e-8	0.50e-9
WPI	0.02	-4	--------	--------
	1.00	-18	0.75e-8	0.76e-9

Table 7.2 shows that, in all studied cases, the maximum electrostatic repulsive force is at least one order of magnitude larger than the turbulent force. This means that the electrostatic barrier is large enough to stabilise the droplets in the hydrodynamic condition of the second processing step. Therefore, the high coalescence frequency is in fact the result of the proximity of naked interfaces. Due to their surface activity, caseinate molecules are able to cover entirely the interfaces. Additionally, as the change in the hydrodynamic condition is carried out on the already established emulsion (at the end of the first processing step), the droplet interfaces are indeed covered. Therefore, only the desorption of proteins from the interfaces will result in high droplet coalescence.

The desorption of proteins is probably caused by a mechanical force exerted by the friction between two droplets. As a high number of collisions is observed at the second step, the likelihood of the droplets rolling over each other increases. This might result in the separation of the proteins from the interface, which in turn exposes naked areas of interfaces. Consequently, when the droplets collide, the collision of two naked interfaces will result in droplet coalescence. This is the reason that, although a higher energy barrier is generated by the droplets in the presence of sodium caseinate, a similar coalescence frequency is observed with WPI, as a result of the similar droplet coalescence mechanism.

It should be noted that previous studies demonstrated that a multi-layer of proteins will form on the interface (Dickinson, 1997; Tcholakova *et al.*, 2006). If multi-layer formation occurs in these experiments, the droplet coalescence caused by the aforementioned mechanism should be suppressed. Nonetheless, the occurrence of formation of multi-layers of proteins on the interface is low during emulsification due to the slower pace of multi-layer formation in comparison with the droplet collision phenomenon. For example, Tcholakova *et al.* (2006) determined the amount of WPC on the interface after emulsification in the absence of hydrodynamic fluctuations, which provided enough time for them to be adsorbed on top of the other protein layer.

An issue arises regarding the lower collision efficiency of an emulsion in the absence of added emulsifier when compared with emulsions with 1 % sodium caseinate or WPI. This is a consequence of the higher collision rate (three times larger, Figure 7.24-a) in comparison to that related to emulsions without emulsifier, which increases the likelihood of droplet coalescence dramatically.

7.4.2.3 Emulsion response to the coalescence dominant regime

It is vitally important to investigate the effect of exposing the emulsion to an environment where droplet coalescence is dominant. For example, when the process is completed and agitation stops, a sudden coalescence regime occurs which can indeed alter the final droplet size. Therefore, in order to investigate this effect, the difference between the initial and final droplet size, which is an indication of the change in droplet size due to coalescence, is shown in Figure 7.26.

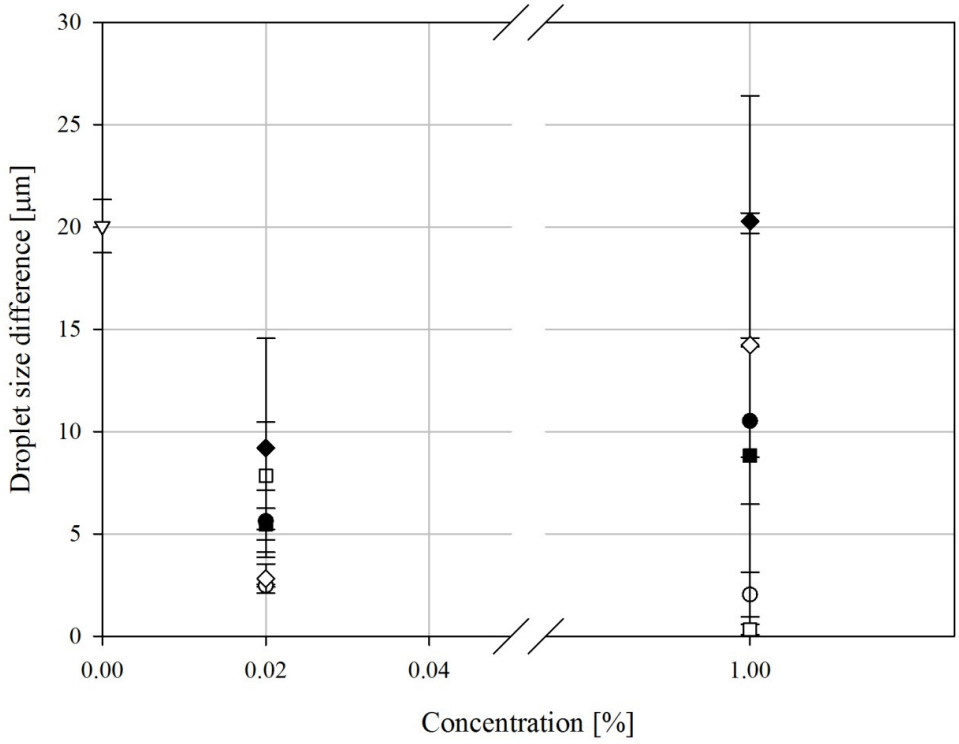

Figure 7.26. Droplet size difference between the initial and final stages of the second processing step for systems containing no emulsifier (▽) and varying concentrations of Tween 20 (●), silica particles (○), silica particles with 0.02 % (■) or 1 % (□) Tween 20 as mixed-emulsifier system, sodium caseinate (♦) and WPI (◊).

Figure 7.26, shows that, although the system in the absence of added emulsifier demonstrates low coalescence, the increase in droplet size during the second processing step is larger in this system in comparison with the systems containing emulsifiers. This demonstrates that, despite the lower collision rates during the coalescence dominant regime, a lower droplet coalescence rate is observed; however, since there is no emulsifier in the systems to cover the interfaces, the droplets continue coalescing. This behaviour has been observed and explained (Chapters 5 and 6). It can be seen that, although high droplet coalescence is observed when 1 % Tween 20 is employed, the droplet size evolution (Figure 7.17) shows that after a sudden increase in droplet size, the droplet size becomes constant. This has been related to the re-adsorption of Tween 20 on the interface, which can stabilise the droplets.

In contrast, it can be seen that the systems containing silica particles show only a small increase in droplet size. This is again related to the adsorption of silica particles on the interface. Since they are not desorbed during the second processing step, it follows that when the droplet size increases (marginally) due to droplet coalescence, the silica particles will be able to stabilise the droplets against droplet coalescence.

It can be seen that the increase in droplet size when proteins are used is large. More specifically, 1 % sodium caseinate and/or WPI show a higher increase in droplet size than lower concentrations of the respective proteins. This demonstrates that, due to their large size, after the droplet coalescence dominant regime, the proteins require longer times than surfactants to re-adsorb on the interface. Thus, a larger droplet size increase is observed.

7.4.3 The third processing step

As has already been mentioned, the third and final step of the experiments was carried out by increasing the impeller speed to the speed of the first processing step. This procedure allows one to observe and investigate the response of the system to the break-up dominant regime.

The droplet size evolution data for all studied systems examined are shown in Figures 7.27-7.29. Figure 7.27 plots the droplet size evolution data for the systems containing varying concentrations of Tween 20 or silica particles. Figure 7.28 plots the droplet size evolution data for varying concentrations of mixed-emulsifier systems. Finally, Figure 7.29 plots the droplet size evolution data for varying concentrations of sodium caseinate and WPI.

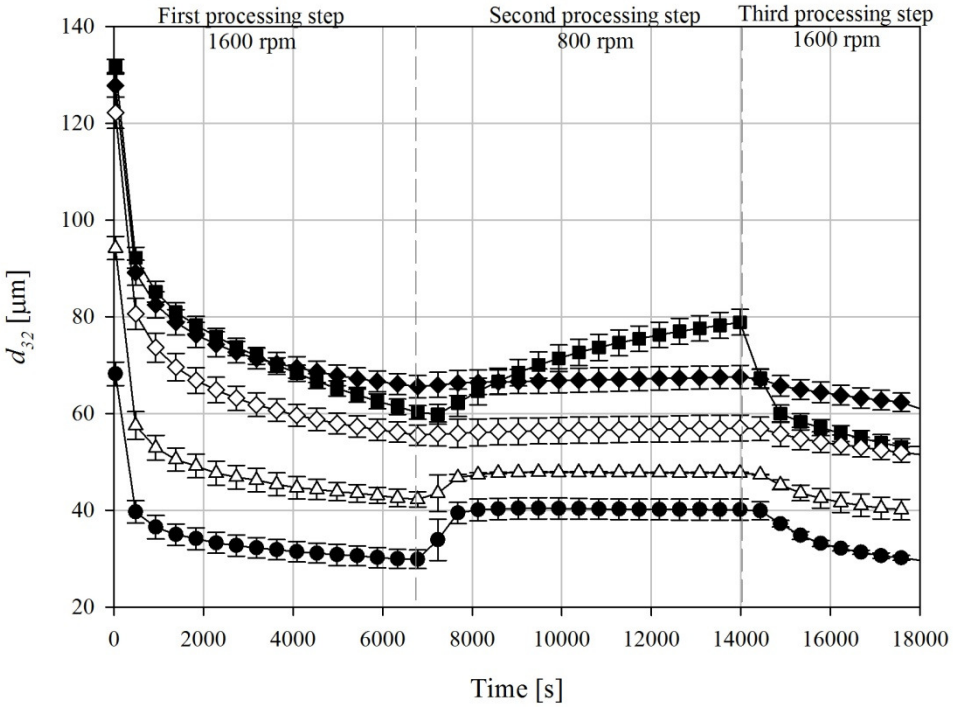

Figure 7.27. Droplet size evolution data for the entire emulsification experiment for systems containing no added emulsifiers (■), 0.02 % (♦) and 1 % (◊) silica particles and 0.02 % (Δ) and 1 % (●) Tween 20.

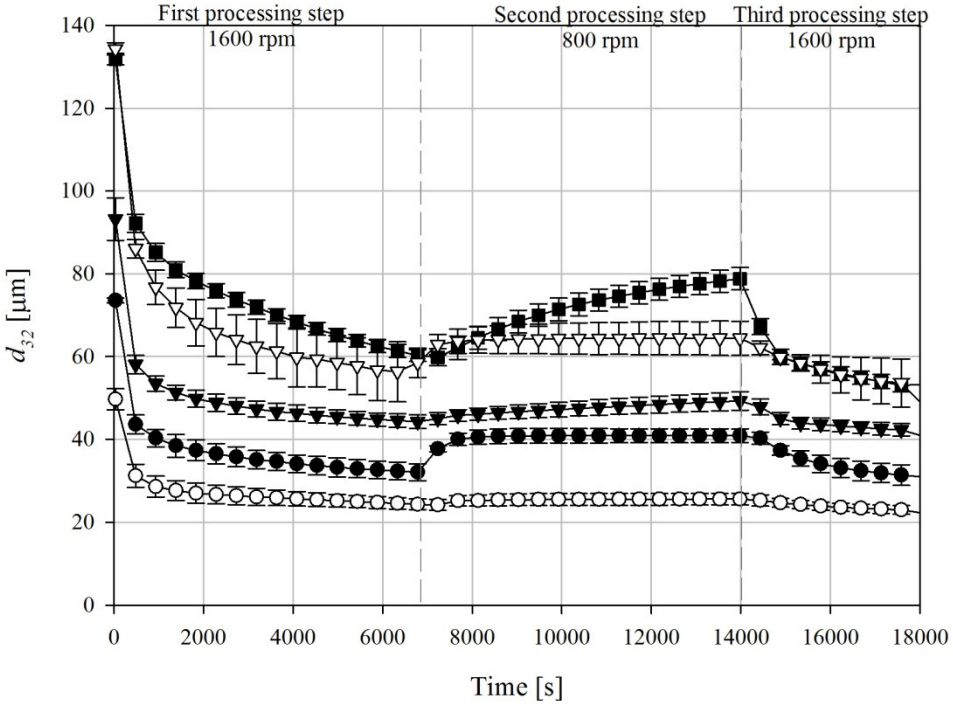

Figure 7.28. Droplet size evolution data for the entire emulsification experiment for systems containing no added emulsifiers (■) and for mixed-emulsifier systems containing 0.02 % silica particles with 0.02 % Tween 20 (▼), 1 % silica particles with 0.02 % Tween 20 (▽), 0.02 % silica particles with 1 % Tween 20 (●) and 1 % silica particles with 1 % Tween 20 (○).

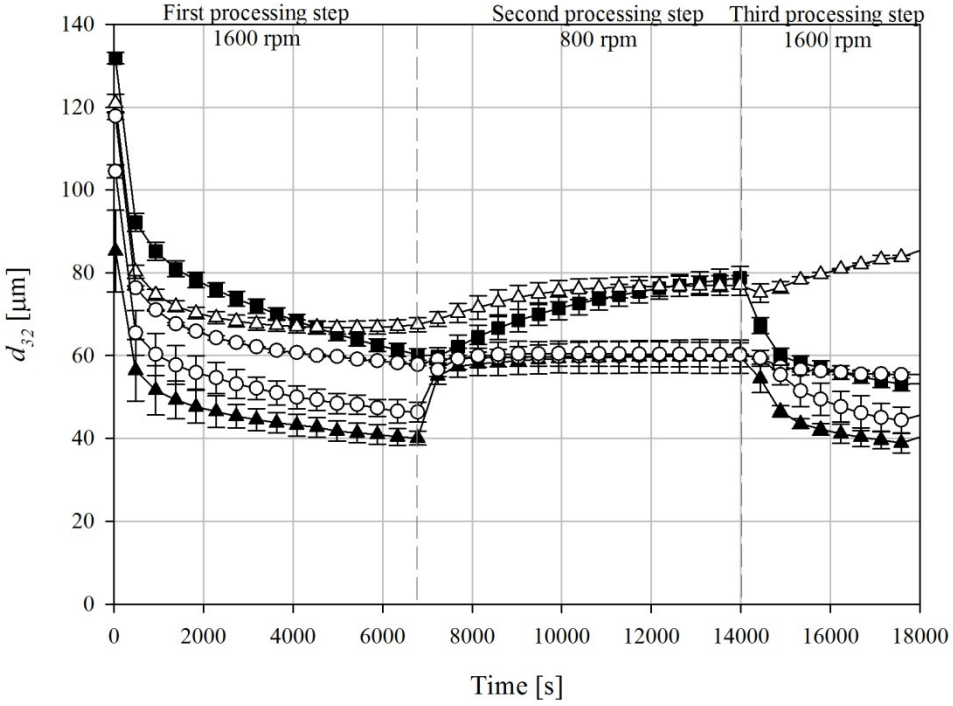

Figure 7.29. Droplet size evolution data for the entire emulsification experiment for systems containing no added emulsifiers (■), 0.02 % (Δ) and 1 % (▲) sodium caseinate and 0.02 % (○) and 1 % (●) WPI.

Figures 7.27-7.29 demonstrate that the droplet size evolution data returns to the value reached at the end of the first processing step. In fact, as shown for other cases (Sections 5.4.3 and 6.2.3), the droplet size evolution data of the third processing step follows the data at the first processing step. This has been related to the adjustment of the emulsions to the hydrodynamic condition of the process. Since the emulsions experience similar hydrodynamic conditions at the first and third processing steps, the emulsions at the initial stages of the third processing step tend to reduce to the droplet size to a value that is stable in the governing hydrodynamic condition. This, in turn, results in the high dependency of droplet break-up at this stage on the initial droplet size of the third processing step (or, equivalently, the final droplet size at the end of the second processing step). If the droplet size increases significantly during the second processing step, a high droplet break-up is expected. Otherwise, there is no

driving force to reduce the droplet size markedly; thus, a low droplet break-up would be expected. These phenomena can be observed in Figure 7.30 which plots the droplet break-up frequency with respect to the concentration of various emulsifiers.

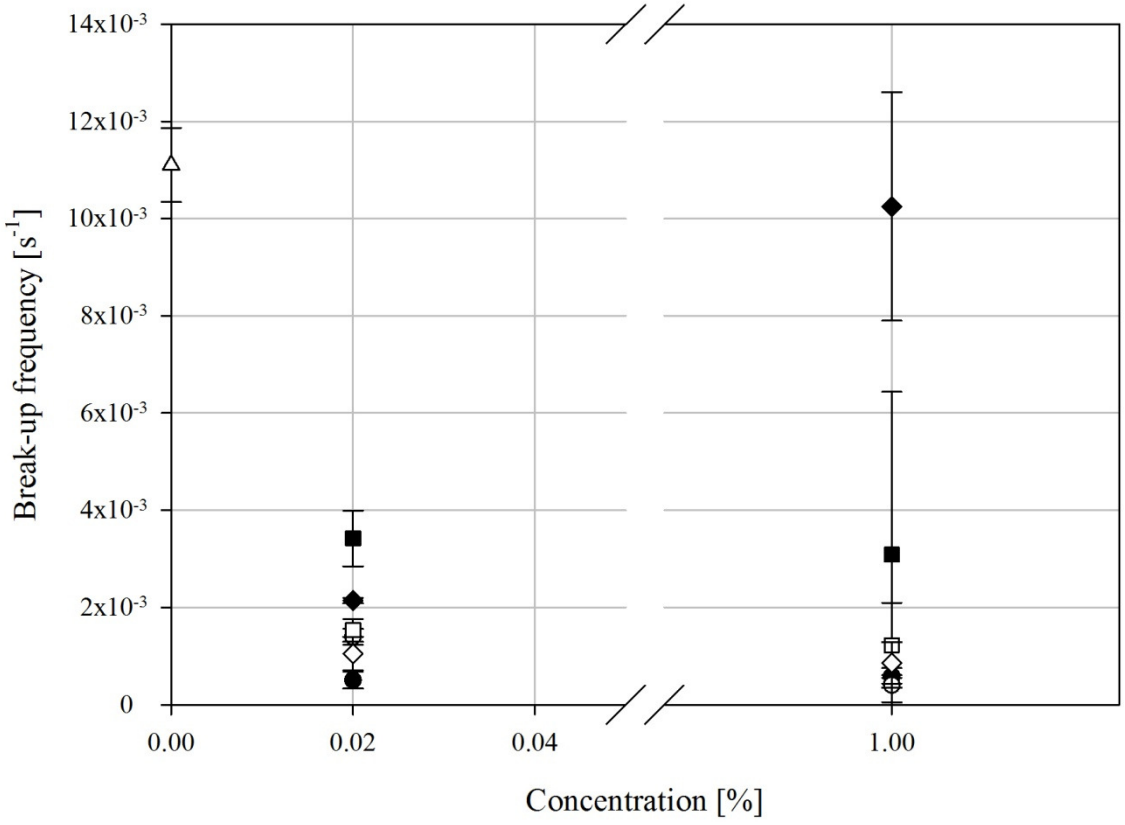

Figure 7.30. Droplet break-up frequencies determined at the initial stages of the third processing step of emulsification for systems with no added emulsifiers (▽) and varying concentrations of Tween 20 (●), silica particles (○), silica particles with 0.02 % Tween 20 as mixed-emulsifier system (■), silica particles with 1 % Tween 20 as mixed emulsifier system (□), sodium caseinate (♦) and WPI (◊).

It can be seen in Figure 7.30 that, in cases which show high increase in droplet size, a higher break-up frequency is observed, further reinforcing the hypothesis outlined above. Nonetheless, a peculiar behaviour is observed when 0.02 % sodium caseinate is employed. Even though the droplet size increases markedly before and after the impeller speed change at the second processing step, a low droplet break-up frequency is observed. In fact, the droplet size evolution data (Figure 7.29) show that after the increase in impeller speed at the third

processing step, the droplet size decreases for a short period and, subsequently, it increases rapidly.

This strange behaviour can be explained by the bridging effect of low concentrations of sodium caseinate. When the droplet sizes is reduced, there is not enough sodium caseinate to cover all the interfaces; therefore, a single molecule may adsorb to two or more droplets. This results in the close proximity of two droplets which, in turn, increases the droplet coalescence. Similar behaviour is observed at the third processing step; when the impeller speed increases, the droplets are too large for the existing hydrodynamic regime. This causes a reduction in the droplet size which significantly increases the interfacial area and, subsequently, results in the bridging of the droplets by casein molecules.

The finding that the rate of increase in droplet size is higher in the first and third processing steps compared to the second processing step may be related to the hydrodynamic condition of the process. Since a more intense hydrodynamic condition is experienced during the first and third processing steps, the interfacial area increases rapidly, promoting, thus, bridging. However, as larger droplets are stable during the second processing step, a lower interfacial area is present; therefore, a smaller bridging effect is experienced at the second processing step.

7.5 Concluding remarks

Chapter 7 focused on the influence of the emulsifier type on the emulsion formation during processes. It can be concluded that the highest droplet break-up frequency was determined by the emulsion in the presence of high concentration (1 %) of Tween 20 either individually or as part of a mixed-emulsifier system. This was caused not only by the higher interfacial tension reduction by Tween 20, but also by the fast adsorption of Tween 20. However, none of these properties are possessed by proteins, as they are larger than surfactant

molecules and their induced interfacial tension is larger; hence, a lower break-up frequency was achieved by proteins.

The lowest final droplet size was achieved by an emulsion containing 1 % Tween 20 as part of a mixed-emulsifier system. Employing mixed-emulsifier systems can lead to the lowest droplet size in comparison with other emulsifiers used. The droplet size evolution data revealed that the droplet size of the systems containing low (0.02 %) concentration of sodium caseinate at the final stages of the first processing step increases. This finding is related to the 'bridging' phenomena of sodium caseinate molecules due to their adsorption to a number of droplets at various places. This increases droplet coalescence and, hence, the droplet size.

The best stability against coalescence was demonstrated by the systems containing 1 % silica particles. As observed in the experiments in the presence of Tween 20, steric repulsive forces are practically ineffective during emulsification due to the desorption of Tween 20. Therefore, the high desorption activation energy of silica particles plays a major role in suppressing the droplet coalescence. This was true even for the mixed-emulsifier system containing 1 % silica particles with 1 % Tween 20, which showed the highest collision rate. Proteins were the least effective emulsifier for suppressing the droplet coalescence although they induce strong electrostatic repulsive forces. This is related to the desorption of proteins which in turn causes the increase in droplet coalescence. Even though high droplet coalescence frequencies were observed in systems containing emulsifiers in comparison with those without any added emulsifier, the droplet size increased continuously for the latter system, whilst it reached a constant value for the former system. This was caused by the absence of any emulsifier to cover the interfaces of the droplets.

Chapter 8

Conclusions and Future work

8.1 Conclusions

The aim of this thesis was to advance the mechanistic understanding of the formation of oil-in-water emulsions during processing. This study is particularly relevant to the food industry where emulsification is a common process. Therefore, the influences of 'food grade' materials were investigated on these processes. The experimental investigation was focused on the online monitoring of the emulsion formation.

To conduct this study, attempts have been initially focused on the development of a technique, and subsequently a methodology, to investigate emulsion behaviour during processing. The developed methodology was employed to investigate the effect of various operating parameters and formulations on the emulsions' droplet size evolution. These parameters include the emulsifier type and concentration, hydrodynamic condition of the process and the dispersed phase volume fraction. The main conclusions of this work are summarised below.

8.1.1 Development of the methodology

- *The reflectance technique can be employed for online droplet size measurements during processing of emulsions in mixing systems.*

A technique based on the relationship between light reflected (Y) from the emulsion and its properties was developed to determine the droplet size evolution in real-time. Calibration curves were produced for each of the dispersed phase volume fractions and emulsifier types employed in this study. All of the calibration curves show a linear dependency between droplet size and the reflectance in a semi-logarithmic diagram. It was shown that the droplet size of the systems in the absence of added emulsifier can be estimated using Tween 20 calibration curves. Finally, it was shown that the droplet size distribution type does not influence the calibration curves.

- *By the proposed experimental procedure it was possible to investigate the droplet break-up and coalescence phenomena individually.*

An experimental procedure was proposed to investigate not only the emulsions response to the hydrodynamic conditions, but also to investigate the droplet break-up and coalescence of the studied processes independently.

- *Droplet break-up and coalescence frequencies could be theoretically calculated using a series of proposed mathematical expressions.*

Droplet break-up and coalescence frequencies were calculated by developing a series of mathematical expressions. These expressions are particularly useful since they do not depend on the hydrodynamic conditions of the system. Therefore, the uncertainties of the hydrodynamic regime of the process did not influence the mathematical expressions.

8.1.2 Emulsion formation during processing

- *The droplet size evolution during emulsification processes is characterised by three regions.*

The first step of the emulsification experiments show that the droplet size evolution data are characterised by three regions. The droplet size in the early stages of the process (rapid decrease region) is only affected by droplet break-up events. The decrease in droplet size caused an increase in the number of droplets, which in turn, increased the occurrence of droplet coalescence phenomenon. This transitional region is followed by a plateau region where droplet break-up and coalescence phenomena were at dynamic equilibrium.

- *The droplet break-up frequency does not depend on the surfactants (Tween 20 and Brij 97), proteins (sodium caseinate and Whey protein isolate) and silica particles concentrations.*

The break-up frequency increased when emulsifiers were used in the studied formulation, however, remained unchanged by further increase in their concentration. This is a consequence of the similar interfacial tension induced by the entire concentration range of emulsifiers which induced similar capillary pressure. Thus, at similar impeller speeds, their respective droplet break-up 'potential' remains the same. The lowest droplet break-up frequency was demonstrated by the experiment in the presence of silica particles, as a result of the fact that silica particles do not affect interfacial tension.

- *The droplet break-up frequency in the presence of the mixed-emulsifier systems depends on their relative ratios (concentrations of Tween 20 and silica particles).*

When mixed-emulsifier systems were employed, most of the mixed-emulsifier systems show similar droplet break-up frequencies to that of Tween 20. This is a result of the faster adsorption of the Tween 20, compared to that of silica particles, which resulted in similar interfacial tension values for those mixed-emulsifier systems as when only Tween 20 was used. The adsorption rate of Tween 20 was significantly reduced when low concentration of Tween 20 (0.02 %) was used with 1 % silica particles. In this experiment the high concentration of silica particles adsorbed faster, suppressing the adsorption of Tween 20, thus the interfacial tension remained the same to that of in the absence of added emulsifier. This experiment showed similar droplet break-up frequency to the experiment when no emulsifier was added.

- *An increase in the volume fraction of the dispersed phase resulted in a minimum in the droplet break-up frequency.*

The observed minimum in the droplet break-up frequency at a dispersed phase volume fraction of 20 %, when the dispersed phase volume fraction was varied up to 50 %, was a result of the influence of two opposing parameters. These include the dampening effect of the

dispersed phase which caused a reduction in the turbulent intensity, and the capillary pressure of the droplets which was lower at higher dispersed phase volume fractions, since the initial droplet sizes were larger.

- *The droplet size evolution in the presence of low concentrations of emulsifier under intense hydrodynamic conditions results in a rapid 'increase and decrease' in droplet size prior to reaching the plateau region.*

A rapid increase and decrease in droplet size at the transitional region was observed in some experimental cases; more specifically, in experiments carried out in the presence of the low concentrations of Tween 20 (0.01 % and 0.02 %) and intense hydrodynamic condition (1600 and/or 2000 *rpm*). This was related to the depletion of Tween 20 due to the high rate of increase in interfacial area caused by the low interfacial tension induced by Tween 20. In turn this resulted, in complete adsorption of the available Tween 20 molecules. This depletion caused the increase in droplet coalescence. This can be avoided by progressively, and not rapidly, increasing the interfacial area to arrest the occurrence of this 'locally high coalescence' region.

- *Lower final droplet size in the presence of higher emulsifier concentration is a result of the extent of droplet break-up, whilst droplet coalescence has a minimal influence.*

Although experiments in the presence of varying concentrations of Tween 20 induced similar droplet break-up frequencies, their equilibrium droplet size at the end of the first processing step was lower when higher concentrations of Tween 20 were used. This is related to the presence of higher amount of 'free' Tween 20 in the aqueous phase which in turn results in higher adsorption rates, thus higher break-up frequencies. This mechanism was observed in all experiments in the presence of proteins, silica particles and mixed-emulsifier systems. It should be noted that the observed behaviour is not resulted from the higher droplet

coalescence. This was demonstrated by the experiment in the presence of mixed-emulsifier system containing Tween 20 and silica particles which showed a similar droplet size to the experiments performed using only Tween 20. Since the presence of silica particles can completely arrest the droplet coalescence, the resulting similar final droplet size was caused by the droplet break-up enhanced by Tween 20 adsorption.

- *Droplet coalescence was not suppressed in the presence of surfactants and proteins in the experiments containing dispersed phase volume fractions lower than 20 %. However droplet coalescence was arrested in the presence of silica particles.*

The surfactant (Tween 20) and proteins (sodium caseinate and Whey protein isolate) used in the studied formulations were not able to suppress droplet coalescence, due to their desorption from the interface. In contrast, the experiments in the presence of silica particles showed them to be able to suppress droplet coalescence. This is a result of a much higher desorption energy of silica particles from the interface compared to surfactants and proteins.

- *The increase in the dispersed phase volume fraction resulted in a decrease in droplet coalescence phenomena.*

Results suggest that droplet coalescence was not suppressed by using Tween 20, except in those cases where a dispersed phase volume fraction of 50 % was employed. A lower droplet coalescence frequency was observed for high dispersed phase volume fractions. These observations relate to the dampening effect of the dispersed phase. At higher dispersed phase volume fractions, not only were lower collision rates observed, but also lower turbulent forces were acting on the colliding droplets, thus reducing the drainage rate of the continuous film between them. At 50 % dispersed phase volume fraction, however, the Tween 20 suppressed the droplet coalescence due to the fact that the steric repulsive forces became comparable to the turbulent forces.

- *The droplet size evolution path is independent of variations in hydrodynamic conditions of the process.*

The third processing step of all experiments showed that the droplet size evolution data rapidly returned to the droplet size already determined at the first processing step. This is a consequence of the fact that droplets should 'age' during processing to reach a certain droplet size. This is demonstrated by the droplet evolution of the third processing step which followed the ones in the first processing step. Therefore, the droplet break-up phenomenon at this step was a function of droplet size at the start of the third processing step and the final droplet size at the end of the first processing step. If there was a significant difference between those two then high droplet break-up frequency would have been observed during the third processing step.

8.2 Future work

This section includes some recommendations for future studies in light of interesting observations and conclusions obtained from the study presented here.

- *Employing the reflectance technique for other emulsification processes.*

The reflectance technique can be employed to measure droplet sizes for other emulsification processes. These may include the newly developed processes such as impinging jet emulsification, or the ones that do not rely on the break-up phenomena for producing the emulsion, such as membrane emulsification.

- *Investigation of only droplet break-up and coalescence.*

The developed methodology was used to observe and understand the mechanisms during processing in the presence of various formulations. By understanding the droplet break-up and coalescence as an individual phenomenon, a better understanding of the

processes can be obtained. This requires feeding a mono-sized emulsion to the process. A mono-sized emulsion, to some extent, can be produced by membrane processes.

- *Characterisation the flow behaviour or detail hydrodynamic condition of the process.*

Extending the usage of the effective techniques such as Positron Emission Particle Tracking (PEPT) can help to clarify the detail influence of the presence of the dispersed phase on the hydrodynamic condition, as this effect was responsible for some interesting results observed in this work.

- *Determining the mathematical expression of the emulsification.*

The mechanistic understanding of the process can be used to mathematically model the emulsification process. Some preliminary studies in this regard were carried out and can be seen in Appendix C. Although useful and detailed models can be found in the literature, however, in order to fully develop a thorough model, a 'fresh look' at the problem in hand based on the gained understanding of the processes is required.

- *Using other forms of food grade particles.*

The usefulness of the particles in emulsions was envisaged in this study. Therefore, it would be interesting to expand the experimental work of this study to include some other particles with different shapes or physicochemical characteristics.

- *Using the reflectance technique in conjunction with other online droplet size measurement techniques.*

The reflectance technique possesses some positive attributes which are required for online droplet size measurement, including fast data acquisition rate and ease of its implementation. However, it generates mean droplet size evolution data which cannot be used for detail study of droplet size distribution. In contrast, other online techniques such as

imaging, provide droplet size distribution, however could not be employed when time scales of the process is small. Therefore, a method based on the combination of both techniques can benefit from the fast data acquisition rate of the reflectance technique and the droplet size distribution determination of the online imaging technique.

Appendix A

The colouring technique and ultrasonic spectroscopy

This Appendix presents the preliminary experimental work carried out to employ the 'colouring technique' and 'ultrasonic spectroscopy' for investigating emulsification processes.

A.1 The colouring technique

A.1.1 Introduction

The colouring technique was originally developed by Danner (2001). The experimental procedure can be summarised as follows. Two coarse emulsions were prepared, each with differently coloured dispersed phases. When the two emulsions were mixed, a third colour was created as a result of the droplet coalescence. Samples were obtained at different times from the process. With the aid of microscope and image analysis software the area taken by the third colour was calculated in each image. The stochastic model (Monte Carlo simulation) was developed in order to determine the coalescence rate from the coalescence probability and the collision efficiency (Schubert *et al.*, 2003). Figure A.1 demonstrates the area occupied by the third colour as a function of processing time.

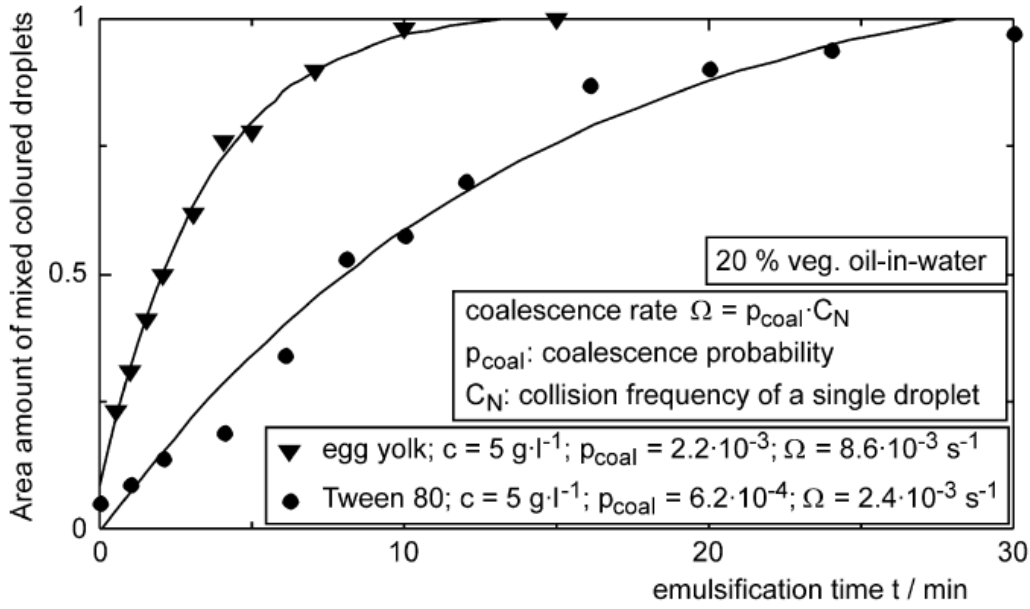

Figure A.1. Area occupied by the generated third colour as a consequence of droplet coalescence during emulsification (Schubert *et al.*, 2003)

Figure A.1 shows that the droplet coalescence increases with processing time. The applicability of this technique is investigated in Danner's thesis (2001). Effort has been made

to employ this technique to determine droplet coalescence frequency in emulsification. The experimental work and results are presented in the following sections.

A.1.2 Materials

Selecting suitable colorant dyes are of the major importance for employing the colouring technique. The oil-soluble and extremely hydrophobic dyes should be selected in order to suppress the diffusion of dyes through continuous phase. These types of dyes are referred to as "Lysochrome". A group that has been widely used in the previous studies are part of 'Sudan family'. Sudan IV has been chosen for generating 'red' colour and Sudan black for generating 'dark blue' colour. The properties of these colorant dyes can be seen in table A.1.

Table A.1. Properties of the dyes employed to colour the oil phase.

Property	**Sudan black**	**Sudan IV**
Common name	Sudan black B	Sudan IV
Other name	Fat black HB	Scarlet R or red Scharlach R
Class	Azo	Azo
Ionisation	Lysochrome	Lysochrome
Solubility in aqueous	Insoluble	Insoluble
Maximum absorption wave length [*nm*]	598.415	520.357
Colour	Blue-black	red

Commercially rapeseed vegetable oil and stilled water were used in these experiments. In order to produce stable emulsions, 1% Tween 20 (Sigma Aldrich, UK) was used as emulsifier.

A.1.3 Methods

A.1.3.1 Preparation of the continuous and the dispersed phases

The continuous phase was prepared by dissolving 1% Tween 20 in the water using the magnetic stirrer. Two differently coloured dispersed phases were prepared by dissolving 1% of Sudan IV and Sudan black in oil by magnetic stirrer at 50 °C. Subsequently, these two

coloured oils were filtered three times with the filter papers to sieve the unsolved colorant particles. A picture of the prepared dispersed phases can be seen in Figure A.2.

Figure A.2. Coloured oil phases red (left) and dark blue (right) prepared for the colouring technique.

A.1.3.2 Emulsification process

All experiments were performed in the experimental set-up (mixing vessel) introduced and used in this work.

A.1.3.3 Optical microscopy

In order to optically observe the droplets in the emulsion, imaging was conducted using a system of microscope with the attached camera. Images were captured from the samples by the coloured camera (3CCD, Colour Vision Camera Module, Donpisha) attached to the microscope (Leica DMRBE, Leica Microsystems Imaging Solution LTD). The images were exported to the connected computer, and they were visualised by the Leica Qwin program (version 2.8, 2003). The system is illustrated in the Figure A.3.

Figure A.3. Optical observation system: the microscope, the coloured camera and the computer.

Droplet size distribution determination and image processing were preformed by ImageJ program. ImageJ is public domain image analysis software which was developed by "NIH image". Calibration was carried out using "stage micrometer" by measuring the number of pixles that construct a known size. The calibration image can be seen in the Figure A.4.

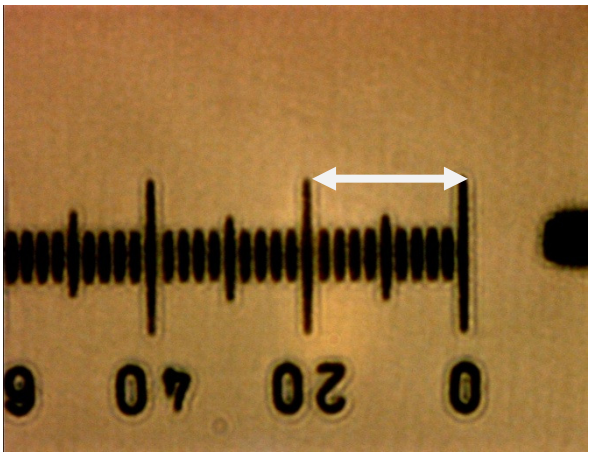

Figure A.4. Calibration image used to measure the droplet size in images obtained by the microscope.

A.1.3.4 Droplet size measurement

In addition to the droplet size distribution determined by optical microscopy, Mastersizer (Malvern Instrument LTD, UK) was also used to measure the droplet sizes.

A.1.4 Results and Discussion

In order to examine the applicability of the colouring technique, two course emulsions were produced using the single coloured dispersed phase which are referred to as 'red emulsion' (prepared by the red coloured oil phase) and 'blue emulsion' (prepared by the blue coloured oil phase). These emulsions were prepared with 5% dispersed phase volume fraction under 300 *rpm* impeller speed. The choice of the Tween 20 concentration (1%) ensures the stability of samples after the process. Samples were obtained from single coloured emulsions at this stage. Subsequently, red emulsion was subjected to processing under 500 *rpm* impeller speed for 30 *s* and subsequently equal volume of the blue emulsion was added to the process. Samples were obtained every 8 *min* during the 40 *min* processing. Some images captured from the samples obtained at different process times are shown in table A.2.

Table A.2. Images captured from the samples obtained every 8 min from the process.

Point in time that samples were obtained	Image
Red emulsion before mixed-emulsion experiment	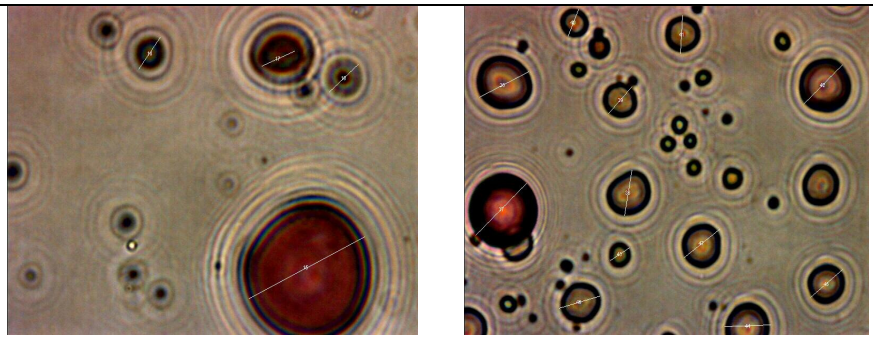
Blue emulsion before mixed-emulsion experiment	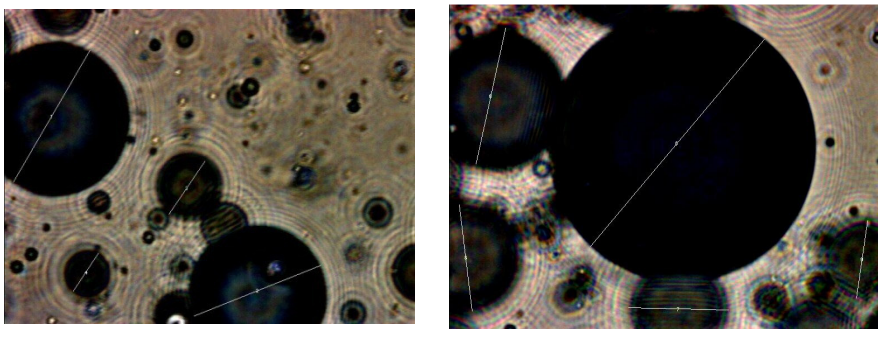

At the start of the mixed-emulsion experiment	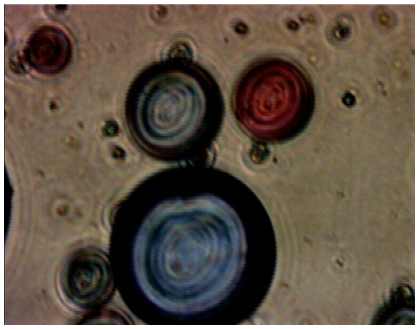	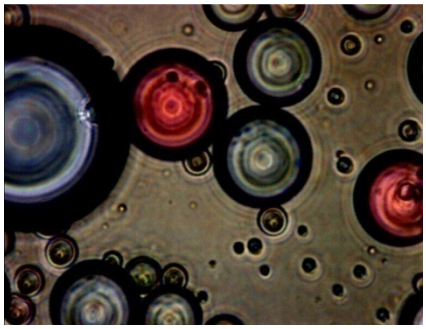
8 min of the mixed-emulsion experiment	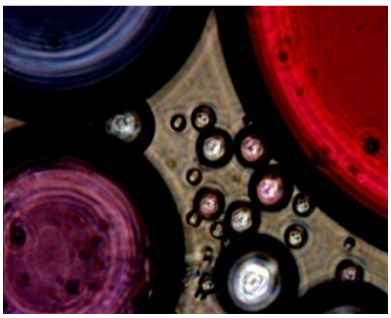	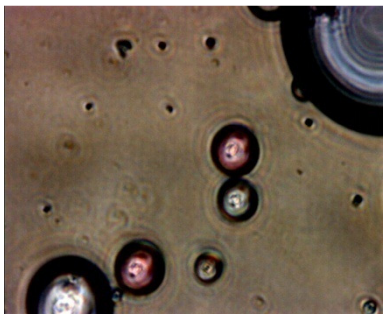
16 min of the mixed-emulsion experiment	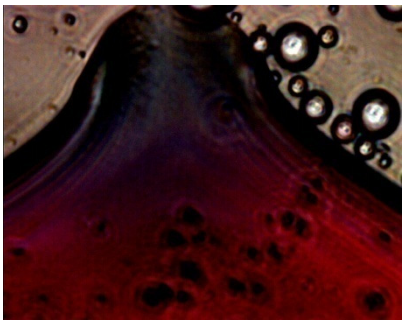	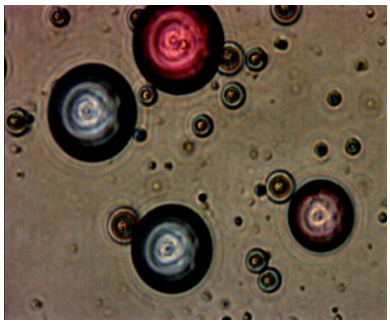
24 min of the mixed-emulsion experiment	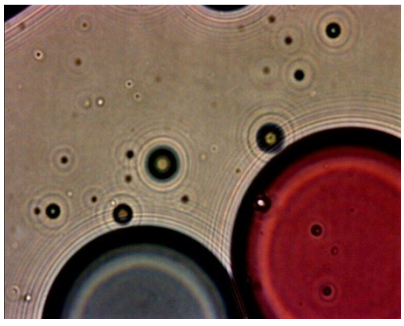	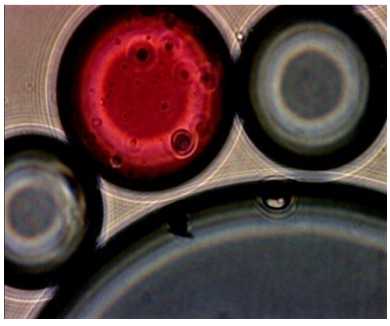
32 min of the mixed-emulsion experiment	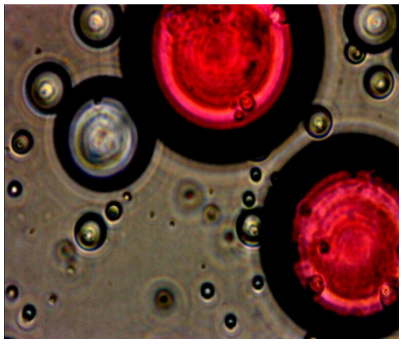	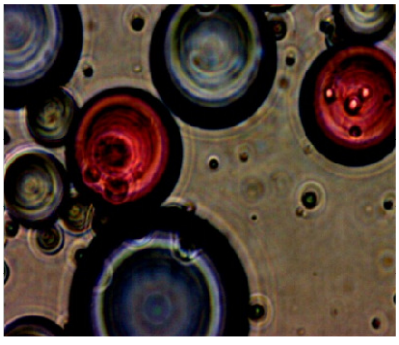

At the end of the mixed-emulsion experiment	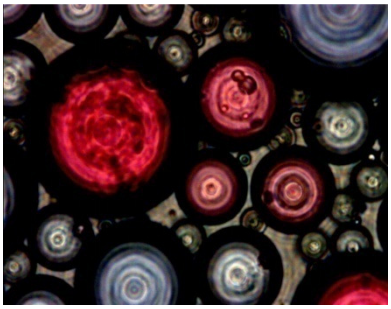	

Careful inspection of the obtained images revealed the (over time) appearance of a third colour (purple) in the mixed-systems. Since the continuous phase of both the single-coloured and the mixed-coloured emulsions remains 'colourless', the development of the third colour via diffusion, of one of the primary colours from one droplet (red or blue) through the continuous phase to another droplet (blue or red), can be dismissed. What can be therefore postulated is that the development of the observed third colour can only be the result of two (or more) droplets, of different primary colours, coalescing. Hence this colour changing process is directly related to the coalescence phenomena taking place in the system under observation.

In order to quantify the colour changes observed, further analysis of the images is needed. This involves constructing an RGB (Red, Green, and Blue) diagram for each image; RGB diagrams are drawn by calculating the 'amount' of each of the three primary colours (red, green and blue) in each pixel. Each pixel is defined by a triplet (r,g,b), in which each value can vary between 0 and 255 in the way that (0,0,0) and (255,255,255) are assigned to colour 'black' and 'white', respectively. In this report, a possible quantification is represented for images captured from the samples obtained at the end of the process (Figure A.5).

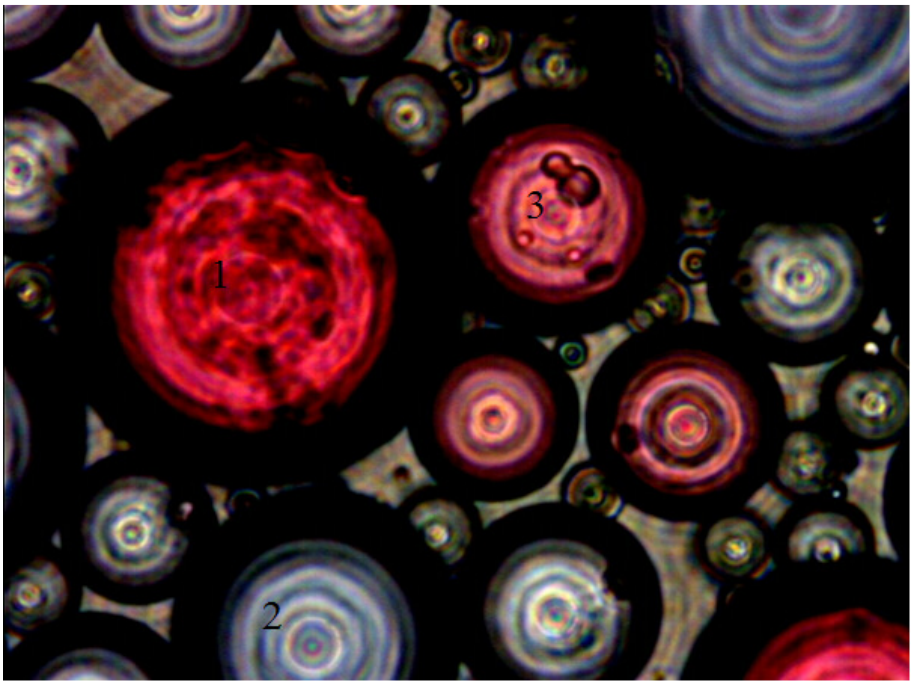

Figure A.5. Image captured from the samples obtained at the end of the mixed-emulsion process.

Figure A.5 clearly shows three colours of red (droplet number 1), blue (droplet number 2) and purple (droplet number 3). In order to study the colours existing in the image, a 3D diagram of RGB is determined from all the pixels in the Figure A.5. This is shown in Figure A.6.

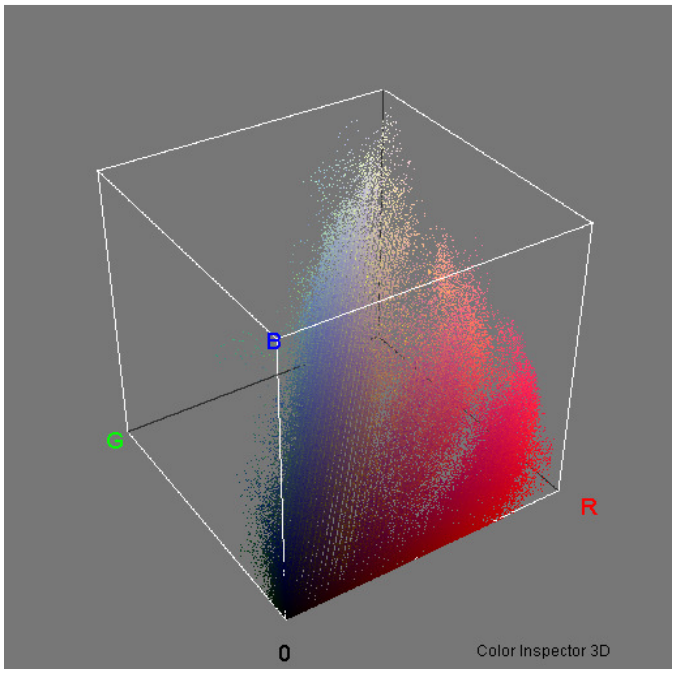

Figure A.6. RGB diagrams of the every pixel in the Figure 5.

Four regions of blue, red, purple and cream are distinguished in Figure A.6, which correspond to the blue and red primary-coloured droplets, the purple-coloured droplets resulting from coalescing primary-coloured droplets and the continuous colourless phase (cream). This shows that, colours or RGB values can be distinguished in each image. In order to clarify the difference in the colour of red, blue and purple droplets, the RGB values are reported in Figures A.7-a, A.7-b and A.7-c for the droplets numbered in Figure A.5 as 1, 2 and 3, respectively. These graphs are the RGB values of pixels on one line which connects two opposing corners of droplets collapsing on the diameter of these droplets.

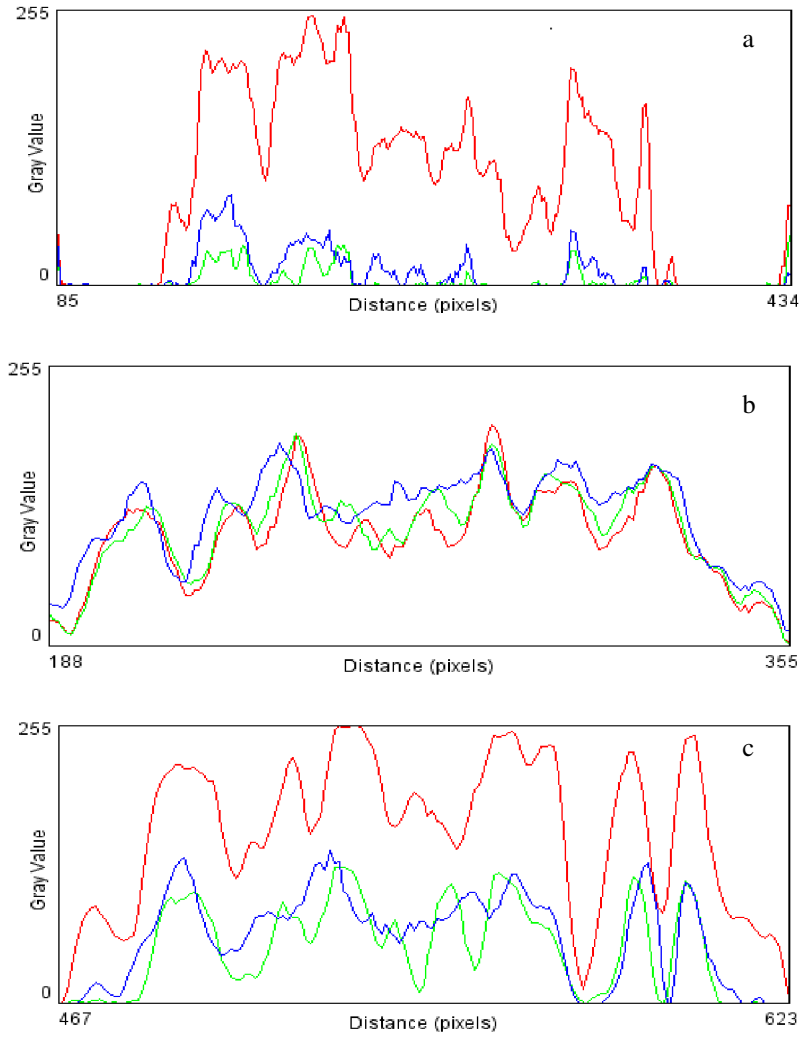

Figure A.7. RGB diagram of the pixels of the diameter of droplets number 1 (a), 2 (b) and 3 (c) in the Figure A.5.

It can be observed that, in the purple droplet more blue and green components exist than red droplet. On the other hand, less blue and green components involved than the blue droplets. It should be noted that the existence of the red component in the blue droplet diagram does not mean that the red dyes are present in the blue droplet. The RGB model is just the method for illustrating the colours as a mathematical viewpoint. It can be deducted from Figures A.6 and A.7 that the difference between the colours of blue, red and purple can be quantified. The proposed procedure for quantifying the colour of droplets is as follows. A calibration RGB values for red and blue droplets from different droplet sizes can be defined using the images of the single-coloured emulsions. The coalesced droplets (purple droplets)

can be identified by comparing the RGB values of the pixels in the mixed-emulsion droplets by the calibration values. Subsequently, the evolution of purple droplets can be used to quantitatively determine the droplet coalescence respect with time.

A.1.5 Reasons for not selecting the colouring technique

Although it seems that the droplet coalescence can be quantified by the proposed protocol, the colouring technique was not employed due to the following shortcomings. The first drawback arises from the limitation of identification of the colour of emulsion by optical observation. The colour intensity is significantly reduced in the smaller droplets as lower amount of colorant is present and the high curvature of droplets. This results in the immergence of the colour of smaller droplets to that of the background (cream) which is the colour of the continuous phase. The experiments show that the smallest droplet that the colour of which can be identified is 20 μm, but the droplet size distributions determined from Mastersizer device show that smaller droplets (10 μm) exist which shows that a certain number of droplets are not included in the colour quantification. Consequently, if more intense hydrodynamic condition is applied, which in turn results in smaller droplets, larger portion of droplets would not be quantified. Additionally, a major drawback of this technique is the amount of sampling involved. Furthermore, this method is extremely time consuming and involves number of steps which each introduces error to the droplet coalescence rate determination.

A.2 Ultrasonic spectroscopy

A.2.1 Introduction

In the search of the online techniques, the ultrasonic spectroscopy has shown to be promising and preliminary studies were conducted in order to implement this method.

A.2.2 Materials

Distilled water and commercially available vegetable oil were used as the continuous and dispersed phases, respectively, for all prepared emulsions. Tween 20 and sodium caseinate (DMV, Netherlands) were used as emulsifiers. All materials were used without further purification or modification of their properties.

A.2.3 Methods

A.2.3.1 Sample preparation

The aqueous phase was prepared by dissolving 1% of emulsifiers (Tween 20 and sodium caseinate) using a magnetic stirrer. The weights of the aqueous and oils phases were selected in order to perform experiments on emulsions containing 10% volume fraction of the dispersed phase.

A.2.3.2 Measurement device

The commercially available Ultrasizer (Malvern, UK) in the University of Leeds was used to perform the ultrasonic measurements. Emulsions were produced using a chamber positioned in the device which used a propeller with variable speed motor with the maximum rotational speed of 650 *rpm*. The device was designed based on the continuous wave method to propagate wide range of ultrasound frequencies.

A.2.4 Result and Discussion

The emulsification was initiated under the impeller speed of 650 *rpm*. A complete measurement of the amplitude of the propagated ultra sound waves as a function of frequencies resulted in the measurement time of 4 *min*. The droplet size and hydrodynamic condition during the measurement time should be unchanged to obtain accurate droplet size. This is the reason that the step-change could not be applied since the condition for the measurements were not consistent during the rapid change in hydrodynamic condition (during

the Four *min* of measurement time). Consequently, experiments were conducted under steady impeller speeds.

In the experiments in the presence of Tween 20, the droplet size distribution could be determined. In contrast, when sodium caseinate was employed, the droplet size distribution could not be determined. This problem was related to the fact that thermophysical properties of the protein solution were not the same as pure water, thus the droplet size could not be determined.

Apart from Ultrasizer (custom-built in University of Leeds), attempts has been made to implement the pulse-echo technique for the stirrer tank. However, by the personal discussion with Professor Povey (Leeds University), it was concluded that a complicated device should have been designed and made since the rig that was available was not suitable for such systems.

A.2.5 Reasons for not selecting the ultrasonic spectroscopy

Although the ultrasonic spectroscopy was shown to operate on emulsions containing high volume fraction of the dispersed phase, it was not able to obtain the droplet size distribution in the presence of all the used emulsifiers. This required the determination of the thermophysical characteristics of each used formulation which reduces the applicability of such technique. Moreover, it was shown that the commercially available device was not suitable for fast occurring processes. The pulse-echo technique attempted to overcome this shortcoming to some extend. However, it was shown that a new system should be designed.

Appendix B

Experimental data of the emulsification in the presence of Brij 97

This Appendix presents the experimental data related to the emulsification experiment in the presence of Brij 97 containing 50% dispersed phase volume fraction.

The emulsion formation containing 50% dispersed phase volume fraction in the presence of nonionic surfactants is examined in Chapter 5. Two different emulsifiers were employed; namely Tween 20 and Brij 97. The experimental data obtained from the emulsification experiments in the presence of Tween 20 is demonstrated in Chapter 5 and the influence of Tween 20 was thoroughly investigated. As the analysis of the experiments in the presence of Brij 97 shows similar trends, the data related to Brij 97 were not included in Chapter 5 and instead they are shown in this Appendix. Since the analyses are already given, only data in the form of graphs are presented herein.

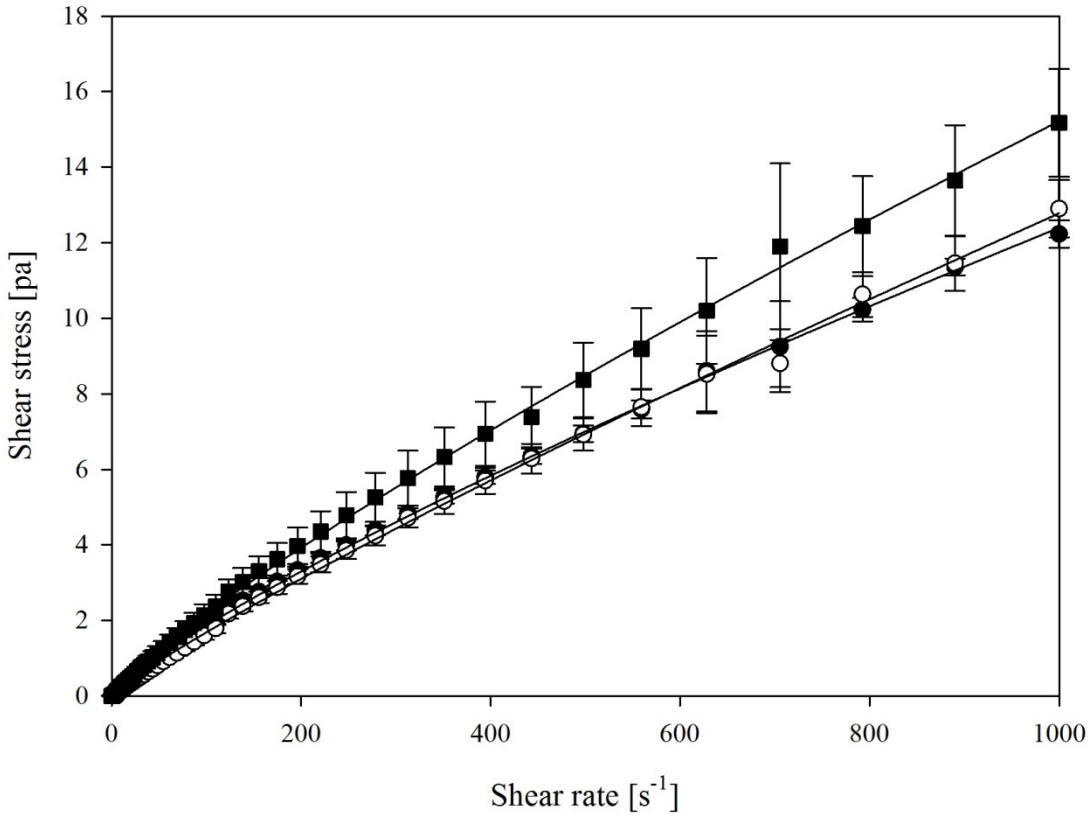

Figure B.1. The flow-curves of shear stress with respect to the shear rate is shown for oil-in-water emulsions containing 50% dispersed phase volume fraction in the presence 1% of Brij 97 produced under different processing conditions; 800 rpm (●), 1600 rpm (○) and 2000 rpm (■) impeller speed.

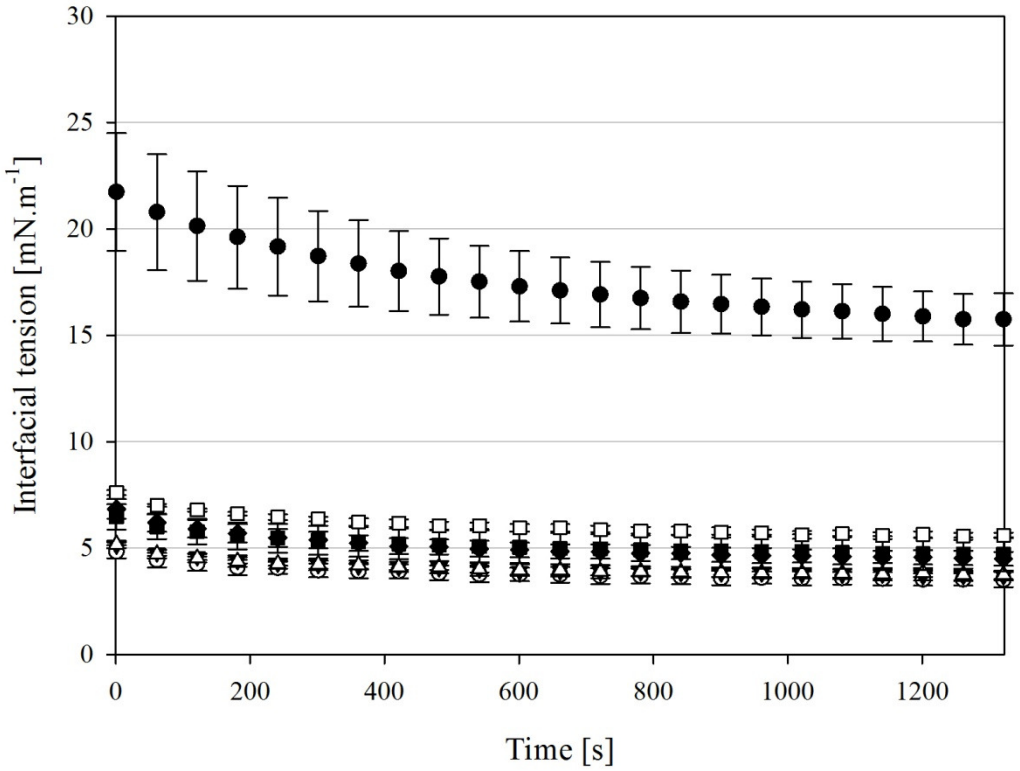

Figure B.2. Interfacial tension measured at the oil and water interface in the absence of added emulsifier (●) and in presence of 0.005% (♦), 0.01% (□), 0.02% (■), 0.2% (Δ), 0.6% (▼) and 1% (○) concentrations of Brij 97.

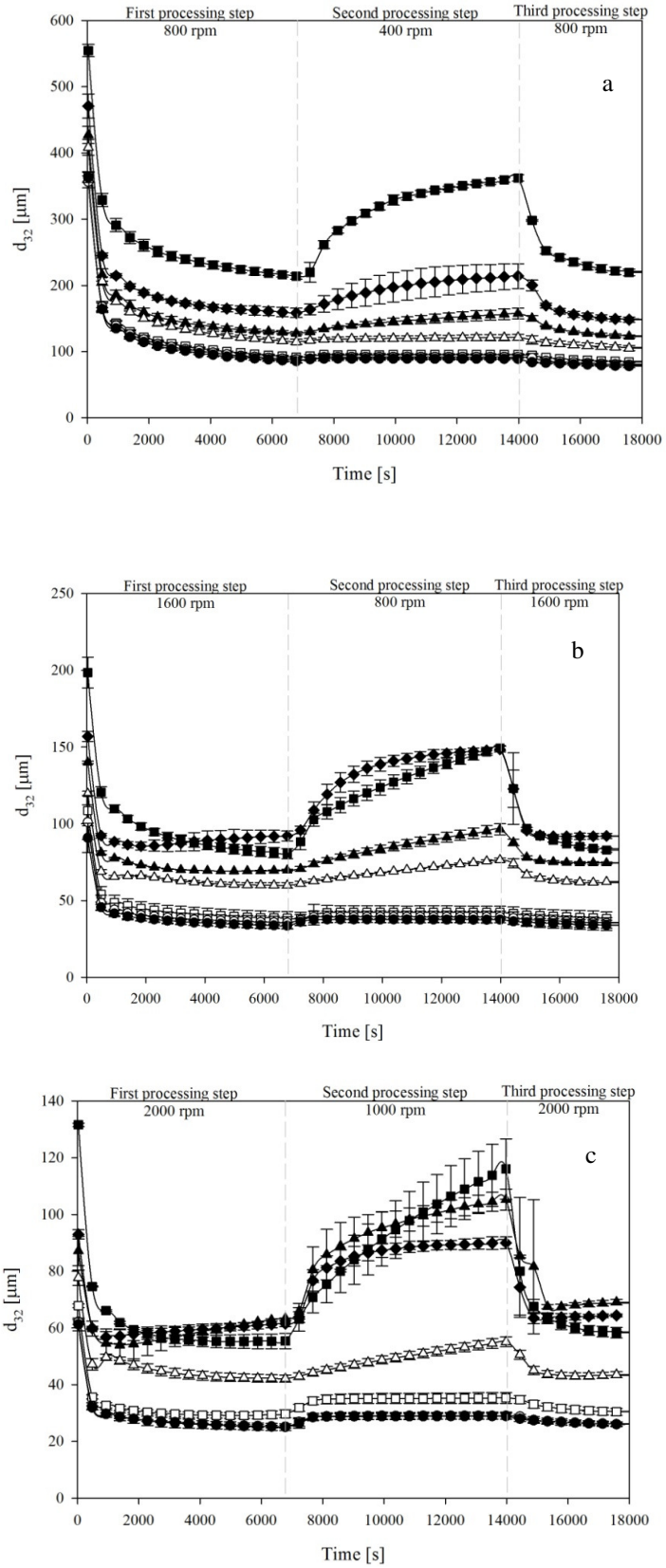

Figure B.3. Droplet size evolution data obtained from the first, the second and the third processing steps of emulsification experiments with 50% dispersed phase volume fraction in absence of added emulsifier (■) and in the presence of 0.005% (♦), 0.01% (▲), 0.02% (Δ), 0.2% (▼), 0.6% (○) and 1% (●) concentrations of Brij 97 under different impeller speeds of (a) 800 rpm, (b) 1600 rpm and (c) 2000 rpm.

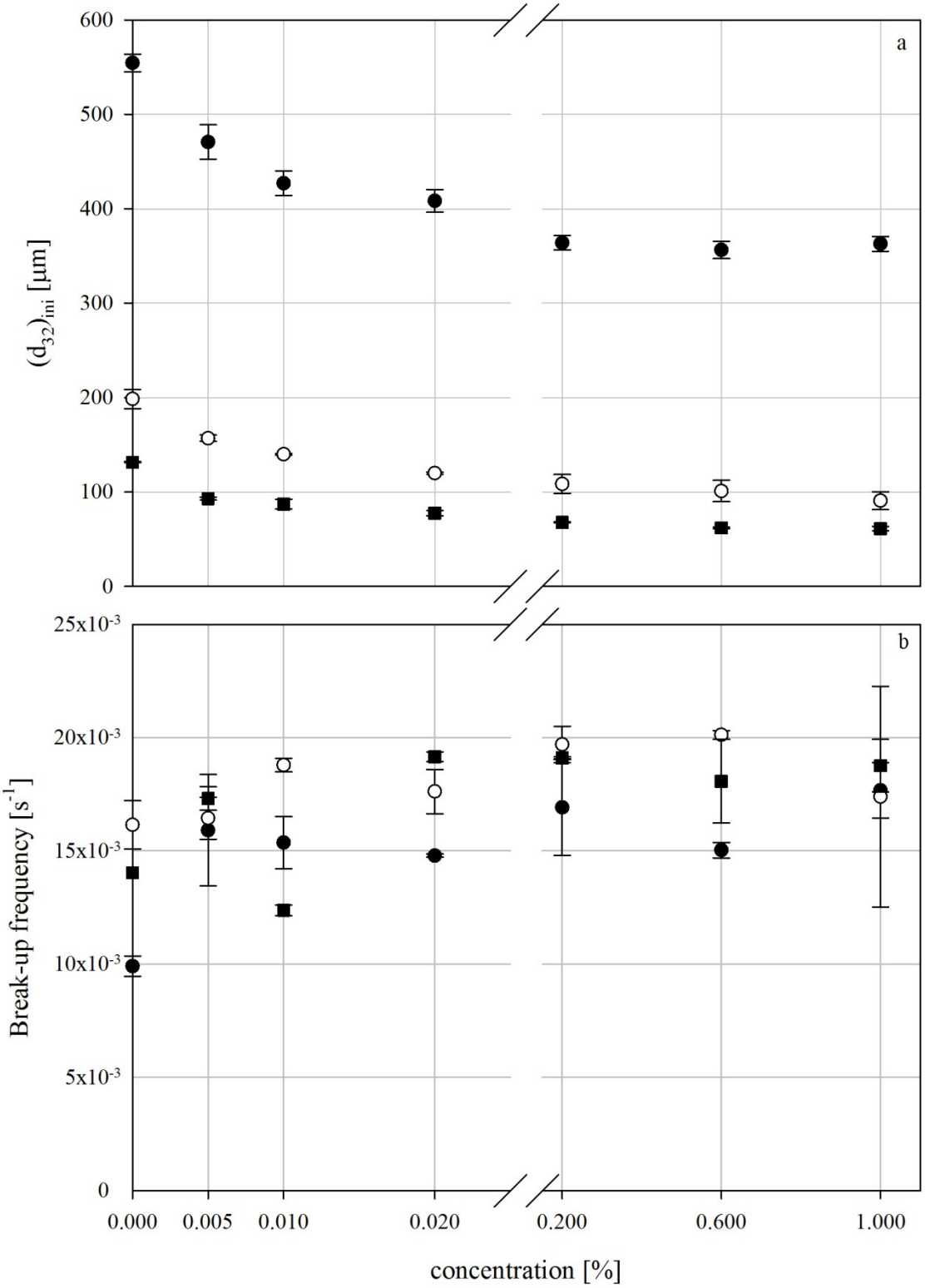

Figure B.4. Initial droplet size (a) and break-up frequencies (b) calculated at the initial stages of the first processing step of the experiments in respect with concentration of Brij 97 for varying impeller speeds of 800 rpm (●), 1600 rpm (○) and 2000 rpm (■).

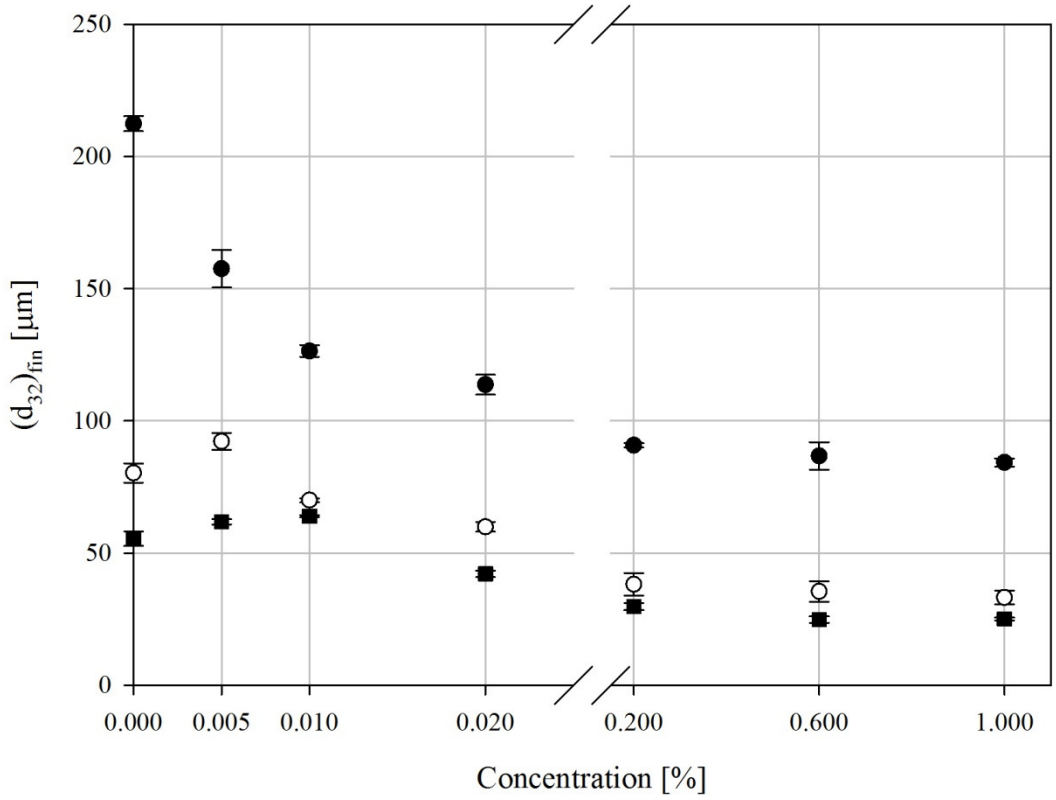

Figure B.5. Droplet sizes determined at the end of the first processing step of experiments in respect with concentrations of Brij 97 for varying impeller speeds of 800 rpm (●), 1600 rpm (○) and 2000 rpm (■).

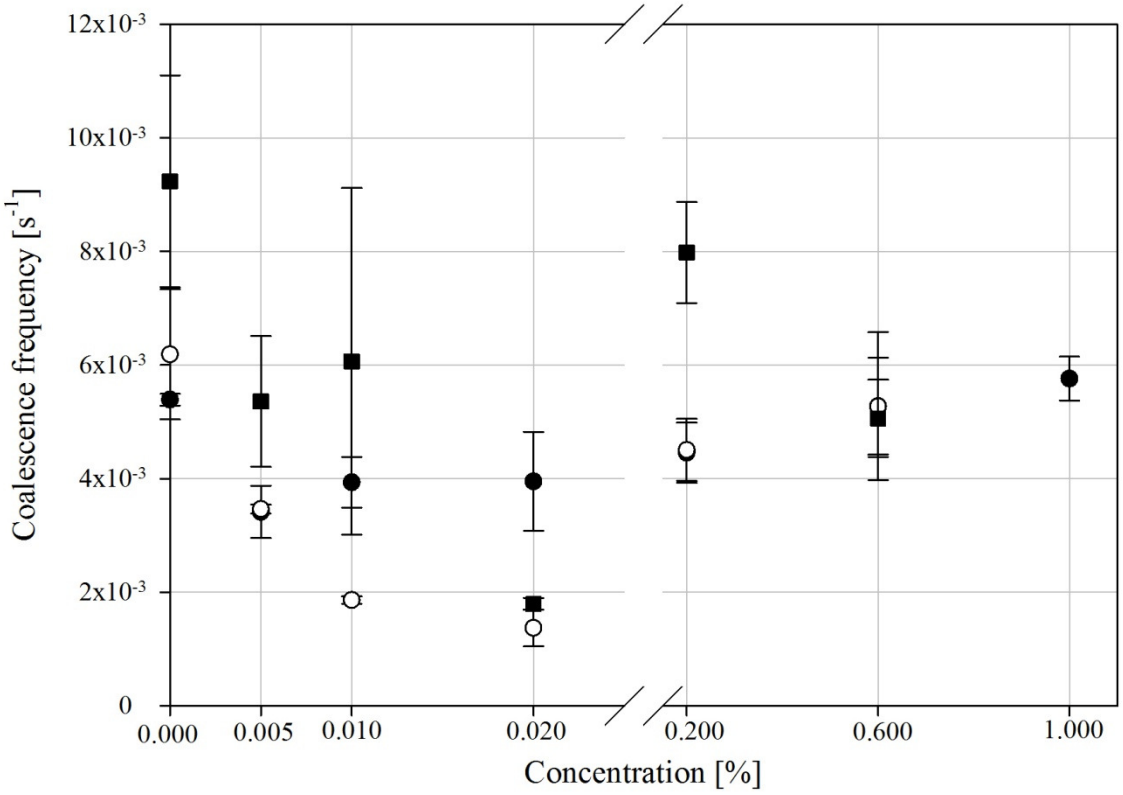

Figure B.6. Droplet coalescence frequencies calculated at the initial stages of the second processing step of experiments with respect to varying concentrations of Brij 97 for varying impeller speeds of 800-400 rpm (●), 1600-800 rpm (○) and 2000-1000 rpm (■).

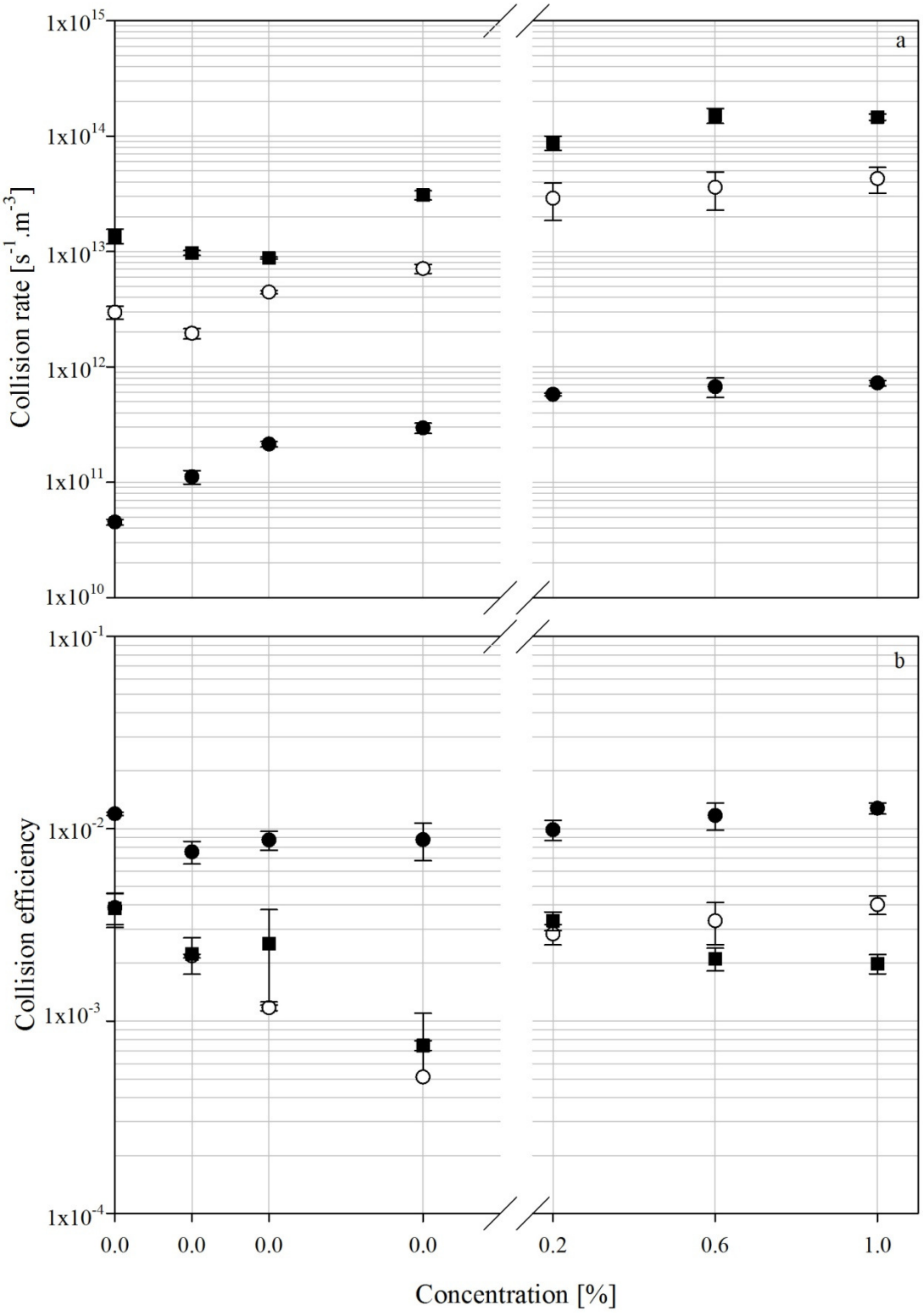

Figure B.7. Collision rates (a) and collision efficiencies (b) calculated at the initial stages of the second processing step of experiments with respect to varying concentrations of Brij 97 for varying impeller speeds of 800-400 rpm (●), 1600-800 rpm (○) and 2000-1000 rpm (■).

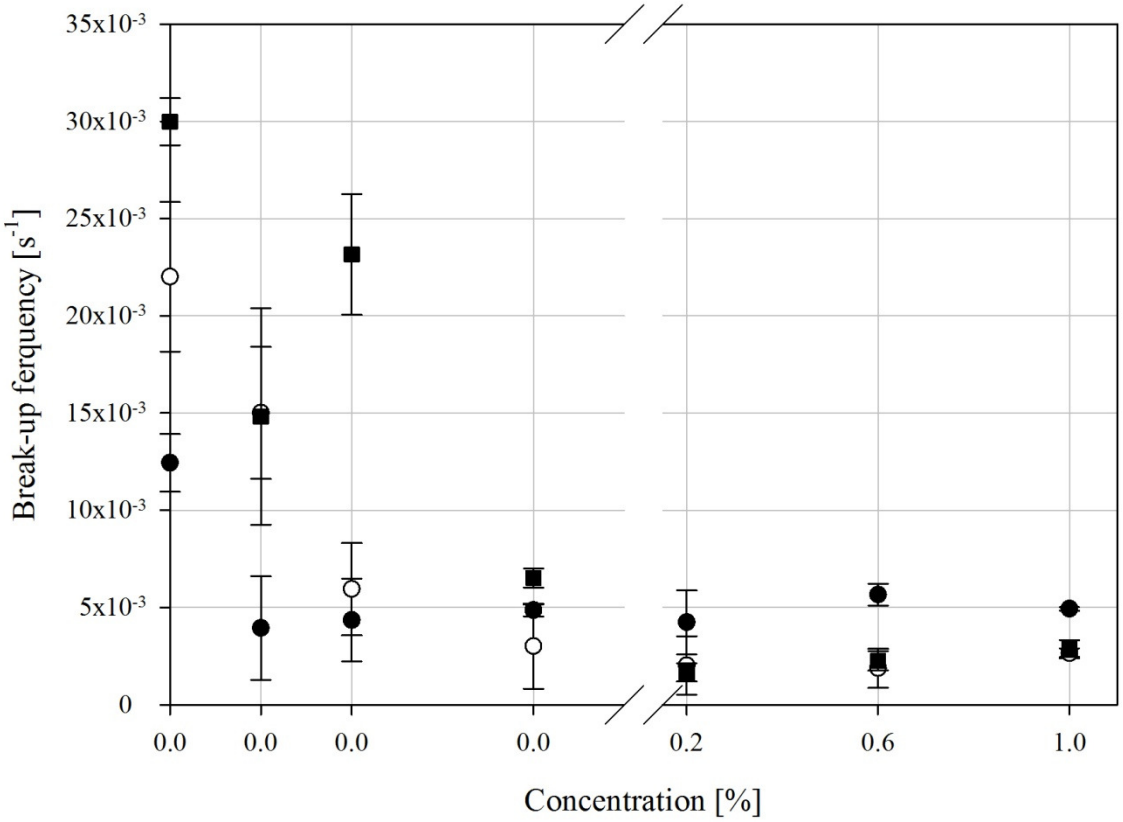

Figure B.8. Break-up frequencies calculated at the initial stages of the third processing step of experiments with respect to varying concentrations of Brij 97 at varying impeller speeds of 800-400-800 rpm (●), 1600-800-1600 rpm (○) and 2000-1000-2000 rpm (■).

Appendix C

Preliminary studies on modelling of the experimental data

In this Appendix the preliminary studies of mathematically modelling the experimentally obtained data, which are effectively the mean droplet diameter evolution, are presented. This section is divided into two sub-sections. Firstly, the empirical method has been used to model the data. Subsequently, mechanistic approach was carried out. After the model development in each of the approaches the drawbacks of each of them are summarised.

C.1 Empirical approach

The literature review of the models developed for estimation of the evolution of the mean droplet size is presented in Section 2.3.2.3. The model of Hong and Lee (Hong and Lee, 1983) was developed to estimate the time required to achieve the steady state droplet size. Validation of this model required estimation of the steady state droplet size, which is effectively the equilibrium droplet size obtained at long processing times (when processing time approaches infinity). Therefore, herein a different approach is considered. It can be assumed that:

$$d_{32_t} - d_{32_{(30)}} = C_1 Ln(t) \quad \text{(C.1)}$$

where d_{32_t} and $d_{32_{(30)}}$ are the emulsion's mean diameters at any given time, and at 30 *s* which is the initial droplet sizes of the experiments and C_1 is the adjustable parameter. In order to validate equation C.1, it is fitted with the experimental data of oil-in-water emulsification with 5% and 50% dispersed phase volume fractions under 1600 rpm impeller speed in the absence of added emulsifier and in the presence of 1% Tween 20 (Figure C.1). It can be seen that satisfactory fittings are determined (R^2>0.9 in all cases).

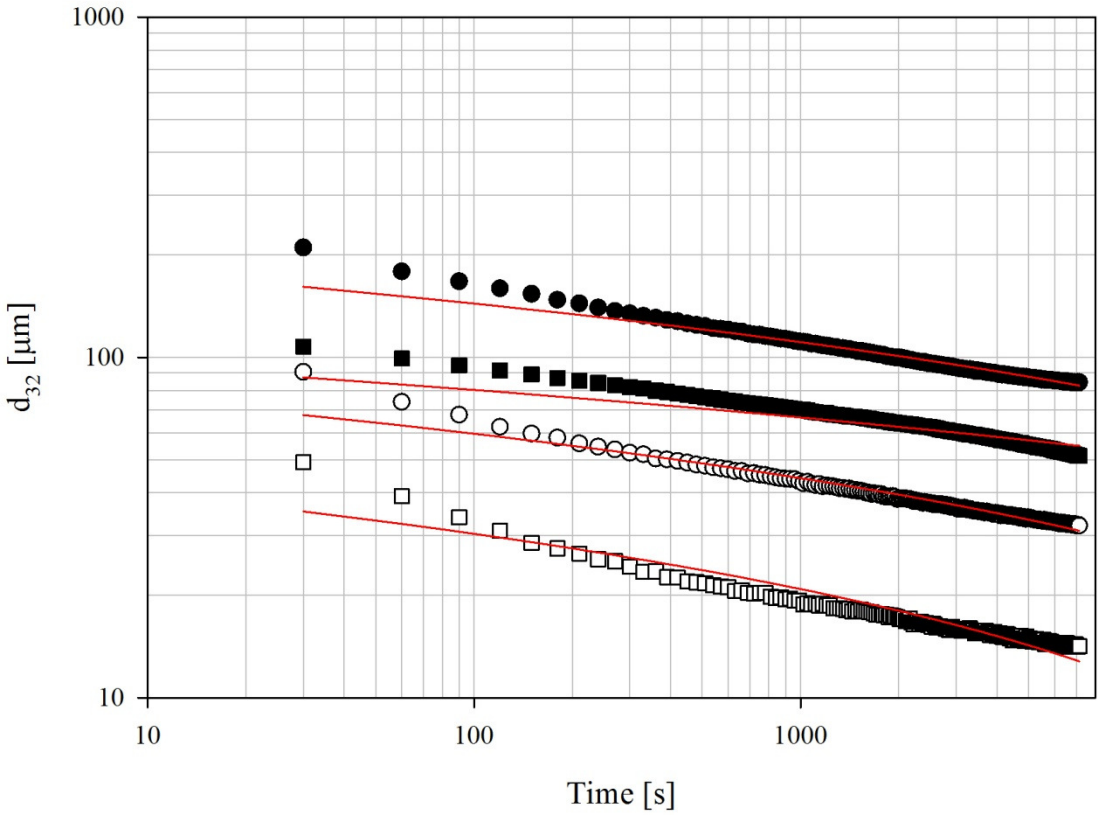

Figure C.1. Fitting of the equation C.1 to the experimental data obtained from the experiments of oil-in-water emulsification with 5% (■, □) and 50% (●, ○) dispersed phase volume fraction under 1600 rpm impeller speed in the absence of added emulsifiers (■, ●) and in the presence of 1% Tween 20 (□, ○) are shown with respect to time. The red lines are shown as the best fit to the data.

One of the benefits of model C.1 is the fact that only one adjustable parameter is used to fit the experimental data and the fact that the initial droplet size is used which is experimentally measureable.

Additionally, the initial droplet size can be written as a function of dispersed phase volume fraction and Tween 20 concentration. Figure C.2 shows the initial droplet sizes obtained from oil-in-water experiments under 1600 rpm in the absence of added emulsifier and in the presence of 1% Tween 20.

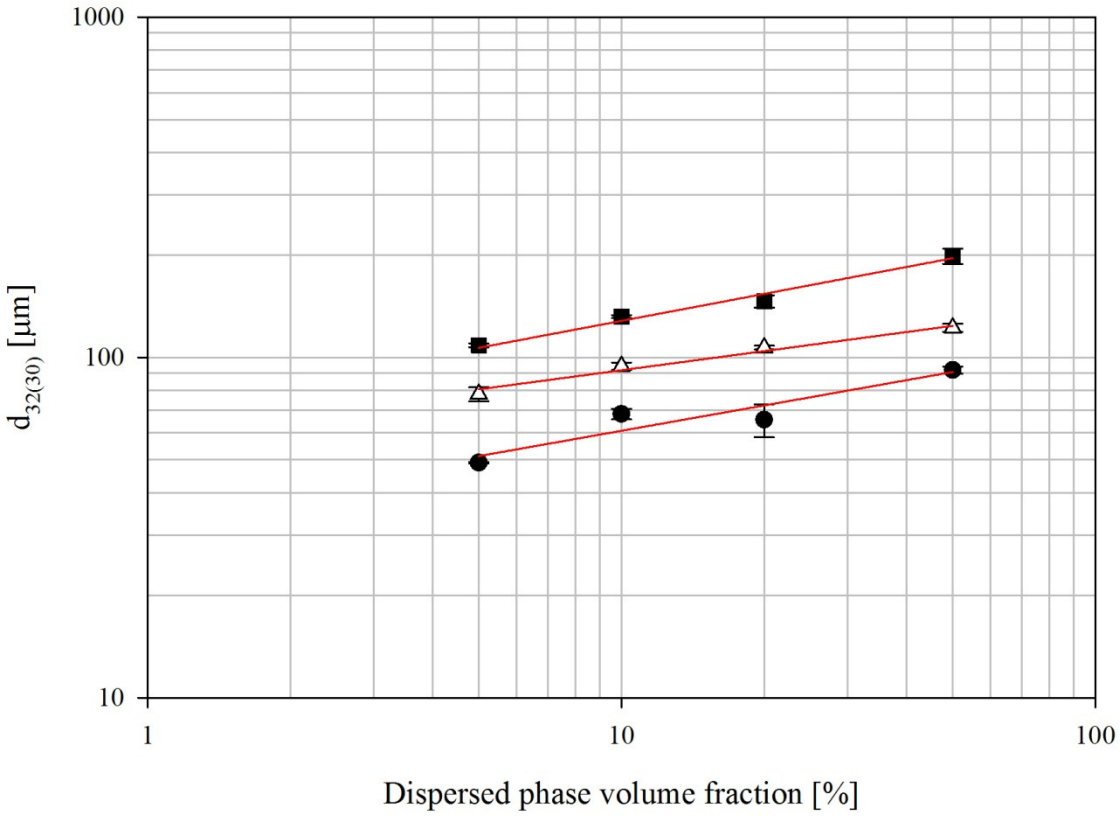

Figure C.2. The initial droplet sizes obtained from oil-in-water experiments under 1600 rpm in the absence of added emulsifier (●) and in the presence of 1% Tween 20 (○). The lines are shown as the best fit to equation A.3.2.

It can be seen that satisfactory fit can be obtained from the fitting of experimental data shown in Figure C.2 and equation C.2:

$$d_{32_{(30)}} = C_2 \varphi^{C_3} \tag{C.2}$$

where φ is the dispersed phase volume fraction. The dependency of initial droplet size on Tween 20 concentration is shown in Figure C.3.

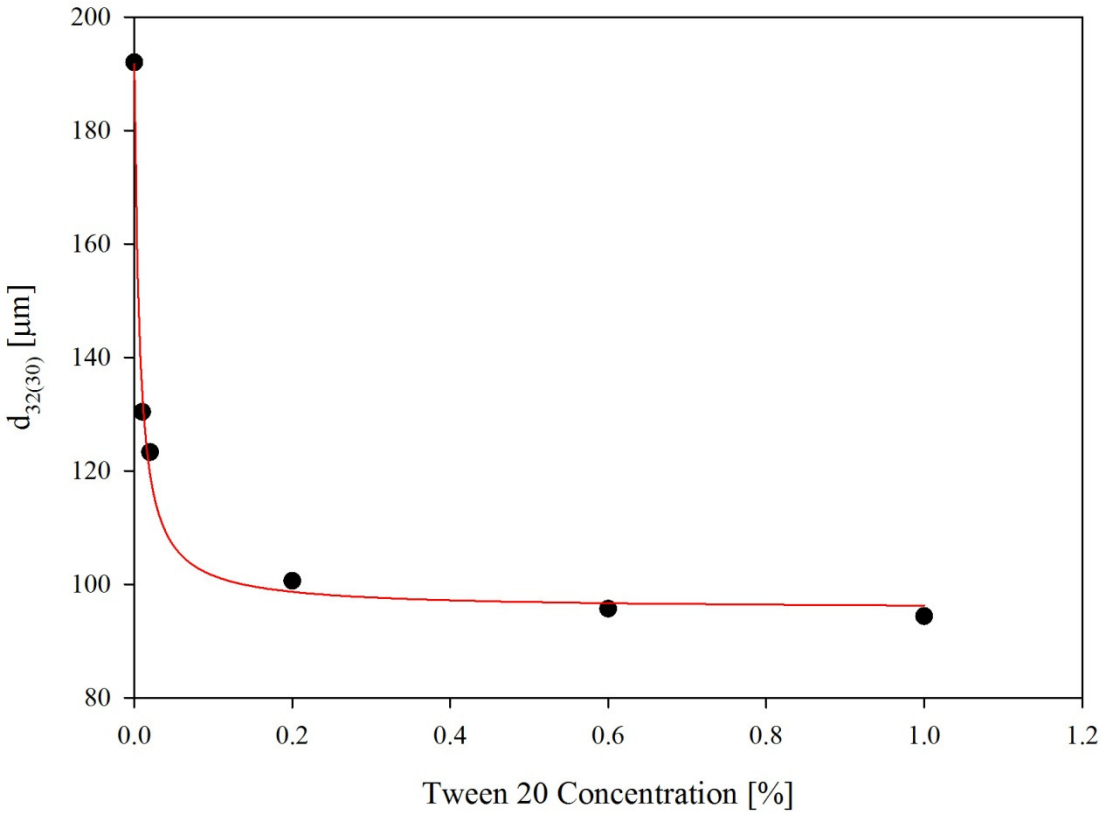

Figure C.3. The initial droplet sizes obtained from oil-in-water experiments under 1600 rpm with respect to Tween 20 concentration is shown. The line is shown as the best fit to equation C.3.

The line in Figure C.3 is determining by Fitting the experimental data to equation C.3:

$$d_{32_{(30)}} = \frac{d_{32_{(30)S=0}} + C_4 S_{Tween\ 20}}{1 + C_5 S_{Tween\ 20}} \tag{C.3}$$

where $d_{32(30)s=0}$ is the initial droplet size in the absence of added emulsifier and $S_{Tween\ 20}$ is the Tween 20 concentration. Equation C.3 is related to the adsorption kinetics of Tween 20 onto the interface of droplets. Conjunction of equations C.2 and C.3 result in the final form for initial droplet size with respect to dispersed phase volume fraction and Tween 20 concentration:

$$d_{32_{(30)}} = C_2 \varphi^{C_3} \left(\frac{d_{32_{(30)S=0}} + C_4 S_{Tween\ 20}}{1 + C_5 S_{Tween\ 20}}\right) \tag{C.4}$$

The general form of equation C.1 can be determined by substitution of equation C.4 into equation C.1:

$$d_{32_t} = C_1 Ln(t) + C_2 \varphi^{C_3}\left(\frac{d_{32(30)s=0} + C_4 S_{Tween\,20}}{1 + C_5 S_{Tween\,20}}\right) \quad \text{(C.5)}$$

Equation C.5 shows that by knowing the process conditions such as dispersed phase volume fraction and Tween 20 concentration the droplet size at any time can be estimated.

Although equation C.5 is useful in determining droplet size, its applicability is limited to the emulsification process in the mixing vessel used in this study. Nonetheless, equation C.5 does not provide any information regarding the mechanism of emulsification or droplet break-up and coalescence at different stages during process. Therefore, it is preferential that the mechanistic approach would be considered.

C.2 Mechanistic approach

This section is focused on the development of a model based on the mechanisms of the phenomena involved in the emulsification. The model development and the benefit and drawbacks are all summarised.

C.2.1 Model development

In order to be able to generate a model, firstly the mechanism of the phenomena involved in the emulsification should be explained. By analogy to reaction kinetics, the emulsification can be assumed to occur according to equation C.6. It is assumed that the droplet break-up and coalescence are forward and back reaction of change in the droplets volume, *v*. Consequently, the final droplet size of the process is determined when the rate of forward reaction (droplet break-up) equals to the back reaction (droplet coalescence). It should be noted that the droplet break-up phenomena is assumed to divide the droplets into two equally sized (same volume) droplets.

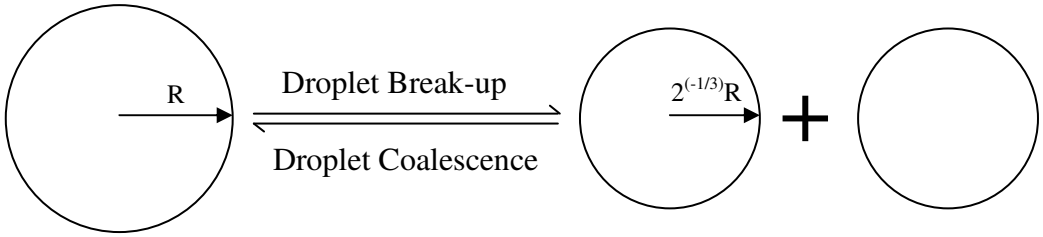

(C.6)

A rate of reaction can be defined for equation C.7 which leads to:

$$\frac{dn}{dt} = Bn - An^2 \qquad \text{(C.7)}$$

where n is the number concentration of droplets, B and A are droplet break-up and coalescence rate constants. Numbers of mechanistic models were developed for droplet break-up and coalescence rate constants which are reviewed in Section 2.3. For droplet break-up rate constant the model based on the eddy-droplet collision developed by Tsouris and Tavlarides (1994) is employed. It should be noted that since the viscosity of the dispersed phase (rapeseed oil) is markedly higher than the continuous phase (water), the model is modified to take account the viscous dissipation inside the droplets as described by Vankova *et al.* (2007b).

The coalescence, as described in Chapter 2, can be defined as a product of collision rate and collision efficiency. Collision rate model is given in section 2.3 and it is employed in this section without any modification. In case of droplet collision efficiency however, although it was shown in Section 2.3 that various models result in contradicting conclusions, the model by Coulaloglou and Tavlarides (1977) developed for deformable droplets with immobile interfaces was used. This model is based on the viscous thinning of the entrapped continuous phase between colliding droplets. The liquid is drained by Laminar flow having a parabolic velocity profile. The drainage continues until a critical thickness is reached which then droplets coalesce. Coulaloglou and Tavlarides (1977) assumed that the initial and critical film thicknesses are constant values, hence simplifying the expression. The reason that this model was selected is that it was decided to first examine the simple models and then employ

more complex models, therefore Coulaloglou and Tavlarides (1977) expression, one of the most acknowledged models was used (Liao and Lucas, 2010).

In order to employ these models the following assumptions have been considered. It has been assumed that the emulsion contained mono-sized droplets at each stage during emulsification with diameter of d_{32}. The average energy dissipation, $\bar{\varepsilon}$, of the mixing tank has been considered as the energy dissipation value. The number concentration, n, is calculated according to:

$$n = \frac{6\varphi}{d_{32}} \tag{C.8}$$

where φ is the dispersed phase volume fraction. Equation C.8 results to:

$$\frac{dn}{dt} = \left(\frac{-18\varphi}{\pi {d_{32}}^4}\right)\frac{d(d_{32})}{dt} \tag{C.9}$$

By incorporation equation C.8 and the droplet break-up and coalescence models in equation C.7, the expression for evolution of droplet diameter is determined by:

$$\frac{d(d_{32})}{dt} =$$

$$-C_6 {d_{32}}^{1/3}\bar{\varepsilon}^{1/3}\exp\left[-C_7\left(\frac{\sigma^{3/5}{\rho_c}^{-3/5}\bar{\varepsilon}^{-2/5}}{d_{32}}\right)^{5/3}\left(1+C_8\frac{\mu_d\bar{\varepsilon}^{1/3}{d_{32}}^{1/3}}{\sigma}\right)\right]+$$

$$C\ \ \frac{\varphi}{\pi}{d_{32}}^{1/3}\bar{\varepsilon}^{1/3}exp\left[-C_{10}\frac{\mu_c\rho_{c\bar{\varepsilon}}}{\sigma}{d_{32}}^4\right]$$

(C.10)

where σ is the interfacial tension between dispersed and continuous phase, ρ_c is the density of the continuous phase, μ_c and μ_d are the viscosities of continuous and dispersed phases, respectively, and C_6-C_{10} are adjustable parameters. The first term at the right hand side is related to droplet break-up phenomenon and the second term on the right hand side is related to the droplet coalescence phenomenaon. It can be seen that the both terms on the right hand side have similar term, ${d_{32}}^{1/3}\bar{\varepsilon}^{1/3}$, which is resulted from the similar methodology used in

calculating the collision rate between eddy-droplet and droplet-droplet in droplet break-up and coalescence rates. C_6 and C_9 are related to the velocity of eddies/droplets in the inertial sub-range of turbulent regime, C_7 is related to the effect of inertial stresses on the droplet, C_8 is for viscous dissipation inside the droplets opposing the droplet break-up and C_{10} is related to the film drainage between two droplets.

C.2.2 Model validation

In order to examine the developed model, the expression given in equation C.10 is fitted to the experimentally obtained data. An experimental case of emulsification of oil-in-water emulsion with 5% dispersed phase volume fraction under impeller speed of 1600 rpm in the absence of added emulsifier is considered. This particular experiment is selected since although 5% dispersed phase volume fraction has minimal effects on the dampening of the energy dissipation, however it was demonstrated that droplet coalescence is significant during processing. The absence of added emulsifier results in the constant interfacial tension between oil and water phases, otherwise, in presence of emulsifier, dynamic interfacial tension should be considered which adds an additional adjustable parameter to the equation C.10. The physical conditions of this process are either calculated or determined experimentally and they are summarised in table C.1.

Table C.1. Physical conditions of experiment used for model validation are shown.

parameter	value
Dispersed phase volume fraction, φ	0.05
Average energy dissipation, $\bar{\varepsilon}$	0.62 $W.kg^{-1}$
Interfacial tension, σ	0.02 N
Density of the continuous phase, ρ_c	1000 $kg.m^{-3}$
Viscosity of the continuous phase, μ_c	0.001 Pa.s
Viscosity of the dispersed phase, μ_d	0.07 Pa.s

The experimental data are obtained in the form of mean diameter, d_{32}, with respect to time, t. In order to fit the data the $d(d_{32})/dt$ is determined numerically and presented in Figure

C.4 with respect to d_{32}. By accounting these parameters equation C.10 was fitted to the data and the adjustable parameters C_1-C_5 were determined.

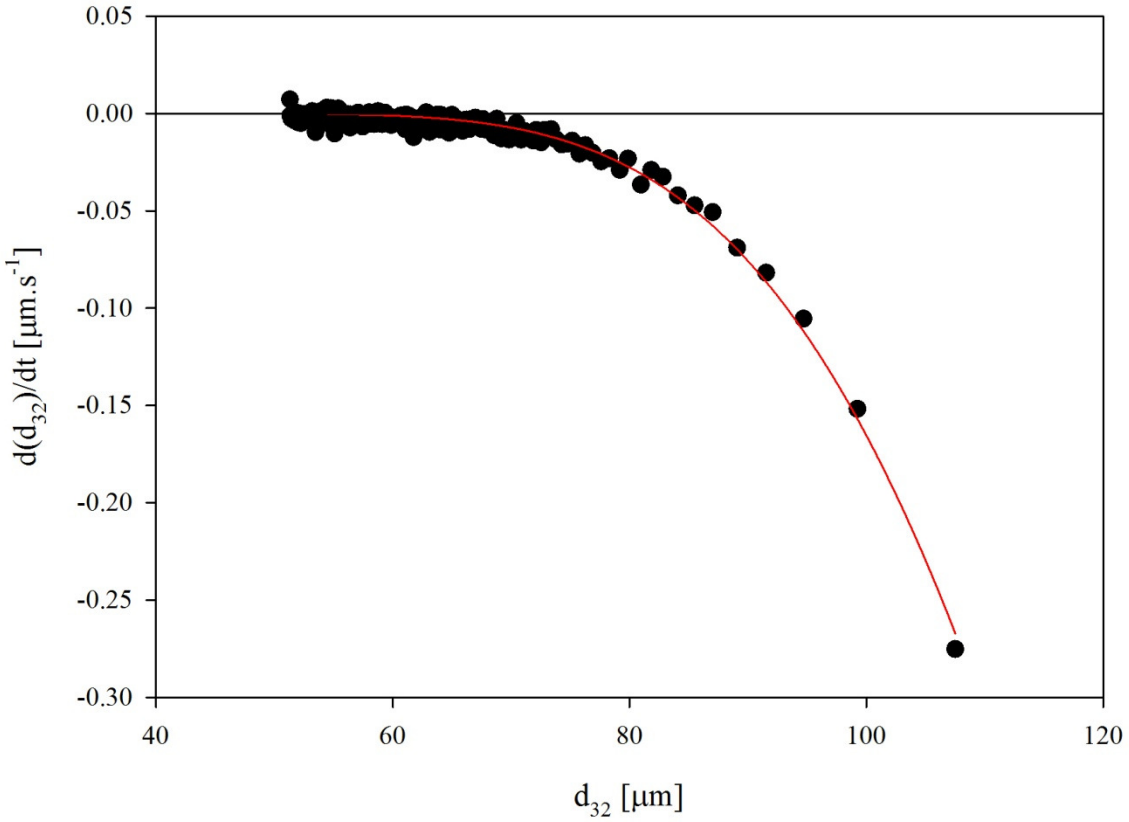

Figure C.4. Graph of $d(d_{32})/dt$ with respect to d_{32} for oil-in-water emulsion with 5% dispersed phase volume fraction in the absence of added emulsifier. The red line is determined by fitting equation C.10 to the experimental data.

As can be seen in Figure C.4, equation C.10 can be fitted to the experimental data (R^2=0.98) and adjustable parameters C_6, C_7 and C_8 were calculated to be 17.74, 1,780,000 and 15.97, respectively. The fitting was shown to not depend on the C_9 and C_{10}. The analysis of the effect of C_9 and C_{10} on the equation C.10 is given below.

Although equation C.10 is shown to be fitted with the experimental data, it has not been used for modelling the experimental data. The reasons are summarised below.

- It can be seen that adjustable parameters of C_9 and C_{10} are not affecting the goodness of the fit of equation C.10 to experimental data. In order to further analyse their effect,

sensitivity analysis was carried out on these parameters. The sensitivity analysis was carried out by assuming similar C_6, C_7 and C_8 as the ones determined by the best fit of equation C.10 to experimental data. Subsequently, two arrays of random values were generated for C_9 and C_{10}. All the possible combinations of these groups were used to calculate $d(d_{32})/dt$ for two cases of high (100 μm) and low (40 μm) mean droplet diameters, selected from the initial and final stages of the experimentally obtained data. The results are shown in Figure C.5.

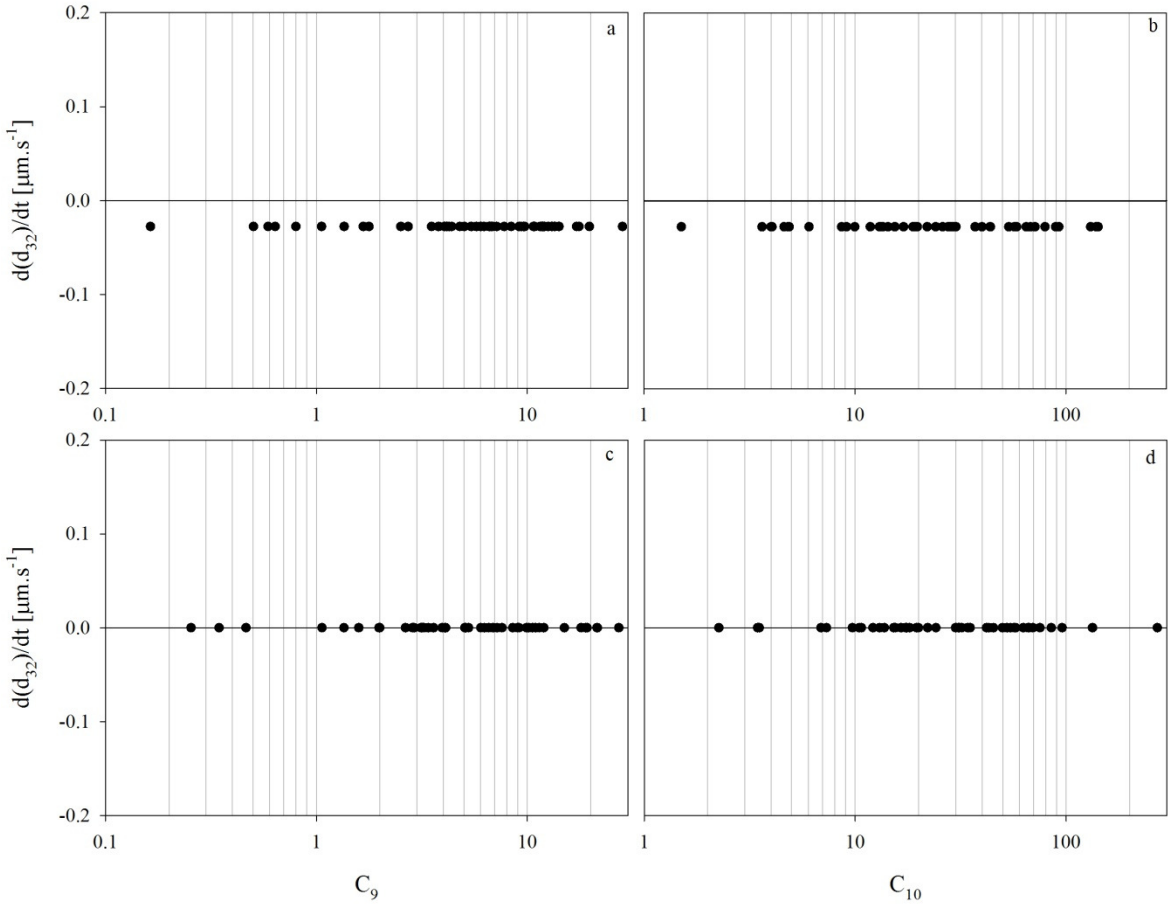

Figure C.5. Sensitivity analysis carried out to determine the effect of C_9 and C_{10} on the equation A.3.10. the combination of two groups of random numbers, generated for C_9 (a and c) and C_{10} (b and d), were employed to calculate $d(d_{32})/dt$ for two droplet sizes of 100 µm (a and b) and 40 µm (c and d).

It can be seen in Figure C.5 that although the values were generated over three orders of magnitudes for C_9 and C_{10}, there is no change in calculated $d(d_{32})/dt$, meaning that they do not influence equation C.10. Since C_9 and C_{10} are both related to the second term in right hand

side of equation C.10, they demonstrate the effect of droplet coalescence on the change in mean droplet diameter. The fact that they do not affect the fitting of equation C.10 suggests that it does not demonstrate the effect of droplet coalescence on determination of the droplet diameter, although it was shown experimentally that the droplet coalescence is not suppressed in this experiment and it is indeed affecting the final droplet size (Chapter 6). In order to include the effect of droplet coalescence in the model, the droplet size evolution data can be divided into the rapid decrease (rapid increase in Figure C.4) and plateau region, and fit two different models to each section. A model based on only droplet break-up can be used for rapid decrease region, and the model demonstrated in equation C.10 can be employed for the plateau region. This method however brings forward the complexity of selecting the threshold for these two regions.

- Equation C.10 was generated with five adjustable parameters. The high number of adjustable parameters, although all of them have a physical meaning, decreases the accuracy of the model.
- In generating equation C.10, the basic model demonstrated in equation C.6 is employed. The rate of reaction for droplet break-up and coalescence have been assumed to obey the 1^{st} and 2^{nd} order reaction kinetics, respectively. Although these assumption are valid when each of these phenomena are occurring individually, when droplet break-up and coalescence occur simultaneously their order of reaction may differ, as contribution of each on the other is not known thoroughly (Walstra, 1993).

All the reasons outlined above suggest that the model developed for mean droplet diameter (equation C.10), although it can be indeed fitted with the experimental data, cannot be used for predicting the droplet evolution data.

References

- Alban, F.B., Sajjadi, S., and Yianneskis, M. 2004. Dynamic tracking of fast liquid-liquid dispersion processes with a real-time in-situ optical technique *Chemical Engineering Research and Design*, 82, (A8) 1054-1060

- Alopaeus, V., Koskinen, J., and Keskinen, K.I. 1999. Simulation of the population balances for liquid-liquid systems in a nonideal stirred tank. Part 1 Description and qualitative validation of the model. *Chemical Engineering Science*, 54, (24) 5887-5899

- Alopaeus, V., Koskinen, J., Keskinen, I., and Majander, J. 2002. Simulation of the population balances for liquid-liquid systems in a nonideal stirred tank. Part 2--parameter fitting and the use of the multiblock model for dense dispersions. *Chemical Engineering Science*, 57, (10) 1815-1825

- Apenten, R.K.O. and Zhu, Q.H. 1996. Interfacial parameters for selected Spans and Tweens at the hydrocarbon-water interface. *Food Hydrocolloids*, 10, (1) 27-30

- Arai, K., N. Konno, Y. Matunaga, and S. Saito (1977). The effect of dispersed phase viscosity on the maximum stable drop size for breakup in turbulent flow, *Journal of Chemical Engineering of Japan.*, 10, 325–330.

- Aveyard, R., Binks, B.P., and Clint, J.H. 2003. Emulsions stabilised solely by colloidal particles. *Advances in Colloid and Interface Science*, 100-102, 503-546

- Bae, J.H. and Tavlarides, L.L. 1989. Laser capillary spectrophotometry for drop-size concentration measurements. *Aiche Journal*, 35, (7) 1073-1084

- Binks, B.P. 2002. Particles as surfactants--similarities and differences. *Current Opinion in Colloid and Interface Science*, 7, (1-2) 21-41

- Binks, B.P. and Kirkland, M. 2002. Interfacial structure of solid-stabilised emulsions studied by scanning electron microscopy. *Physical Chemistry Chemical Physics*, 4, (15) 3727-3733

- Binks, B.P. and Lumsdon, S.O. 2000a. Effects of oil type and aqueous phase composition on oil-water mixtures containing particles of intermediate hydrophobicity. *Physical Chemistry Chemical Physics*, 2, (13) 2959-2967

- Binks, B.P. and Lumsdon, S.O. 2000b. Influence of particle wettability on the type and stability of surfactant-free emulsions. *Langmuir*, 16, (23) 8622-8631

- Binks, B.P. and Rodrigues, J.A. 2007. Enhanced Stabilization of Emulsions Due to Surfactant-Induced Nanoparticle Flocculation. *Langmuir*, 23, (14) 7436-7439

- Boscher, V., Helleboid, R., Lasuye, T., Stasik, B., and Riess, G.+. 2009. On-line acoustic attenuation spectroscopy of emulsions stabilized by vinyl alcoholΓÇôvinyl acetate copolymers: a model system for the suspension polymerization of vinyl chloride. *Polymer International*, 58, (10) 1209-1216

- Britten M. and Groux H.J. 1990. Emulsifying Properties of Whey Protein and Casein Composite Blends. Food Research and Development Centre Contribution

- Calabrese, R.V., Chang, T.P.K., & Dang, P.T. 1986a. Drop Breakup in Turbulent Stirred-Tank Contactors .1. Effect of Dispersed-Phase Viscosity. *AIchE Journal*, 32, (4) 657-666

- Calabrese, R.V., Wang, C.Y., & Bryner, N.P. 1986b. Drop Breakup in Turbulent Stirred-Tank Contactors .3. Correlations for Mean Size and Drop Size Distribution. *AIchE Journal*, 32, (4) 677-681

- Chanamai, R., Coupland, J.N., and McClements, D.J. 1998. Effect of temperature on the ultrasonic properties of oil-in-water emulsions. *Colloids and Surfaces A: Physicochemical and Engineering Aspects*, 139, (2) 241-250

- Chanamai, R., Horn, G., and McClements, D.J. 2002. Influence of Oil Polarity on Droplet Growth in Oil-in-Water Emulsions Stabilized by a Weakly Adsorbing Biopolymer or a Nonionic Surfactant. *Journal of Colloid and Interface Science*, 247, (1) 167-176

- Chantrapornchai, W., Clydesdale, F., and McClements, D.J. 1998. Influence of droplet size and concentration on the color of oil-in-water emulsions. *Journal of Agricultural and Food Chemistry*, 46, (8) 2914-2920

- Chantrapornchai, W., Clydesdale, F., and McClements, D.J. 1999. Influence of droplet characteristics on the optical properties of colored oil-in-water emulsions. *Colloids and Surfaces A-Physicochemical and Engineering Aspects*, 155, (2-3) 373-382

- Chantrapornchai, W., Clydesdale, F.M., and McClements, D.J. 2001a. Influence of Flocculation on Optical Properties of Emulsions. *Journal of Food Science*, 66, (3) 464-469

- Chantrapornchai, W., Clydesdale, F.M., and McClements, D.J. 2001b. Influence of relative refractive index on optical properties of emulsions. *Food Research International*, 34, (9) 827-835

- Chatzi, E. and Lee, J.M. 1987. Analysis of Interactions for Liquid Liquid Dispersions in Agitated Vessels. *Industrial and Engineering Chemistry Research*, 26, (11) 2263-2267

- Chatzi, E.G. and Kiparssides, C. 1995. Steady-state drop-size distributions in high holup fraction dispersion systems. *Aiche Journal*, 41, (7) 1640-1652

- Chatzi, E.G., Boutris, C.J., and Kiparissides, C. 1991. Online Monitoring of Drop Size Distributions in Agitated Vessels .1. Effects of Temperature and Impeller Speed. *Industrial and Engineering Chemistry Research*, 30, (3) 536-543

- Chesters, A.K. 1991. The Modeling of Coalescence Processes in Fluid Liquid Dispersions - A Review of Current Understanding. *Chemical Engineering Research and Design*, 69, (4) 259-270

- Chung, K.H.K., Barigou, M., and Simmons, M.J.H. 2007. Reconstruction of 3-D Flow Field Inside Miniature Stirred Vessels Using a 2-D PIV Technique. *Chemical Engineering Research and Design*, 85, (5) 560-567

- Chung, K.H.K., Simmons, M.J.H., and Barigou, M. 2008. Angle-Resolved Particle Image Velocimetry Measurements of Flow and Turbulence Fields in Small-Scale Stirred Vessels of Different Mixer Configurations. *Industrial and Engineering Chemistry Research*, 48, (2) 1008-1018

- Coulaloglou, C.A. and Tavlarides, L.L. 1977. Description of Interaction Processes in Agitated Liquid-Liquid Dispersions. *Chemical Engineering Science*, 32, (11) 1289-1297

- Danner, T. (2001). Tropfenkoaleszenz in Emulsionen. PhD Thesis, Universitat Karlsruhe (TH)
- Das, K.P. and Kinsella, J.E. 1993. Droplet Size and Coalescence Stability of Whey-Protein Stabilized Milkfat Peanut Oil-Emulsions. *Journal of Food Science*, 58, (2) 439-444
- Delsa Nano series. The solution for all your nano prticle sizing and zeta potential needs. 2010. Beckman Coulter. Ref type: catalog
- Desnoyer, C., Masbernat, O., & Gourdon, C. 2003. Experimental study of drop size distributions at high phase ratio in liquid-liquid dispersions. *Chemical Engineering Science*, 58, (7) 1353-1363
- Dickinson, E. 1994. Colloidal aspects of beverages. *Food Chemistry*, 51, (4) 343-347
- Dickinson, E. 1997. Properties of emulsions stabilized with milk proteins: Overview of some recent developments. *Journal of Dairy Science*, 80, (10) 2607-2619
- Dickinson, E. 1998, Rheology of emulsions-the relation to structure and stability, In: B. P. Binks, ed., *Modern aspects of emulsions.* Cambridge: The Royal Society of Chemistry.
- Dickinson, E. 2001. Milk protein interfacial layers and the relationship to emulsion stability and rheology. *Colloids and Surfaces B: Biointerfaces*, 20, (3) 197-210
- Dickinson, E. and Gelin, J.L. 1992. Influence of Emulsifier on Competitive Adsorption of Alpha-S-Casein Plus Beta-Lactoglobulin in Oil-In-Water Emulsions. *Colloids and Surfaces*, 63, (3-4) 329-335
- Dickinson, E. and Golding, M. 1997. Rheology of Sodium Caseinate Stabilized Oil-in-Water Emulsions. *Journal of Colloid and Interface Science*, 191, (1) 166-176
- Dickinson, E. and McClements, D.J., 1995. *Advances in Food Colloids,* Chapman and Hall, London.
- Dickinson, E., 1992. *Introduction to Food Colloids,* Oxford University Press, Oxford,.

- Dickinson, E., Murray, B.S., and Stainsby, G. 1985. Time-dependent surface viscosity of adsorbed films of casein + gelatin at the oil-water interface. *Journal of Colloid and Interface Science*, 106, (1) 259-262

- Dickinson, E., Pogson, D.J., Robson, E.W., and Stainsby, G. 1985. Time-dependent surface pressures of adsorbed films of caseinate + gelatin at the oil--water interface. *Colloids and Surfaces*, 14, (1) 135-141

- Djakovic, L., Dokic, P., Radivojevic, P., Sefer, I., and Sovilj, V. 1987. Action of Emulsifiers During Homogenization of O/W Emulsions. *Colloid and Polymer Science*, 265, (11) 993-1000

- Doulah, M.S. 1975. Effect of Hold-Up on Drop Sizes in Liquid-Liquid Dispersions. *Industrial and Engineering Chemistry Fundamentals*, 14, (2) 137-138

- Dukhin, A. and Goetz, P. 2005. Evolution of water-in-oil emulsion controlled by droplet-bulk ion exchange: acoustic, electroacoustic, conductivity and image analysis. *Colloids and Surfaces A: Physicochemical and Engineering Aspects*, 253, (1-3) 51-64

- Euston, R., Hirst, L., and Hill, P. 1999. The emulsifying properties of [beta]-lactoglobulin genetic variants A, B and C. *Colloids and Surfaces B: Biointerfaces*, 12, (3-6) 193-202

- Everett, D.H., 1988. *Basic Principles of Colloid Science,* Royal Society of Chemistry, Cambridge.

- Fainerman, V.B., Miller, R., and Joos, P. 1994. The Measurement of Dynamic Surface-Tension by the Maximum Bubble Pressure Method. *Colloid and Polymer Science*, 272, (6) 731-739

- Galindo, E., Larralde-Corona, C.P., Brito, T., C≤rdova-Aguilar, M., Taboada, B., Vega-Alvarado, L., and Corkidi, G. 2005. Development of advanced image analysis techniques for the in situ characterization of multiphase dispersions occurring in bioreactors. *Journal of Biotechnology*, 116, (3) 261-270

- Ghouchi Eskandar, N., Simovic, S., and Prestidge, C.A. 2007. Synergistic effect of silica nanoparticles and charged surfactants in the formation and stability of submicron oil-in-water emulsions. *Physical Chemistry Chemical Physics*, 9, (48) 6426-6434

- Golemanov, K., Tcholakova, S., Kralchevsky, P.A., Ananthapadmanabhan, K.P., and Lips, A. 2006. Latex-Particle-Stabilized Emulsions of Anti-Bancroft Type. *Langmuir*, 22, (11) 4968-4977

- Graham, D.E. and Phillips, M.C. 1979. Proteins at Liquid Interfaces .1. Kinetics of Adsorption and Surface Denaturation. *Journal of Colloid and Interface Science*, 70, (3) 403-414

- Grigoriev, D.O. and Miller, R. 2009. Mono- and multilayer covered drops as carriers. *Current Opinion in Colloid and Interface Science*, 14, (1) 48-59

- Hall, J.F., Barigou, M., Simmons, M.J.H., and Stitt, E.H. 2005a. Comparative study of different mixing strategies in small high throughput experimentation reactors. *Chemical Engineering Science*, 60, (8-9) 2355-2368

- Hall, J.F., Barigou, M., Simmons, M.J.H., and Stitt, E.H. 2005b. Just Because It's Small Doesn't Mean It's Well Mixed: Ensuring Good Mixing in Mesoscale Reactors. *Industrial and Engineering Chemistry Research*, 44, (25) 9695-9704

- Harnby, N., Edwards, M.F. and Nienow, A.W. Eds. 1985, *Mixing in the Process Industry*, Oxford: Butterworth and Co. Ltd.

- Henry, J.V.L., Fryer, P.J., Frith, W.J., and Norton, I.T. 2009. Emulsification mechanism and storage instabilities of hydrocarbon-in-water sub-micron emulsions stabilised with Tweens (20 and 80), Brij 96v and sucrose monoesters. *Journal of Colloid and Interface Science*, 338, (1) 201-206

- Hocq, S., Milot, J.F., Gourdon, C., and Casamatta, G. 1994. Electrical conductivity capillary technique: a new method for bivariate drop-size--concentration distribution measurements. *Chemical Engineering Science*, 49, (4) 481-489

- Hollingsworth, K.G., Sederman, A.J., Buckley, C., Gladden, L.F., and Johns, M.L. 2004. Fast emulsion droplet sizing using NMR self-diffusion measurements. *Journal of Colloid and Interface Science*, 274, (1) 244-250

- Hollingsworth, P., Food research: Cooperation is the key, *Food Technology,* 49(2), 67, 1995.

- Holt, C., 1992. *Advances in Protein Chemistry volume 43,* San Diego: Academic Press.
- Hong, P.O. and Lee, J.M. 1983. Unsteady-State Liquid Liquid Dispersions in Agitated Vessels. *Industrial and Engineering Chemistry Process Design and Development*, 22, (1) 130-135
- Howarth, W.J. 1964. Coalescence of Drops in A Turbulent Flow Field. *Chemical Engineering Science*, 19, (1) 33-38
- Hsu, C.T., Chang, C.H., and Lin, S.Y. 1997. Comments on the adsorption isotherm and determination of adsorption kinetics. *Langmuir*, 13, (23) 6204-6210
- Hsu, C.T., Chang, C.H., and Lin, S.Y. 2000. Study on Surfactant Adsorption Kinetics: Effects of Interfacial Curvature and Molecular Interaction. *Langmuir*, 16, (3) 1211-1215
- Hu, B., Angeli, P., Matar, O.K., Lawrence, C.J., and Hewitt, G.F. 2006. Evaluation of drop size distribution from chord length measurements. *AIchE Journal*, 52, (3) 931-939
- Hu, B., Nienow, A.W., and Pacek, A.W. 2003. The effect of sodium caseinate concentration and processing conditions on bubble sizes and their break-up and coalescence in turbulent, batch air/aqueous dispersions at atmospheric and elevated pressures. *Colloids and Surfaces B: Biointerfaces*, 31, (1-4) 3-11
- Hunter, R.J., 1986. *Foundations of Colloid Science,* Vol. 1, Oxford: Oxford University Press.
- Hunter, T.N., Pugh, R.J., Franks, G.V., and Jameson, G.J. 2008. The role of particles in stabilising foams and emulsions. *Advances in Colloid and Interface Science*, 137, (2) 57-81
- Israelachvili, J. 1994. The Science and Applications of Emulsions - An Overview. *Colloids and Surfaces A-Physicochemical and Engineering Aspects*, 91, 1-8
- Israelachvili, J., 1997. *Intermolecular and surface forces*, Second edition, London: Academic press limited.
- Ivanov, I. B. 1988, *Thin liquid films: fundamentals and applications*, New York: M. Decker

- Jafari, S.M., Assadpoor, E., He, Y., and Bhandari, B. 2008. Re-coalescence of emulsion droplets during high-energy emulsification. *Food Hydrocolloids*, 22, (7), 1191-1202

- Johansson, D., Bergenstahl, B., and Lundgren, E. 1995. Water-In-Triglyceride Oil-Emulsions - Effect of Fat Crystals on Stability. *Journal of the American Oil Chemists Society*, 72, (8) 939-950

- Koopal, L.K., Goloub, T., de Keizer, A., and Sidorova, M.P. 1999. The effect of cationic surfactants on wetting, colloid stability and flotation of silica. *Colloids and Surfaces A: Physicochemical and Engineering Aspects*, 151, (1-2) 15-25

- Kralchevsky, P. A., Danov, K. D., and Denkov, N. D. 2009, Chemical Physics of Colloid *In Handbook of surface and colloid chemistry*, Third ed. K. S. Birdi, ed., Boca Ratan: CRC Press.

- Kruss, 2011, *The plate method*, [Online] Available at: < http://www.kruss.de/en/theory/measurements/surface-tension/plate-method.html?PHPSESSID=0053da47327d68bccb353127ac7d74f0> [Accessed 1 october 2011]

- Krynke, K.K. and Sek, J.P. 2004. Predicting viscosity of emulsions in the broad range of inner phase concentrations. *Colloids and Surfaces A: Physicochemical and Engineering Aspects*, 245, (1-3) 81-92

- Kumar, S., Kumar, R., and Gandhi, K.S. 1991. Alternative mechanisms of drop breakage in stirred vessels. *Chemical Engineering Science*, 46, (10) 2483-2489

- Kumar, S., Kumar, R., and Gandhi, K.S. 1993. A new model for coalescence efficiency of drops in stirred dispersions. *Chemical Engineering Science*, 48, (11) 2025-2038

- Laats, M. K. and Frishman, F. A. Development of techniques and investigation of turbulence energy at the axis of a two-phase turbulent jet. *Fluid Dynamics* 8 (2), 304-307. 1973.

- Lagisetty, J.S., Das, P.K., Kumar, R., & Gandhi, K.S. 1986. Breakage of Viscous and Non-Newtonian Drops in Stirred Dispersions. *Chemical Engineering Science*, 41, (1) 65-72

- Lam, A., A. N. Sathyagal, S. Kumar, and D. Ramkrishna (1996). Maximum stable drop diameter in stirred dispersions, *AIChE J.*, **42**, 1547–1552.

- Lan, Q., Yang, F., Zhang, S., Liu, S., Xu, J., and Sun, D. 2007. Synergistic effect of silica nanoparticle and cetyltrimethyl ammonium bromide on the stabilization of O/W emulsions. *Colloids and Surfaces A: Physicochemical and Engineering Aspects*, 302, (1-3) 126-135

- Lasheras, J.C., Eastwood, C., Martinez-Bazan, C., and Montanes, J.L. 2002. A review of statistical models for the break-up of an immiscible fluid immersed into a fully developed turbulent flow. *International Journal of Multiphase Flow*, 28, (2) 247-278

- Leng, D. A. and Calabrese R.V. 2004, Immiscible liquid-liquid systems, In: E.L. Paul, V.A. Atiemo-obeng, and S.M. Kresta, Eds. *Handbook of industrial mixing, science and practice*, New Jersey: Wiley-interscience.

- Levich, V.G. 1962. *Physicochemical hydrodynamics* New Jersey: Prentice-Hall.

- Liao, Y. and Lucas, D. 2009. A literature review of theoretical models for drop and bubble breakup in turbulent dispersions. *Chemical Engineering Science*, 64, (15) 3389-3406

- Liao, Y. and Lucas, D. 2010. A literature review on mechanisms and models for the coalescence process of fluid particles. *Chemical Engineering Science*, 65, (10) 2851-2864

- Liu, S.P. and Li, D.M. 1999. Drop coalescence in turbulent dispersions. *Chemical Engineering Science*, 54, (23) 5667-5675

- Lobo, L. and Svereika, A. 2003. Coalescence during emulsification 2. Role of small molecule surfactants. *Journal of Colloid and Interface Science*, 261, (2) 498-507

- Lobo, L., Svereika, A., and Nair, M. 2002. Coalescence during emulsification - 1. Method development. *Journal of Colloid and Interface Science*, 253, (2) 409-418

- Maass, S., Grunig, J., and Kraume, M. 2009. Measurement Techniques for Drop Size Distributions in Stirred Liquid-Liquid Systems. *Chemical and Process Engineering-Inzynieria Chemiczna I Procesowa*, 30, (4) 635-651

- Malvern Instruments - Web Site Technical Support. (2011. *Refractive index of solutions*).
- Mastersizer 2000. Refractive index of materials. 2009. Malvern instruments. Ref Type: Catalog
- McClements, D.J. 2002a. Colloidal basis of emulsion color. *Current Opinion in Colloid and Interface Science*, 7, (5-6) 451-455
- McClements, D.J. 2002b. Theoretical prediction of emulsion color. *Advances in Colloid and Interface Science*, 97, (1-3) 61-87
- McClements, D.J. 2005. *Food Emulsion; Principles, Practices, and Techniques,* London: CRC press LLC.
- Midmore, B.R. 1998. Synergy between silica and polyoxyethylene surfactants in the formation of O/W emulsions. *Colloids and Surfaces A: Physicochemical and Engineering Aspects*, 145, (1-3) 133-143
- Mohan, S. and Narsimhan, G. 1997. Coalescence of protein-stabilized emulsions in a high-pressure homogenizer. *Journal of Colloid and Interface Science*, 192, (1) 1-15
- Morishita, C. and Kawaguchi, M. 2009. Rheological and interfacial properties of Pickering emulsions prepared by fumed silica suspensions pre-adsorbed poly(N-isopropylacrylamide). *Colloids and Surfaces A: Physicochemical and Engineering Aspects*, 335, (1-3) 138-143
- Muralidhar, R. and Ramkrishna, D. 1986. Analysis of Droplet Coalescence in Turbulent Liquid-Liquid Dispersions. *Industrial and Engineering Chemistry Fundamentals*, 25, (4) 554-560
- Muralidhar, R., Ramkrishna, D., Das, P.K., and Kumar, R. 1988. Coalescence of Rigid Droplets in A Stirred Dispersion .2. Band-Limited Force Fluctuations. *Chemical Engineering Science*, 43, (7) 1559-1568
- Murray, B.S., Durga, K., Yusoff, A., and Stoyanov, S.D. 2011. Stabilization of foams and emulsions by mixtures of surface active food-grade particles and proteins. *Food Hydrocolloids*, 25, (4) 627-638
- Myers, D., 1988. *Surfactant Science Technology,* Weinheim: VCH Publishers.

- Narsimhan, G. 2004. Model for drop coalescence in a locally isotropic turbulent flow field. *Journal of Colloid and Interface Science*, 272, (1) 197-209

- Narsimhan, G. and Goel, P. 2001. Drop coalescence during emulsion formation in a high-pressure homogenizer for tetradecane-in-water emulsion stabilized by sodium dodecyl sulfate. *Journal of Colloid and Interface Science*, 238, (2) 420-432

- Narsimhan, G., D. Ramkrishna, and J. P. Gupta (1980). Analysis of drop size distributions in lean liquid–liquid dispersions, *Aiche Journal*, 26, 991–1000.

- Narsimhan, G., Ramkrishna, D., and Gupta, J.P. 1980. Analysis of drop size distributions in lean liquid-liquid dispersions. *Aiche Journal*, 26, (6) 991-1000

- Nciri, H., Huang, N., Rosilio, V., Trabelsi-Ayadi, M., Benna-Zayani, M.., and Grossiord, J.L. 2010. Rheological studies in the bulk and at the interface of Pickering oil/water emulsions. *Rheologica Acta*, 49, (9) 961-969

- Niknafs, N., Spyropoulos, F., and Norton, I.T. 2011. Development of a new reflectance technique to investigate the mechanism of emulsification. *Journal of Food Engineering*, 104, (4) 603-611

- Norton I.T., Spyropoulos F., and Cox P.W. Effect of emulsifiers and fat crystals on shear induced droplet break-up, coalescence and phase inversion. 2008. *Food Hydrocolloids*, 23, (6) 1521-1526

- O'Rourke, A.M. and MacLoughlin, P.F. 2005. A comparison of measurement techniques used in the analysis of evolving liquid-liquid dispersions. *Chemical Engineering and Processing*, 44, (8) 885-894

- Pacek, A.W., Moore, I.P.T., Nienow, A.W., and Calabrese, R.V. 1994. Video Technique for Measuring Dynamics of Liquid-Liquid Dispersion During Phase Inversion. *Aiche Journal*, 40, (12) 1940-1949

- Petrak, D. 2002. Simultaneous Measurement of Particle Size and Particle Velocity by the Spatial Filtering Technique. *Particle and Particle Systems Characterization*, 19, (6) 391-400

- Pichot, R., Spyropoulos, F., and Norton, I.T. 2009. Mixed-emulsifier stabilised emulsions: Investigation of the effect of monoolein and hydrophilic silica particle mixtures on the stability against coalescence. *Journal of Colloid and Interface Science*, 329, (2) 284-291

- Pickering, S.U. 1907. Emulsions. *Journal of the Chemical Society*, 91, 2001-2021

- Prince, M.J. and Blanch, H.W. 1990. Bubble Coalescence and Break-Up in Air-Sparged Bubble-Columns. *AIchE Journal*, 36, (10) 1485-1499

- Richter, A., Voigt, T., and Ripperger, S. 2007. Ultrasonic attenuation spectroscopy of emulsions with droplet sizes greater than 10 um. *Journal of Colloid and Interface Science*, 315, (2) 482-492

- Rodney J.B., 1999, Milk coagulation and protein denaturation, In: R. Jenness, N.P. Wong, E.H. Marth, M. Keeney, eds, *Fundamentals of Dairy Chemistry*, third edition, Aspend publishers, Ch. 11.

- Ruiz, C.C., Molina-Bolivar, J.A., Aguiar, J., MacIsaac, G., Moroze, S., and Palepu, R. 2003. Effect of ethylene glycol on the thermodynamic and micellar properties of Tween 20. *Colloid and Polymer Science*, 281, (6) 531-541

- Sanchez, M.C., Berjano, M., Guerrero, A., and Gallegos, C. 2001. Emulsification rheokinetics of nonionic surfactant-stabilized oil-in-water emulsions. *Langmuir*, 17, (18) 5410-5416

- Simon, S., Theiler, S., Knudsen, A., Φye, G., and Sjoblom, J. 2010. Rheological Properties of Particle-Stabilized Emulsions. *Journal of Dispersion Science and Technology*, 31, (5) 632-640

- Sis, H. and Chander, S. 2004. Kinetics of emulsification of dodecane in the absence and presence of nonionic surfactants. *Colloids and Surfaces A: Physicochemical and Engineering Aspects*, 235, (1-3) 113-120

- Sis, H., Kelbaliyev, G., and Chander, S. 2005. Kinetics of Drop Breakage in Stirred Vessels under Turbulent Conditions. *Journal of Dispersion Science and Technology*, 26, (5) 565-573

- Tadayyon, A. and Rohani, S. 1998. Determination of Particle Size Distribution by Par-Tec® 100: Modeling and Experimental Results. *Particle and Particle Systems Characterization*, 15, (3) 127-135

- Taisne, L., Walstra, P., and Cabane, B. 1996. Transfer of oil between emulsion droplets. *Journal of Colloid and Interface Science*, 184, (2) 378-390

- Tcholakova, S., Denkov, N.D., and Danner, T. 2004. Role of surfactant type and concentration for the mean drop size during emulsification in turbulent flow. *Langmuir*, 20, (18) 7444-7458

- Tcholakova, S., Denkov, N.D., and Lips, A. 2008. Comparison of solid particles, globular proteins and surfactants as emulsifiers. *Physical Chemistry Chemical Physics*, 10, (12) 1608-1627

- Tcholakova, S., Denkov, N.D., Ivanov, I.B., and Campbell, B. 2006. Coalescence stability of emulsions containing globular milk proteins. *Advances in Colloid and Interface Science*, 123, 259-293

- Tcholakova, S., Denkov, N.D., Sidzhakova, D., Ivanov, I.B., and Campbell, B. 2003. Interrelation between drop size and protein adsorption at various emulsification conditions. *Langmuir*, 19, (14) 5640-5649

- Tcholakova, S., Vankova, N., Denkov, N.D., and Danner, T. 2007. Emulsification in turbulent flow: 3. Daughter drop-size distribution. *Journal of Colloid and Interface Science*, 310, (2) 570-589

- Tigges, B., Dederichs, T., Mo¦êller, M., Liu, T., Richtering, W., and Weichold, O. 2010. Interfacial Properties of Emulsions Stabilized with Surfactant and Nonsurfactant Coated Boehmite Nanoparticles. *Langmuir*, 26, (23) 17913-17918

- Tobin, T. and Ramkrishna, D. 1999. Modeling the effect of drop charge on coalescence in turbulent liquid - liquid dispersions. *The Canadian Journal of Chemical Engineering*. 77, (6), 1090-1104.

- Tong, J. and Povey, M.J.W. 2002. Pulse echo comparison method with FSUPER to measure velocity dispersion in n-tetradecane in water emulsions. *Ultrasonics*, 40, (1-8) 37-41

- Torres, L.G., Iturbe, R., Snowden, M.J., Chowdhry, B.Z., and Leharne, S.A. 2007. Preparation of o/w emulsions stabilized by solid particles and their characterization by oscillatory rheology. *Colloids and Surfaces A: Physicochemical and Engineering Aspects*, 302, (1-3) 439-448

- Tsouris, C. and Tavlarides, L.L. 1994. Breakage and Coalescence Models for Drops in Turbulent Dispersions. *AIchE Journal*, 40, (3) 395-406

- Tween 20-product information. 2007. Sigma-Aldrich Inc. Ref Type: Catalog

- Vankova, N., Tcholakova, S., Denkov, N.D., Ivanov, I.B., Vulchev, V.D., and Danner, T. 2007a. Emulsification in turbulent flow - 1. Mean and maximum drop diameters in inertial and viscous regimes. *Journal of Colloid and Interface Science*, 312, (2) 363-380

- Vankova, N., Tcholakova, S., Denkov, N.D., Vulchev, V.D., and Danner, T. 2007b. Emulsification in turbulent flow 2. Breakage rate constants. *Journal of Colloid and Interface Science*, 313, (2) 612-629

- Vashisth, C., Whitby, C.P., Fornasiero, D., and Ralston, J. 2010. Interfacial displacement of nanoparticles by surfactant molecules in emulsions. *Journal of Colloid and Interface Science*, 349, (2) 537-543

- Vermant, J., Cioccolo, G., Nair, K.G., and Moldenaers, P. 2004. Coalescence suppression in model immiscible polymer blends by nano-sized colloidal particles. *Rheologica Acta*, 43, (5) 529-538

- Walstra, P. 1968. Estimating globule-size distribution of oil-in-water emulsions by spectroturbidimetry. *Journal of Colloid and Interface Science*, 27, (3) 493-500

- Walstra, P. 1993. Principles of Emulsion Formation. *Chemical Engineering Science*, 48, (2) 333-349

- Walstra, P. and Smulders, P. E. A. 1998, Emulsion formation, In: B. P. Binks, Ed., *Modern Aspects of Emulsion Science*. London: The Royal Society of Chemistry.

- Walstra, P., 1987, Fat crystallization, In: J.M.V. Blanshard, , P. Lillford, Eds., *Food Structure and Behaviour*, London: Academic Press.

- Wang, C.Y. and Calabrese, R.V. 1986. Drop Breakup in Turbulent Stirred-Tank Contractors .2. Relative Influence of Viscosity and Interfacial-Tension. *AIchE Journal*, 32, (4) 667-676

- Wang, J., Yang, F., Tan, J., Liu, G., Xu, J., and Sun, D. 2009. Pickering Emulsions Stabilized by a Lipophilic Surfactant and Hydrophilic Platelike Particles. *Langmuir*, 26, (8) 5397-5404

- Weiss, J. and McClements, D.J. 2001. Color Changes in Hydrocarbon Oil-in-Water Emulsions Caused by Ostwald Ripening. *Journal of Agricultural and Food Chemistry*, 49, (9) 4372-4377

- Whitby, C.P., Fornasiero, D., and Ralston, J. 2009. Effect of adding anionic surfactant on the stability of Pickering emulsions. *Journal of Colloid and Interface Science*, 329, (1) 173-181

- Wille, M., Langer, G., and Werner, U. 2001. PDA Measurement of Drop Size Distribution for Liquid-Liquid Dispersing in Agitated Tanks. *Chemical Engineering and Technology*, 24, (5) 475-479

- Windhab, E.J., Dressler, M., Feigl, K., Fischer, P., and Megias-Alguacil, D. 2005. Emulsion processing - from single-drop deformation to design of complex processes and products *Chemical Engineering Science*, 60, (8-9) 2101-2113

- Worlitschek, J., Hocker, T., and Mazzotti, M. 2005. Restoration of PSD from Chord Length Distribution Data using the Method of Projections onto Convex Sets. *Particle and Particle Systems Characterization*, 22, (2) 81-98

- Wright, H. and Ramkrishna, D. 1994. Factors Affecting Coalescence Frequency of Droplets in A Stirred Liquid-Liquid Dispersion. *AIchE Journal*, 40, (5) 767-776

- Yang, B., Matsumura, H., and Furusawa, K. 1999. Adsorption behavior of phospholipid vesicles at oil/water interfaces. *Colloids and Surfaces B: Biointerfaces*, 14, (1-4) 161-168

- Zhai, X. and Efrima, S. 1996. Chemical and Physical Aspects of Macroemulsions Stabilized by Interfacial Colloids. *The Journal of Physical Chemistry*, 100, (26) 11019-11028

- Zhou, G.W. and Kresta, S.M. 1996. Impact of tank geometry on the maximum turbulence energy dissipation rate for impellers. *AIchE Journal*, 42, (9) 2476-2490

- Zhou, G.W. and Kresta, S.M. 1998. Evolution of drop size distribution in liquid-liquid dispersions for various impellers. *Chemical Engineering Science*, 53, (11) 2099-2113